REST and the regulation of stress resistance, brain aging, and Alzheimer's disease

REST and the regulation of stress resistance, brain aging, and Alzheimer's disease

A dissertation presented

by

Derek Mark Drake

to

The Division of Medical Sciences

in partial fulfillment of the requirements

for the degree of

Doctor of Philosophy

in the subject of

Genetics and Genomics

Harvard University

Cambridge, Massachusetts

October 2015

REST and the regulation of stress resistance, brain aging, and Alzheimer's disease

Abstract

Understanding how age-related stress in the brain is managed over a lifetime to maintain neuronal and cognitive function and prevent neurodegeneration will be critical for developing therapies to promote healthy aging. Here we show that repressor element 1-silencing transcription factor (REST) is induced in neurons of cognitively-intact aged individuals, but not those with Alzheimer's disease (AD). REST protects against factors associated with AD, such as neuronal apoptosis and AD neuropathology, through direct binding and repression of pro-apoptotic genes and genes that contribute to AD neuropathology. REST nuclear levels in prefrontal cortex pyramidal neurons also correlate with increased AD age of onset and decreased AD neuropathology. REST protects against toxic insults associated with aging, such as oxidative stress. Moreover, REST regulates FOXO1, a fundamental regulator of the response to oxidative stress, to provide oxidative stress protection. REST and FOXO1 nuclear levels correlate in aging human cortical neurons. Furthermore, REST and FOXO1 expression are correlated with the expression of FOXO1-regulated genes that protect against oxidative stress in aged prefrontal cortex. REST also downregulates miR-132 and miR-212, microRNAs that repress FOXO1 expression, and sensitize to oxidative stress. High levels of REST in the nucleus correlate with reduced longitudinal cognitive decline during aging. Moreover, REST nuclear levels account for a significant fraction of the variability of cognitive decline in the aging human population by a mixed model analysis. These results suggest that the neuroprotective function of REST is mediated, at least in part, through regulation of FOXO1 and miR-132/miR-212, and that REST is a critical determinant of stress resistance and cognitive preservation during aging.

Contents

Abbreviations

REST repressor element 1-silencing transcription factor

RE1 repressor element 1

FOXO forkhead box O

miR-132/miR-212 miR-132 and miR-212

ROSMAP Religious Orders Study and Memory and Aging Project

AD Alzheimers disease

MCI mild cognitive impairment

PFC prefrontal cortex

miRNA, miR microRNA

RNAi RNA interference

RT-qPCR real time quantitative PCR

shRNA short hairpin RNA

sgRNA short guide RNA

DN dominant negative

H_2O_2 hydrogen peroxide

ROS reactive oxygen species

NAC N-acetyl-L-cysteine

RA retinoic acid

FUDR fluorodeoxyuridine

IIS insulin/IGF-1 signaling

MEFs mouse embryonic fibroblasts

SEM, SE standard error of the mean

Acknowledgements

I would like to thank my thesis advisor Bruce Yankner for providing an ideal environment to study brain aging, the opportunity to work on several projects, and helpful advice concerning scientific and personal matters. My colleagues also provided invaluable support: Liviu Aron for help with immunolabeling, providing mice, dissertation advice, scientific criticism, and advice for graduating; Tao Lu for discussions, technical guidance, samples, and many reagents; Joe Zullo for collaboration, discussions, references, and technical assistance; Haeyoung Kim for reagents and technical advice; Monlan Yuan for lab management and training; and Ying Pan for reagents. My dissertation advisory committee, Raul Mostoslavsky, Alexander Meissner, and Yang Shi, also provided excellent scientific and experimental advice. I also want to thank David Bennett and Gregory Klein for valuable data from the Religious Orders Study and Memory and Aging Project, and the Paul F. Glenn Center for the Biology of Aging for supporting the local aging community through the Boston Aging Data Meetings, Harvard/Glenn Symposium on Aging, and other events.

Thanks to my grandmother Eleanor for support and keeping in touch. Finally, I thank my beautiful wife Rachel Drake for providing an incredible amount of support, understanding, encouragement, and dedication throughout the past 9 years.

Chapter 1

Introduction

Overview

Aging is associated with increased stress in the brain, and is the greatest risk factor for cognitive decline and Alzheimer's disease (AD). Most individuals will experience some degree of age-related cognitive decline which can negatively impact the quality of life for those affected and their families. Moreover, estimates suggest almost 50% of United States individuals aged 85 or older have AD (Hebert $\mathrm{et\ al.}$, 2003), and this number will continue to grow with our aging population placing an increasing burden on our health care system. The molecular changes that cause increased stress and predispose to AD and cognitive decline are incompletely understood. Understanding how age-related stress is managed will be critical for developing therapies to promote healthy aging.

In chapter 2 we provide evidence that induction of repressor element 1-silencing transcription factor (REST) in cortical and hippocampal neurons is a critical feature of healthy cognitive aging, and this process is lost in AD (Lu $\mathrm{et\ al.}$, 2014). REST directly represses expression of cell death and AD-promoting genes, protects against oxidative stress, and conditional deletion of REST in the mouse brain causes age-related neurodegeneration. Therefore, REST can be considered to be a fundamental regulator of stress responses dur-

ing brain aging, and may differentiate healthy aging from neurodegeneration. Chapters 3–5 focus on further investigation of the role of REST in oxidative stress resistance, cognitive decline during aging, and AD. First, we provide a general overview of brain aging, cognitive decline, AD, and oxidative stress and stress responses in the brain. Then, we review REST and the two REST-regulated targets pursued here, FOXO1 and miR-132/miR-212.

General overview of brain aging

At a functional level cross sectional and longitudinal studies show age-related decreases in several memory functions including delayed recall, working memory, processing speed, and spatial memory although there are unaffected functions including verbal ability (reviewed in Hedden and Gabrieli (2004); Yankner $\mathrm{et\ al.}$ (2008)). Human functional imaging studies show aged individuals have reduced coordinated activation of separate brain regions normally utilized by young, and that this is associated with reduced performance (Andrews-Hanna $\mathrm{et\ al.}$, 2007).

At a structural level there is minimal age-related neuronal loss in most areas of the frontal cortex and hippocampus (Burke and Barnes, 2006). However, most aged brains have lower grey matter volume due to reduced synaptic densities and dendritic branching especially in particular regions of the prefrontal cortex (PFC) (Burke and Barnes, 2006; Hedden and Gabrieli, 2004). There are also reductions in white matter integrity, particularly in the PFC, which correlate with reduced memory performance and may contribute to the reduced coordinated activation of separated brain regions (Hedden and Gabrieli, 2004).

At the molecular level common features of brain aging which are typically exacerbated in neurodegenerative diseases include reduced mitochondrial function, increased oxidative damage, increased redox-active iron (Zecca $\mathrm{et\ al.}$, 2004), protein aggregation, reduced protein clearance through the autophagic and ubiquitin-proteasome pathways, excitotoxicity, and inflammation (reviewed in Halliwell (2006); Mariani $\mathrm{et\ al.}$ (2005); Yankner $\mathrm{et\ al.}$ (2008)).

In agreement, there is substantial evidence for conserved gene expression changes in the aging mammalian brain (Lee et al., 2000; Loerch et al., 2008; Lu et al., 2004; Rowe et al., 2007; Yankner et al., 2008). There is strong decreased expression of genes involved in neural plasticity, the immediate-early response, synaptic function, vesicular transport, calcium homeostasis, and mitochondrial function. There is also increased expression of genes involved in stress response pathways, antioxidant function, DNA damage repair, metal ion homeostasis, and inflammation. Currently, the mechanism behind these age-related gene expression changes is unknown but may represent a coordinated stress response. It is also unknown whether the strong decrease in genes related to neuronal function is responsible for cognitive decline during aging.

Cognitive decline during aging

Memory is the process of information encoding, storage, and retrieval. Memory domains and function including episodic memory (autobiographical events), semantic memory (general factual knowledge), working memory (short term holding and processing of new information), processing speed, and perceptual orientation (visuospatial ability) can be assessed through testing, and an aggregate measure of global cognitive function can be derived.

Using these memory tests, age-related cognitive decline can be defined as reduced cognitive function relative to normal young adult function and includes deficits in short-term recall, working memory, spatial memory, naming, processing speed, or ability to encode new memories, but not severe loss of memory, reasoning, and language which are characteristic of dementias (Hedden and Gabrieli, 2004; Yankner et al., 2008). Most individuals experience some degree of cognitive decline during aging although there is significant interindividual heterogeneity. Some individuals remain cognitively intact or decline slowly while others develop dementia or mild cognitive impairment primarily

due to AD, cerebrovascular disease, or Lewy body disease. We currently have a poor understanding of the molecular mechanisms underlying this heterogeneity. However, we do know that the neuropathologies commonly associated with dementia and AD such as tangles, amyloid, infarcts, and lewy bodies are involved in cognitive decline because these neuropathologies accumulate in nondemented individuals and are associated with increased rates of cognitive decline (Boyle $\mathrm{et\ al.}$, 2013b). Other factors are involved because the levels of these neuropathologies account for less than half of the variation in cognitive decline (Boyle $\mathrm{et\ al.}$, 2013a). These factors include stochastic developmental and life events (Wilson $\mathrm{et\ al.}$, 2013), genetic differences (De Jager $\mathrm{et\ al.}$, 2012), diet, education, and REST nuclear levels as we show here.

Alzheimer's disease

AD is a progressive neurodegenerative disease with early stages characterized by short-term memory deficits and reduced cognitive function and late stages characterized by long-term memory deficits, loss of independence, and death usually within 10 years (Holtzman $\mathrm{et\ al.}$, 2011). AD is diagnosed clinically using memory tests such as the mini mental state exam (MMSE) and interviews with the patient and close acquaintances. AD is the most common form of dementia which is category of brain diseases characterized by loss of memory and reduced cognitive function severe enough to interfere with normal daily life and can include language and emotional problems (Holtzman $\mathrm{et\ al.}$, 2011). Other types of dementias include Lewy body dementia characterized by α-synuclein aggregates and cerebrovascular dementia characterized by blood supply problems and infarcts. Mild cognitive impairment (MCI) is characterized by cognitive impairments greater than expected for age but not severe enough to interfere with daily function. MCI may represent a transitional stage between normal aging and dementia.

AD differs from normal brain aging in several ways. Macroscopically, AD brains have

severe atrophy. There is also region-specific neuron death particularly in the entorhinal cortex and hippocampus in early stages and frontal cortex in later stages (Yankner $\mathrm{et\ al.}$, 2008). Loss of synapses and dendritic spines is also more pronounced (Holtzman $\mathrm{et\ al.}$, 2011). One neuropathological characteristic of AD is the typically pronounced accumulation of two protein aggregates, amyloid plaques and neurofibrillary tangles (NFTs). Amyloid plaques are typically found extracellularly and consist primarily of aggregated, insoluble amyloid-β which is a cleaved product of APP. NFTs are typically found within neurons and consist of aggregated hyperphosphorylated tau, a microtubule-binding protein. Both of these protein aggregates are neurotoxic and inflammatory through numerous mechanisms (Holtzman $\mathrm{et\ al.}$, 2011; Yankner $\mathrm{et\ al.}$, 2008). Amyloid plaques typically precede NFTs, but NFTs correlate better with AD diagnosis (Braak and Braak, 1991) and cognitive status (Giannakopoulos $\mathrm{et\ al.}$, 2003).

AD has a strong genetic component with early-onset and late-onset forms of the disease (reviewed in Karch $\mathrm{et\ al.}$ (2014)). Early-onset or familial AD is characterized by age of onset before age 65 and is due to highly penetrant mutations in APP and genes that process APP including PSEN1 and PSEN2 (Holtzman $\mathrm{et\ al.}$, 2011; Yankner $\mathrm{et\ al.}$, 2008). Late-onset or sporadic AD symptoms typically begin after age 60 and is the form of AD considered here. The strongest risk factor for AD is apolipoprotein E (*APOE*) which is involved with lipid and cholesterol catabolism and transport. Roughly 50% of AD individuals have an *APOE*$\varepsilon 4$ allele of *APOE* which increases risk of AD 3–4-fold and accelerates AD age of onset (Holtzman $\mathrm{et\ al.}$, 2012). Meta-analysis of several large cohort genome wide association studies (GWAS) using SNP arrays for common variants associated with AD have discovered 19 loci (OR range $[0.77, 1.22]$) in addition to *APOE*$\varepsilon 4$ (Lambert $\mathrm{et\ al.}$, 2013). How these intergenic and intronic SNPs alter risk of AD is unknown. Sequencing studies have identified rare variants (minor allele frequency (MAF) typically less than 0.05 or 0.01) in TREM2 (Jonsson $\mathrm{et\ al.}$, 2013) and possibly PLD3 (Cruchaga $\mathrm{et\ al.}$, 2014) that increase risk of AD. Recently, rare loss-of-function variants in ABCA7, which was associated with

increased risk of AD through common variant GWAS, were shown to increase risk of AD (OR $= 2.03$).

Oxidative stress and stress responses in the brain

Reactive species are molecules that can modify molecules and macromolecules through redox reactions (reviewed in Halliwell (2006)). Reactive oxygen species (ROS) are reactive species that contain oxygen including hydrogen peroxide (H_2O_2), superoxide ($O_2^{\cdot -}$), and hydroxyl radical ($^{\cdot}OH$). ROS are used by several intracellular signaling pathways during signal propagation. For example insulin binding and signaling through its receptor requires H_2O_2 generation and reversible oxidation of a phosphatase that acts on the receptor (Mahadev $\mathrm{et\ al.}$, 2001). ROS are also generated during normal metabolism as unintended by-products with the major source being superoxide and hydrogen peroxide generated during electron transport in mitochondria (reviewed in Murphy (2009)).

The problem with ROS is inappropriate modification of macromolecules potentially disrupting their function. ROS are normally eliminated by the cell's antioxidant machinery as part of its stress response mechanisms. Many cellular processes involve balance, and oxidative stress can be thought to occur when there is an imbalance between ROS production and removal. While the rate of mitochondrial ROS production is normally low it can increase if mitochondria become dysfunctional, O_2 concentration increases, in response to toxins, and during aging (Halliwell, 2006). For example, paraquat toxicity is likely due to it acting as a redox cycler first being reduced to a free radical state in mitochondria and then being oxidized by O_2 to form superoxide (Bus and Gibson, 1984; Castello $\mathrm{et\ al.}$, 2007; Cochemé and Murphy, 2008). One of the early theories of aging termed "The Free Radical Theory of Aging" hypothesized that inappropriate ROS that causes macromolecule damage causes aging (Harman, 1956). In support, expression of the antioxidant enzyme catalase targeted to the mitochondria extends

mouse lifespan (Schriner et al., 2005). However, while current evidence suggests that this theory is not strictly correct oxidative stress is harmful and can accelerate disease and functional decline. Throughout the existence of a living system at both the organismal and cellular level there is continual need to respond to the internal and external environment. These stimuli or the response may induce damage such as inappropriate ROS-induced macromolecule modification, protein misfolding and aggregation, improper modifications, improper restoration of previous state, or physical trauma. The events that cause damage can be considered to be stress. The cell has mechanisms to sense, prevent, and repair this stress-induced damage termed stress response pathways (reviewed in Haigis and Yankner (2010)). In one view, aging could be considered to be the outcome of the inability of living systems to properly manage the stress-induced damage of life.

The brain may be exceptionally sensitive to oxidative stress because of its high oxygen utilization (approximately 20% of the basal oxygen consumption) to provide for the high energy demand functions it performs such as action potential propagation and neurotransmission and the fact that neurons are postmitotic and cannot dilute damaged macromolecules through cell division (reviewed in Halliwell (2006); Mariani et al. (2005)). The brain also contains high concentrations of polyunsaturated fatty acids that are prone to oxidation, redox-active iron and other transition metals, and glutamate which can be excitotoxic if improperly regulated. For example, transition metals such as iron and copper ions, can convert H_2O_2, which is stable and can diffuse throughout the cell, to the damaging hydroxyl radical by splitting the $O-O$ bond in the Fenton reaction which can cause lipid peroxidation (Halliwell and Gutteridge, 1984; Yankner et al., 2008). In agreement, many studies find increased oxidative damage to proteins, lipids, mitochondrial DNA, and nuclear DNA in the aging brain and further increases in AD (reviewed in Mariani et al. (2005)). In addition, highly oxidized proteins can resist degradation and aggregate (Grune et al., 2004) including amyloid-β and tau (Dyrks et al., 1993; Troncoso et al., 1993). Interestingly, the oxidative damage to proteins in AD is selective (Sultana et al., 2006). The aging mam-

malian brain also has decreased expression of genes involved in mitochondrial function and increased expression of genes involved in stress response pathways, antioxidant function, and metal ion homeostasis suggesting increased oxidative stress potentially due to dysfunctional mitochondria (Lee et al., 2000; Loerch et al., 2008; Lu et al., 2004; Yankner et al., 2008). These observations suggest the brain's stress response mechanisms are engaged, but the rate at which age-related stress-induced damage occurs exceeds the rate at which the stress response mechanisms are able to prevent and repair the damage. Further, mitochondrial dysfunction during aging and AD may lead to energy deficits and increasing oxidative stress causing ROS-induced macromolecule damage which could further damage mitochondria exacerbating the situation. As an example, the large pyramidal projection neurons of the cortex that degenerate in AD have high energy demands and are vulnerable to mitochondrial dysfunction (Yankner et al., 2008). However, antioxidant feeding can prevent age-related gene expression changes in cerebellum (Park et al., 2009), and oxidative damage and age-related memory loss in rats can be partially rescued by antioxidant feeding (Liu et al., 2002) suggesting that intervention is possible.

REST

REST, also known as neuron-restrictive silencer factor (NRSF), was originally discovered as a transcriptional repressor of neuronal genes in differentiated non-neuronal cells (Chong et al., 1995; Schoenherr and Anderson, 1995). REST represses transcription by direct DNA binding though its eight zinc fingers and recruiting two corepressor complexes, SIN3A at the N-terminus and COREST/RCOR1 at the C-terminus (reviewed in Ballas and Mandel (2005); Ooi and Wood (2007)). The N-terminal complex consists of SIN3A and at least the histone deacetylases HDAC1 and HDAC2 and is thought to mediate short term repression. The C-terminal complex consists of COREST and several other chromatin modifiers including HDAC1, HDAC2, LSD1 (H3K4 demethylase), EHMT2/G9a (H3K9 methyltransferase),

MECP2 (methyl DNA-binding protein), and SMARCA4/BRG1 (nucleosome remodeler) and is thought to mediate long term repression by inducing a more compact chromatin configuration through eventual recruitment of DNMT1 (DNA methyltransferase) and HP1 (heterochromatin protein) at methylated H3K9. Once assembled these complexes are thought to act in a stepwise manner to remove activating marks and add repressive marks to the nearby histones and DNA. REST target genes are marked by a 21 base pair motif called a repressor element 1 (RE1) site although left and right half variants of this motif are also able to recruit REST (Bruce et al., 2004; Johnson et al., 2007). At some REST-regulated genes different combinations of the corepressor complexes can be present which may be dependent on the specific type and sequence of the RE1 motif and may be responsible for differential regulation (Ooi and Wood, 2007).

REST is expressed in non-neuronal cells and in embryonic stem cells and neuronal progenitor cells where its downregulation and degradation is required for differentiation into neurons (Ballas and Mandel, 2005). REST's degradation is regulated by ubiquitin-mediated proteolysis through the E3 ubiquitin ligase SCF$^{\beta\text{-TRCP}}$ (Westbrook et al., 2008). This ubiquitination requires phosphorylation by at least CK1 (Kaneko et al., 2014) or ERK1/2 (MAPK1/MAPK3) (Nesti et al., 2014), and REST can be stabilized by dephosphorylation at these sites by CTDSP1 (Nesti et al., 2014).

In addition to repressing neuronal genes REST also represses several brain-enriched miRNAs including miR-124 which inhibits expression of non-neuronal genes (Conaco et al., 2006; Wu and Xie, 2006). REST also may have other functions such as tumor supression through reduced PI3K signaling determined by reduced P-S473-AKT (Singh et al., 2013; Westbrook et al., 2005).

REST is transcriptionally regulated by WNT signaling (Lu et al., 2014; Nishihara et al., 2003), neuronal activity induced by the glutamate analog kainic acid (Palm et al., 1998), SP1 transcription factor (Ravache et al., 2010), and Oct4 and Nanog. HIPPI/IFT57 can bind to the REST promoter to activate transcription which is dependent on nuclear translocation

of HIPPI by HIP1 (Datta and Bhattacharyya, 2011; Datta et al., 2011).

REST nuclear localization is only partly understood. REST has a nuclear localization signal. PRICKLE1/RILP, which is expressed in adult human brain neurons (Bassuk et al., 2008), is localized to the outer nuclear membrane and required for REST nuclear import (Shimojo and Hersh, 2003, 2006). DCTN1 (dynactin 1, dynactin p150^{Glued}) is a subunit of dynactin complex that can bind dynein motor proteins to cargo to be transported along microtubules. DCTN1 directly interacts with PRICKLE1 and huntingtin (HTT) (Shimojo, 2008). In non-neuronal cells this complex transports REST to the nucleus. In contrast, HAP1, which is enriched in neurons (Li and Li, 2005; Rong et al., 2007), binds HTT and helps retain REST in the cytoplasm through the HTT/DCTN1/PRICKLE1 complex (Shimojo, 2008). However, there are conflicting reports that show PRICKLE1 directly binds REST and retains it in the cytoplasm (Bassuk et al., 2008).

There are several reports suggesting that REST may be neuroprotective. REST knockout mice are embryonic lethal with apoptotic cell death (Chen et al., 1998). REST is induced and protects against hyperexcitability in hippocampal neurons (Pozzi et al., 2013), and REST protects forebrain neurons in mouse models of epilepsy (Hu et al., 2011). Finally, REST conditional knockout mice are more vulnerable to the dopaminergic neurotoxin MPTP potentially suggesting a reduced stress response (Yu et al., 2013). However, REST may be detrimental in ischemia (Calderone et al., 2003)

In chapter 2 we find that REST is induced in cortical and hippocampal neurons in cognitively-intact aged individuals, but REST is lost from the nucleus in AD and MCI (Lu et al., 2014). Interestingly, REST is induced in cerebellar Purkinje and granule cell neurons and in dentate gyrus granule cell neurons in both aged and AD individuals which are relatively unaffected areas in AD indicating specificity. In AD REST is lost from the nucleus and appears in autophagosomes, but not lysosomes, with other pathologically misfolded proteins such as amyloid-β and phosphorylated tau. REST is induced by stress and provides neuroprotection from oxidative stress and amyloid-β toxicity *in vitro*. REST

also represses genes associated with AD including PSEN2, PSENEN/PEN2, GSK3β, CDK5R1/p35, and CDK5R2/p39 and cell death including FAS, FADD, TRADD, BAX, BID, DAXX, PUMA/BBC3, and BIM/BCL2L11. In agreement, REST conditional knockout mice have increased neuronal apoptosis at 8 months. However, it is unclear whether regulation of any of these pro-apoptotic and AD-associated genes would provide direct protection against oxidative stress. Finally, REST was associated with reduced cognitive decline and neuropathology in a cross-sectional analysis.

Chapters 3 and 4 are a further investigation of two central unanswered questions of Chapter 2. First, how does REST protect against oxidative stress? Second, what is the relationship between REST nuclear levels and longitudinal cognitive decline if neuropathologies are also considered?

FOXO1

FOXO1 is a member of the FOXO family of transcription factors characterized by a DNA binding domain called a forkhead box. There are four FOXO members in mammals: FOXO1, FOXO3, FOXO4, and FOXO6. FOXOs typically function as transcriptional activators and regulate several processes including the response to oxidative stress, apoptosis, cell cycle, autophagy (Zhao $\mathrm{et\ al.}$, 2010), and metabolism (reviewed in Greer and Brunet (2005); van der Horst and Burgering (2007)). FOXO1 can provide ROS protection through transcriptional activation of at least catalase/CAT, MnSOD/SOD2, PA26/SESN1, selenoprotein P/SEPP1, and paraoxonase 2/PON2 (Klotz $\mathrm{et\ al.}$, 2015; Sengupta $\mathrm{et\ al.}$, 2011; Shao $\mathrm{et\ al.}$, 2014; Tothova $\mathrm{et\ al.}$, 2007). For example, neural and hematopoietic stem cells from FOXO conditional knockout mice have higher levels of intracellular ROS (Paik $\mathrm{et\ al.}$, 2009; Tothova $\mathrm{et\ al.}$, 2007), and cardiomyoctes subjected to oxidative stress are protected by FOXO overexpression and more vulnerable with loss of FOXO function (Sengupta $\mathrm{et\ al.}$, 2011). FOXO1 can induce apoptosis through transcriptional activation

of pro-apoptotic BCL-2 family members BNIP3 and BIM/BCL2L11, death cytokines Fas ligand/FASLG and TRAIL/TNFSF10, and the transcriptional repressor BCL6 which down-regulates anti-apoptotic BCL-2 family member BCL-XL/BCL2L1. FOXO1 regulates cell cycle arrest through transcriptional activation of several genes including p27KIP1/CDKN1B, p21/CDKN1A, cyclin G2/CDK1, and GADD45.

FOXOs can be regulated at the post-translational level by numerous mechanisms (reviewed in Greer and Brunet (2005); Xie $\mathrm{et\ al.}$ (2012)). These post-translational modifications can affect FOXO subcellular localization, DNA binding ability, protein-protein interactions, transcriptional activity, and degradation. The first pathway found to regulate FOXOs was the insulin/IGF-1 signaling (IIS) pathway (Brunet $\mathrm{et\ al.}$, 1999). FOXOs have a nuclear localization signal and nuclear export signal, and in the absence of signals are typically localized in the nucleus. Stimulation of IIS by insulin or IGF-1 binding to their receptors eventually results in activation of PI3K then AKT which can then translocate to the nucleus to phosphorylate FOXO1 at Thr24, Ser256, and Ser319. Phosphorylation at these sites induces FOXO1 nuclear export through enhanced binding to 14-3-3 proteins in the nucleus followed by nuclear export. FOXOs are subject to ubiquitination and degradation by the proteasome which is enhanced by AKT phosphorylation at Ser256. Several E3 ubiquitin ligase proteins for FOXO1 are known including SKP2 (F-box) and MDM2 (RING-finger).

The regulation of FOXO1 by oxidative stress-induced signaling has been thoroughly studied (reviewed in Klotz $\mathrm{et\ al.}$ (2015)). Several kinases phosphorylate FOXO1 in response to increased ROS including ERK and p38MAPK. FOXOs can be acetylated by CBP, P300, and PCAF which suppresses transcriptional activity by reducing DNA binding ability. Oxidative stress can induce deacetylation of FOXO1 by SIRT1 which promotes nuclear retention, activates FOXO1-mediated stress response genes, reduces apoptotic genes, and suppresses FOXO1-induced apoptosis (Qiang $\mathrm{et\ al.}$, 2010; Yang $\mathrm{et\ al.}$, 2005). SIRT1 also protects against oxidative stress through FOXO1 (Alcendor $\mathrm{et\ al.}$, 2007).

miR-132/miR-212

microRNAs (miRNAs) are small noncoding RNAs that function as post-transcriptional regulators of gene expression. miRNAs function as part of a ribonucleoprotein complex with the miRNA imperfectly hybridizing to a short region usually in the 3'-UTR of mRNAs and act primarily through repression of protein synthesis or degradation of the target mRNA by deadenylation and decapping (Fabian et al., 2010). miRNAs can maintain homeostasis and provide resistance to stress (Leung and Sharp, 2010). Because increased stress resistance is highly correlated with increased life span, miRNAs may function to regulate life span and health span. Many miRNAs are brain-specific or brain-enriched (Sempere et al., 2004) and have been shown to play an important role in mammalian brain function and development. Dysregulation of these miRNAs could play an important role in brain aging.

By profiling miRNAs with microarrays, we find that miR-132 and miR-212, a forebrain-enriched (Olsen et al., 2009) pair of miRNAs derived from the same noncoding RNA transcript, are downregulated in the aging brain. miR-132/miR-212 have been implicated in many neural processes such as regulation of dendrite length and number (Vo et al., 2005), hippocampal spine density (Magill et al., 2010), circadian rhythms (Cheng et al., 2007), and novel object recognition memory (Hansen et al., 2013). However, high levels of miR-132 have been shown to promote to short term memory impairment (Scott et al., 2012), stress-induced cognitive impairment (Shaltiel et al., 2013), and learning impairment (Hansen et al., 2013). In addition, miR-132/miR-212 have been shown to be pro-apoptotic in some cancers (Formosa et al., 2013), downregulated after the neuroprotective event of ischemic preconditioning (Lusardi et al., 2010), and their downregulation after status epilepticus is neuroprotective (Jimenez-Mateos et al., 2011). Thus, reduced miR-132/miR-212 levels during aging could be one important contributor to cognitive decline. miR-132/miR-212 are also predicted to target several genes that regulate oxidative stress responses, and we

find that they directly target FOXO1, sensitize to oxidative stress, and are pro-apoptotic.

miR-132/miR-212 are upregulated by BDNF and neural activity (Wayman et al., 2008) through the MAPK-ERK1/2 signalling pathway (Remenyi et al., 2010) and are bound by CREB (Vo et al., 2005). miR-132/miR-212 are also known to be regulated by REST (Conaco et al., 2006; Johnson et al., 2008; Wu and Xie, 2006). Thus, one of these pathways may be responsible for decreased miR-132/miR-212 during aging, and we provide evidence that increased repression by REST is involved.

Dissertation results and model

Figure 1.1 provides a summary model encapsulating the results presented in this dissertation and the chapters where the related data are presented. Chapter 2 presents the first paper to show that REST is induced in the nucleus of neurons of cognitively-intact aged individuals, but this process is lost in AD (Lu et al., 2014). Moreover, REST directly protects against apoptosis by repression of pro-apoptotic genes and protects against oxidative stress through unidentified mechanisms (dashed line). Cross-sectional data indicates that REST also protects against cognitive decline and neuropathology. Chapter 3 is a follow-up to Chapter 2 to investigate how REST provides protection against oxidative stress. The primary findings are that REST regulates FOXO1 expression and localization, and REST provides stress resistance partly through FOXO1. Based on gene expression analysis, REST may also regulate FOXO1 for stress resistance in the aged human brain. Chapter 4 expands on the cross-sectional analysis of cognitive decline and neuropathology in Chapter 2. The relationship between REST nuclear levels, AD neuropathologies, and longitudinal cognitive decline is investigated using a mixed model to determine if REST nuclear levels are associated with cognitive decline independently of AD neuropathologies. The contribution of REST nuclear levels to the variability of cognitive decline is also investigated. Lastly, Chapter 5 investigates an age-regulated REST target, miR-132/miR-212,

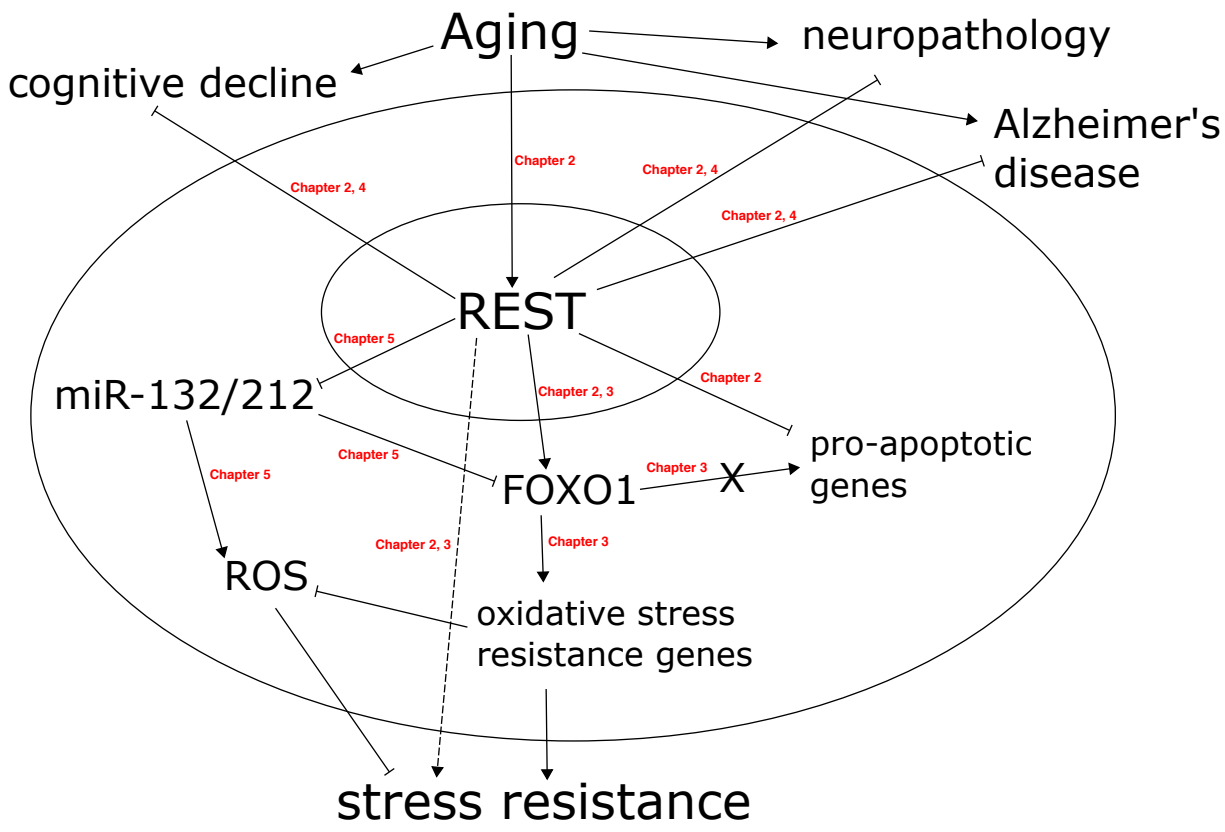

Figure 1.1: **Summary model of results and interrelations of chapters.**

and their role in regulating FOXO1 and oxidative stress resistance.

Chapter 2

REST and stress resistance in aging and Alzheimers disease

Abstract

Human neurons are functional over an entire lifetime, yet the mechanisms that preserve function and protect against neurodegeneration during aging are unknown. Here we show that induction of the repressor element 1-silencing transcription/neuron-restrictive silencer factor (REST/NRSF) is a universal feature of normal aging in human cortical and hippocampal neurons. REST is lost, however, in mild cognitive impairment (MCI) and Alzheimers disease (AD). Chromatin immunoprecipitation with deep sequencing (ChIP-seq) and expression analysis show that REST represses genes that promote cell death and AD pathology, and induces the expression of stress response genes. Moreover, REST potently protects neurons from oxidative stress and amyloid β-protein (Aβ) toxicity, and conditional deletion of REST in the mouse brain leads to age-related neurodegeneration. A functional ortholog of REST, C. elegans SPR-4, also protects against oxidative stress and Aβ toxicity. During normal aging, REST is induced in part by cell non-autonomous Wnt signaling. However, in AD, frontotemporal dementia and dementia with Lewy bodies, REST

is lost from the nucleus and appears in autophagosomes together with pathologic misfolded proteins. Finally, REST levels during aging are closely correlated with cognitive preservation and longevity. Thus, the activation state of REST may distinguish neuroprotection from neurodegeneration in the aging brain.

Contributing authors

Adapted from Lu $\mathrm{et\ al.}$ (2014).

Tao Lu[1], Liviu Aron[1], Joseph Zullo[1], Ying Pan[1], Haeyoung Kim[1], Yiwen Chen[2], Tun-Hsiang Yang[1], Hyun-Min Kim[1], Derek Drake[1], Xiaole Liu[2], David A. Bennett[3], Monica P. Colaicovo[1] and Bruce A. Yankner[1]

[1]Department of Genetics, Harvard Medical School, Boston, MA 02115, [2] Department of Biostatistics and Computational Biology, Dana-Faber Cancer Institute and Harvard School of Public Health, Boston, MA 02215, [3]Rush Alzheimer's Disease Center, Rush University Medical Center, Chicago, IL 60612.

Author Contributions

T.L, L.A., J.Z., Y.P., H.K., and H.-M.K. performed experiments. T.L., L.A., J.Z., M.C. and B.A.Y. contributed to the overall study design. T.L., Y.C., T.-H.Y., D.D. and X.L. performed informatics analysis. D.A.B. contributed tissue samples, cognitive test data and analysis. B.A.Y. directed the study and B.A.Y., T.L., L.A. and J.Z. wrote the manuscript, which was edited by all the coauthors.

Introduction

The preservation of cognitive function during aging has emerged as one of the major medical challenges of the 21st century. A fundamental question is why some individuals age with their cognitive function relatively intact whereas others decline and develop Alzheimers disease (AD). Early studies suggested that neuronal loss was an integral feature of the aging brain. With the advent of stereological neuronal quantification, however, it became clear that neuronal cell number is largely preserved in the neocortex and hippocampus of the aging human brain, declining only in the setting of neurodegenerative disease (Gómez-Isla et al., 1996; Peters et al., 1998; Yankner et al., 2008). Robust stress response mechanisms must have evolved, therefore, to preserve neurons and cognitive function across an entire lifespan (Kenyon, 2010; Spalding et al., 2005).

REST is a repressor of neuronal genes during embryonic development that is downregulated once terminal neuronal differentiation has occurred (Ballas et al., 2005; Chong et al., 1995; Schoenherr and Anderson, 1995). Here we show that REST is induced in the aging human brain and regulates a network of genes that mediate cell death, stress resistance and AD pathology. This gene network becomes dysregulated at early stages of AD when REST is lost from the nucleus. Conditional REST knockout mice and C. elegans models suggest that REST protects neurons from age-related toxic insults. In aging humans, elevated REST levels are associated with preservation of cognitive function and increased longevity, even in the presence of AD pathology. Hence, REST regulates a neuroprotective stress response that may be central to cognitive preservation during aging.

Results

REST is induced in the aging human brain and declines in AD

Transcriptional profiling has demonstrated significant changes in the expression of neuronal genes in the prefrontal cortex of aging humans (Loerch $\mathrm{et\ al.}$, 2008; Lu $\mathrm{et\ al.}$, 2004). Analysis of this dataset using the Ingenuity Systems IPA platform suggests that the transcription factor most strongly predicted to be activated in the aging brain is REST/NRSF (P =9E-10). Moreover, the 21-bp canonical RE1 recognition motif for REST is highly enriched in the age-downregulated gene set (P =3E-7) (Figure 2.1a).

To explore the role of REST in the aging brain, we measured REST levels in extracts of prefrontal cortex (PFC) from young adult (20-35 years) and aged (73-106 years) individuals without AD. REST expression was significantly increased in the aging human PFC at both the mRNA and protein levels, as determined by quantitative real time RT-PCR (qRT-PCR) and Western blotting (Figure 2.1b, c). Full-length REST was markedly increased; the truncated splice variant REST4 was a minor component, comprising 0.1-0.5% of REST mRNA. Immunofluorescence microscopy using three different antibodies against the N- or C-terminal domains of REST showed a striking induction of REST in the nucleus of aging neurons in the PFC and hippocampus (Figure 2.1d, e; Figure 2.7). Much lower levels of REST were detected in microglial cells and astrocytes (data not shown). REST antibody specificity was indicated by ablation of immunoreactivity after antibody preabsorption with a REST blocking peptide, absence of immunoreactivity with matched nonspecific IgG, and loss of immunoreactivity after shRNA-mediated REST knockdown in neural SH-SY5Y cells (Figure 2.7b, c).

We then asked whether induction of REST in aging neurons leads to increased REST-RE1 site binding. To assess REST targeting specifically in neurons, we isolated neuronal nuclei from the PFC by fluorescence-activated cell sorting (FACS) of NeuN-positive nuclei (Spalding $\mathrm{et\ al.}$, 2005) (Methods). ChIP-PCR analysis showed a marked induction of

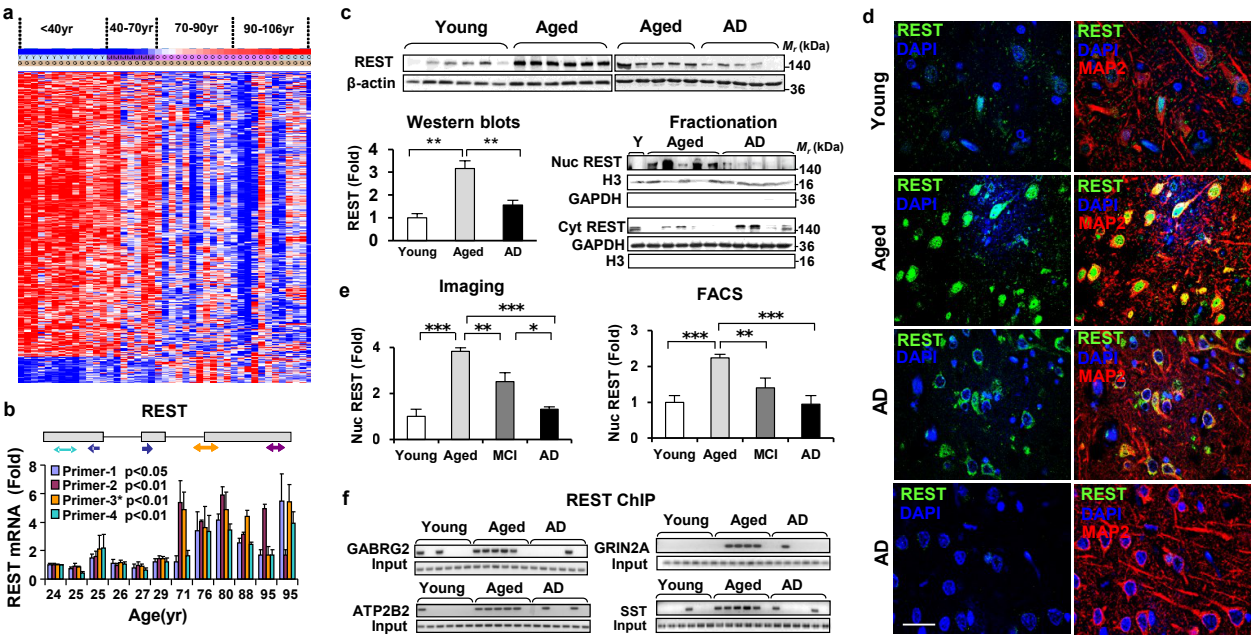

Figure 2.1: **Induction of REST in the aging human prefrontal cortex. A.** Hierarchical cluster analysis of predicted REST targets, based on the presence of the canonical RE1 motif (Bruce et al., 2004), shows relatively high expression in young adults (red) and lower expression (blue) in the aging population. Each lane represents an individual prefrontal cortical brain sample. **B.** qRT-PCR shows age-dependent induction of REST mRNA in the PFC. Values represent the mean$\pm$S.D., n=3. Shown are p-values indicating significance for the mean of aged (71-95 yrs) versus young (24-29 yrs) cases for each primer. **C.** Age-dependent increase in total REST protein level in the PFC of controls but not AD patients. REST levels were also measured in isolated nuclear (Nuc REST; lower right panel, upper blot) and cytoplasmic (Cyt REST; lower right panel, lower blot) fractions. Each lane represents an individual case. Young, n=12; Aged, n=15; AD, n=10. **D.** Confocal immunofluorescence labeling for REST (green), the neuronal marker MAP2 (red) and DNA (DAPI, blue) in the PFC of young adult, aged and AD cases. Scale bar: 25 μm. **E.** Quantitative analysis of nuclear REST levels by in situ imaging (left panel: Young, n=11; Aged, n=77; AD, n=72; MCI=11) or FACS analysis of isolated PFC neuronal nuclei (right panel: Young, n=11; Aged, n=22; AD, n=11; MCI n=12). For c and e, values are expressed as fold change relative to the young adult group, and represent the mean+S.E.M. *P <0.05, **P <0.01, ***P <0.001 by Students unpaired t test. **F.** ChIP analysis shows induction of REST-RE1 site binding in normal aging PFC neurons but not in AD.

REST binding to canonical RE1 motifs in REST target genes in the aged PFC (Figure 2.1f). These results suggest that REST expression and function is increased in aging neurons.

We next examined REST in aging individuals with mild cognitive impairment (MCI) or AD. REST was almost absent from the nucleus of cortical and hippocampal neurons in AD (Figure 2.1d, Figure 2.7a, d). Punctate cytoplasmic REST immunoreactivity was detected in some AD neurons, but was not detectable in other neurons (Figure 2.1d). Loss of nuclear REST was confirmed by quantitative immunocytochemical analysis of 77 cases of sporadic AD compared with 72 age-matched cognitively intact controls, and confirmed by FACS analysis of neuronal nuclei in a subset of cases (Figure 2.1e). In 23 of 24 cases of amnestic MCI, nuclear REST levels were reduced relative to the mean of aged controls (Figure 2.1e). A survey of brain regions showed significantly reduced nuclear REST levels in affected neuronal populations in AD, including prefrontal cortical neurons, and neurons of the CA1, CA3 and CA4 subfields of the hippocampus (Figure 2.7a, c). In contrast, nuclear REST was not reduced in neurons of the dentate gyrus and cerebellum, which are relatively unaffected in AD (Figure 2.7a, d). Reduced REST levels in AD were confirmed by Western blotting of prefrontal cortical grey matter samples, as well as isolated cortical nuclei (Figure 2.1c, upper and far right panels, respectively). Furthermore, ChIP-PCR analysis of neuronal nuclei showed significantly reduced or absent REST-RE1 site binding in AD relative to normal aging controls (Figure 2.1f, Figure 2.2a). Thus, REST is induced during normal brain aging, but is markedly reduced in AD in vulnerable neuronal populations.

REST represses genes involved in cell death and AD

To obtain greater insight into the functional consequences of REST induction in the aging brain, we explored REST targets by chromatin immunoprecipitation and deep sequencing (ChIP-seq) in the neural cell line SH-SY5Y. REST binding to a subset of the identified target genes was confirmed by ChIP-qPCR (Figure 2.8). REST ChIP-seq sites were

significantly enriched among age-regulated genes in human PFC (P =1.65E-12), and were predominantly downregulated from the third to the tenth decades of life (Figure 2.8a). Pathway analysis of the ChIP-seq database showed a highly significant enrichment for genes in cell death pathways and genes that are associated with AD/dementia (Figure 2.8b, c). Cell death genes include p38 MAP kinase (MAPK11), fas, fadd, tradd, bax, bid, daxx, PUMA, the mitochondrial permeability transition pore ANT1 and cytochrome C. REST targets related to the pathology of AD include the gamma secretase complex members presenilin-2 and pen-2 implicated in Aβ generation, and cdk5R1 (p35), cdk5R2 (p39), p38 MAP kinase and 14-3-3zeta implicated in tau phosphorylation. REST repressed the expression of these genes in SH-SY5Y cells (Figure 2.9a, b), and strongly inhibited tau phosphorylation at the AT8 and PHF1 epitopes associated with AD (Figure 2.9c).

We next examined the regulation of these REST target genes in the normal aging brain and AD. To distinguish effects at different stages of cognitive decline, we stratified the AD population for least severe (AD1; MMSE score $>$18) and most severe (AD2; MMSE score $<$8). REST targets related to cell death and AD pathology showed reduced REST binding and elevated mRNA expression at both stages of AD (Figure 2.2a, b). REST target genes related to neurotransmission, however, showed elevated mRNA expression in early stage AD1, but reduced expression in later stage AD2 (Figure 2.2b). Regression analysis of protein levels showed that nuclear REST is inversely correlated with levels of pro-apoptotic (BAX and DAXX) and AD-related (presenilin-2) proteins in normal aging and AD neurons (Figure 2.2c, d). This was also observed for REST targets associated with neurotransmission (SST and CALB1) during normal aging and early stage AD1, but not in late stage AD2 (Figure 2.2c). The activation-associated histone modification H3K9ac, which is typically reduced by REST, was globally downregulated in normal aging PFC neurons (Figure 2.2e) and was inversely correlated with REST levels (Figure 2.2c, d). In contrast, neuronal H3K9ac increased significantly in early AD (Figure 2.2e). Thus, loss of nuclear REST in AD is associated with epigenetic derepression of potentially pathogenic

genes.

REST is neuroprotective

Since REST represses pro-apoptotic genes, we explored a role in neuroprotection by assessing vulnerability to oxidative stress and oligomeric Aβ, stressors associated with brain aging (Lu $\mathrm{et\ al.}$, 2004) and AD (Holtzman $\mathrm{et\ al.}$, 2011). Primary cultures of mouse E16 cortical neurons were established from Nestin-Cre:REST$^{lx/lx}$ (REST cKO) and littermate control embryos. After 1-2 weeks in culture, neuronal differentiation was comparable in REST-deficient and control cultures. Upon treatment with hydrogen peroxide or oligomeric Aβ42, REST-deficient neurons showed markedly increased degeneration and cell death relative to controls (Figure 2.3a, Figure 2.10a). REST-deficient neurons were rescued by lentiviral transduction of wild-type REST, leading to expression levels 2-2.5-fold that of wild-type (Figure 2.3a, Figure 2.10a). In contrast, a REST mutant that is deficient in nuclear translocation ($\triangle$REST) was unable to rescue (Figure 2.3a, b). REST-deficient neurons showed increased expression of pro-apoptotic genes in response to oxidative stress and oligomeric Aβ (Figure 2.10b). Thus, endogenous REST is neuroprotective.

REST-deficient mice showed a progressive age-related neurodegenerative phenotype. At one month of age, neuronal numbers in the cortex and hippocampus of REST cKO mice were not significantly different from controls. Neuronal degeneration and apoptosis appeared by 8 months of age, as indicated by positive neuronal labeling for cleaved caspase-3 and TUNEL (Figure 2.3c, d). This was accompanied by significant neuronal loss in the cerebral cortex and hippocampus, and pronounced gliosis (Figure 2.3c, d). These results suggest that REST is essential for maintaining neuronal viability in the aging brain. To confirm the findings on REST-deficient neurons, we assessed vulnerability to oxidative stress after REST overexpression or shRNA-mediated knockdown in neural SH-SY5Y cells. Cell death induced by hydrogen peroxide was significantly reduced when REST was overexpressed by 3-to 20-fold (Figure 2.10c). Higher levels of REST overexpression

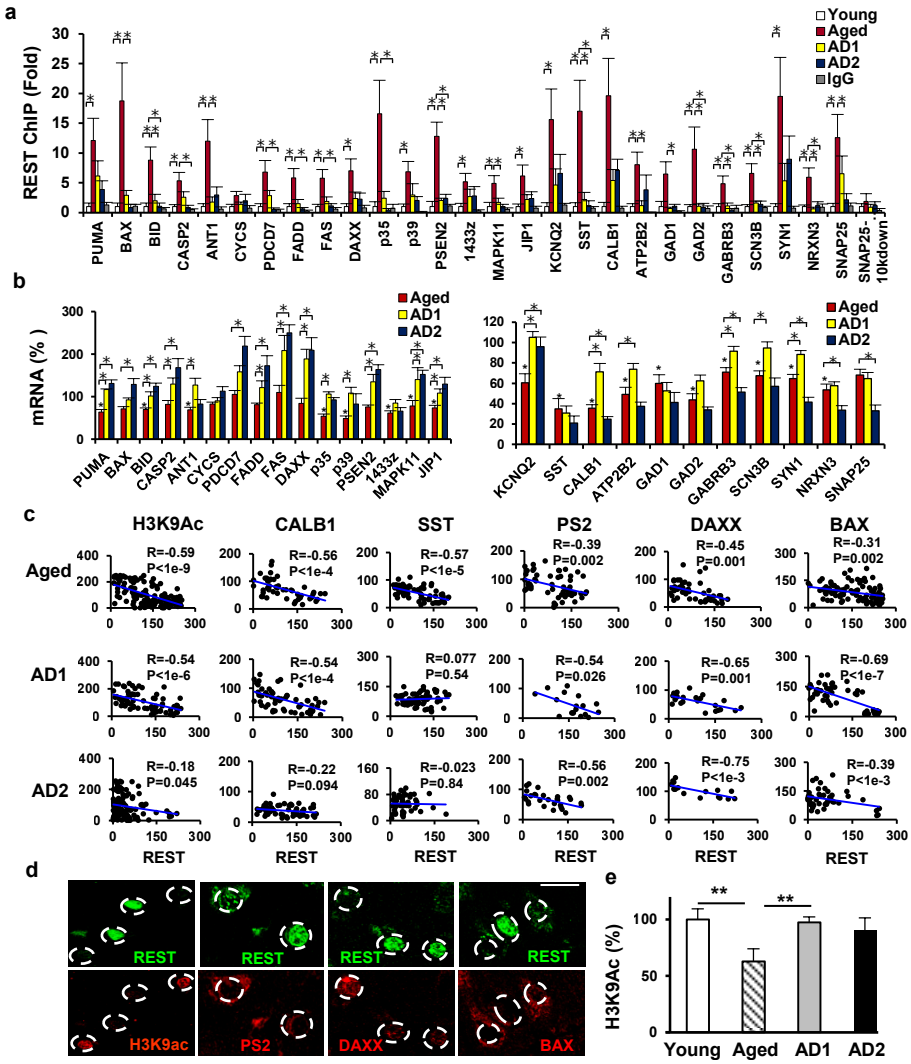

Figure 2.2: **Regulation of REST target genes in aging and AD. A.** ChIP-qPCR analysis of REST binding to target genes in isolated PFC neuronal nuclei. Shown are young adult (Young), normal aged (Aged) and AD cases, which were stratified as AD1 and AD2. Values represent fold change relative to the mean young adult value, and represent the mean+S.E.M., n=7. *P <0.05 by the Mann-Whitney test. **B.** mRNA expression of REST target genes determined by qRT-PCR of PFC. Shown are REST target genes related to cell death pathways and AD pathology (left panel), and neurotransmission (right panel). Values are normalized to the mean young adult expression level (100%) and represent the mean+S.E.M. Young, n=9; Aged, n=10; AD1, n=10; AD2, n=10. *P <0.05 by the Mann-Whitney test. **C.** Linear regression analysis of nuclear REST versus levels of protein targets or histone H3K9ac in double-labeled PFC neurons. **D.** Representative images showing inverse relationships between nuclear REST and H3K9ac, PS2, DAXX and BAX in AD1 neurons. Scale bar: 20 μm. **E.** Global epigenetic regulation in aging and AD. Histone modification H3K9ac was determined in isolated PFC neuronal nuclei. Values are normalized to the mean of the young adult group (100%), and represent the mean+S.E.M., **P <0.005 by t-test. Young, n= 8; Aged, n=11; AD1, n=4; AD2, n=4.

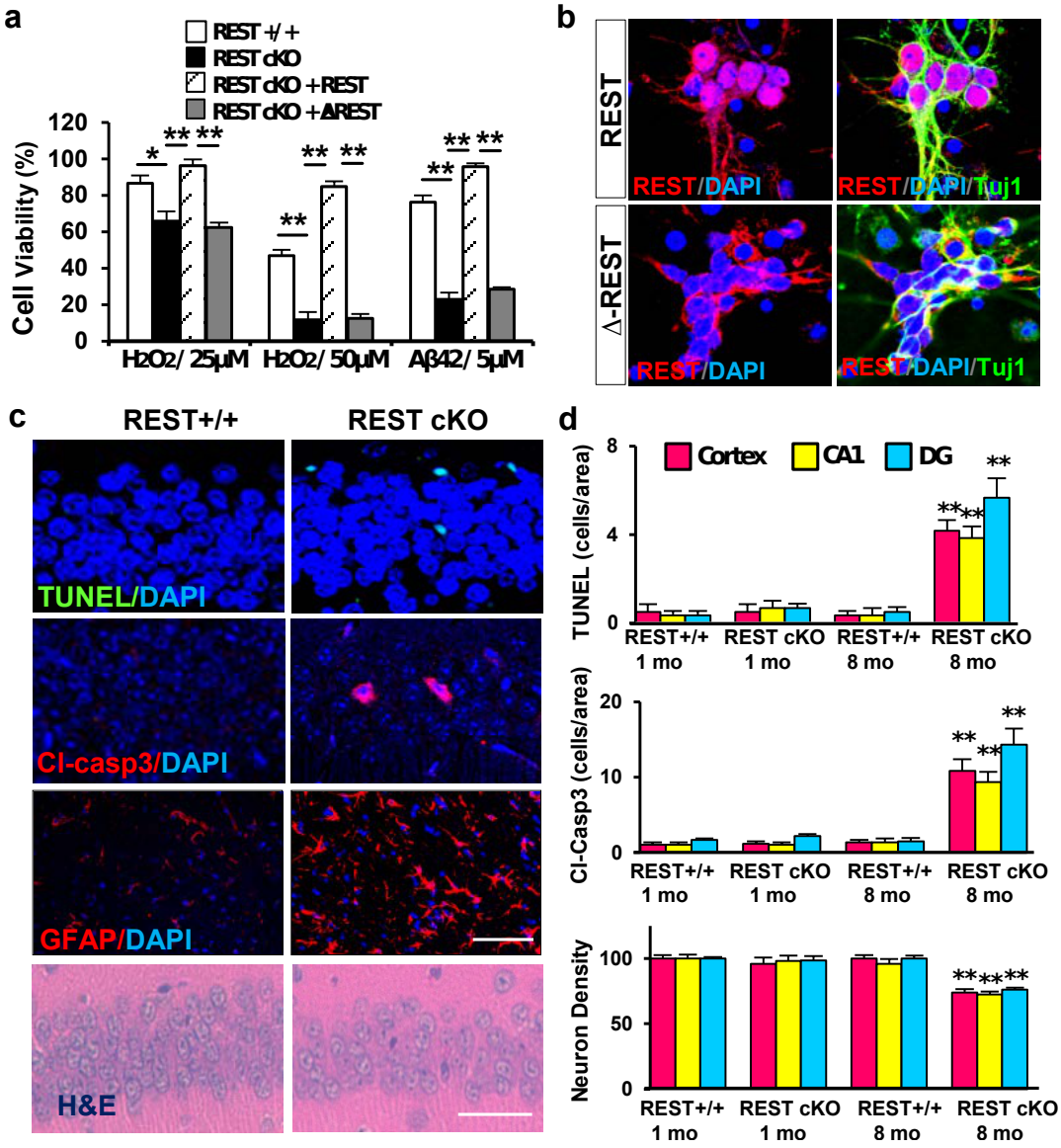

Figure 2.3: **REST is neuroprotective A.** REST-deficient cortical neurons cultured from REST cKO mouse embryos show increased vulnerability to H2O2 and oligomeric Aβ42 toxicity. Cell viability is expressed as percent of the value in untreated cultures. Values represent the mean + S.E.M., n=6-8. *P <0.05, **P <0.01 by Students unpaired t-test. **B.** Reduced nuclear translocation of the ΔREST mutant. **C.** REST cKO mice exhibit age-related neurodegeneration. Shown are sections of the hippocampal CA1 subfield from 8 month old REST cKO mice labeled for TUNEL, cleaved caspase 3 (cl-casp3) and GFAP, or stained with hematoxylin and eosin (H&E). **D.** Neurodegeneration in 8 months but not 1 month old REST cKO mice in the cortex, and in hippocampal CA1 and dentate gyrus (DG) regions. Values represent the mean + S.E.M., n=6 mice; **P <0.001 relative to control by Students unpaired t-test. Scale bars: 20 μm.

increased cell death. REST knockdown by lentiviral shRNA transduction significantly increased H2O2-induced apoptosis in both SH-SY5Y cells and cultured human cortical neurons, which was prevented by shRNA-resistant mREST (Figure 2.10c, d). Furthermore, shRNA-mediated REST knockdown increased levels of reactive oxygen species (ROS), which was prevented by the antioxidant N-acetyl-cysteine (NAC) (Figure 2.10e, f). Moreover, REST knockdown increased oxidative DNA damage, which was reduced by REST overexpression (Figure 2.10g). To examine the relationship of REST expression to oxidative DNA damage in the human brain, we double-labeled for REST and the oxidative DNA damage marker 8-oxoguanine (8-oxoG). Linear regression analysis showed a significant inverse relationship between nuclear REST and 8-oxoG levels in normal aging neurons and in AD (Figure 2.10h). Thus, REST expression during aging may reduce oxidative damage.

The nematode C. elegans has served as a model system of aging and stress resistance (Kenyon, 2010). Two multi-zinc finger transcription factors in C. elegans structurally resemble mammalian REST (spr-3 and spr-4)(Lakowski $\mathrm{et\ al.}$, 2003; Wen $\mathrm{et\ al.}$, 2000), and another gene is closely homologous to CoREST (spr-1) (Jarriault and Greenwald, 2002). To test the role of these genes in oxidative stress resistance, we placed adult worms on nematode growth medium supplemented with paraquat, a superoxide generator. C. elegans lines with mutations in spr-1, spr-3, and spr-4 all showed significantly reduced survival relative to wild-type controls (Figure 2.4a, Figure 2.11a). The spr-4(by105) mutant showed the greatest vulnerability. Furthermore, depletion of spr-4 by RNAi significantly reduced survival in wild-type worms after treatment with paraquat (Figure 2.11b). SPR-4 was expressed predominantly in neurons (Figure 2.11c), and was induced by oxidative stress (Figure 2.11d).

The increased sensitivity of the spr-4 mutant worms to oxidative stress was significantly reduced by transgenic expression of either wild-type SPR-4 or human REST (Figure 2.4a, b). To ascertain whether SPR-4 and REST directly modulate ROS levels,

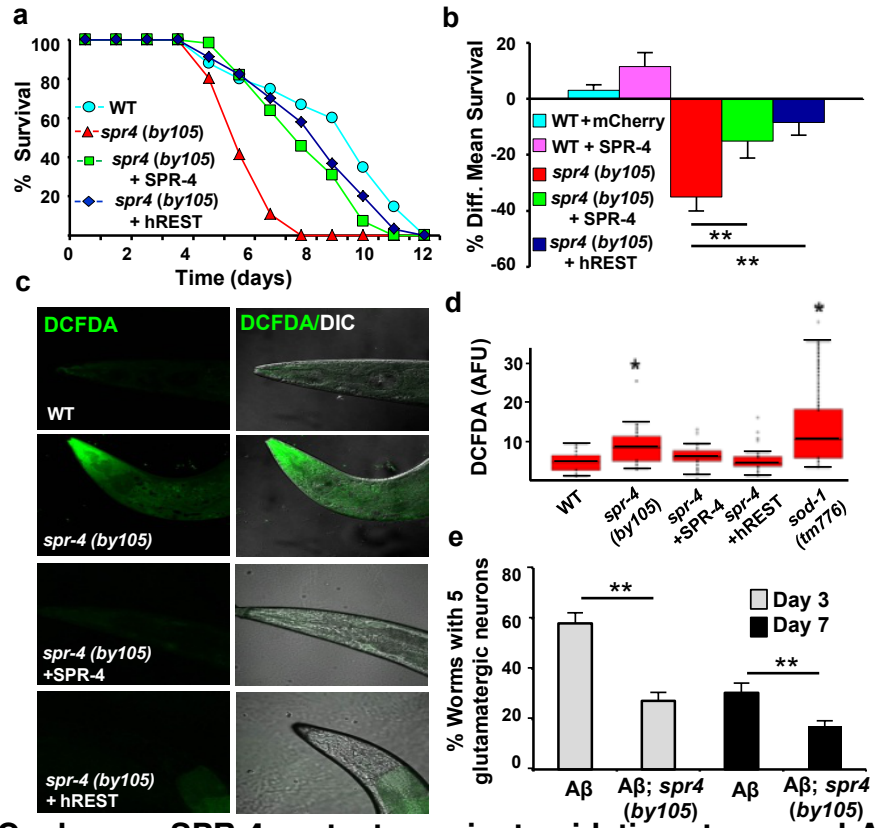

Figure 2.4: **C. elegans SPR-4 protects against oxidative stress and Aβ toxicity. A.** Spr-4(by105) worms incubated continuously with paraquat (5 mM) exhibit increased mortality rescued by wild-type SPR-4 or human REST. Shown is a representative experiment replicated three times. **B.** Quantitative analysis of survival in wild-type worms expressing mCherry or SPR-4 (WT+mCherry and WT+SPR-4), spr-4(by105) mutants, and spr-4(by105) mutants expressing SPR-4 or human REST [spr4(by105)+SPR4 and spr4(by105)+hREST]. Shown is the percent change in mean survival relative to wild-type. Values represent the mean + S.D., n=3 independent replicates of at least 30 animals per genotype; *P <0.05 relative to wild-type by the log-rank test. **C.** REST and SPR-4 reduce levels of reactive oxygen species (ROS). Shown are representative confocal images of paraquat-treated worms labeled with the ROS-sensitive dye DCFDA. Scale bar: 30 μm. **D.** Quantitation of ROS levels by DCFDA labeling. Horizontal bars indicate the median; boxed areas represent the second and third quartiles. *P <0.05 relative to wild-type by ANOVA with post-hoc Tukey test; n=30 worms. **E.** SPR-4 protects against Aβ neurotoxicity. Shown are Aβ worms (expressing a stably integrated Aβ1-42 transgene (Treusch et al., 2011)) and Aβ;spr4(by105) worms. Neuronal degeneration does not occur in WT worms or spr4(by105) mutants in the absence of the Aβ transgene. Values represent the % of worms that retain 5 glutamatergic tail neurons at the indicated age (day), and are the mean+S.D., n=3. *P <0.05 by unpaired t-test.

worms were labeled with the fluorescent ROS indicator 2',7'-dichlorodihydrofluorescein diacetate (DCFDA). Spr-4(by105) mutants treated with paraquat showed significantly elevated ROS levels relative to wild-type, which was reduced by transgenic expression of either wild-type SPR-4 or human REST (Figure 2.4c, d). To determine whether REST can substitute for SPR-4 as a transcriptional repressor, we assessed the expression of the presenilin gene hop-1, which is repressed by SPR-4. The expression of hop-1 was elevated in adult spr-4 mutants relative to wild-type worms, and was repressed by both wild-type SPR-4 and hREST (Figure 2.11e). These results suggest that human REST can functionally substitute for SPR-4 in C. elegans.

SPR-4 also modulated the neurotoxicity of Aβ in a C. elegans line that expresses Aβ42 in glutamatergic neurons and undergoes age-dependent neuronal loss (Treusch $\mathrm{et\ al.}$, 2011). When this Aβ-expressing line was crossed with the spr-4(by105) mutant, the resulting line expressed Aβ42 in an SPR-4 loss-of-function background and showed significantly accelerated neurodegeneration (Figure 2.4e). Thus, SPR-4 protects against both oxidative stress and Aβ toxicity, consistent with a general role in stress resistance.

Induction of REST by stress and Wnt signaling

To determine whether REST might be induced by oxidative and other forms of stress in the aging brain, we subjected primary human cortical neuronal cultures to a variety of stressors. Incubation with redox-active iron (Fe^{+2}), hydrogen peroxide, the glutathione synthesis inhibitor buthionine sulfoxide (BSO), or Aβ42 induced REST mRNA and protein and increased REST-RE1 site binding (Figure 2.12a-f). To determine whether secreted factors might contribute to REST induction, cortical neurons were incubated with H2O2 followed by removal of H2O2 and generation of conditioned medium. Addition of stress-related conditioned medium to nave neuronal cultures resulted in a marked induction of REST mRNA expression (Figure 2.12g). Thus, a variety of stressors induce REST expression, which is mediated at least in part through cell non-autonomous signaling.

To explore the role of cell non-autonomous signaling in the aging brain, we generated extracts of human PFC from young adult and aged samples and assessed their effects on SH-SY5Y cells. REST was robustly induced by extracts of aged human cortex, but minimally by extracts of young adult cortex (Figure 2.12h). Furthermore, extracts of AD cortex showed reduced REST-inducing activity relative to age-matched controls (Figure 2.12h). Since REST has been identified as a target of canonical Wnt-β-catenin signaling (Willert $\mathrm{et\ al.}$, 2002), we examined the role of this cell non-autonomous signaling pathway. Extracts of aged cortex and conditioned medium from stressed cells treated with H2O2, tunicamycin or wortmannin induced β-catenin in parallel with REST (Figure 2.12h, Figure 2.13a, b). Induction of REST and β-catenin was partially inhibited by the Wnt signaling antagonist Dickkopf (Figure 2.13a, b). REST was also induced by addition of purified Wnt-3a and Wnt-7a. Moreover, the GSK3-β inhibitors lithium chloride and Chiron 99021 that activate Wnt signaling induced REST, increased REST-RE1 site binding, and augmented nuclear translocation (Figure 2.13c-f). To assess Wnt signaling in the human brain, we measured nuclear β-catenin levels in the PFC of young adult and aged cases. Nuclear β-catenin was significantly elevated in aging PFC neurons and co-localized with REST (Figure 2.13g, h). These results suggest that Wnt-β-catenin signaling may contribute to the induction of REST in the aging brain.

Autophagy of REST in neurodegenerative disorders

In AD, loss of REST from the nucleus was often accompanied by localization to punctate cytoplasmic structures that were labeled with the autophagosome markers LC3, Atg 7 and Atg 12, but not the lysosomal markers LAMP1 and LAMP2 (Figure 2.14a). To determine if autophagy could alter the nuclear-cytoplasmic distribution of REST, autophagy was activated in SH-SY5Y cells by serum deprivation. This resulted in significantly reduced nuclear REST, which was reversed by treatment with 3-methyladenine (3-MA) or bafilomycin, inhibitors of autophagy (Figure 2.14b, c). Since activation of autophagy is characteristic of

many age-related neurodegenerative disorders, we asked whether REST is also depleted in other dementing diseases. Examination of cortical sections from patients with frontotemporal dementia (FTD) or dementia with Lewy bodies (DLB) showed marked depletion of nuclear REST (Figure 2.5a).

Induction of autophagy in neurodegenerative disorders has been associated with pathogenic misfolded proteins such as Aβ (Lipinski $\mathrm{et\ al.}$, 2010). In AD, many cortical and hippocampal neurons showed a striking co-localization of REST with Aβ in LC3-positive autophagosomes (Figure 2.5b). In contrast, REST did not colocalize with Aβ in amyloid plaques. Phosphorylated tau and TDP-43 have been implicated as abnormally folded pathogenic proteins in FTD, whereas α-synuclein has been implicated in DLB. Every case (8) of tau-positive FTD examined showed co-localization of REST with phosphorylated tau (PHF1) in LC3-positive autophagosomes (Figure 2.5b). Similarly, every case (6) of TDP-43-positive FTD showed co-localization of REST with TDP-43 and LC3 (Figure 2.5b). All ten cases of DLB examined showed partial co-localization of REST with α-synuclein in autophagosomes (Figure 2.5b). Thus, autophagy of REST, together with pathogenic misfolded proteins, may reduce nuclear translocation in AD and other neurodegenerative disorders.

REST is associated with cognitive preservation and longevity

A central question is whether loss of REST in AD contributes to cognitive decline. We explored this question by using measures of cognitive function derived from neuropsychiatric assessments performed longitudinally in the Religious Orders Study and the Rush Memory and Aging Project (Methods). Linear regression analysis showed that nuclear REST levels in prefrontal cortical neurons are positively correlated with a measure of global cognition, and separate measures of episodic, semantic and working memory with high levels of statistical significance (Figure 2.6a, Figure 2.15a). Similar results were obtained in pyramidal neurons in the hippocampal CA1 region. For both brain regions,

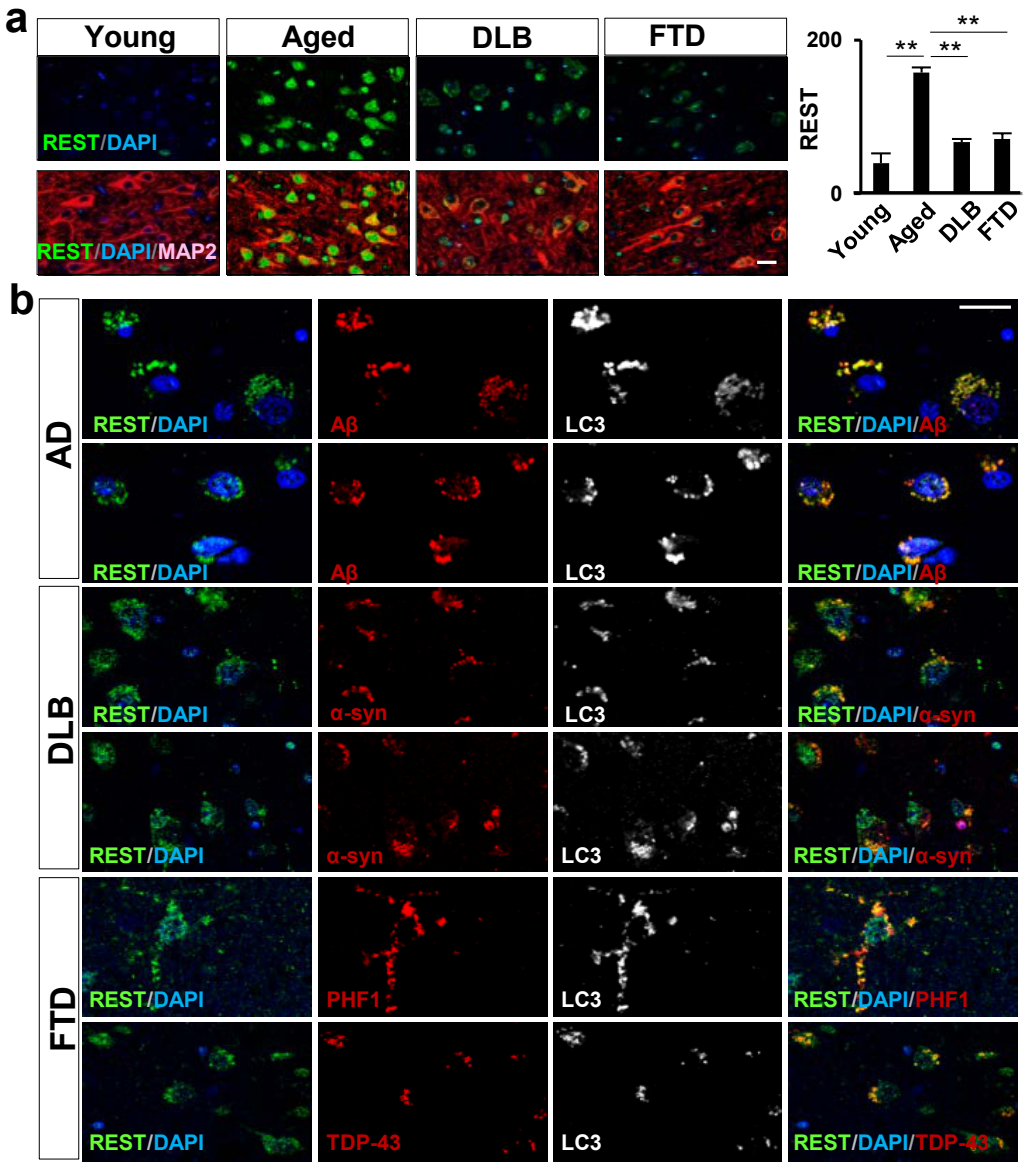

Figure 2.5: **REST, autophagy and proteostasis in AD, DLB and FTD. A.** Loss of nuclear REST in DLB and FTD. Left Panel: Immunofluorescence microscopy with labeling for REST (green), the neuronal marker MAP2 (red) and DNA (DAPI, blue). Right Panel: Quantitative analysis of immunfluorescence. Values represent the mean+S.E.M., Young, n=11; Aged, n=21; DLB, n=18; FTD, n=16. $^{**}P$ <0.001 by Students unpaired t-test. **B.** Co-localization of REST with disease-associated misfolded proteins in autophagosomes. Cortical sections were triple-labeled for REST, LC3, and either Aβ in AD, α-synuclein (α-syn) in DLB, or phosphorylated tau (PHF1) or TDP-43 in FTD. Two different representative cases are shown for each disease. Scale bars: 20 μm.

REST levels were most robustly correlated with episodic memory, which typically declines early in the course of AD. Elevated REST levels also predicted reduced AD neuropathology (Figure 2.6b, Figure 2.15b).

We then asked if elevated REST levels might confer resistance to AD pathology. Cases with NIA-Reagan and CERAD pathology scores indicative of pathologic AD, but with mild or no cognitive impairment, were compared to cases with pathologic AD together with severe cognitive impairment. Nuclear REST levels were significantly elevated in cognitively preserved cases relative to cognitively impaired cases, despite the fact that both groups met pathologic criteria for AD (Figure 2.6c). Thus, elevated REST levels are associated with cognitive preservation in individuals who meet pathologic criteria for AD.

Since REST is associated with stress resistance and preservation of cognitive function, we explored the relationship to human lifespan. Nuclear REST levels in PFC neurons showed a significant positive correlation with longevity (R=0.53; $P <$1e-4) (Figure 2.6d). This relationship remained significant after multivariate adjustment for cognitive test scores and indices of neuropathology. Furthermore, the expression of REST target genes showed a highly significant inverse correlation with longevity (Figure 2.8a). Examination of the neuroanatomical distribution of REST in individuals with extreme longevity showed marked induction in neurons of the PFC and hippocampus, but not in the Purkinje or granule cell neurons of the cerebellum (Figure 2.16a). Thus, REST expression in specific neuronal populations correlates with longevity.

We then asked if REST regulates genes that have been implicated in stress resistance and the aging process. In addition to repressing cell death genes, REST also promoted expression of the anti-apoptotic gene bcl-2, the antioxidants catalase and SOD1, and the FOXO transcription factor FOXO1a (Figure 2.9a, Figure 2.16b). As FOXO1a has been implicated in oxidative stress resistance (Tothova $\mathrm{et\ al.}$, 2007) and human longevity (Li $\mathrm{et\ al.}$, 2009), we assessed its regulation by REST at the protein level. REST knockdown by shRNA transduction in SH-SY5Y cells almost completely abolished FOXO1a expression,

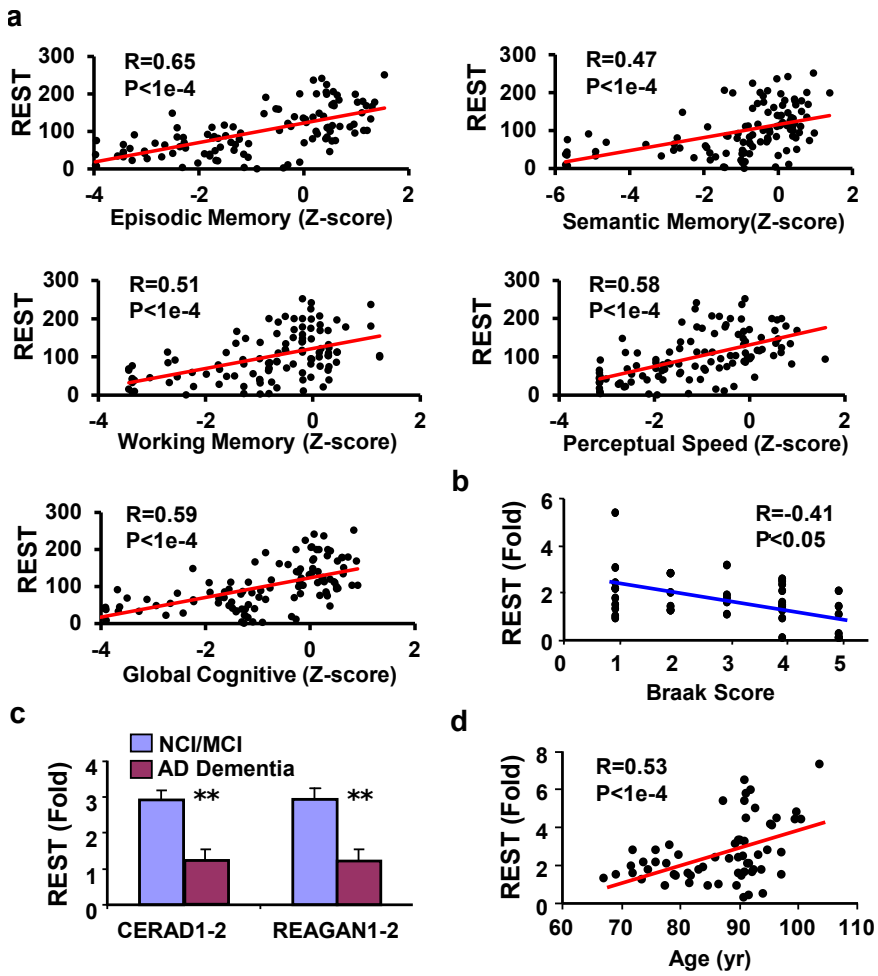

Figure 2.6: **Nuclear REST is positively correlated with cognitive function and longevity A.** Linear regression analysis of nuclear REST levels in PFC neurons and cognitive test scores. Nuclear REST was imaged by anti-REST immunofluorescence and quantified by Metamorph. Each point represents an individual case. n=111 cases (59 females, 52 males), age range 71-90 yrs. **B.** Nuclear REST levels are inversely correlated with Braak stage (extent of neurofibrillary tangle formation). **C.** Nuclear REST levels in PFC from cases with neuropathologic AD (moderate/frequent plaques by CERAD score and intermediate/high likelihood AD by NIA-Reagan criteria) that had mild or no cognitive impairment (NCI/MCI), or AD dementia. Values are the mean+S.E.M. *P <0.01 by Students unpaired t-test; NCI/MCI n=30, AD dementia n=21. **D.** Nuclear REST levels in aging neurons correlate positively with longevity. REST levels were quantified by FACS analysis of isolated PFC neuronal nuclei in 61 individuals without AD (age range 67-104 years).

which was reversed by an shRNA-resistant mREST vector (Figure 2.16c). Thus, REST may broadly confer stress resistance during aging.

Discussion

We have demonstrated a striking induction of the developmental transcriptional repressor REST in specific neuronal populations of the aging human brain together with epigenetic repression of REST target genes. REST has been investigated extensively as a repressor of neuronal genes during embryonic development, a function that persists in adult non-neuronal cells (Ballas and Mandel, 2005). Our findings suggest that REST additionally plays a role as a neuroprotective modulator, in part by repressing genes that promote cell death and the pathology of AD. Moreover, REST increases the expression of FOXO transcription factors that mediate oxidative stress resistance (Tothova $\mathrm{et\ al.}$, 2007), as well as the antioxidant enzymes catalase and SOD1, possibly through indirect mechanisms such as repression of micro RNAs. Consistent with these findings, REST confers oxidative stress resistance and protects against toxic insults associated with AD, including Aβ oligomers and tau phosphorylation. Furthermore, REST appears to be essential for maintaining neuronal viability in the normal aging cortex and hippocampus. This protective function is conserved in C.elegans. Previous ChIP-SACO (Otto $\mathrm{et\ al.}$, 2007) and ChIP-chip (Abrajano $\mathrm{et\ al.}$, 2009) studies also identified REST target genes involved in cell death. In addition, a recent study suggests that REST protects against the toxicity of 1-methyl-4-phenyl-1,2,3,6-tetrahydropyridine (MPTP), a model of Parkinsons disease (Yu $\mathrm{et\ al.}$, 2013). Thus, REST may coordinate a stress response that is broadly neuroprotective in the aging brain.

REST dysfunction may contribute to the pathogenesis of a number of different neurodegenerative disorders. In addition to AD, REST was also significantly depleted in frontotemporal dementia and dementia with Lewy bodies. In each of these disorders, REST was lost from the nucleus and appeared in autophagosomes together with patho-

logic misfolded proteins, including Aβ, phosphorylated tau, TDP-43 and α-synuclein. This may represent a common pathogenic mechanism that links altered proteostasis to aberrant gene expression.

Recent studies suggest that epigenetic regulation of chromatin may modulate the cognitive outcome of a variety of neuropathological states (Fischer $\mathrm{et\ al.}$, 2007; Gräff and Tsai, 2013; Ronan $\mathrm{et\ al.}$, 2013). It is intriguing that aging individuals who harbor substantial AD pathology do not appear to progress to dementia when neuronal REST levels are high. This raises the possibility that structural pathology, such as Aβ deposition and neurofibrillary tangles, may not be sufficient to cause dementia. Rather, failure of the brains stress response system may also be necessary, suggesting new possibilities for therapeutic intervention.

Acknowledgements

We thank members of the Yankner laboratory for suggestions and discussion, Monlan Yuan, Allison Harwick, Kelly Dakin and Gregory Klein for assistance, and Cheng Li and Dana Gabuzda for helpful discussion. We also acknowledge the Rush Alzheimer's Disease Center, the Brigham and Womens Hospital Brain Bank, the Massachusetts General Hospital ADRC Brain Bank, and the Kathleen Price Bryan Brain Bank at Duke University for providing tissue samples. This work was supported by an NIH Directors Pioneer Award (DP1OD006849) and NIH grants PO1AG27916 and RO1AG26651 to B.A.Y., RO1GM072551 to M.P.C., P30AG10161, R01AG15819 and R01AG17917 to D.A.B, and a grant from the Glenn Foundation for Medical Research to B.A.Y. J.Z. is a Molecular Biology of Neurodegeneration fellow at Harvard Medical School.

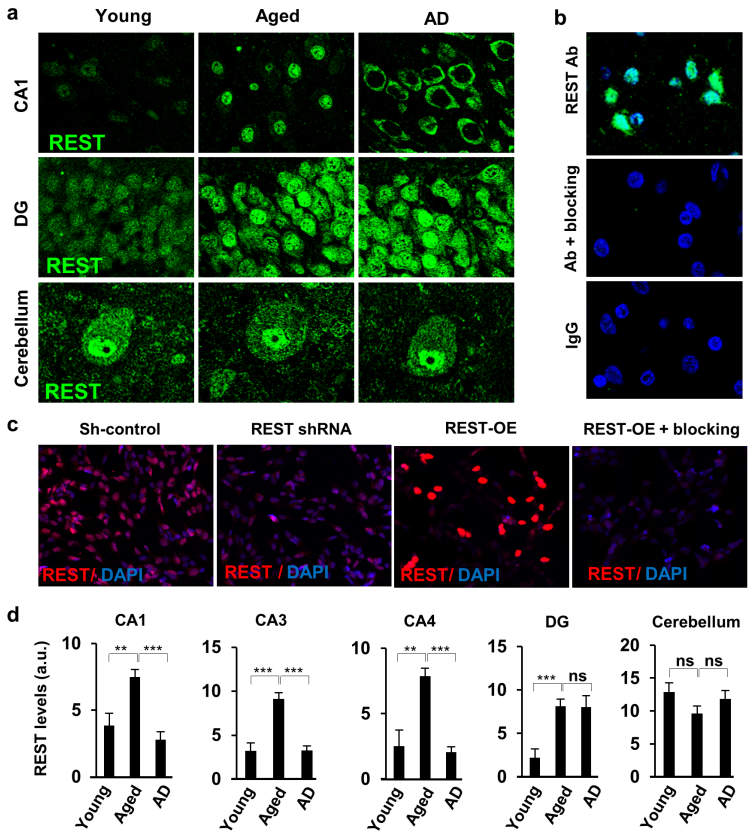

Figure 2.7: **Neuroanatomical distribution of REST induction in the aging human brain.** **A.** Representative confocal photomicrographs of hippocampal CA1 pyramidal neurons (upper panel), dentate gyrus granule neurons (middle panel, DG) and cerebellar Purkinje and granule cell neurons (lower panel), from young, aged or AD cases that were labeled for REST (green). Note the increased expression of REST in hippocampal CA1 pyramidal and dentate granule cell neurons in aged cases relative to young adult cases. Also note that nuclear REST is markedly reduced in AD in hippocampal CA1 neurons, but not in dentate granule cell or cerebellar neurons. **B.** Specificity of REST immunohistochemistry. Shown are sections of normal aged PFC labeled with anti-REST (Bethyl) (upper panel), anti-REST preincubated with a REST blocking peptide (middle panel), and non-specific IgG (lower panel). REST labeling is green; nuclear labeling with DAPI is blue. **C.** REST knockdown (REST shRNA) and overexpession (REST-OE) in SH-SY5Y cells confirm antibody specificity. Also shown is labeling with antibody preincubated with REST blocking peptide (REST-OE+blocking). REST knockdown and oeverexpression were confirmed by Western blotting (Extended Data Fig. 3b). **D.** Quantification of nuclear REST levels in hippocampal CA1, CA3, CA4 regions, in dentate gyrus granule cells (DG), and in cerebellar Purkinje cell neurons. REST is induced with age in CA1, CA3, CA4 and DG neurons, but not in cerebellar neurons. REST expression is reduced in AD in CA1, CA3, and CA4 neurons, but not in DG or cerebellar neurons. CA1: young n=11, aged n=30, AD n=33. CA3, CA4, DG and cerebellum: young n=8-9, aged n=7-8, AD= 9-10. Values are the mean +S.E.M., * P <0.05, ** P <0.01 and *** P <0.001 by Students unpaired t test. Scale bar: 25 μm.

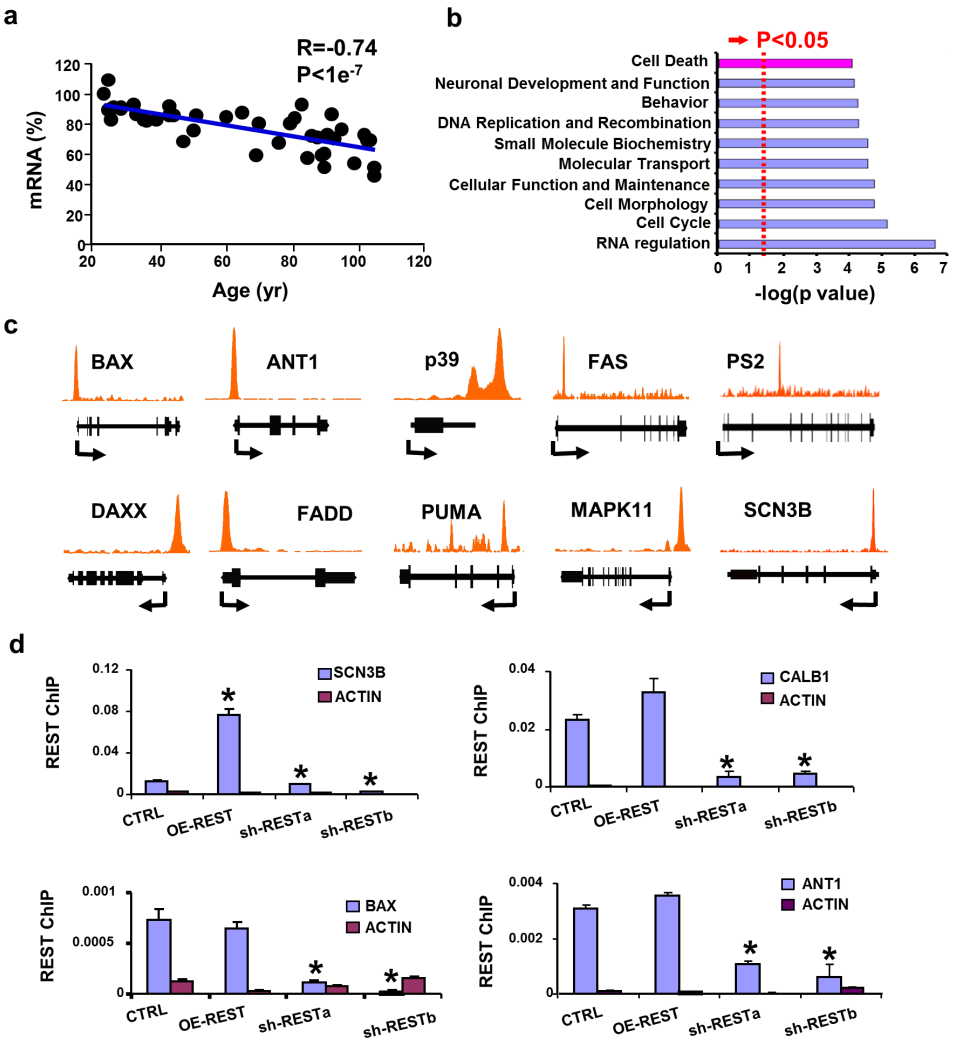

Figure 2.8: **ChIP-seq analysis of REST target genes shows enrichment for genes related to cell death and the pathology of AD. A.** Genes identified by REST ChIP-seq in SH-SY5Y cells are downregulated in the aging human PFC. Expression of age-regulated REST target genes identified by ChIP-seq shows a highly significant inverse correlation with age at death. For each case, a weighted expression index was derived for age-regulated target genes based on microarray analysis. These values were normalized to the youngest adult value (24 yrs; 100%). N=43, age range 24-106 yrs. **B.** Canonical pathways by Ingenuity IPA analysis of REST ChiP-seq targets. **C.** REST ChIP-seq binding peaks in genes related to cell death pathways and AD pathology. **D.** Confirmation of ChIP-seq targets by quantitative ChIP-PCR following REST overexpression (OE-REST) or REST knockdown (sh-RESTa and sh-RESTb) in SH-SY5Y cells. Shown is ChIP followed by real time PCR using primers that amplify REST binding sites identified by ChIP-seq. PCR amplification of a region of the actin promoter not proximal to a known RE1 site was used as a negative control. Values are normalized to the input control and represent the mean+S.E.M., n=3. *P <0.05 relative to control by Students unpaired t-test.

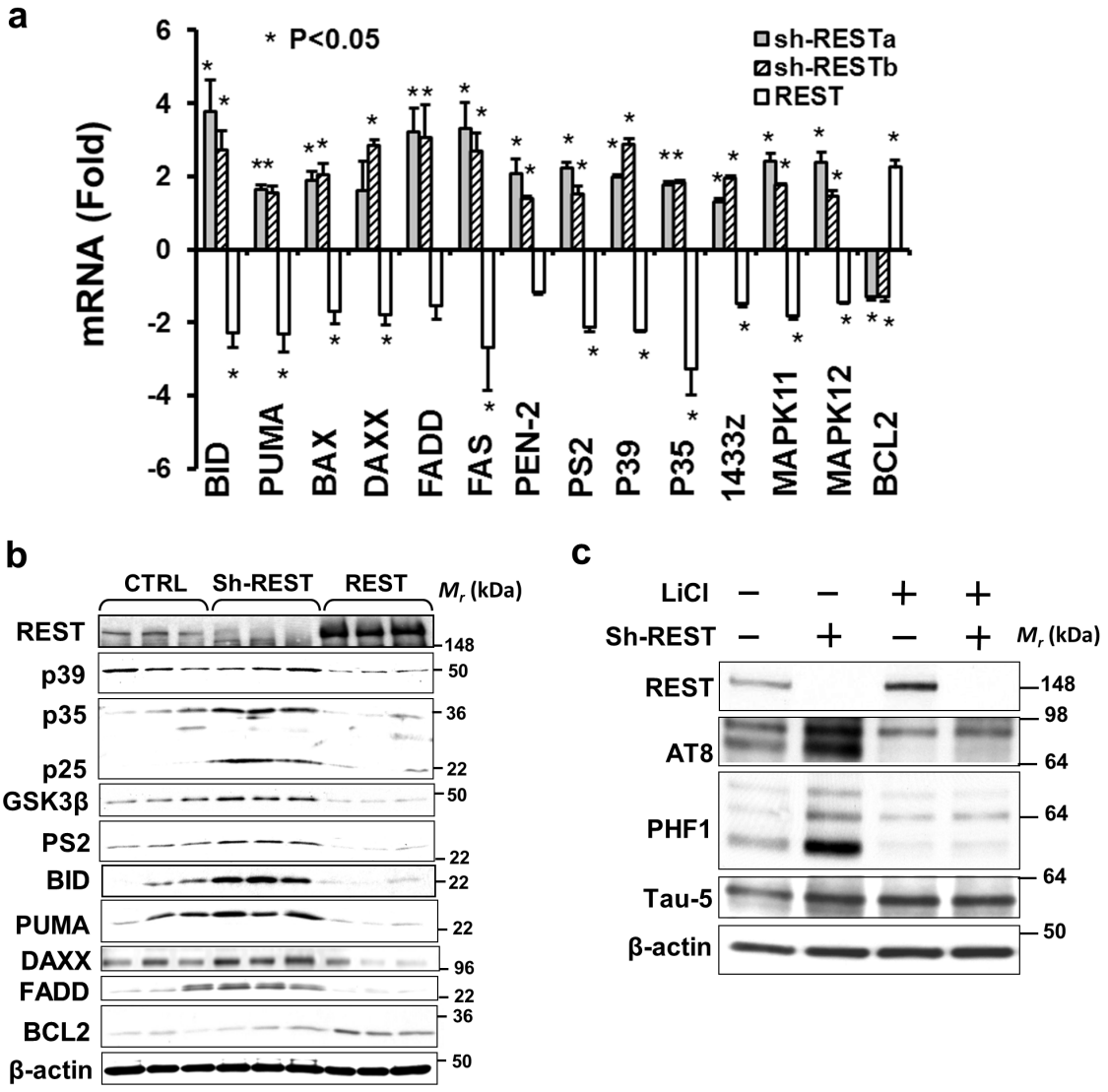

Figure 2.9: **REST regulates expression of genes related to cell death and the neuropathology of AD. A.** REST knockdown with either of two distinct shRNAs (sh-RESTa and sh-RESTb) significantly increase mRNA expression of ChIP-seq targets related to cell death and AD pathology, whereas REST overexpression (REST) represses gene expression. Values are the mean + S.D., n=3. *P <0.05 by Students unpaired t-test. **B.** Shown are Western blots of lysates from SH-SY5Y cells transduced with a control lentiviral vector (CTRL), or 3 separate REST shRNAs (sh-REST; each lane represents a different shRNA) or REST cDNA (REST) to knockdown or overexpress REST, respectively. **C.** REST knockdown (sh-REST) markedly induces phosho-tau epitopes (PHF-1 and AT8). Induction of these epitopes is blocked by lithium chloride (LiCl), an inhibitor of the tau kinase GSK3β.

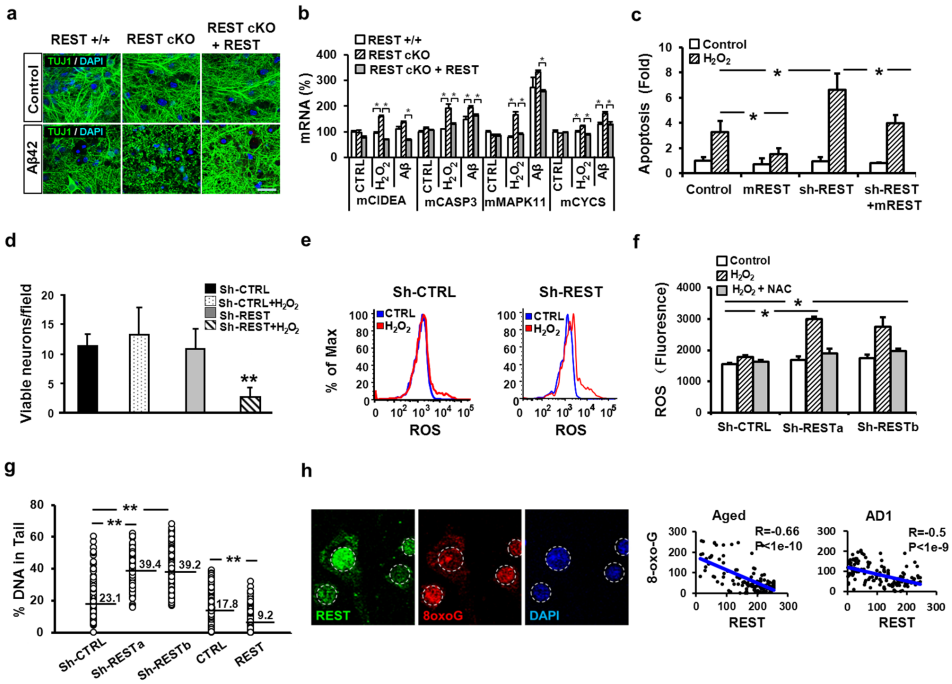

Figure 2.10: **REST protects against oxidative stress.** **A.** Cortical neuronal cultures from REST-deficient (REST cKO) mice show extensive neuritic degeneration relative to control cultures after incubation with 5 μM oligomeric Aβ42 for 24 hrs, which is prevented by lentiviral transduction of REST (REST cKO + REST). Neuritic processes are labeled with antibody TUJ1. Scale bar: 30 μm. **B.** Pro-apoptotic genes show increased mRNA expression in REST-deficient cortical neuronal cultures after treatment with hydrogen peroxide (50 μM H2O2, 3 hrs) or oligomeric Aβ42 (5 μM, 8 hrs). Values are the mean +S.E.M., n=4. $^{*}P$ <0.05 by t-test. **C.** REST knockdown potentiates hydrogen peroxide-induced apoptosis in SH-SY5Y cells. Cells were incubated with 800 μM H2O2 for 2 hrs, and apoptotic cells were quantified by FACS analysis of Annexin V-APC. Values represent fold change relative to the untreated control. **D.** REST knockdown (sh-REST) increases vulnerability to oxidative stress in cultured primary human cortical neurons treated with 100 μM H2O2 for 2 hrs relative to control cultures (Sh-CTRL). **E.** REST knockdown increases generation of reactive oxygen species (ROS). Shown are FACS profiles of a fluorescent ROS indicator (CellRox). Note right-ward shift (increased ROS) in H2O2-treated (600 μM, 2 hrs) SH-SY5Y cells (red) vs untreated controls (blue) following lentiviral transduction of REST shRNA (Sh-REST). **F.** Increased ROS levels in SH-SY5Y cells expressing either of two different REST shRNAs (sh-RESTa and sh-RESTb) is reversed by the antioxidant N-acetyl cysteine (NAC, 5 mM). **G.** REST protects against oxidative DNA damage. Shown is a measure of DNA fragmentation in the Comet Assay following treatment of SH-SY5Y cells with H2O2. Horizontal bars indicate the mean value. $^{**}P$ <0.0001 by the Mann-Whitney test; n=114-134. Values in b, c, d and f represent the mean + S.E.M, n=6-10, $^{*}P$ <0.05, $^{**}P$ <0.01 by t-test. **H.** Inverse correlation between oxidative DNA damage and nuclear REST levels in normal aging and early AD (AD1). Shown is double-labeling for REST and 8-oxoguanine (8oxoG) in hippocampal CA1 neurons.

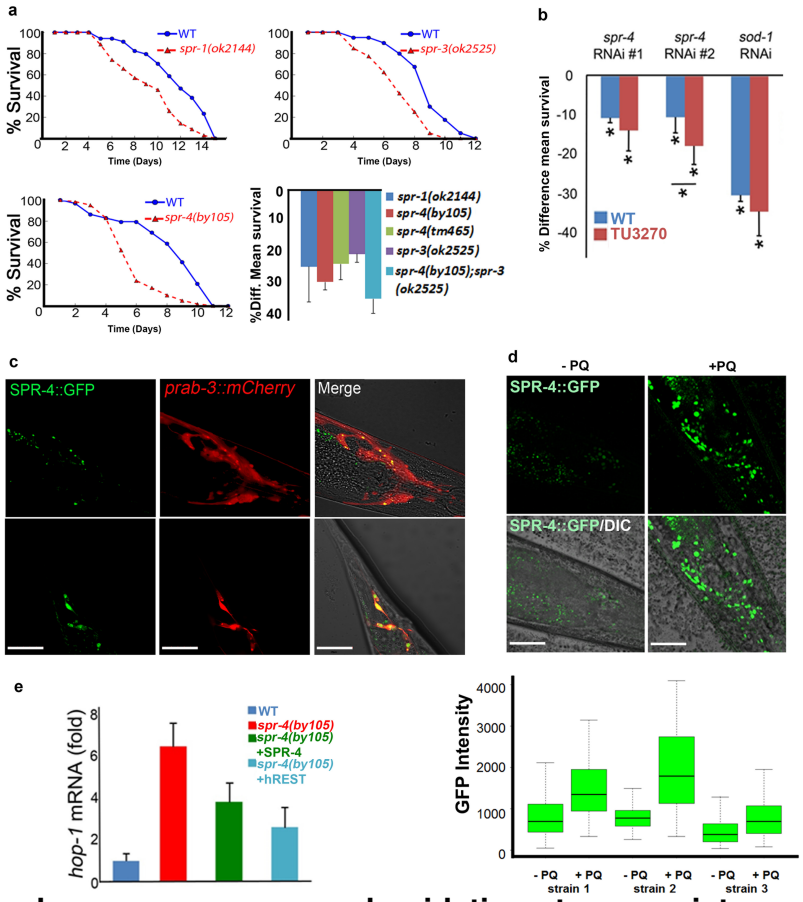

Figure 2.11: **C. elegans spr genes and oxidative stress resistance.** **A.** Worms were incubated with paraquat (5 mM). Shown are representative time courses of survival, and quantification of reduced mean lifespan relative to wild-type. Values represent the decrease in mean lifespan as % relative to wild-type and represent the mean + S.D., n=3. *P <0.05 by log-rank test. **B.** Worms were fed RNAi against the indicated genes and then transferred to plates seeded with standard OP50 bacteria and containing 5 mM paraquat. Shown is the percent decrease in mean survival relative to the empty vector control from 3 independent experiments. Values are the mean + S.D., n=3. *P <0.05 by log-rank test. **C.** A stably integrated spr-4-gfp construct under the control of the endogenous spr-4 promoter is expressed predominantly in neurons in adult worms, as indicated by co-localization with the neuronal marker prab-3::mCherry. Upper panels: pharyngeal ring neurons; lower panels: tail neurons. Scale bar: 20 μm. **D.** Treatment of adult worms with paraquat (+PQ) from day 1 to day 4 induces expression of spr-4-gfp. Untreated worms (-PQ). Upper panels show confocal imaging of a representative strain; the lower panel graph shows quantitative analysis of SPR4::GFP expression in 3 separate strains. Horizontal bars indicate the median; boxed areas represent the second and third quartiles. N=3 (15 worms each); ***P <0.001 by t-test. **E.** Expression of hop-1 mRNA was measured by qRT-PCR in 24-hour post L4 worms of the indicated genotypes. Transcript values were normalized to cdc-42. Values represent fold change relative to WT and represent the mean + S.D., n=3. *P <0.05 by t-test.

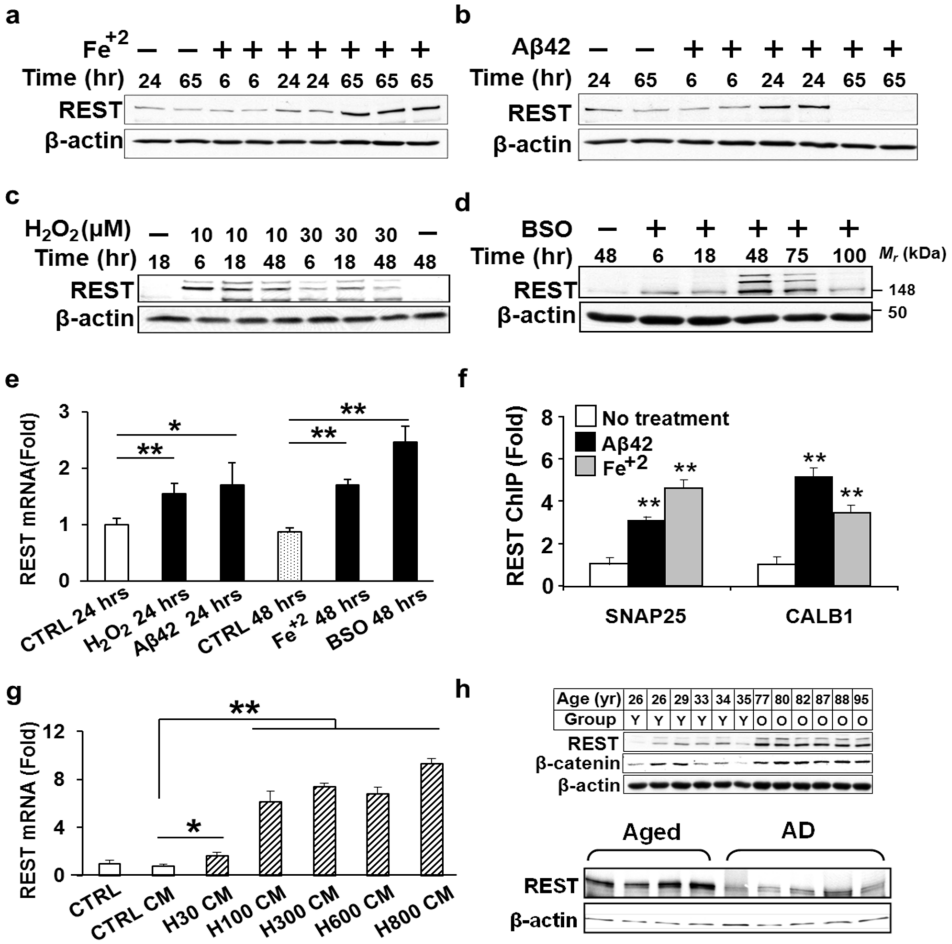

Figure 2.12: **Induction of REST by stress and cell non-autonomous signaling. A–D.** Redox-active Fe^{+2} (15 μM), Aβ42 (15 μM), H2O2 (indicated concentrations), and the glutathione synthesis inhibitor BSO (50 μM) increase REST protein levels in primary human cortical neuronal cultures. Shown are Western blots for REST and actin. **E.** REST mRNA levels determined by qRT-PCR. **F.** Treatment of human neurons with Fe^{+2} or Aβ42 increase REST-RE1 site binding in the SNAP25 and calbindin 1 genes as determined by ChIP-qPCR. **G.** REST mRNA levels measured by qRT-PCR after addition of conditioned medium from H2O2-treated (30 μM- H30, 100 μM-H100, 300 μM-H300, 600 μM- H600, 800 μM- H800) or control neuronal cultures (CTL-CM) to nave neurons. **H.** Extracts from aged human PFC (O) induce REST when added to SH-SY5Y cells. Much lower levels of induction are induced by extracts derived from young adult (Y) or AD cortex. Shown are Western blots for REST, β-catenin and β-actin. Values in e-g represent the mean+S.D., n=3. *P <0.05, **P <0.01 by Students unpaired t-test.

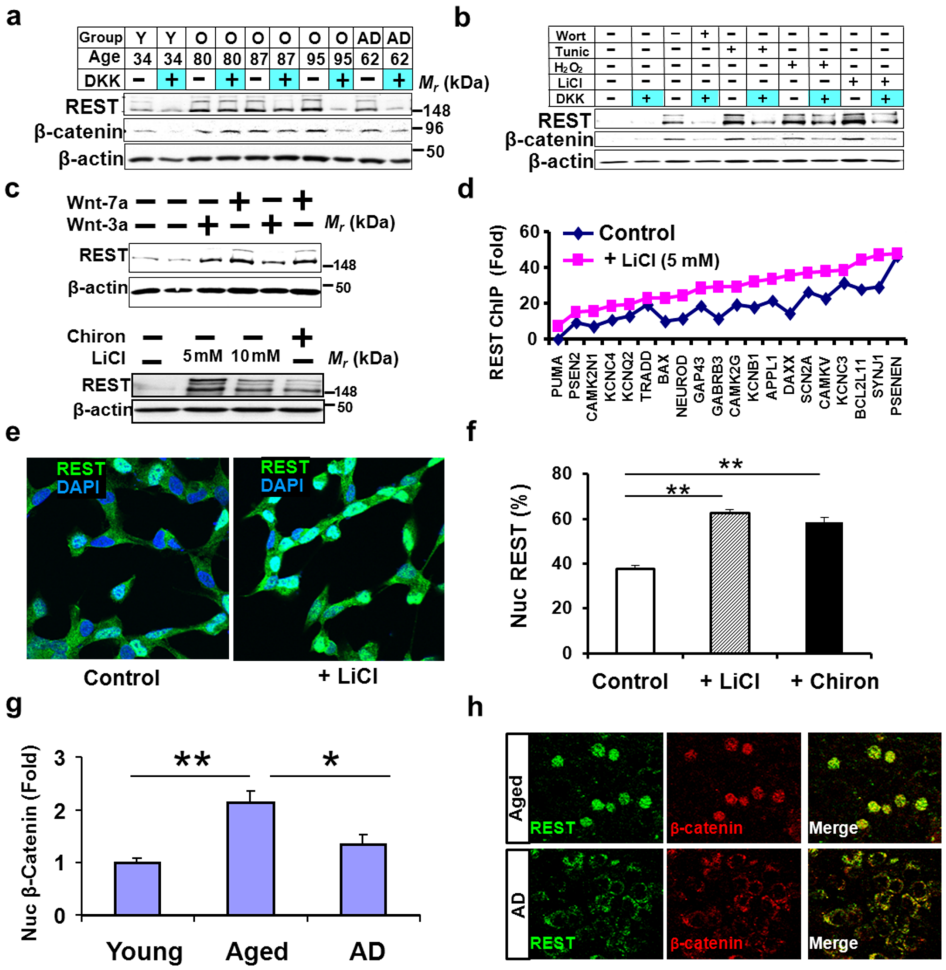

Figure 2.13: **Induction of REST by Wnt signaling. A.** Cell non-autonomous induction of REST by aged brain extracts is partially inhibited by the Wnt antagonist Dickkopf (DKK). Extracts were derived from young adult (Y), aged (O) or AD PFC and then incubated with SH-SY5Y cells in the absence (-) or presence (+) of DKK (250 ng/ml). **B.** Conditioned medium transferred from SH-SY5Y cells, treated with either wortmannin (2 μM), tunicamycin (2 μM), H2O2 (100 μM) or LiCl (10 mM), induce REST when added to nave cells, which is inhibited by DKK. **C.** REST levels are increased by treatment of SH-SY5Y cells with Wnt 3a or 7a (250 ng/ml, 16 hrs; upper Western blot), and by LiCl (5 or 10 mM, 6 hrs) or Chiron 99021 (20 nM, 6 hrs) (lower Western blot). **D.** REST ChIP-seq shows that the Wnt activator LiCl (5 mM) broadly increases REST binding to target genes. Shown are REST targets (P <1E-5) with REST-RE1 site binding within 10 kb of the transcription start site. **E–F.** SH-SY5Y cells incubated with LiCl (10 mM, 24 hrs) or Chiron 99021 (100 nM, 24 hrs) exhibit increased nuclear REST. (e). Quantitative analysis of % REST-positive nuclei (f). **G.** Increased nuclear β-catenin in the PFC in normal aging, and reduced levels in AD. Shown is FACS analysis of neuronal nuclei isolated from PFC. Values are the mean+S.E.M. *P <0.05, **P <0.01 by Students unpaired t-test. Young, n=13; Aged, n=18; AD, n=10. **H.** Co-localization of REST and β-catenin in the nucleus of aging neurons in the PFC. Aged and AD cases were double-labeled for REST (green) and β-catenin (red).

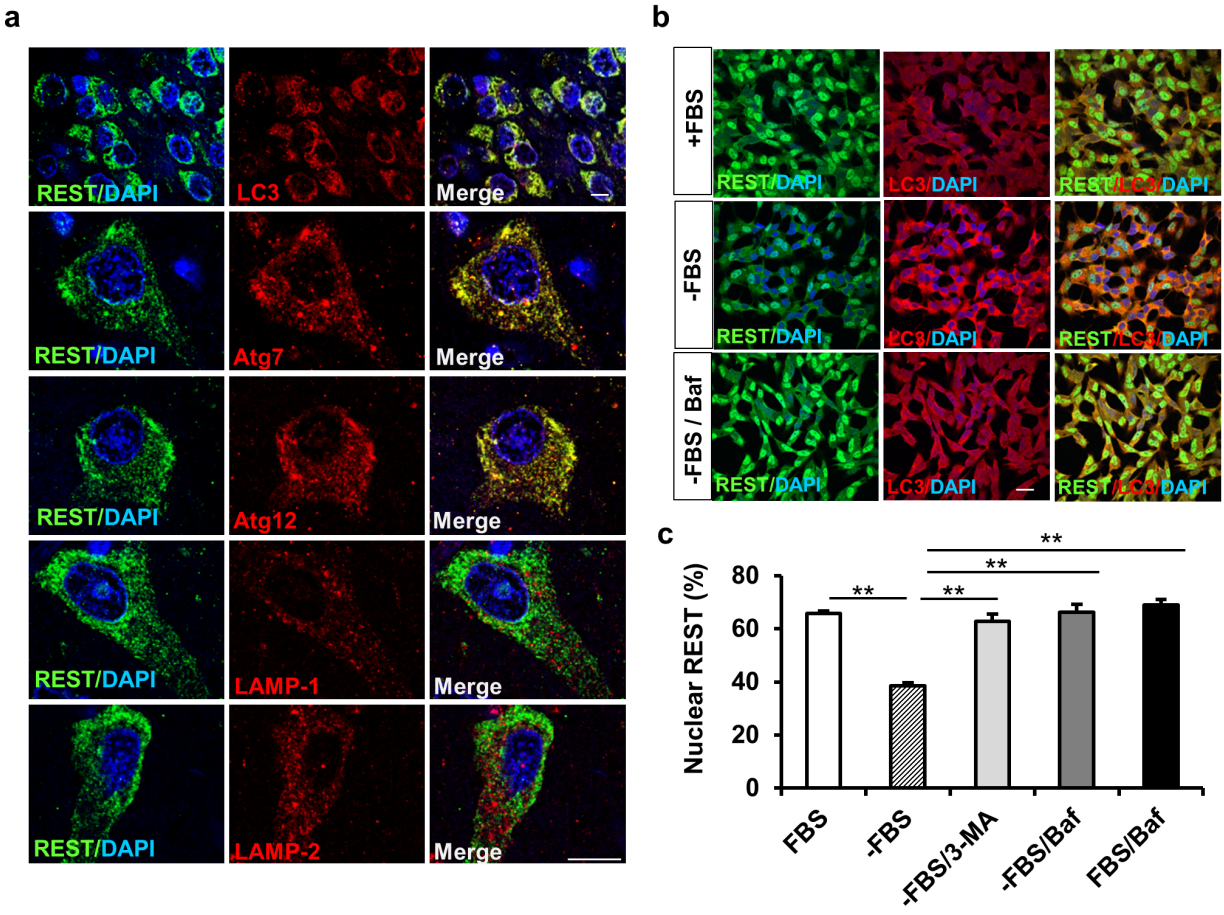

Figure 2.14: **Autophagy and REST. A.** REST is distributed in a vesicular punctate distribution in the cytoplasm of cortical neurons in AD. Confocal immunofluorescence microscopy shows co-localization of REST with the autophagosome markers LC3, Atg 7 and Atg 12, but not with the lysosomal markers LAMP-1 or LAMP-2. **B.** Nuclear REST levels are reduced by activation of autophagy. SH-SY5Y cells were subject to serum withdrawal (-FBS, 40 hrs) to induce autophagy and maintained in Opti-MEM to preserve cell viability. Note that serum withdrawal results in depletion of nuclear REST (loss of green labeling that overlaps with the blue DAPI nuclear stain), which is restored by bafilomycin (-FBS/Baf). **C.** The autophagy inhibitors 3-methyladenine (3-MA, 5 mM) and bafilomycin (Baf, 150 nM) increase nuclear REST. Values represent % of cells positive for nuclear REST, and represent the mean + S.E.M., n=3; $^{**}P < 0.01$ by Students t-test. Scale bars: 15 μm.

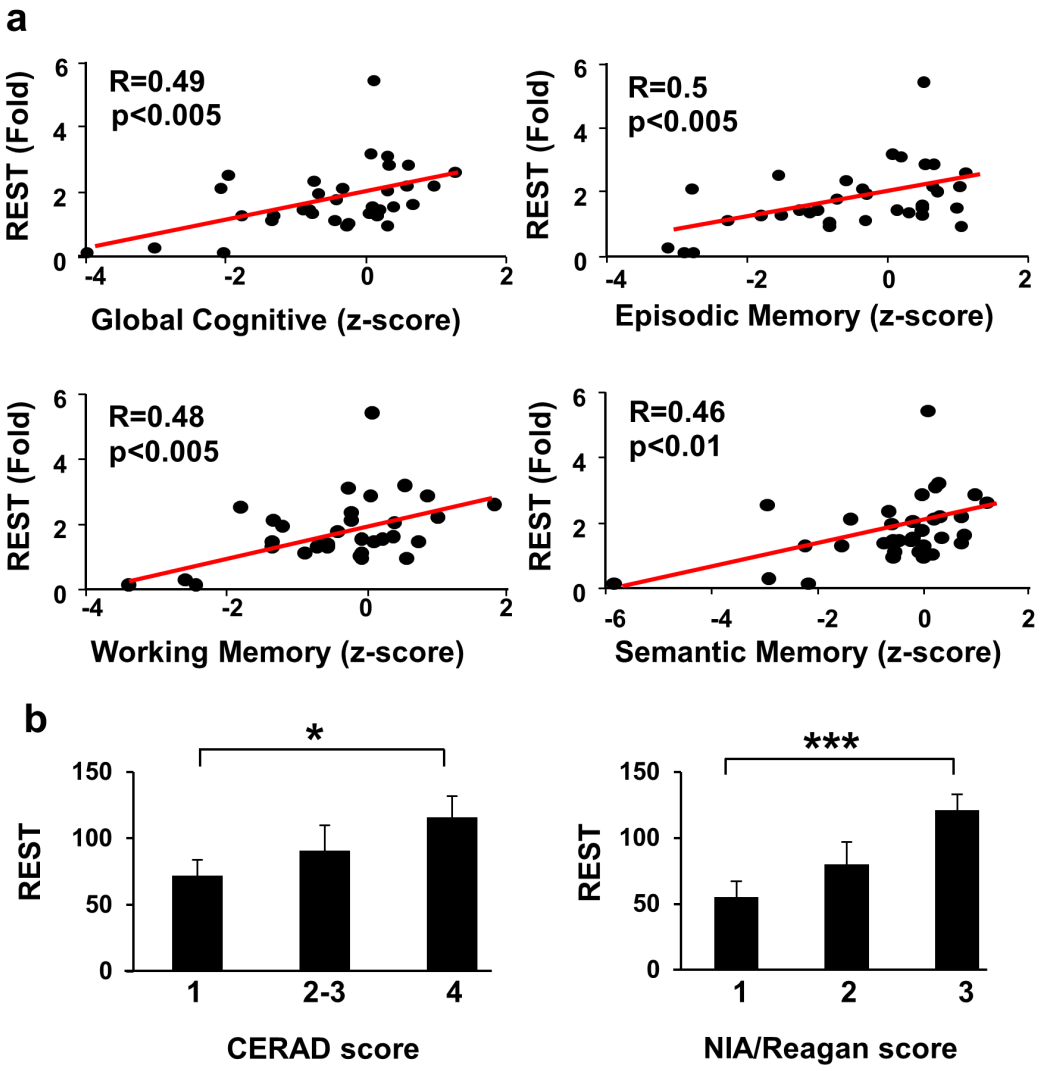

Figure 2.15: **Neuronal REST levels are positively correlated with cognitive function and inversely correlated with AD neuropathology. A.** Linear regression analysis shows that nuclear REST levels in PFC neurons are positively correlated with measures of cognition function. REST levels were determined by FACS analysis of isolated PFC neuronal nuclei. Each point represents an individual case, and is normalized as fold change relative to the mean value of the young adult group. N=37, age range 67-90 yrs. **B.** Nuclear REST levels in prefrontal cortical neurons decrease with increasing AD pathology. Shown are CERAD (1-frequent plaques, 2-3 sparse/moderate plaques, 4-no plaques) and NIA-Reagan scores (composite index of neuritic plaques and neurofibrillary tangles; 1-high likelihood of AD, 2-intermediate likelihood, 3-low likelihood). Values are the mean+S.E.M. CERAD 1, n=20; 2-3, n=11; 4, n=9; NIA-Reagan 1, n=12; 2, n=14; 3, n=14. * P <0.05, *** P <0.001.

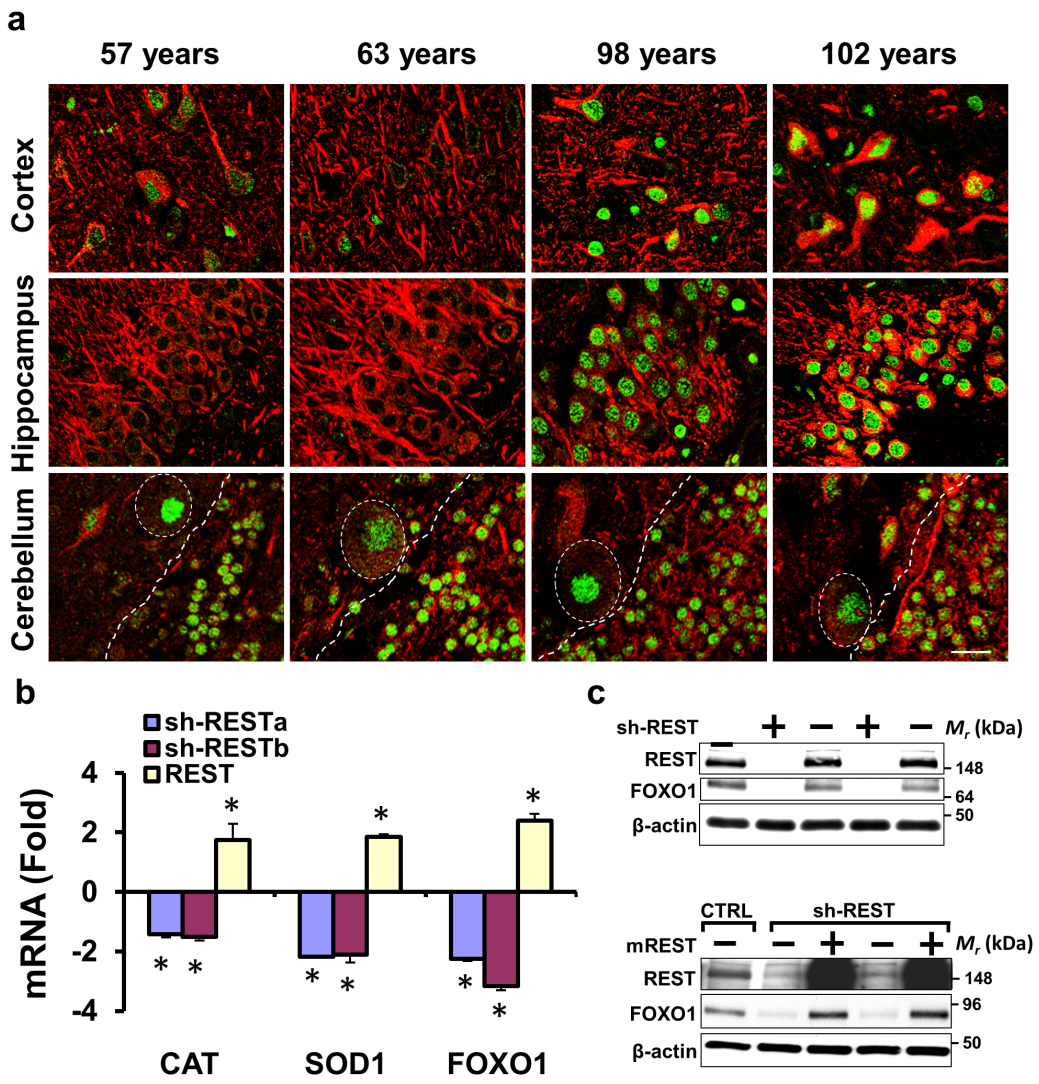

Figure 2.16: **REST, longevity and stress resistance.** **A.** Prefrontal cortical (upper panel), hippocampal CA1 (middle panel) and cerebellar (lower panel) sections of individuals ranging in age from 57-102 years were double-labeled for REST (green) and the neuronal marker MAP2 (red). Cases with extreme longevity (98, 102 years) are associated with marked induction of REST in prefrontal cortical and hippocampal CA1 neurons, but not in cerebellar Purkinje cell (ovals) or granule cell neurons (to the right of the dashed line). Scale bar: 20 μm. **B.** REST increases the expression of genes associated with stress resistance and longevity. Shown are fold changes in mRNA levels for catalase (CAT), superoxide dismutase (SOD1) and FOXO1a (FOXO1) following REST knockdown (sh-RESTa or sh-RESTb) or overexpression (REST). Values represent the mean+S.D., *P <0.05 by Students unpaired t-test. n=3. **C.** FOXO1a expression is dependent on REST. Western blotting of SH-SY5Y cells shows that shRNA-mediated REST knockdown (sh-REST +) almost completely abolishes FOXO1a protein, which is prevented by shRNA-resistant mREST.

Methods

Brain sample procurement. Postmortem human brain material was procured in accordance with institutional guidelines governed by approved protocols. Tissue samples were procured from the Rush University Medical Center, the University of Maryland, Duke University, the Brigham and Womens Hospital, and the Massachusetts General Hospital. Tissue samples from Rush University Medical Center were derived from participants in the Religious Order Study (ROS) and Rush Memory and Aging Project (MAP) at the Rush Alzheimers Disease Center, which are longitudinal, clinical-pathologic studies of aging, cognitive decline and AD (Bennett $\mathrm{et\ al.}$, 2012$\mathrm{a,b}$). Study participants agreed to comprehensive annual clinical and neuropsychological evaluation and brain donation at death.

Cognitive function tests and neuropathology. Measures of cognitive function were derived from neuropsychiatric assessments performed longitudinally in the Religious Orders Study and the Rush Memory and Aging Project (MAP). This population includes individuals across the cognitive spectrum, ranging from normal to AD. The last cognitive test scores obtained during life were related to nuclear REST levels in postmortem prefrontal cortical brain samples by quantitative immunocytochemistry (111 cases, Figure 2.6a) and FACS analysis of isolated neuronal nuclei (37 additional cases, Figure 2.15a). Nineteen cognitive function tests were employed in the present study, including a summary score of all 19 tests used as a measure of global cognition, and separate measures of episodic, semantic, and working memory, and perceptual speed. The follow-up rate exceeds 95% and the autopsy rate exceeds 90%.

Autopsy cases in the Religious Orders and MAP studies underwent a uniform structured neuropathologic evaluation of AD, including assignment of Braak (measure of number and distribution of neurofibrillary tangles), CERAD (Aβ plaque pathology), and NIA-Reagan (composite measure of neurofibrillary tangles and amyloid plaques) scores. The clinical

diagnoses of AD and MCI have been described in detail and pathologic confirmation of AD approaches 90% (Bennett et al., 2006, 2002; Schneider et al., 2009). Frozen brain tissue specimens used in this study were from the prefrontal cortical grey matter (Brodmann area 9, 10) and were snap-frozen and stored at -140℃. Paraffin-embedded brain samples were also obtained from the Massachusetts General Hospital and Brigham and Womens Hospital. These samples included young adult cases without neurological abnormalities, aged subjects that did not carry a diagnosis of AD or another neurodegenerative disease and showed neuropathological findings within the normal range for age, and cases of AD, FTD and DLB with clinical histories of these disorders and subsequent pathological confirmation. A total of 239 brain specimens with an age range from 19-106 years were utilized for molecular and histopathological analyses. The characteristics of these cases are provided in Supplementary Information Table 1.

Microarray analysis. Gene expression profiling using microarrays has been described previously (Loerch et al., 2008). Human brain samples with tissue pH$<$6.5 or postmortem interval (PMI) $>$20 hrs were excluded. Prefrontal cortical samples with acceptable parameters of RNA quality were hybridized to Affymetrix Human Genome U133plus 2.0 arrays, which were then scanned and expression data extracted using Affymetrix Microarray Suite Software. The Probe-level Linear Model (PLM) platform was used for analysis of microarray data (Bolstad et al., 2003). A subset of the data was additionally analyzed using RMA or dCHIP platforms yielding similar results. Significance Analysis of Microarrays (SAM) software (Tusher et al., 2001) was used for 2-group comparisons of young adult versus aged with the following criteria for identifying age-related expression changes: 1000 permutations and median false discovery rate (FDR) $\leq$ 0.01. Age-regulated genes that overlap with RE1-containing genes (Bruce et al., 2004) were visualized by hierarchical clustering using dChip software (Li and Wong, 2001) (Fig. 1a). The display range used was 1.5 (a value greater than 1.5 standard deviations above the mean is pure red, below is pure blue, and equal to the mean is white).

Real time RT-PCR and PCR. Primers were designed for 90-300-base-pair (bp) segments to span exon boundaries if possible. PCR or real-time PCR were run for 30-40 cycles (Appendix Table 2.2). The purity of both PCR and RT-PCR products were determined by single peak melting curves, and further confirmed by agarose gel electrophoresis. To extract RNA, the Cells-to-cDNA II Kit was used for cells, and Trizol (Invitrogen) was used for tissue samples. All RNAs were DNase treated. A standard curve for each primer pair was generated by serial dilution of a pool of titrated RNA or DNA. Beta-actin or GAPDH were used as internal controls. Positive control primers for the REST ChIP assay, SYN- RE1 primers, were from Millipore (Cat#17-641), and the C-terminal truncated splice variant, REST4 primers: RES4-F: 5-GTGAGCGAGTATCACTGGAGG-3, REST4-R: 5-CCATCTAGATCACACTCTGAATG-3 have been reported previously (Yu $\mathrm{et\ al.}$, 2009). Other primers used in this study were designed using Primer3.0, and are listed in Supplementary Table 2.

Western blotting. Tissues were homogenized, whereas cells were directly lysed using RIPA-DOC buffer supplemented with protease and phosphatase inhibitors (Complete and Phosphostop, Roche). A sonication step was performed prior to centrifugation at 10,000 rpm for 10 min at 4C. The supernatant was removed and the protein concentration determined (BioRad protein assay). SDS sample buffer containing beta mercaptoethanol was added and 20 μg protein was loaded per lane and resolved by 4-20% Mini-PROTEAN TGX precast gels (Biorad). Western blots were quantified by densitometry using the ImageJ software. The antibodies used for this study are described in Supplementary Table 3.

Immunohistochemical analysis of human brain. Antibodies used in this study are described in Appendix Table 2.3, The following REST-specific antibodies were used for immunolabeling studies: (i) a rabbit polyclonal IgG recognizing a region between residues 1050 and the C-terminus (residue 1097) of REST (Bethyl laboratories, IHC-00141); (ii) a rabbit polyclonal IgG recognizing a region between residues 801 and the C-terminus

(residue 1097) of REST (Millipore, 07-579); (iii) a goat polyclonal IgG recognizing an internal region of REST (Santa Cruz, sc-15118); and (iv) rabbit monoclonal IgG recognizing a region near the N-terminus of REST (Abcam, ab28018).

Immunohistochemical/immunofluorescence analysis using paraffin-embedded brain sections was performed in the following regions: (1) the prefrontal cortex (Broadmann areas 9, 10 and 47, (2) the hippocampal formation, including the CA1, CA3, CA4 and DG sectors, and (3) the cerebellum. Analysis of REST expression by immunohistochemistry using paraffin-embedded sections obtained from the various sources indicated above led to very similar conclusions.

Paraffin-embedded tissue sections were first deparaffinized in xylene, then rehydrated with decreasing concentrations of ethanol and placed in water. Sections then underwent antigen retrieval using either citrate buffer (Vectorlabs, USA) or the Diva decloaker (BioCare, USA). For diaminobenzidine (DAB) labeling, sections were additionally treated with 3% hydrogen peroxide for 30 minutes. They were then washed and blocked with 3% BSA, 0.2% Triton X-100 in PBS for 1 hr at room temperature. Primary antibodies were diluted in 2% BSA, 0.1% Triton in PBS. Following overnight incubations, sections were washed three times with PBS. Secondary antibodies, diluted in 2% BSA, 0.1% Triton in PBS were either biotin-coupled (1:200, Vector Labs, USA) or coupled to Alexa fluorophores (1:300, Invitrogen). For DAB labeling, sections were additionally incubated with a pre-formed biotin-avidin-HRP complex (1:100, VectorLabs). For immunofluorescence labeling, sections were also incubated with 1% Sudan Black in 70% ethanol, for 10 minutes, to suppress lipofuscin autofluorescence. Following washes in PBS, sections were mounted and imaged using confocal or bright field microscopy. To quantify immunofluorescence or DAB labeling, images were randomly acquired in selected brain regions. Antigen-expressing areas within each neuron and in cellular compartments (such as the nucleus) were selected using the Metamorph image analysis system and the average signal intensity measured. Values were corrected by subtracting the average slide background intensity (measured outside

of cells). Between 50 -100 neurons were analyzed for each case. The investigator was blinded to sample origin or diagnosis.

For linear regression analysis of the relationship between nuclear REST and the levels of (i) proteins encoded by REST targets (BAX, DAXX, PSEN2, calbindin and somatostatin) (Figure 2.2c, d); (ii) the activating histone mark H3K9Ac (Figure 2.2c, d), or (iii) oxidative DNA damage (8-oxoguanine) (Figure 2.10h), we performed double-label immunofluorescence for REST (Bethyl antibody) and each individual protein or marker. Multiple 40x pictures were acquired (at various locations) within the prefrontal cortex displaying pyramidal neurons using an Olympus Fluoview Confocal Microscope. For cases displaying a majority of pyramidal neurons with very high (or very low) nuclear REST levels, fields were also included that displayed lower (or higher, respectively) REST levels, to test for potential correlations between REST and each target. Antigen-expressing areas within each neuron (such as the nucleus or the cytoplasm) were selected using the Metamorph image analysis system and the average signal intensity was measured. Values were corrected by subtracting the average slide background intensity (measured outside of cells). Between 25 and 75 pyramidal neurons were quantified for each case for linear regression.

Image acquisition. Images were acquired using an Olympus Fluoview confocal microscope, or using a bright field microscope coupled to a CCD camera (Diagnostic Instruments, Inc.). No image processing was performed on the acquired images, with the exception of (i) Fig. 3c (the H&E image) and (ii) Fig, 5b (the DAPI channel in DLB and FTD panels), which were contrasted to allow better visualization of cell nuclei.

Fluorescence-activated cell sorting (FACS). Antibodies against nuclear proteins, as well as isotype-matched control IgGs, were preconjugated to Allophycocyanin (APC) using lightning-link APC conjugation kit (Innova Biosciences). The monoclonal antibody against NeuN coupled to Alexa-Fluor 488 (Millipore, MAB 477X) was used for neuron-specific labeling. The antibodies and reagents used in this study are listed in Supplementary

Table 3. Approximately 1-2 μg of antibody was added to 1×10^6 nuclei/ml and incubated at 4C for 12 hrs with gentle rocking in the dark. Labeled nuclei were washed twice by centrifugation and filtered to remove clumps before performing FACS. The DNA binding dyes DAPI or propidium iodide were used for gating of nuclei. Aggregate discrimination was achieved based on the height, area and width parameters for FSC and SSC. The purity and identity of isolated neuronal nuclei was further confirmed by microscopy and epigenetic analysis. For each antibody, the geometric mean value of single-nuclei events that is above the matched nonspecific IgG control was determined. An average of 10,000 events was acquired for FACS analysis. For ChIP assays, 1×10^6 FACS-sorted neuronal nuclei were collected by centrifugation.

Chromatin immunoprecipitation (ChIP) and nuclear isolation. The ChIP assay protocol has been described previously (Lu $\mathrm{et\ al.}$, 2004). Cells or tissue homogenates were cross-linked using 1% formaldehyde (37% solution, sigma) at room temperature for 10min. Then the reaction was then stopped by adding glycine (1.25M, 10X) and washed twice by centrifugation. The cell pellet was dissolved in SDS lysis buffer (1% SDS, 10mM EDTA and 50mM Tris-HCl, pH 8.1). The genomic DNA was sheared into 300-1000bp by sonication (Bioruptor), followed by centrifugation. The supernatant was removed, diluted with ChIP dilution buffer (0.01%SDS, 1.1% TritonX-100, 1.2mM EDTA, 167mM NaCl, 16.7mM Tris-HCl, pH 8.1), and pre-cleared with Protein A Sephorose beads (Invitrogen) before adding antibody-conjugated beads. 5% of the sheared DNA was used as input control. After incubation with rocking at 4C for 12 hrs, chromatin bound beads were washed twice with low salt wash buffer (0.1% SDS.1% Triton X-100, 2mM EDTA, 150mM NaCl, 20mM Tris-HCl, pH 8.1), once with high salt wash buffer (0.1% SDS, 1% Triton X-100, 2mM EDTA, 500mM NaCl, 20mM Tris-HCl, pH 8.1), once with LiCl wash buffer (0.25M LiCl, 1% NP-40, 1% deoxycholic acid, 1mM EDTA, 10mM Tris-HCl, pH 8.1), and twice with TE buffer (1mM EDTA, 10mM Tris-HCl pH 8.1). The beads were then incubated with elution buffer (1% SDS, 0.1M NaHCO3), followed by de-cross-linking at 65 C for 5 hrs. The

eluted preparation was then treated with RNase A and proteinase K followed by isolation of DNA using the Qiagen PCR purification kit. For ChIP-PCR (Figure 2.1f, Figure 2.2a; Figure 2.8d, Figure 2.12f), primers were directed to binding sites identified by ChIP-seq analysis of SH-SY5Y cells.

The isolation of nuclei from human brain tissue was performed using a protocol adapted from previously described methods (Siegmund $\mathrm{et\ al.}$, 2007; Spalding $\mathrm{et\ al.}$, 2005). Briefly, 0.5 g of frozen tissue was dounce-homogenized in 10 ml of NF1 hypotonic buffer (0.4% Triton X100, 0.3 M Sucrose, 5 mM MgCl2, 0.1 mM EGTA, 1mM DTT, 10 mM Tris-HCl pH 8.0, supplemented with Complete protease inhibitors from Roche) on ice, incubated for 30min, and then dounce-homogenized with 30 additional strokes. The homogenates were then centrifuged in a swinging-bucket rotor at 1000 rpm for 10 min at 4C. The pellet was washed once with rocking at 4C for 0.5 hr, and then resuspended in NF1 buffer. Crude nuclei were carefully layered onto a cushion of 5 ml sucrose solution [1.2 M (40%) sucrose, 3 mM MgCl2, 1 mM DTT, 10 mM Tris-HCl, ph 8.0], and centrifuged at 5000 rpm for 30 min at 4C. The isolated nuclear preparation was resuspended in 1 ml NF2 buffer (0.1 M Sucrose, 5 mM MgCl2, 0.1 mM EDTA, 1% BSA, 10 mM Tris-HCl, pH 8.0), filtered with a 40 μm strainer (BD Falcon), and the number of nuclei was quantified after DAPI labeling, and then diluted to a concentration of 1×10^6 nuclei/ml. For FACS-ChIP assays, 1g of brain tissue was dounce-homogenized in 10 ml PBS with protease inhibitors (Complete, Roche) using pestle A, fixed with 1% formaldehyde for 10 min at room temperature, and then washed twice with NF1 buffer by centrifugation and gentle resuspension. The preparation was then treated as described above for brain tissue samples that did not undergo fixation.

ChIP sequencing. For ChIP-seq analysis, 10x15 cm2 dishes of SH-SY5Y cells at 80% confluence were incubated in the absence or presence of 5 mM LiCl (to induce REST expression) in SH-SY5Y cell culture medium (see Cell cultures below) for 12 hrs. ChIP was performed as described above, except that genomic DNA was sheared to 150-300 bp fragments confirmed by agarose gel electrophoresis. For normalization and analysis of

enrichment, input controls for each sample were sequenced. ChIP-DNA (2 ng) was used for library preparation followed by deep sequencing at the High Throughput Sequencing Facility of the University of North Carolina. Approximately 30 million ChIP-seq reads with read length of 36 were aligned to the hg18 genome assembly using ELAND with the default parameters. Sequence reads within REST binding sites were identified from ChIP-seq data using the latest version of MACS (Zhang et al., 2008) algorithm (1.4) with the default parameters. Genes that harbor REST binding sites within 10 kb of transcription start sites with at least 3-fold enrichment relative to the input control, statistical q-value$<$0.01 and P-value$<$1E-5 were considered as putative REST targets. Binding sites showed the canonical RE1 motif (Schoenherr and Anderson, 1995), as well as previously identified noncanonical REST-binding motifs (Johnson et al., 2007; Otto et al., 2007) (Appendix Table 2.4a, 2.4b). Fishers exact test was used to assess the statistical significance of the overlap between REST targets and genes that are age-regulated in the human prefrontal cortex.

REST-deficient mice. Animal housing and experimental procedures were approved by the Institutional Animal Care and Use Committees of Harvard Medical School. Mice carrying floxed alleles of REST flanking exon 2 were described previously (Mao et al., 2011). These mice were crossed to Nestin-Cre transgenic mice (Jackson laboratory; strain No. 003771) to achieve REST conditional inactivation in the nervous system. The Nes-Cre transgene is in the C57BL/6J background, and the $REST^{lx/lx}$ alleles were in a hybrid C57BL/6J and 129Sv/Ev background. The resulting Nestin-Cre:$REST^{lx/lx}$ conditional knockout mice (hybrid C57BL/6J and 129Sv/Ev background), referred to as REST cKO, were born at expected Mendelian ratios, were viable and fertile, and did not display any visible alterations. The control group included $REST^{lx/lx}$ and Nes-Cre mice. Mouse genotyping by PCR was performed using the following primers to amplify a region in the REST gene flanking exon 2: re08 (5CATGCGAGTACTGCCATACCCAAC-3), re09 (5GTGATGGGGCAGTCTTCTGGAGG3), and re11 (5 GGGCACACCTTTAATCCTAGCTTC3); this allowed the identification of WT (220 bp), floxed (264 bp) or recombined (375 bp)

REST alleles (Mao et al., 2011). The experimental groups included both male and female mice. The REST cKO and REST$^{+/+}$ control groups were composed of littermate mice (same genetic background). Mice were identified by eartag numbers, and were randomly selected for histological processing (perfusion, brain dissection, etc.). The investigator was blind to age and genotype.

Immunohistochemical and histological analysis of mouse brain. Mice were anesthetized with isofulorane and carbon dioxide and then perfused with cold PBS buffer for 20 minutes. Brains were rapidly removed and placed in 4% PFA overnight. They were then processed for paraffin embedding, according to standard procedures. TUNEL labeling was performed following manufacturer's instructions. For quantification of neuronal density, randomly selected areas within the hippocampus or the cortex, and at various depths within these structures, were imaged at 20x magnification. The number of cells (using either H&E or NeuN labeling) was determined using the Metamorph image analysis software and was then divided by the area occupied by these cells. The investigator was blind to the genotype.

Cell culture. REST cKO embryos and littermate controls were used to establish primary cortical and hippocampal cultures as described previously (Lorenzo et al., 2000). Each embryo was individually genotyped by PCR. Moreover, PCR analysis of DNA isolated from primary E16 embryonic neurons confirmed the excision of the REST floxed allele by Cre, in contrast to DNA derived from embryo tails. qRT-PCR was performed on the corresponding neuronal cultures or brain samples for genotype confirmation (RT-PCR: Forward primer: 5-CTTTGTCCTTACTCAAGCTCTC-3 Reverse primer: 5-TTCCTGAGACTCGTTTTCAGCC-3 Product size is 2034 bp). Embryonic cultures from E16 fetuses were plated on either coverslips or culture dishes that were pre-coated with both poly-D-lysine (Beckton-Dickinson) and laminin, and maintained in serum-free neurobasal medium containing B27 supplements and glutamax. Hippocampal cultures (7 DIV) or cortical cultures (14 DIV) were treated with either oligomeric Aβ42 for 24 hrs or H2O2 for 5 hrs. Oligomeric Aβ was

prepared as described previously (Busciglio and Yankner, 1995) and confirmed by SDS gel electrophoresis with and without boiling. Neuronal differentiation was comparable in REST cKO and control cultures after 1-2 weeks, as indicated by immunofluorescence labeling with antibody Tuj1 (MAB1637, Millipore), and Western blotting for the neuronal differentiation marker NeuN (MAB377, Millipore).

The SH-SY5Y neural cell line was maintained in Dulbecco's Modified Eagle Medium (DMEM) with 4.5 mg/L D-glucose, 2 mM L-glutamine, 1 mM sodium pyruvate, 100 U/mL penicillin, 100 μg/mL streptomycin (all from Invitrogen), supplemented with 10% fetal bovine serum. To induce autophagy, SH-SY5Y cells were maintained in serum-free Opti-MEM medium (Invitrogen) for 24 hrs, and then treated with inhibitors (5 mM 3-methyladenine or 150 nM bafilomycin) or maintained in Opti-MEM without inhibitors for an additional 16 hrs prior to fixation and imaging. The cells did not show morphological changes or evidence of reduced viability under these conditions. Human cortical neuronal cultures (HCNC) were established as previously described (Busciglio and Yankner, 1995), and were maintained in neurobasal media with 2 mM L-glutamine and B27 supplements (Invitrogen). Mature HCNCs (14 DIV) were used for experiments. B27 supplements without added antioxidants were used for oxidative stress-related experiments.

Assessment of cell viability and apoptosis. Cell viability was assessed using a chromogenic assay that involves the biological reduction by viable cells of the tetrazolium compound 3-(4,5-dimethylthiazol-2-yl)-5-(3-carboxymethoxyphenyl)-2-(4-sulfophenyl)-2H-tetrazolium (MTS). Cells were seeded in either 48- or 96-well plates and treated at 80% confluence. After adding MTS to culture medium and incubating for 2 hrs in the dark at 37C, absorbance was measured at 490 nm against a blank control with a plate reader. For detection of apoptotic cells, cells were incubated with Annexin V, Allophycocyanin Conjugate (APC Annexin V, Invitrogen) for 15 mins in 1x binding buffer (10 mM HEPES pH7.4, 0.14 M NaCl, 2.5 mM CaCl2). Cells were washed twice by centrifugation and resuspension and analyzed immediately by FACS. Analysis of reactive oxygen species

(ROS). ROS levels were measured using the cell-permeable fluorescent indicator CellROX Deep Red (#C10422, Invitrogen) with detection by FACS. SH-SY5Y cells were incubated in the absence or presence of hydrogen peroxide for 1 hr, which was removed followed by centrifugation and resuspension twice. The cells were then incubated with the CellROX Deep Red reagent for 30 mins at 37C, placed on ice and then analyzed by FACS.

Immunocytochemical analysis of cultured cells. Cells plated on laminin/polylysine-coated coverslips were fixed by incubation with 4% (v/v) paraformaldehyde in PBS for 30 minutes at room temperature, followed by three washes in PBS, and then permeabilized with 0.1% Triton X-100 in PBS for 15 minutes at room temperature. After 3 additional washes in PBS, cells were blocked with 10% goat serum in PBS for 1 hour at room temperature. Primary antibodies were diluted to the appropriate concentration using 10% goat serum, and incubated overnight at 4C. Cells were then washed 3 times in 1% goat serum in PBS for 10 minutes before adding fluorophore-conjugated secondary antibodies for 2 hours at room temperature. Fluorophore labeled cells were then washed in 1% goat serum in PBS for 3x10 minutes, and then mounted using Prolong Gold mounting medium with DAPI and anti-fade reagent (Invitrogen). To score endogenous nuclear REST in SH-SY5Ycells, Pearson correlations between DAPI and REST were generated from 200-300 cells from multiple coverslips using confocal analysis software. A threshold of $R > 0.6$ was used to indicate positive nuclear localization.

Single cell gel electrophoresis (comet assay). SH-SY5Y cells were treated with 100 μM hydrogen peroxide for 20 min at 4C and then suspended in PBS containing 1 mM EDTA on ice. The alkaline comet assay was then performed using the CometAssay HT kit (Trevigen) according to the manufacturer's protocol. The percentage of DNA in the comet tail was measured in 114-132 cells for each sample using CometScore image analysis software (TriTek).

Generation of cell-conditioned medium and cortical extracts. For conditioned medium transfer experiments (Figure 2.12g,h and Figure 2.13a, b), cells were incubated

with stress-inducing agents, followed by removal of the medium and 2 changes of fresh medium prior to the final addition of conditioning medium. After a 6 hr incubation period, the medium was removed and centrifuged twice to remove suspended cells or debris. The medium was then transferred to a new well containing nave cells. After a 10 hr incubation period, the treated cells were harvested and analyzed. To generate extracts of human prefrontal cortex, 200 mg cortical grey matter tissue samples were gently homogenized on ice using a dounce A pestle in 2 ml of cell culture medium supplemented with protease inhibitors (Complete, Roche). Brain extracts were cleared by sequential centrifugation and resuspension (2x1000rpm, 2x5000rpm and 14,000xrpm spin, each for 10 min at 40C). The tissue extracts were normalized to the DNA concentration of the starting material, and added to cultured SH-SY5Y cells at 25% of total medium volume.

Generation of recombinant lentiviruses. Viral particles were generated in HEK293T cells by co-transfection of transfer vectors, packaging plasmid (pRSV-REV and pMDLg) and envelope plasmid (pCMV-VSVG) using Lipofectamine 2000 (Invitrogen). Cells were cultured for 2 days and the medium was collected, centrifuged at 1000 rpm for 5 min, and passed through a 0.45 μm low protein binding filter (VWR). Viruses were then centrifuged at 25,000 rpm for 2 hrs at 4C (Beckman SW28) and then resuspended in 200 μl of PBS. Viruses were titered by infecting SH-SY5Y cells at serial dilution. The percentage of transduced cells, identified by EGFP fluorescence, was measured by flow cytometry 72 hrs post-infection. Cells that express REST-IRS-GFP were sorted into low, middle and high expression populations based on GFP intensity, and the corresponding REST levels were determined by qRT-PCR.

C. elegans strains. The N2 Bristol strain was used as the wild-type background for these studies. C. elegans strains were cultured at 20C under standard conditions (Brenner, 1974). The following mutations and chromosome rearrangements were used: LGI: spr-4(by105) (Lakowski $\mathrm{et\ al.}$, 2003), spr-4(tm465) (this study), daf-16(mu86) (Lin $\mathrm{et\ al.}$, 1997), hT2[bli-4(e937) qIs48] (I;III); LGII: sod-1(tm776) (Van Raamsdonk and Hekimi, 2009); LGV:

spr-1(ok2144); and LGX: spr-3(ok2525) (this study). All strains, except for spr-4(tm465), were provided by the Caenorhabditis Genetics Center (CGC), which is funded by the NIH Office of Research Infrastructure Programs (P40 OD010440). Strains obtained from external sources which had been outcrossed previously were outcrossed to our N2 strains twice. Worms which had not been outcrossed previously were outcrossed six times.

C. elegans RNAi. RNAi feeding experiments were performed at 200C. HT115 bacterial clones from a C. elegans RNAi feeding library (Geneservice) were used for spr-4 (C09H6.1), sod-1 (C15F1.7), and sod-2 (F10D11.1). Control RNAi was performed by feeding HT115 bacteria carrying the empty pL440 vector. Clones were sequence validated and knockdown was confirmed by semi-quantitative RT-PCR. The TU3270 (uIs57 [Punc-119::sid-1+ Punc-119::YFP+Pmec-6::mec-6]) strain was also used to assess neuronal loss-of-function (Calixto $\mathrm{et\ al.}$, 2010).

C. elegans microinjection and transgenic strains. Transgenic C. elegans lines were generated by microinjecting the relevant constructs into the gonads of the indicated strains. Prab-3::mCherry (pGH8, Addgene: 19359) was used as a coinjection marker labeling neurons. Three independent lines that demonstrated reliable transmission of the marker were propagated as described above for each experiment. Transgene expression was verified by qRT-PCR (see below), utilizing primers that spanned exon junctions for spr-4 or hREST, normalized for possible DNA carryover by utilizing two pairs of primers to the ampicillin resistance gene (present in all plasmids) and a specific site in pD152.79 (see table below for primer sequences). The spr-4 transgene was overexpressed by 18-24-fold relative to endogenous spr-4 expression in wild-type worms. The hREST transgene was expressed at levels comparable to the cdc-42 housekeeping gene.

To analyze RNA from transgenic lines, 100 Prab-3::mCherry positive worms (24 hours post-L4) of each strain (including controls) were placed into 1.5 ml M9 buffer. Worms were washed once in M9, pelleted by centrifugation, resuspended in 200 μl Trizol, vortexed for 2 minutes and flash frozen in liquid nitrogen. Worms were then freeze-cracked by thawing

in a 37C water bath and re-freezing in liquid nitrogen. This was repeated 2 more times. After the final thaw, 100 μl of Trizol was added and the tubes were maintained at room temperature for 5 minutes. RNA was then extracted with 140 μl of chloroform, precipitated with an equal volume of 70% ethanol and transferred to an RNeasy spin column (Qiagen) and purified. Quantitative RT-PCR was performed directly from isolated RNA, using 1ng of RNA and the Qiagen One Step qPCR mix. All reactions were performed in triplicate.

Analysis of Aβ toxicity in C. elegans. The UA198 Aβ-expressing strain (baIn34 [Peat-4::Abeta42, Pmyo-2::mCherry]; adIs1240[Peat-4::GFP]) was provided by the Caldwell lab (Treusch $\mathrm{et\ al.}$, 2011). This strain was crossed to wild-type males, and the resulting male progeny were crossed to spr-4(by105) homozygotes. Single F1 progeny bearing both fluorescent markers were each placed on individual plates (singled) and the subsequent F2 generation was singled and genotyped for spr-4. Homozygous spr-4(by105) mutants were then singled for several generations to ensure homozygosity of the transgenes before analysis. To assess toxicity of the Aβ42 transgene, worms were synchronized by transferring 8-10 young adults (24 hours post-L4) to a fresh plate, and allowing them to lay eggs for 12-14 hours. The adults were then removed and eggs were allowed to hatch at 200C. Worms were then aged by transferring adults to fresh, seeded plates every other day. At days 3 and 7 of adulthood, approximately 25-40 worms were immobilized with sodium azide on 2% agarose pads on slides. Confocal z-sections covering the entire depth of the worms were taken on an Olympus Fluoview Confocal Microscope using the 488 laser and a GFP filter. The image files were then assigned to randomly named folders to blind the scoring of the number of tail neurons per worm. Control and mutant worms were always hatched, grown, aged and imaged in parallel, and the assay was repeated three times. Statistical significance was assessed by paired t-test on both the distribution of neuronal number and the mean percent of the population without neurodegeneration.

SPR-4 localization and induction by paraquat. To create SPR-4::GFP transgenic animals, unc-119(ed3) worms were bombarded with a cosmid that had been subjected

to recombineering to introduce a GFP cassette onto the last exon of spr-4, creating a C-terminal fusion. Wild-type moving worms were isolated and singled. GFP signal was examined by confocal microscopy and worms with a bright, reproducible, and stable fluorescence were propagated. As described for the stress assay, worms were then transferred to plates containing either 5 mM paraquat and 100 μg/ml fluorodeoxyuridine (FUdR) or FUdR alone. On day four of treatment, worms were mounted on 2% agarose pads with sodium azide, and imaged by confocal microscopy at 60x magnification with a 1.5x digital zoom and 488 laser and GFP filter. Z-stacks were taken throughout the head and tail regions of the worms, and fluorescence intensity of the punctate GFP signal was analyzed in ImageJ. To assess statistical significance, a paired t-test between control and treated fluorescence intensity distributions was performed. Images were taken for at least 15 worms for each condition and each strain was analyzed in an independent paraquat treatment. For localization, SPR-4::GFP transgenic animals were mated to wild type males carrying the Prab-3::mCherry extrachromosomal array, and images were taken by confocal microscopy.

ROS detection in C. elegans. To measure ROS levels, 100 4-day old adult worms, grown as described for the paraquat survival assays, were transferred to eppendorf tubes containing 1.5 ml of M9 buffer, washed once in M9, and then stained for 1 hour in 500 μl of M9 containing 25 μM 2',7'-dichlorodihydrofluorescein diacetate (DCFDA, Life Sciences/Invitrogen) while rotating in the dark. Worms were then washed once with M9, and transferred to 1.5% agarose pads on glass slides, covered, and immediately imaged within 1 hour of washing out the DCFDA. Imaging was performed on an Olympus Fluoview Confocal Microscope using the 488 laser and GFP filter. At least 15 images were taken per genotype per replicate. Images were analyzed in ImageJ, where average intensity of the head region above the terminal pharyngeal bulb was scored and plotted using the boxplot function in R.

REST cDNA constructs and shRNAs. The pHAGE-CMV-Flag-hREST-IRES-ZsGreen

and pHAGE-CMV-ZsGreen plasmids were generously provided by Peter Mulligan (Mulligan et al., 2008; Westbrook et al., 2008). The cDNA for wild type mouse REST/NRSF (mREST) in the pCS2+MT vector (Shimojo and Hersh, 2006) was amplified by high fidelity PCR with BamH I and EcoR I restriction sites at 5' and 3' ends, respectively. The PCR amplicon was digested with BamH I and EcoR I followed by gel purification and ligation into the FUGW lentiviral vector driven by the human ubiquitin C gene promoter (Lois et al., 2002), and sequence verified. To generate the nuclear translocation-defective mutant $\triangle$REST (Figure 2.3a, b), a nuclear localization signal (amino acids 515-525) (Shimojo, 2006) and the fifth zinc finger motif (amino acids 294-324) (Shimojo, 2006) were deleted by high fidelity PCR using primers listed in Supplementary Table 2. The restriction site Xba I replaces amino acids 515-525 and adds two new amino acids Ser-Arg. The restriction site Nhe I replaces amino acids 294-324 and adds two new amino acids Ala-Ser.

Short-hairpin RNAs against human REST/NRSF were expressed from the lentiviral plasmid pGIPZ (Open Biosystems). Mature antisense sequences of effective shRNAs are TCGATTAGTATTGTAGCCG (663-681) (shRESTa) and TTTGAACTGTAAATATCTG (392-410) (shRESTb). Numbers in parenthesis indicate the position of mature antisense sequences corresponding to the coding domain sequence (CDS) of human REST/NRSF (3294 bp). As a control, the GIPZ non-silencing shRNAmir was used (Open Biosystems).

For C. elegans studies, full length spr-4 was isolated from fosmid DNA (WRM0628bF09, from the Sanger Institute collection) by PCR amplification with primers specific to the promoter regions (1.5 kb upstream of the transcriptional start site) and the UTR. The PCR product was sequence verified and used directly for injection. Human REST was isolated from cDNA and cloned into the vector pD152.79 MCS, downstream of the dpy-30 promoter and upstream of GFP. Sequencing verified the correct reading frame. The SPR-4::GFP fusion fosmid used in bombardment (Clone: 3167840880351681 C09) was provided by the Transgenome consortium (Sarov et al., 2012). Primers for sub-cloning are listed in Supplementary Table 2.

Statistical Analysis Statistical analysis was performed using Graphpad software and the R program. Student's t-tests were used to make comparisons between two groups with a normal distribution of data points. The Mann-Whitney-Wilcoxon Test was used for multiple samples without knowledge of their distribution. Age-related gene expression changes were identified by the Significant Analysis of Microarray (SAM) in R program. SAM identifies differentially expressed genes between young adult (less than 40 yrs, n=12) and Aged (greater than 70 yrs, n=16) by carrying out gene specific t-tests. Power analysis was used to ensure adequate statistical power for detecting significant differentially expressed genes in the microarray analysis. For sample n$>$12 in each group, there is 80% power to detect 1.5-fold changes at p-value $<$ 0.01. We therefore report significant age-related gene expression changes using the cutoff q-value $<$ 0.01 and fold change $>$ 1.5. The overlap of age-regulated genes with REST targets genes identified by ChIP-seq was assessed using the Hypergeometric test (p-value$=$1.65E-12). Age-down-regulated genes are enriched in ChIP-seq targets based on the binomial test (p-value$=$3.5E-7). Pathway and upstream regulator enrichment for age-regulated genes and ChIP-seq target genes were analyzed by the Hypergeometric test using Ingenuity pathway analysis (IPA). Pearson's correlation is used in this paper. By the central limit theorem, the distribution of the correlation coefficient is asymptotically normally distributed when the sample size is sufficiently large (n$>$30). Hence, the p-value for the Pearson's correlation coefficient for Figure 2.6 a, b, and d are calculated based on the normal distribution. Figure 2.6a shows plots for REST protein levels vs. cognitive test scores for multiple individual subjects. The correlation coefficient between REST protein level and cognitive variables are calculated based on n$=$111. Figure 2.6b shows a plot of REST protein level vs. Braak Score. The correlation coefficient between REST protein level and Braak Score is calculated based on n$=$37. Figure 2.6d shows a plot of REST protein level vs. age at death. The correlation coefficient between REST protein level and age is calculated based on n$=$61. Figure 2.8a compares the weighted mean expression level of REST target genes vs. age at death.

Each point represents the mean of weighted expression of 342 REST target probe-sets that are age-regulated based on microarray. These mean values were weighted by the total expression level for each probe-set across all samples and were further normalized to the youngest adult value (24 yrs; 100%).

Chapter 3

REST regulates FOXO1 for protection against oxidative stress

The data in this chapter will be submitted for publication (manuscript in preparation with Joseph Zullo):

REST regulates FOXO1 for protection against oxidative stress

Derek Drake[1,*], Joseph Zullo[1,*], Liviu Aron[1], Tao Lu[1], David A. Bennett[2], Monica P. Colaicovo[1] and Bruce A. Yankner[1]

[1]Department of Genetics, Harvard Medical School, Boston, MA 02115, [2]Rush Alzheimer's Disease Center, Rush University Medical Center, Chicago, IL 60612, [*]These authors contributed equally to this work.

Author Contributions

D.D., J.Z., L.A., and T.L. performed experiments. D.D., J.Z., L.A., T.L., M.C. and B.A.Y. contributed to the overall study design. D.D. and J.Z. performed informatics analysis. D.A.B. contributed tissue samples and analysis. B.A.Y. directed the study and B.A.Y., D.D. and

J.Z. wrote the manuscript, which was edited by all the coauthors.

Tao Lu (Yankner lab) cultured cells and sent samples for gene expression profiling (Figure 3.1A). Tao Lu and Liviu Aron (Yankner lab) performed the REST overexpression/knockdown experiment with immunofluorescent labeling for REST and FOXO1 shown in Figure 3.1D. Immunofluorescent labeling of brains shown in Figure 3.4C and Figure 3.5 was performed with Liviu Aron. Haeyoung Kim (Yankner lab) generated $REST^{lx/lx}$ and $REST^{-/-}$ MEFs. Joseph Zullo (Yankner lab) performed all *C. elegans* experiments and created associated Figure 3.7, Figure 3.8, Figure 3.9, Figure 3.10, and Figure 3.11. David Bennett (Rush Alzheimer's Disease Center) provided processed RNA-seq data. Candidate performed all other experiments and analyses in this chapter.

Introduction

Oxidative stress increases in the aging brain, and how this stress is managed to maintain neurons and neuronal function is critically important. We showed that REST is induced in neurons in the aging brain, REST directly represses expression of pro-apoptotic genes, and REST is induced by and protects against oxidative stress *in vitro* through an undetermined mechanism (Chapter 2, Lu $\mathrm{et\ al.}$ (2014)). While repression of pro-apoptotic genes is likely important for maintaining irreplaceable neurons during aging it is unlikely to provide direct protection against oxidative stress. Here we show that REST regulates FOXO1, a master regulator of the response to oxidative stress, and REST provides oxidative stress protection at least partially through FOXO1. We also provide evidence that REST may induce FOXO1 in neurons of the aging human brain and provide neuroprotection through FOXO1 target genes.

The phenotypic manifestations of aging are well conserved among metazoans, allowing model systems with relatively short lifespans such as the nematode worm *C. elegans* to be used to understand aging at both the organismal and cellular levels. Studies in these model

systems have discovered that pathways that regulate lifespan also tend to regulate stress resistance (Johnson et al., 2002). The best studied pathway is the insulin/IGF signaling (IIS) pathway where attenuation of IIS extends lifespan and promotes stress resistance (Kenyon, 2010). In worms, this lifespan extension and stress resistance, including resistance to thermal, genotoxic, oxidative, and proteotoxic stress, requires the forkhead transcription factor *daf-16*/FOXO (Kenyon, 2010). As an alternative system to investigate the role of REST in aging and stress resistance, we have focused on the *C. elegans* orthologs of the REST/COREST repressor complex, the suppressor of presenilin (spr) family (Lakowski et al., 2003; Wen et al., 2000). Using this system, we have previously shown that spr mutant worms are sensitive to oxidative stress, and that REST can substitute functionally for its ortholog, *spr-4*, to restore stress resistance (Chapter 2). Here we expand our analysis of the stress sensitivities of these mutants and identify spr genes as key players in the lifespan extension resulting from reduced IIS through regulation of *daf-16*/FOXO. The results presented in this chapter suggest that the stress resistance provided by REST through regulation of FOXOs is evolutionarily conserved, and that REST may promote healthy human aging.

Results

REST regulates FOXO1 expression and nuclear localization

To investigate how REST may provide protection against oxidative stress as shown in Chapter 2 we altered REST levels by overexpression or short hairpin RNA-mediated knockdown in neural SH-SY5Y cells and performed gene expression profiling by microarrays. Of those genes with Gene Ontology Biological Process annotations related to oxidative stress we found that FOXO1 expression was increased by REST overexpression and decreased by REST knockdown (Figure 3.1A). Since FOXOs are well characterized regulators of

the response to oxidative stress we investigated if the regulation of FOXO1 was involved in the stress resistance provided by REST. First, we sought to understand at what levels REST regulates FOXO1. We confirmed the microarray result using RT-qPCR which showed that FOXO1 mRNA is increased 2.2-fold in REST overexpressing cells relative to GFP expressing cells and decreased 3.1-fold in sh4-REST knockdown cells relative to sh-con cells (Figure 3.1B). FOXO1 protein levels were also strongly increased in REST overexpressing cells relative to GFP expressing cells (Figure 3.1C) which is consistent with the strong decrease in FOXO1 protein in SH-SY5Y cells when REST protein is decreased by short hairpin RNA-mediated knockdown (Chapter 2). In addition to increasing FOXO1 protein levels, immunofluorescent labeling showed that REST overexpressing cells also induced FOXO1 nuclear translocation relative to GFP expressing cells (Figure 3.1D). Thus, REST regulates FOXO1 expression at the mRNA and protein levels and promotes nuclear translocation.

As an alternative system to investigate REST's regulation of FOXO1 expression and nuclear translocation at baseline and in response to oxidative stress we used mouse embryonic fibroblasts (MEFs) from $REST^{lx/lx}$ mice (Chapter 2). To create REST-deficient ($REST^{-/-}$) MEFs we transduced $REST^{lx/lx}$ MEFs with a Cre lentivirus. At baseline without oxidative stress $REST^{-/-}$ MEFs had reduced nuclear FOXO1 (Figure 3.2A, B). In response to paraquat, which promotes the generation of reactive oxygen species, $REST^{lx/lx}$ MEFs showed increased levels of nuclear FOXO1 compared to $REST^{-/-}$ MEFs (Figure 3.2A, B). $REST^{lx/lx}$ MEFs also showed increased nuclear FOXO1 at all doses compared to the control treatment, whereas $REST^{-/-}$ MEFs only showed increased nuclear FOXO1 at 250 μM paraquat (Figure 3.2A, B). Moreover, $REST^{lx/lx}$ MEFs showed better survival than $REST^{lx/lx}$ MEFs at 250 μM paraquat, as evidenced by reduced cell density in $REST^{-/-}$ MEFs, confirming that REST-deficiency sensitizes to oxidative stress. Thus, REST-deficiency leads to reduced nuclear FOXO1 levels and reduced survival in response to oxidative stress, suggesting that FOXO1 may mediate part of the ability of REST to protect against

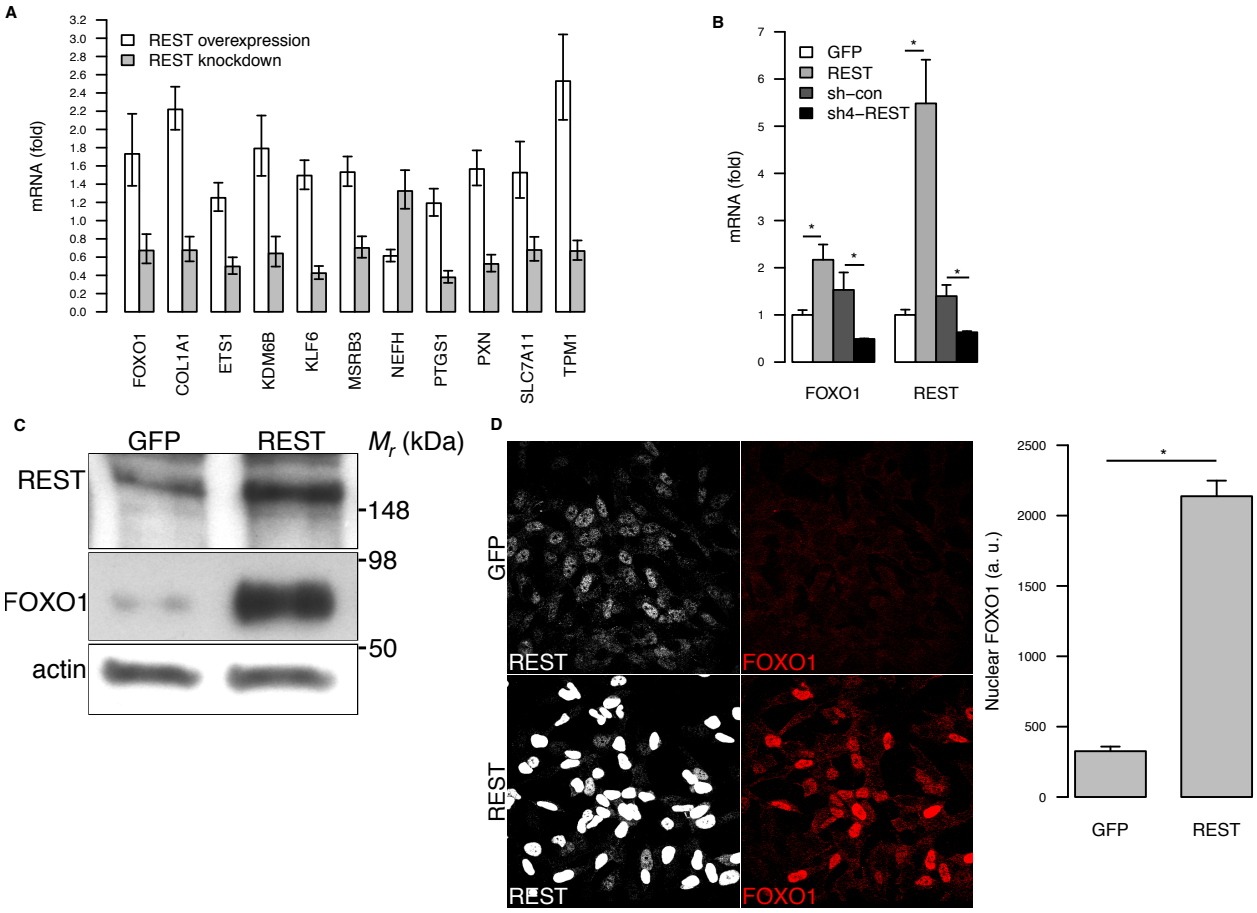

Figure 3.1: **REST regulates FOXO1 expression and nuclear localization in SH-SY5Y cells.** **A.** Gene expression profiling by microarrays of genes involved in oxidative stress in SH-SY5Y cells with altered REST levels. For overexpression lentiviral transduction of viruses encoding GFP or REST were used. For knockdown lentiviral transduction of viruses encoding a control short hairpin or short hairpin against REST were used. Only genes significantly different compared to control with false discovery rate < 0.05 in REST overexpression and REST knockdown with opposite direction of change that had Gene Ontology Biological Process annotations related to oxidative stress are shown (Methods). Values represent the mean fold change relative to control, and represent a 95% confidence interval for the mean. GFP, $n = 5$; REST, $n = 5$; sh-control, $n = 5$; sh-REST, $n = 4$. **B.** REST regulates FOXO1 mRNA expression. SH-SY5Y cells were transduced as described in A. Expression was normalized to β-actin. Values represent fold change relative to GFP, and represent the mean $\pm$ SE. $n = 3$ per group. * $p < 0.05$, t-test. **C.** SH-SY5Y cells were transduced using lentivirus encoding control (GFP) or REST and protein extracts were analyzed by western blotting. **D.** SH-SY5Y cells were transduced using lentivirus encoding control (GFP) or REST and cells were immunofluorescently labeled to determine REST and FOXO1 localization. FOXO1 nuclear levels were quantified using DAPI to delineate the nucleus. Values represent the mean FOXO1 nuclear intensity, and represent the mean $\pm$ SE. * $p < 0.05$, t-test.

oxidative stress. However, it is noteworthy that FOXO1 could be induced by high dose paraquat (250 μM) in REST$^{-/-}$ MEFs. Thus, REST is not absolutely required for FOXO1 induction, but it is necessary for optimal induction by oxidative stress.

REST, oxidative stress resistance, and FOXO1

REST can induce the expression of genes that protect against oxidative stress, such as FOXO1, as well as genes that are FOXO1 targets, such as catalase (Chapter 2, Figure 3.1A,B). To investigate if REST protects against oxidative stress through induction of FOXO1, we overexpressed REST using lentiviral transduction and inhibited endogenous FOXO1 function using a dominant negative FOXO1 construct (FOXO1-DN). The FOXO1-DN construct (Wang $\mathrm{et\ al.}$, 2011) encodes amino acids 1–255 of FOXO1, which contains the DNA binding domain but not the transactivation domain, and competes with endogenous FOXO1 for binding to target sites without activating their expression (Wang $\mathrm{et\ al.}$, 2011). In SH-SY5Y cells, REST overexpression provided protection against oxidative stress compared to GFP expression, as previously shown (Chapter 2, Lu $\mathrm{et\ al.}$ (2014)), but this protection was significantly reduced in the FOXO1-DN expressing cells (Figure 3.3A). This suggests that FOXO1 mediates part of REST's ability to protect against oxidative stress.

As an alternative approach, we used short hairpin RNA-mediated knockdown of FOXO1 to reduce FOXO1 protein levels in REST$^{lx/lx}$ and REST$^{-/-}$ MEFs. First, we confirmed that the sh-FOXO1 constructs reduce FOXO1 protein levels relative to sh-control constructs (Figure 3.3B). REST$^{lx/lx}$ FOXO1 knockdown, REST$^{-/-}$ control knockdown, and REST$^{-/-}$ FOXO1 knockdown cells all showed increased but similar sensitivity to oxidative stress relative to REST$^{lx/lx}$ control knockdown cells (Figure 3.3C). This suggests that REST provides oxidative stress resistance through FOXO1, and that the increased sensitivity of REST$^{-/-}$ cells to oxidative stress relates, at least in part, to to reduced FOXO1.

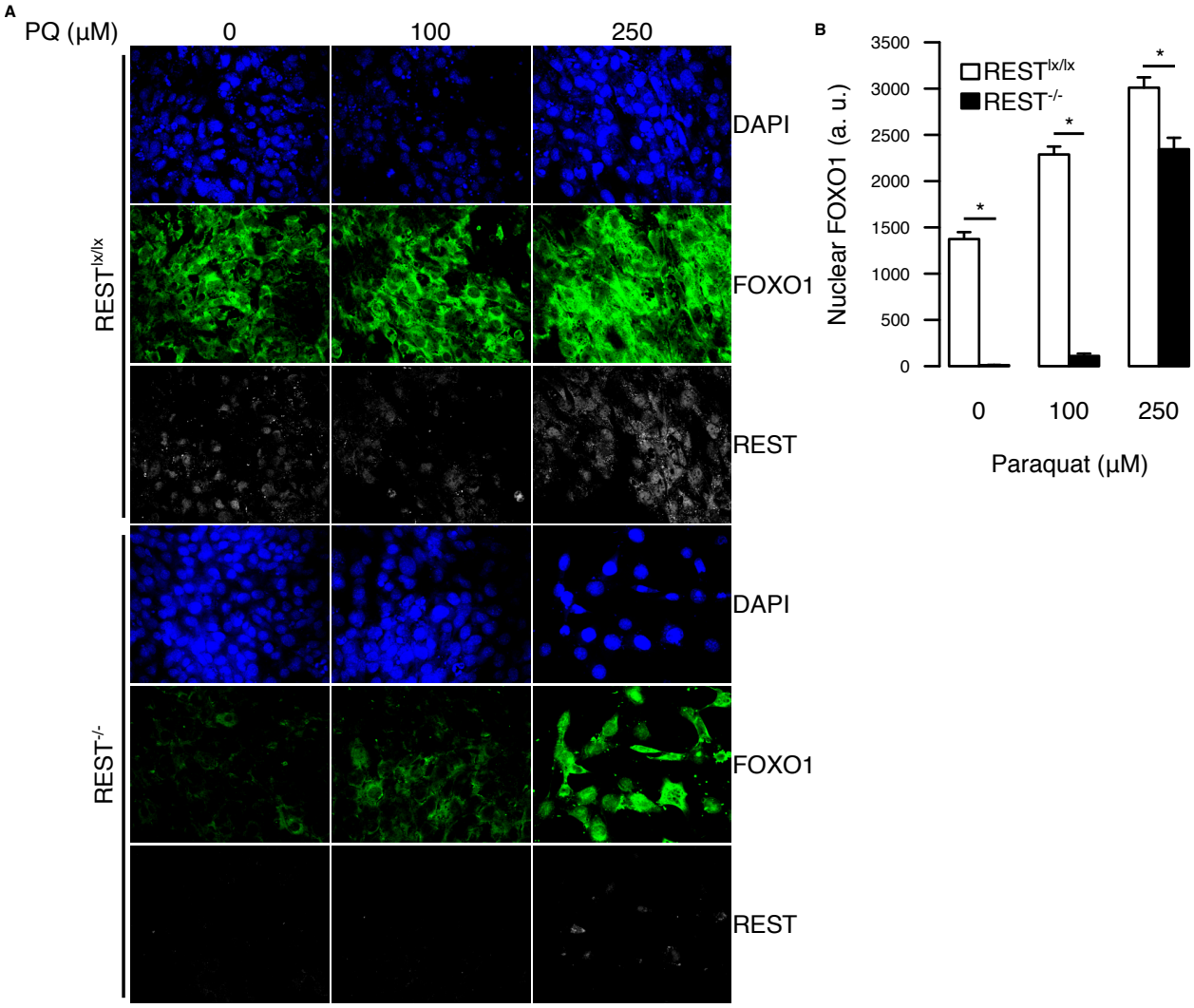

Figure 3.2: **REST regulates FOXO1 expression and nuclear localization in REST$^{-/-}$ MEFs. A.** REST-deficient (REST$^{-/-}$) and control (REST$^{lx/lx}$) MEFs were treated with 0 μM, 100 μM, or 250 μM paraquat (PQ) for 48 hours and then immunofluorescently labeled to determine REST and FOXO1 localization. **B.** FOXO1 nuclear levels were quantified using DAPI to delineate the nucleus. Values represent the mean FOXO1 nuclear intensity, and represent the mean $\pm$ SE. * $p < 0.05$, ANOVA followed by Tukey's HSD test.

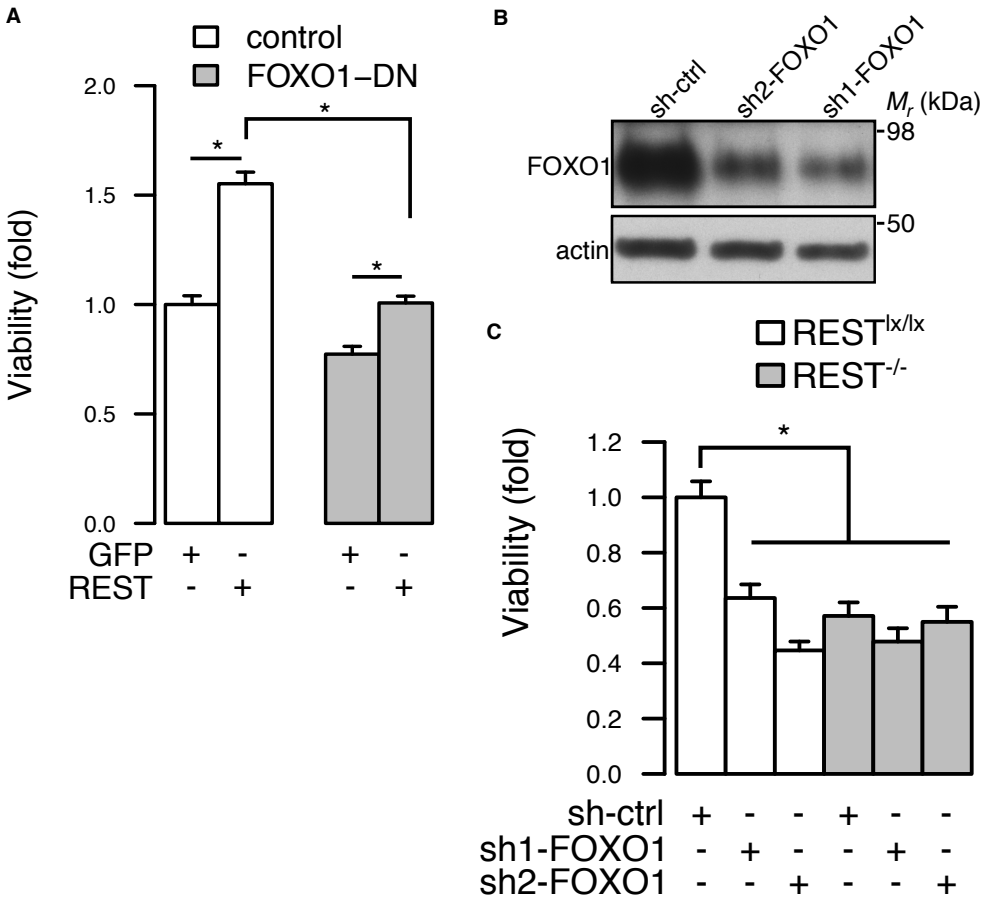

Figure 3.3: **REST provides stress resistance partially through FOXO1. A.** Stable SH-SY5Y cells were generated by neomycin selection expressing a control vector or FOXO1-dominant negative (FOXO1-DN) construct. Cells were transduced with GFP or REST lentivirus then treated with 0 μM or 100 μM H_2O_2 for 1 hour. Viability was determined using the MTS assay. Values were normalized to the mean viability of the control cells transduced with GFP and represent the mean $\pm$ SE. $n = 6$ per group. * $p < 0.05$, ANOVA followed by Tukey's HSD test. **B.** Confirmation of short hairpin RNA-mediated knockdown of FOXO1 protein levels. **C.** Control (REST$^{lx/lx}$) and REST-deficient (REST$^{-/-}$) MEFs were transduced with lentiviral vectors encoding control short hairpin (sh-ctrl) or short hairpin against FOXO1 (sh1-FOXO1 or sh2-FOXO1) then treated with 0 μM or 250 μM paraquat for 48 hours. Viability was determined using the the MTS assay. Values were normalized to the mean viability of REST$^{lx/lx}$ MEFs transduced with sh-ctrl and represent the mean $\pm$ SE. $n = 6$ per group. * $p < 0.05$, ANOVA followed by Tukey's HSD test.

REST and FOXO1 regulation in the aging brain

To explore the regulation of FOXO1 by REST during brain aging, we labeled coronal brain sections from 9- and 18-month-old $REST^{lx/lx}$ and $REST^{-/-}$ mice with a FOXO1-specific antibody. We found a robust induction of FOXO1 expression in the aging 18-month-old mouse cortex relative to 9-month-old mice, in particular in neurons in cortical layers 4 and 5. In contrast, FOXO1 induction in the aging mouse brain was significantly reduced in REST-deficient mice (Figure 3.4A). This suggests that REST may also regulate FOXO1 expression *in vivo* in neurons of the aging brain. To determine if FOXO1 is induced by REST in the aging human brain, we performed Western blotting on post-mortem human brain samples. FOXO1 trended toward a 3.6-fold increase in aged compared to young individuals (Figure 3.4B). To further investigate if REST regulates FOXO1 nuclear localization in the human brain, we performed immunofluorescent microscopy on 15 brains from young, aged, centenarian, and AD individuals for REST and FOXO1 (Figure 3.4C) and quantified nuclear levels in prefrontal cortical pyramidal neurons (Figure 3.5). REST nuclear levels were increased in aged cases, consistent with our previous results (Chapter 2). FOXO1 nuclear levels also trended toward an increase in the aged and the combined aged and centenarian groups in this small sample (data not shown). REST and FOXO1 also exhibited similar nuclear-cytoplasmic localization in pyramidal neurons; cells with high levels of nuclear REST showed high levels of nuclear FOXO1 and cells with low nuclear REST showed low levels of nuclear FOXO1. This was confirmed by linear regression analysis which showed highly significant correlations between REST and FOXO1 nuclear levels in all groups (Figure 3.5). Taken together with our observations in the aging mouse brain, these findings suggest that FOXO1 expression may be induced by REST in aging cortical neurons.

To investigate if the correlation between REST and FOXO1 in the aging brain may be related to stress resistance, we utilized a large RNA sequencing dataset from aged human prefrontal cortex. In 179 aged cognitively-intact individuals, the expression of REST and FOXO1 mRNA was highly correlated (Figure 3.6A). Further, REST and FOXO1 expres-

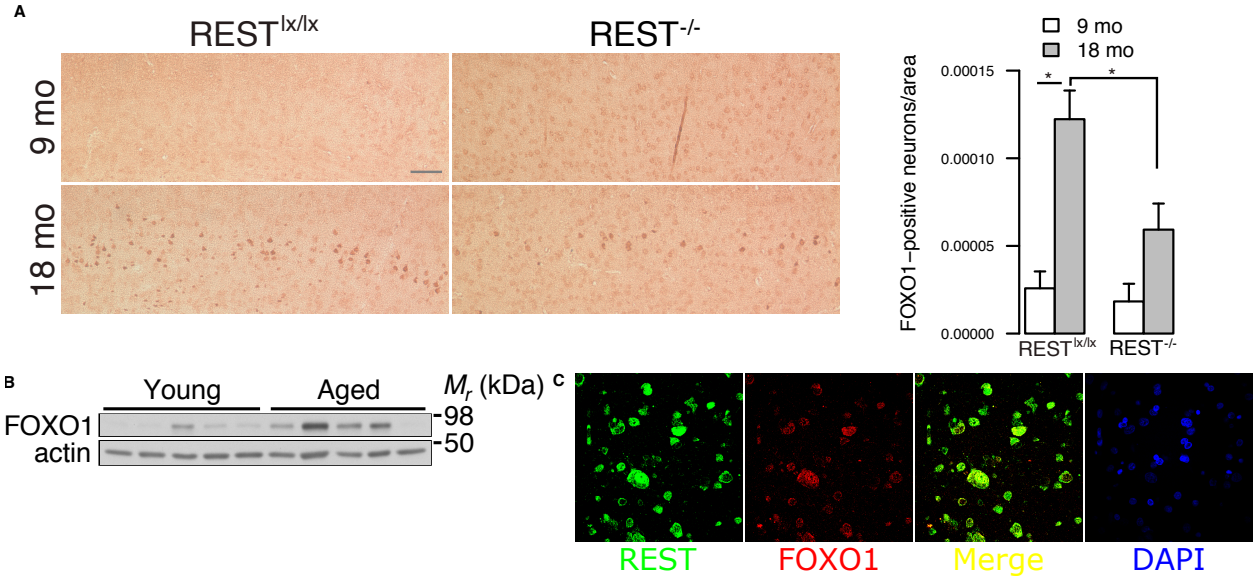

Figure 3.4: **FOXO1 induction in aged frontal cortex. A.** Increased FOXO1 expression in the aging mouse cortex. Immunolabeling of mouse cortical sections with a FOXO1-specific antibody revealed increased FOXO1 expression in 18-month-old REST$^{lx/lx}$ mice relative to 9-month-old REST$^{lx/lx}$ mice. The increase in FOXO1 expression was seen predominantly in the cortical layers 4–5. Scale bar represents 250 μm. REST$^{lx/lx}$, 9-month-old: $n = 4$; REST$^{lx/lx}$, 18-month-old: $n = 9$; REST$^{-/-}$, 9-month-old: $n = 3$; REST$^{-/-}$, 18-month-old: $n = 5$. Values represent the number of large FOXO1-positive cells per unit area and represent the mean $\pm$ SE. * $p < 0.05$, ANOVA followed by Tukey's HSD test. **B.** Aged individuals have increased FOXO1 protein levels in human prefrontal cortex. FOXO1 protein levels quantified relative to actin trended toward a significant 3.6-fold increase ($P = 0.063$, t-test) in aged individuals relative to young individuals. $n = 5$ per group. **C.** Colocalization of REST and FOXO1 in aged human prefrontal cortex. Representative immunofluorescent labeling of an aged human brain for REST (green) and FOXO1 (red) using DAPI (blue) signal to delineate the nucleus.

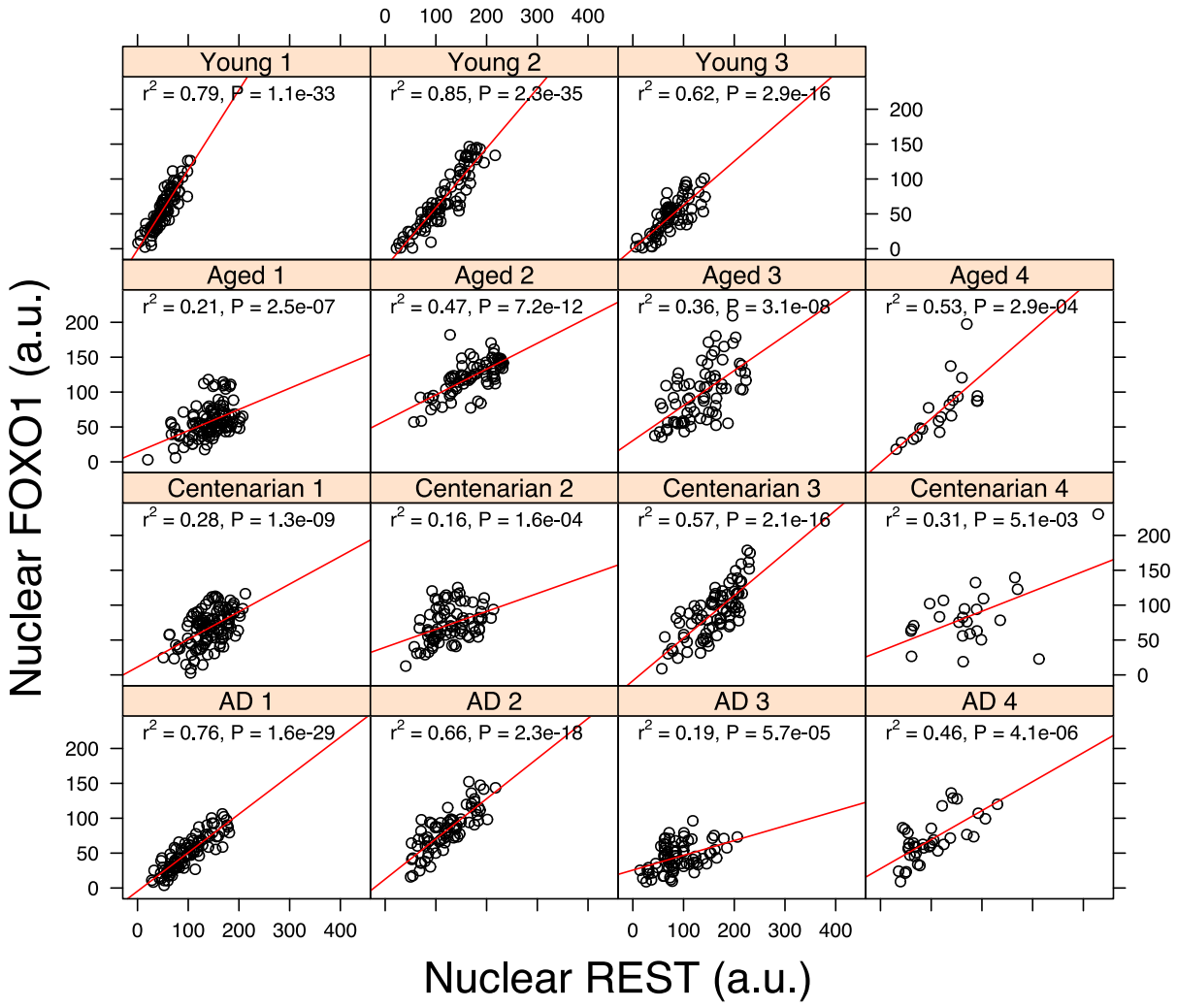

Figure 3.5: **Coregulation of REST and FOXO1 in aged human prefrontal cortex.** Scatterplots and coefficient of determination (r^2) of nuclear FOXO1 and nuclear REST levels in pyramidal neurons of the human prefrontal cortex determined by immunofluorescent labeling. Young, $n = 3$; Aged, $n = 4$; Centenarian, $n = 4$; AD, $n = 4$.

sion positively correlated with the expression of several known FOXO-regulated genes involved in oxidative stress protection including catalase (CAT, an antioxidant enzyme that converts H_2O_2 to water and oxygen), periredoxin-6 (PRDX6, a redox regulator that can protect against oxidative stress by reducing H_2O_2 and phospholipid hydroperoxides), paraoxonase 2 (PON2, a membrane-bound antioxidant), selenoprotein P (SEPP1, an extracellular antioxidant), methionine sulfoxide reductase B3 (MSRB3, reduces the sulfoxide of methionine back to methionine), metallothionein 2A (MT2A, a member of a class of heavy-metal binding proteins that protect against toxic heavy metal ions), metallothionein 1E (MT1E), nuclear factor erythroid 2-like 2 (NFE2L2/NRF2, a transcription factor that regulates several antioxidant response genes (Nguyen $\mathrm{et\ al.}$, 2009)), and sirtuin 1 (SIRT1, a transcription factor that regulates aging and directly deacetylates FOXO1 (Yang $\mathrm{et\ al.}$, 2005)). Surprisingly, there was no correlation with superoxide dismutase 2 (SOD2/MnSOD) expression (Figure 3.6A, Figure 3.6B). Consistent with this, PRDX6, PON2, and SEPP1 mRNA expression was also upregulated in the aging human prefrontal cortex (Lu $\mathrm{et\ al.}$, 2004). We also found that REST and FOXO1 expression were positively correlated with the expression of the anti-apoptotic gene BCL2 (Figure 3.6A, Figure 3.6B). Importantly, REST and FOXO1 expression did not correlate, or was inversely correlated, with canonical pro-apoptotic targets of FOXO1, including BIM (BCL2L11), BNIP3, TRAIL (TNFSF10), and PUMA (BBC3) or with cell cycle targets of FOXO1, including p27KIP1 (CDKN1B) and cyclin G2 (CDK1) (Figure 3.6A, Figure 3.6B). These results suggest that FOXO1 activity is modulated for stress resistance and neuroprotection in the aging brain, and that its potential pro-apoptotic activity is inhibited.

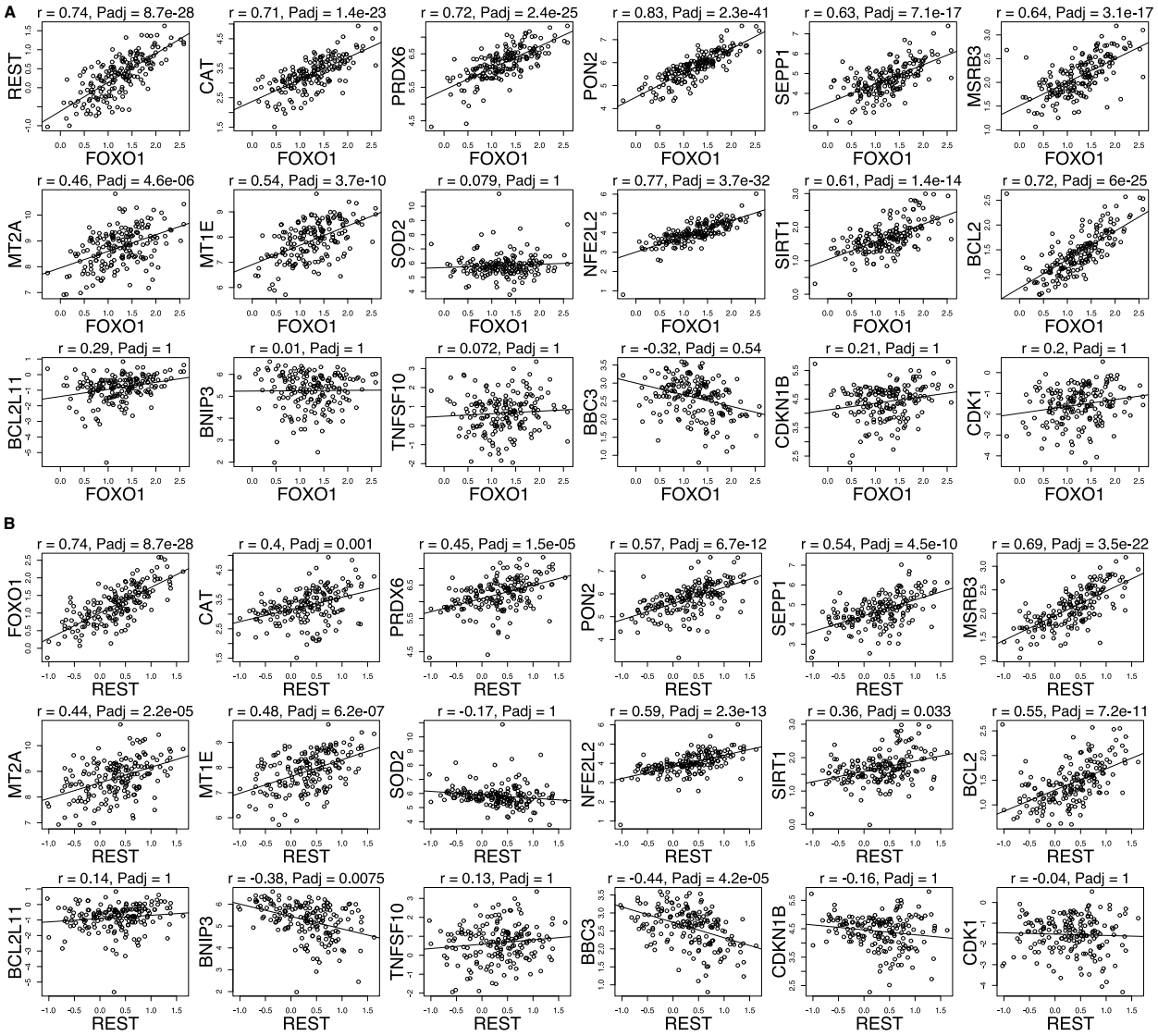

Figure 3.6: **FOXO1 and REST mRNA expression correlate with the expression of protective FOXO1 target genes in the aged human brain.** mRNA expression from the gray matter of the dorsolateral prefrontal cortex of 179 cognitively-intact aged individuals was measured by RNA-seq. Log-transformed FPKM expression data is plotted. Expression was regressed on FOXO1 (**A**) or REST (**B**) using a linear model, and the significance of the regression coefficient was adjusted by Bonferroni correction (Padj).

REST orthologs regulate lifespan and stress resistance through the insulin/IGF-1 signaling pathway

We have previously shown that in aging human neurons, REST nuclear levels are positively correlated with longevity, consistent with its protective effect against Alzheimers disease (Chapter 2). We have expanded on this finding by examining the brains of 7 centenarians, individuals who lived to a hundred years or greater. We found that even relative to the high levels of REST seen in individuals 70–90 years of age, REST levels were significantly higher in the centenarian group (Figure 3.8A). This raises the possibility that REST may promote longevity. To directly test this hypothesis, we utilized the nematode *C. elegans*, which has orthologs of the REST corepressor complex (Lakowski et al., 2003; Wen et al., 2000). We have previously shown that the *C. elegans* gene *spr-4* is a functional ortholog of mammalian REST (Lu et al., 2014). To obtain greater insight into the role of REST in aging, we determined whether increasing the expression of *spr-4* would have an effect on lifespan. To accomplish this, we developed a new system of gene induction in the worm that would enable us to activate the transcription of the endogenous *spr-4* locus. First, a worm expression cassette was generated for a nuclease deficient CAS9-VP64 transcriptional activator similar to those that have been used in mammalian cell culture (Gilbert et al., 2013; Maeder et al., 2013). In this construct, dCas9::VP64 is driven by the ubiquitous *eft-3* promoter, and appended by the *tbb-2* UTR, enabling expression of transgenes in the germline (Merritt et al., 2008). This construct was then introduced into the worm genome using the MosSCI procedure (Zeiser et al., 2011). Integration was confirmed by genotyping, and expression of dCas9::VP64 was verified by Western blotting (data not shown). A mix of four unique small guide RNAs (sgRNAs) targeting the dCas9::VP64 fusion protein to the *spr-4* promoter was introduced by microinjection along with a myo-2::mCherry fluorescent marker. Three independent transgenic lines were established from the injections. Increased expression of *spr-4* mRNA was observed

by RT-qPCR in sgRNA-bearing worms relative to their non-array bearing counterparts (Figure 3.7A). We also observed increased SPR-4 protein by crossing sgRNA positive worms to worms bearing an integrated *spr-4*::gfp fusion construct (Figure 3.7B), consistent with the RT-qPCR results.

We next performed lifespan analysis on *spr-4* overexpressing worms. Progeny either with or without the sgRNA targeting array were segregated from the three transgenic lines described above and placed on NGM plates containing 100 μg/mL FUDR to inhibit progeny production. The worms were then maintained over the ensuing 30 days and scored for viability every two days. Lines bearing the sgRNA arrays showed significantly increased mean lifespan relative to worms without the targeting array and wildtype worms (Figure 3.8B). This lifespan extension phenotype required the dCas9::VP64 transgene as it did not occur in worms bearing only the sgRNAs in which the transgene had been crossed out (Figure 3.8C). As a control for off-target effects, we also assessed the construct in the tm465 *spr-4* mutant. This is a null allele that consists of a large deletion of the second and third exon of the *spr-4* transcript with a subsequent frameshift. These worms, lacking a functional copy of *spr-4*, did not exhibit any lifespan increase from targeting dCas9::VP64 to the *spr-4* promoter via the same sgRNA transgenic arrays (Figure 3.8C, D). Thus, modest overexpression of *spr-4* from the endogenous locus results in a robust and specific extension of lifespan.

The most well studied regulator of aging in *C. elegans* is the *daf-2*/insulin-IGF signaling (IIS) pathway (Kenyon, 2010). Worms with *daf-2* mutations, the sole insulin receptor ortholog, exhibit increased stress resistance (Lithgow $\mathrm{et\ al.}$, 1995) and longevity (Kenyon $\mathrm{et\ al.}$, 1993). To determine if the spr genes affect this pathway, we investigated the effects of spr mutants on lifespan. Two *spr-4* mutants (by105 and tm465), one *spr-3* mutant (ok2525), and one double mutant for *spr-3*(ok2525)/*spr-4*(by105) (*spr-3*/*spr-4*) were examined. All of these alleles are loss of function alleles. We found that none of these mutations affected lifespan under normal conditions (Figure 3.9A,B). However, since these mutants exhibit

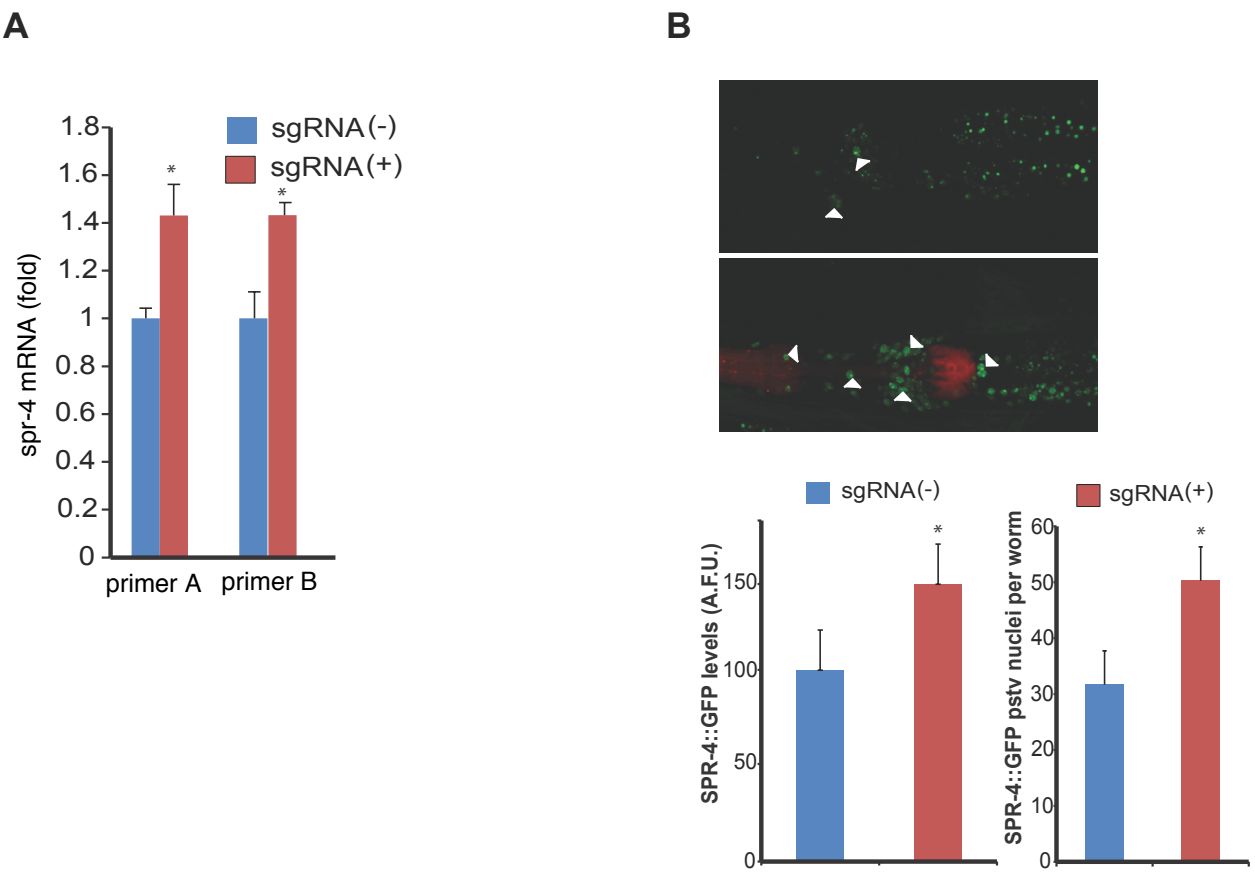

Figure 3.7: **dCas9::VP64-mediated activation of *spr-4*. A.** Worms bearing a stably integrated and ubiquitously expressed peft-3::dCas9::VP64::tbb-2utr transgene were injected with a cocktail of 4 constructs which express small guide RNA (sgRNAs) targeted to distinct regions of the *spr-4* promoter, along with a myo-2::mCherry fluorescent marker. 8 adult and 8 L4 stage animals were picked per strain (with and without sgRNA extrachromosomal array). 60 hours later, worms were harvested and RNA was collected. Transcript levels are normalized to wildtype controls using the cdc-42 housekeeping gene and represent the mean $\pm$ SEM. Primer A and B amplify different regions of the *spr-4* transcript. $n = 3$ independent lines. * $p < 0.05$, t-test. **B.** sgRNA+ worms were mated to worms bearing an integrated pspr-4::spr-4::gfp::spr-4utr transgene. Heterozygous progeny from this cross which either received (sgRNA+) or did not receive (sgRNA-) the transgenic array containing the guide RNAs were examined to assess efficacy of the sgRNAs in upregulating SPR-4::GFP. Arrowheads indicate SPR-4::GFP+ nuclei. Quantification of the experiments for 2 independent lines and two separate crosses is shown. Data represent the mean $\pm$ SEM. * $p < 0.05$, t-test.

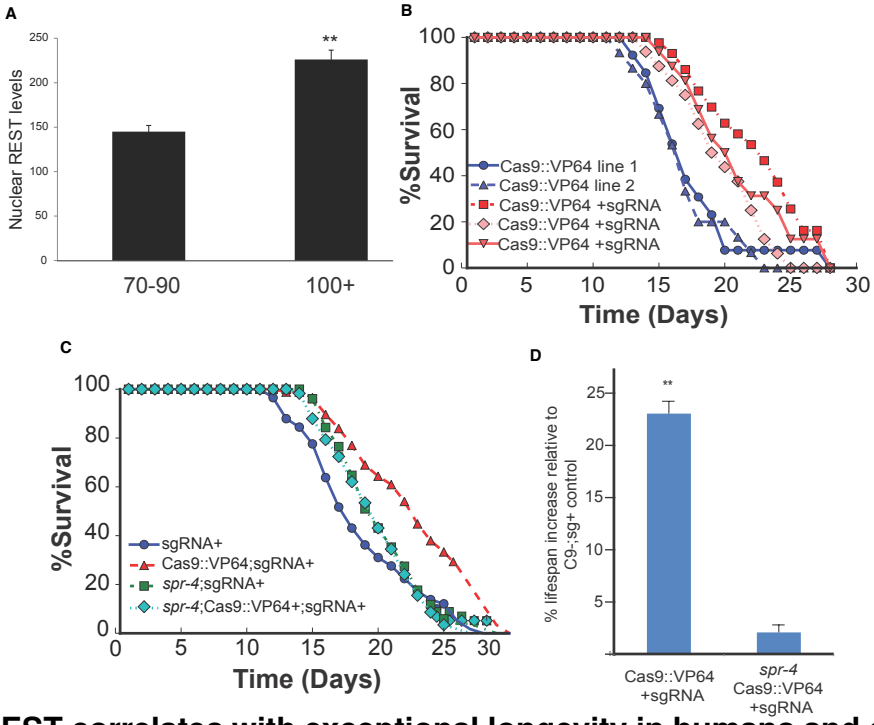

Figure 3.8: **REST correlates with exceptional longevity in humans and extends lifespan in worms.** **A.** Quantification REST nuclear levels in human neurons, as determined by DAPI staining and immunohistochemistry, in brains from individuals of the indicated ages. Values represent the mean REST nuclear intensity, and represent the mean $\pm$ SEM. 70–90, $n = 50$; 100+, $n = 7$. ** $p < 0.005$, t-test. **B.** Lifespans of worms with integrated copies of the dCas9::VP64 transgene, bearing extrachromosomal arrays composed of a myo-2::mCherry transgene and 4 distinct sgRNAs targeted to different regions of the *spr-4* promoter. Three lines were derived from independent injections. As a control, mCherry negative worms were isolated from these populations and lifespan analysis was performed in parallel. 25–30 day 1 adult worms of the indicated genotypes were transferred from standard NGM to NGM supplemented with 100 μg/mL FUDR, stored at 20 ℃ in a humidified chamber, and scored every other day for viability, by reactive movement to prodding with a platinum wire. Lifespans are plotted as Kaplan-Meir survival curves, and significance was assessed by log-rank test. All transgenic lines were significantly different than control by log rank test ($p < 0.05$). **C.** Representative lifespans of worms bearing sgRNA arrays, with or without dCas9::VP64 transgenes and functional *spr-4*. *spr-4*(tm465) is a putative null allele containing a large internal deletion and frameshift of the *spr-4* transcript. Each lifespan trace represents 2 independent strains of the same genotype, with $n >= 20$ animals per plate. **D.** Mean values from three experiments performed as described in (C), error bars are SEM. ** $p < 0.05$.

impaired stress resistance (Chapter 2), we tested whether they were required for the extended longevity resulting from reduced IIS. Since DAF-2 is the major upstream regulator of the IIS pathway, we first used RNAi to knockdown *daf-2*. As previously shown, worms grown on RNAi feeding clones targeting *daf-2* live approximately 50% longer than those grown on an empty vector control. The spr mutants, however, showed a reduced lifespan extension on *daf-2* RNAi (Figure 3.9C, D), despite equivalent *daf-2* knockdown efficiency (Figure 3.11A). Worms with the *daf-2(e1370)* allele live approximately two-fold longer than wildtype worms and are highly resistant to a variety of stresses (Lithgow $\mathrm{et\ al.}$, 1995). Introduction of spr mutations into this background reduced lifespan extension by 25–50%, depending on the spr allele (Figure 3.9E). This effect of the spr mutants was observed at both 20℃ (Figure 3.9F), the temperature at which our previous experiments were done, and at 25℃, where the *daf-2(e1370)* allele is fully penetrant at initiating dauer arrest in larval stage 1 animals (Gems $\mathrm{et\ al.}$, 1998). *daf-2* mutant worms are also resistant to thermal and oxidative stress. However, *daf-2* worms bearing spr mutations showed significantly reduced thermal and oxidative stress resistance (Figure 3.11B). Taken together, these results suggest that spr genes can modulate the effects of IIS signaling on stress resistance and aging.

The forkhead transcription factor *daf-16* is the sole worm ortholog of the FOXO family of transcription factors, and is required for the lifespan and stress resistance phenotypes of *daf-2* mutant worms (Kenyon $\mathrm{et\ al.}$, 1993). In this chapter and in Chapter 2 we have shown that REST regulates FOXO1 expression. To determine if this is a conserved mechanism by which REST and spr genes could promote longevity and stress resistance, we crossed a DAF-16::GFP transgene into the *spr-3*/*spr-4* double mutant. Untreated *spr-3*/*spr-4* double mutants showed modestly decreased DAF-16::GFP levels (Figure 3.10A,B). Treatment with the pro-oxidant paraquat induced nuclear translocation of DAF-16::GFP (data not shown). However, treatment of *spr-3*/*spr-4* double mutants with paraquat resulted in markedly reduced nuclear levels of DAF-16::GFP (Figure 3.10A,B). These data are consistent with

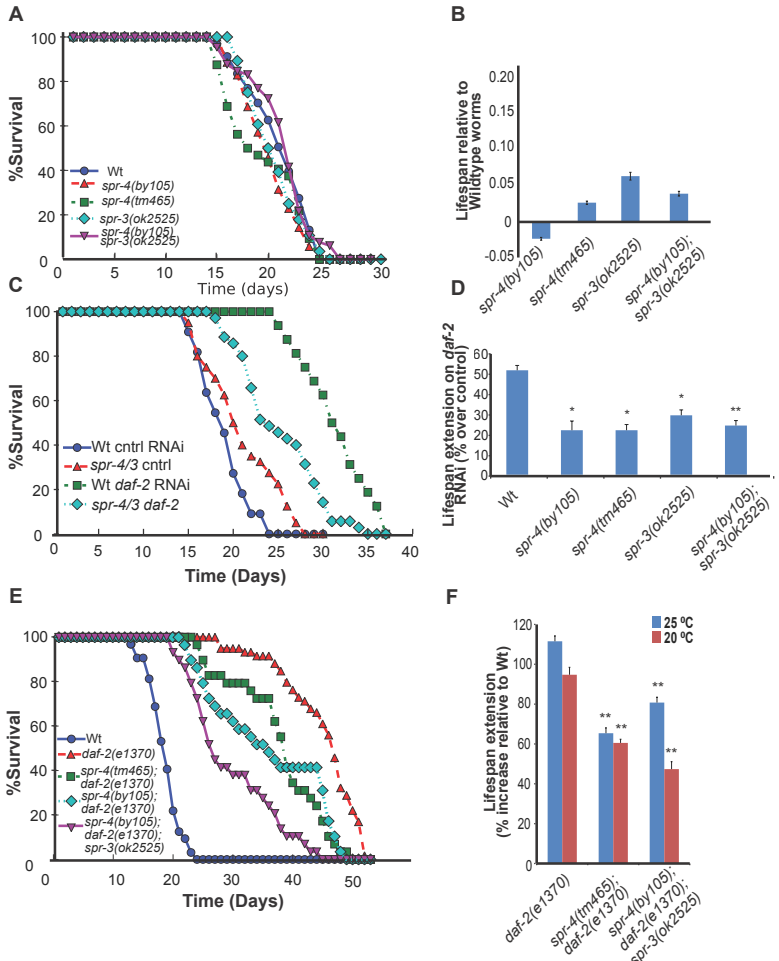

Figure 3.9: **The transcription factors *spr-4* and *spr-3* are required for long life of *daf-2* mutants.** spr genes are specifically required for the extended longevity via reduced insulin/IGF signaling (IIS). **A.** Representative lifespan analysis of spr mutants and wildtype controls. Experiments were performed as described in Figure 3.8B. **B.** Quantification of 3 independent experiments performed as described in A. No reproducible significant differences were found by log-rank test or t-test on average lifespan. **C.** Representative lifespan analysis of *spr-4*(by105);*spr-3*(ok2525) double mutants and wildtype controls on plates seeded with bacteria carrying either an empty vector control or expressing doublestranded RNAi targeting the *daf-2* transcript. **D.** Quantification of 3 independent experiments described in C, with additional spr mutants of the indicated genotypes. **E.** Lifespan analysis of the spr mutants on a *daf-2(e1370)* background. For C–F: All mutants lifespans were significantly different from wildtype by log-rank test in individual trials, and differences in mean lifespan extension were significant at the indicated levels by t-test (* $p < 0.05$, ** $p < 0.001$).

the lifespan experiments, in which spr mutants have normal lifespans under baseline conditions, but in the setting of oxidative stress and reduced insulin signaling, exhibit reduced survival. To confirm a role for *daf-16* in the stress resistance phenotype of spr mutants, we generated wildtype and *spr-3*/*spr-4* mutant lines bearing extrachromosomal transgenic arrays of a full length DAF-16::GFP transgene (Lin $\mathrm{et\ al.}$, 1997). If DAF-16 deficiency is the basis of the spr stress phenotypes, then driving *daf-16* expression at a high level should rescue the reduced survival phenotype. As previously observed, *spr-3*/*spr-4* mutant worms treated with 5 mM paraquat exhibited decreased survival relative to wildtype worms (Figure 3.10C). This phenotype was almost completely suppressed by *daf-16* overexpression (Figure 3.10D). Taken together, these findings demonstrate that the regulation of *daf-16*/FOXO1 by spr/REST is conserved and plays a major role in the mechanism of REST-mediated stress resistance.

REST regulates insulin/IGF-1 signaling in mammalian cells

Since spr genes affect the insulin/IGF-1 signaling (IIS) pathway in *C. elegans*, we determined if REST regulates the IIS pathway in mammalian cells. AKT is a central hub of the IIS pathway. Activation of the IIS pathway leads to AKT activation by phosphorylation at residues T308 and S473. Activated AKT can then directly phosphorylate FOXO1 leading to its nuclear exclusion and degradation. Thus, we used phosphorylated AKT as a surrogate for IIS activity. REST overexpressing cells showed decreased P-T308-AKT at baseline (0.63-fold) and in response to insulin (0.65-fold), while REST knockdown cells showed increased P-T308-AKT at baseline (1.68-fold) and an increased response to insulin (1.32-fold) (Figure 3.12A), suggesting that REST downregulates insulin signaling. P-S473-AKT was unchanged by REST overexpression or knockdown (data not shown). One candidate REST-regulated gene identified by gene expression profiling is the insulin binding protein IGFBP3. This was validated by RT-qPCR as showing induction following REST overexpression and reduction upon REST knockdown (Figure 3.12B). Since IGFBP3

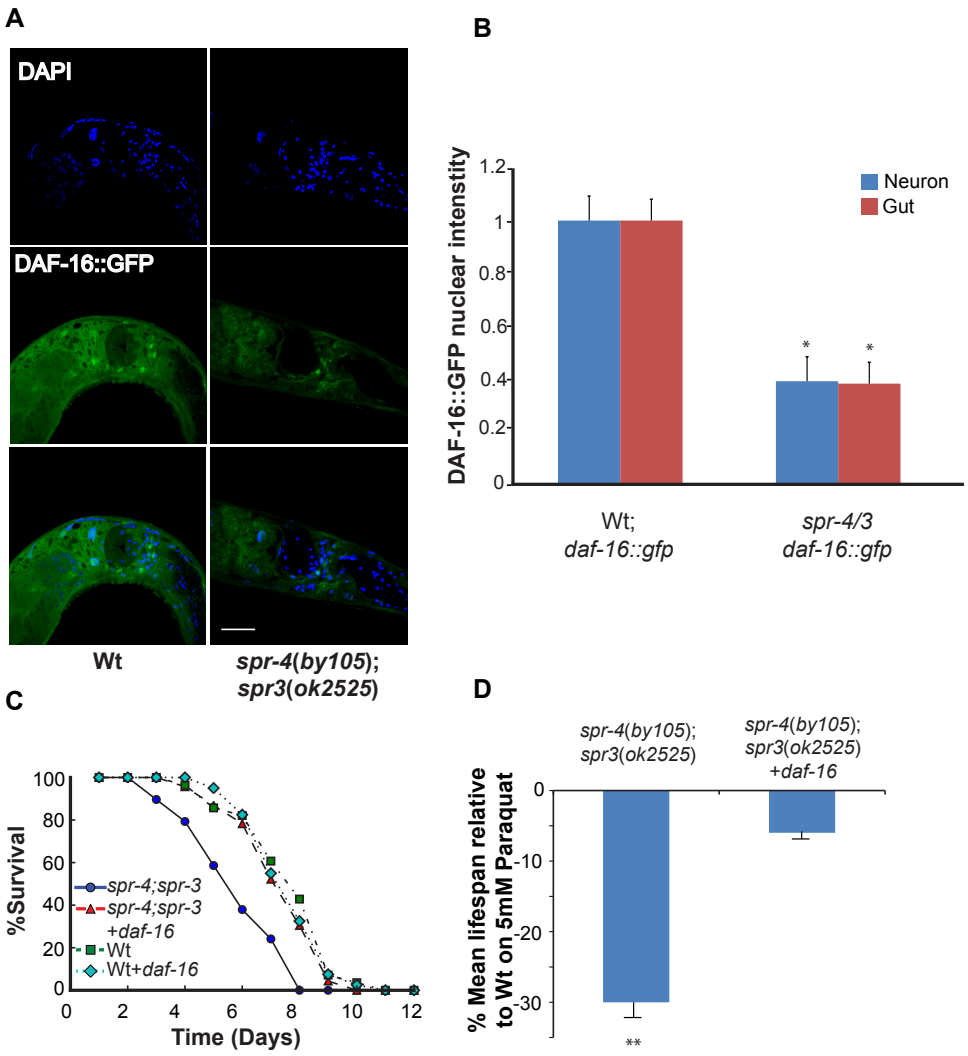

Figure 3.10: **spr mutations impair *daf-16* levels. A.** Worms bearing an integrated *daf-16*::gfp construct were mated to *spr-4*/*spr-3* double mutants and transgene bearing homozygous mutant progeny were isolated from the F2 generation. Animals were plated to 10 mM paraquat for 3 days to induce oxidative stress, picked off the plate, fixed, stained with DAPI, and assayed for DAF-16::GFP nuclear translocation by confocal microscopy. Shown are representative images. **B.** Quantification of the experiments described in A. **C.** Transgenic rescue of *spr-4*/*spr-3* double mutant paraquat sensitivity by *daf-16* overexpression. Two independent *spr-4*/*spr-3* double mutant and wildtype lines bearing either myo-mCherry;*daf-16*::GFP or myo-2::mCherry extrachromosomal arrays were incubated continuously on plates containing 5 mM paraquat and 100 μg/μl FUDR. Shown is the time course of survival from a representative experiment replicated three times. **D.** Quantification of mean lifespan relative to wildtype myo-2::mcherry controls from 3 independent experiments, utilizing two independent lines per genotype per experiment.

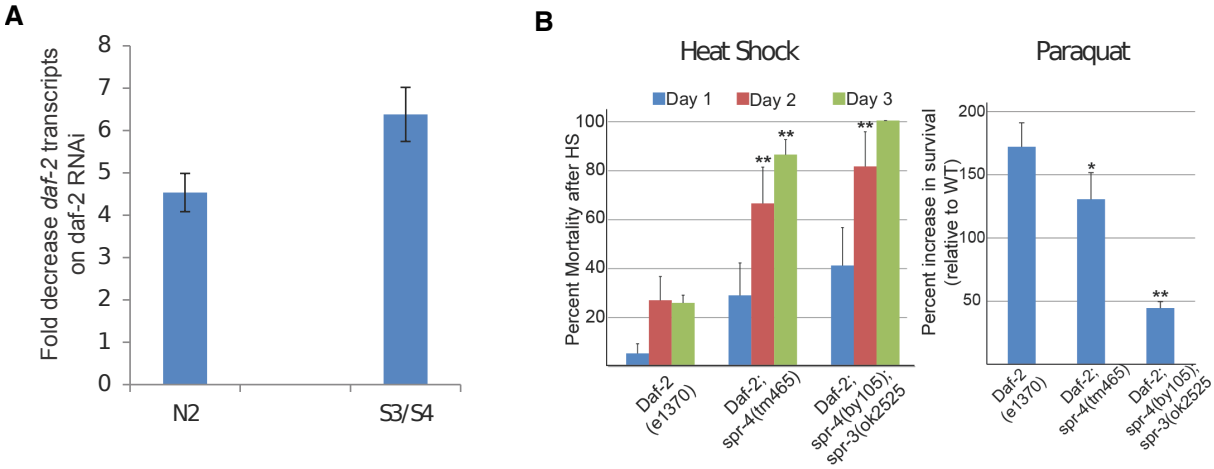

Figure 3.11: **spr mutants exhibit sensitivity to oxidative and thermal stress, and are crucial for *daf-2*-mediated stress resistance. A.** Confirmation of *daf-2* knockdown by RNAi. $n = 2$ independent treatments with 2 plates per group. **B.** Mean survival rates for spr mutants in a *daf-2* mutant background for heat shock and paraquat stress resistance assays. For heat shock, Day 1 adults (24 hours post L4) of the indicated genotypes were plated to standard NGM media and heat shocked for a sublethal interval of 6 hrs at 34 ℃. Every 24 hours following, plates were scored for viability by reactive movement to prodding with a sterilized platinum wire. Shown are the averaged data from 2 independent experiments, using approximately 25 animals per plate, and utilizing two plates per genotype (for a total approximately $n = 50$ per experiment). For paraquat, worms were assayed as in Figure 3.10C, with the paraquat concentration being increased to 15 mM.

downregulates IIS, this is a potential mechanism for suppression of this pathway by REST. These results suggest that REST induces FOXO1 in part by inhibition of insulin/IGF-1 signaling. Thus, REST is likely to regulate insulin signaling by affecting multiple components of the insulin/IGF-1 signaling pathway.

Discussion

Here we have shown that REST regulates the expression and nuclear localization of forkhead transcription factors from worms to humans. REST and orthologous spr genes provide protection against oxidative stress in part through induction of FOXO1 or *daf-16*, respectively. Furthermore, the REST-FOXO1 pathway is upregulated in aging human neurons, where it may protect against neurodegeneration and cognitive decline.

There is a large body of evidence showing that FOXO proteins protect against oxidative stress by promoting the expression of genes that reduce the levels of reactive oxygen species, such as catalase (Alcendor $\mathrm{et\ al.}$, 2007; Choi $\mathrm{et\ al.}$, 2009). FOXO1 deficiency is associated with increased reactive oxygen species (Sengupta $\mathrm{et\ al.}$, 2011). Conversely, we have found that oxidative stress induces both REST and FOXO1, and that REST-deficient cells have reduced FOXO1 expression at baseline and after treatment with paraquat, and that this is associated with reduced cell viability (Figure 3.2). Interfering with FOXO1 function using a dominant negative FOXO1 construct also reduced the oxidative stress protection provided by REST (Figure 3.3A). Further, FOXO1-deficiency sensitizes to oxidative stress *in vitro* (Figure 3.2, Figure 3.3), and REST-deficient, FOXO1 knockdown, and REST-deficient-FOXO1 knockdown cells were all equally sensitive to paraquat treatment (Figure 3.3B), suggesting that the oxidative stress sensitivity of REST-deficient cells is due, at least in part, to reduced FOXO1. Regulation of FOXO1 by REST may contribute to oxidative stress protection in the aging human brain because we find that REST and FOXO1 expression are highly correlated and the proteins colocalize. Importantly,

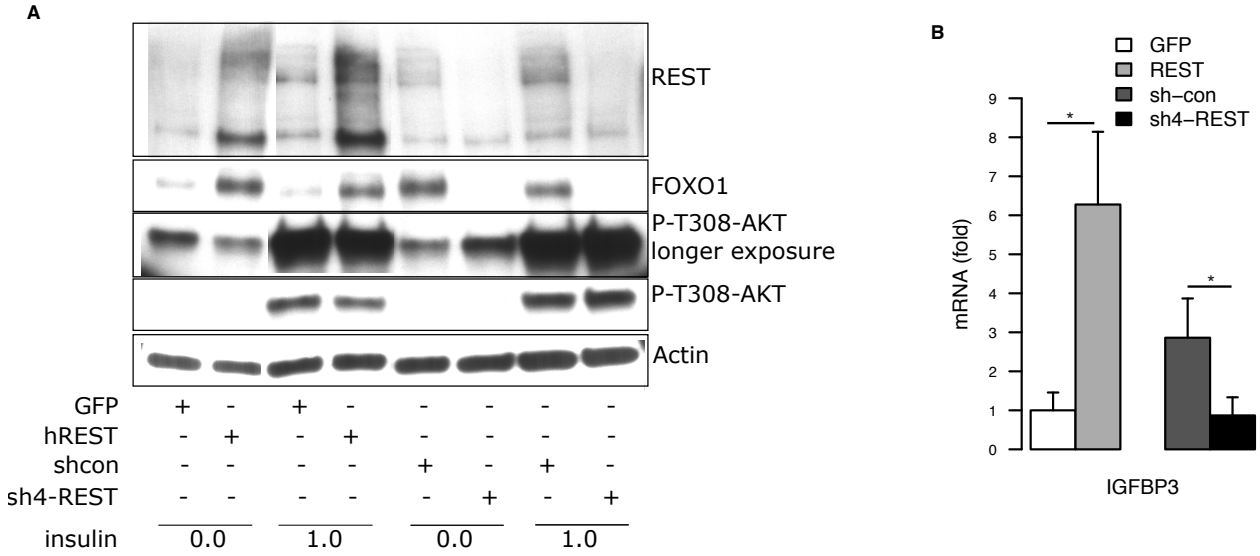

Figure 3.12: **REST regulates FOXO1 protein levels partially through the insulin signaling pathway. A.** SH-SY5Y were transduced with lentivirus to modulate REST levels. For overexpression control (GFP) or human REST (hREST) were used. For knockdown a control short hairpin (shcon) or short hairpin against REST (sh4-REST) were used. Cell medium was changed to low serum medium (1% serum) for 24 hours followed by 0 ng/mL or 1 ng/mL insulin in low serum medium for 24 hours before cell lysates were prepared for Western blotting. Some internal lanes were cropped out to simplify the figure. **B.** In SH-SY5Y cells REST levels were altered by lentiviral transduction using viruses encoding control (GFP) or REST for overexpression or short hairpin control (sh-con) or short hairpin against REST (sh4-REST) for knockdown. Expression was normalized to β-actin. Values represent fold change relative to control, and represent the mean $\pm$ SE. $n = 3$ per group. * $p < 0.05$, t-test.

REST and FOXO1 expression are positively correlated with the expression of genes that directly protect against oxidative stress, such as catalase and periredoxin-6, as well as genes that regulate the oxidative stress response, such as NRF2 and SIRT1 (Figure 3.6).

Our findings suggest that FOXO regulation by REST is evolutionarily conserved from worms to humans. Moreover, the REST ortholog *spr-4* promotes longevity when overexpressed, consistent with the correlation between REST nuclear levels and longevity in humans. In the worm, stress resistance and longevity are closely related. In worms, lifespan extension and stress resistance are mediated by several pathways (Boulias and Horvitz, 2012; Hamilton et al., 2005; Hansen et al., 2005; Kenyon et al., 1993; Landis and Murphy, 2010), most of which are integrated through effects on *daf-16*/FOXO generally through modulation of IIS. We have found that *spr-3* and *spr-4* are non-redundantly required for the lengthened lifespan of *daf-2* mutant worms with reduced IIS. Consistent with this phenotype, DAF-16 protein levels are reduced in spr loss of function mutants following the induction of oxidative stress by paraquat. This is likely a key deficiency in the stress phenotypes of these worms, as *daf-16* overexpression rescues the paraquat sensitivity of the *spr-4*/*spr-3* double mutants to wildtype levels. These findings provide additional evidence for the role of REST in the stress resistance and lifespan effects of forkhead transcription factors. They also provide the first direct evidence that REST promotes longevity.

Adult worms have little programmed cell death, as the soma of these animals is entirely postmitotic (Kimble and Hirsh, 1979; Sulston and Horvitz, 1977). As such, the protective mechanism for spr activity is unlikely to include the suppression of apoptosis following *daf-16* induction. However, FOXO proteins can promote apoptosis in a context-dependent manner by activating expression of pro-apoptotic genes, such as BIM, TRAIL, BNIP3, and PUMA (Zhang et al., 2011b), which could be detrimental for neuronal survival in the aging brain. In this regard, it is noteworthy that REST and FOXO1 expression are positively correlated with the anti-apoptotic gene BCL2, but are not correlated, or are

inversely correlated, with the FOXO1 pro-apoptotic target genes BIM, BNIP3, TRAIL, and PUMA (Figure 3.6). This suggests that FOXO1 induction by REST is not detrimental. One possibility is that FOXO1 is protective because REST not only induces FOXO1, but also represses pro-apoptotic FOXO1 target genes. In support of this hypothesis, we have shown that REST directly binds to and represses pro-apoptotic FOXO1-induced genes, including BIM/BCL2L11 and PUMA/BBC3 (Lu et al., 2014), and that REST expression is inversely correlated with PUMA expression (Figure 3.6, (Lu et al., 2014)). Another possible contributory mechanism may be modulation of FOXO1 transcriptional activity by REST. REST may indirectly promote the deacetylation of FOXO1, which could shift FOXO activity from apoptosis-promoting to stress resistance (Brunet et al., 2004). Overall, our findings support the idea that FOXO1 activity is specifically tuned for stress resistance and neuroprotection in the aging brain, and that this contributes to the neuroprotective and longevity-promoting effects of REST.

Methods

Chemicals and antibodies

DMSO, paraquat, H_2O_2, and insulin were from Sigma. Antibodies: FOXO1 (Cell Signaling Technology C29H4), FOXO1 (LS Biosciences), phospho-T308-AKT (Cell Signaling Technology C31E5E), beta-actin (Sigma A2103), REST (Millipore 05-579), REST (Bethyl IHC-00141).

Brain sample procurement and description

Postmortem human brain material was procured in accordance with institutional guidelines governed by approved protocols. Tissue samples were procured from the Rush University Medical Center, the University of Maryland, Duke University, the Brigham and Womens

Hospital, and the Massachusetts General Hospital. Tissue samples from Rush University Medical Center were derived from participants in the Religious Order Study (ROS) and Rush Memory and Aging Project (MAP) at the Rush Alzheimers Disease Center, which are longitudinal, clinical-pathologic studies of aging, cognitive decline and AD (Bennett et al., 2012a,b). Study participants agreed to comprehensive annual clinical and neuropsychological evaluation and brain donation at death. Autopsy cases in the Religious Orders and MAP studies underwent a uniform structured neuropathologic evaluation of AD, including assignment of Braak (measure of number and distribution of neurofibrillary tangles), CERAD (Aβ plaque pathology), and NIA-Reagan (composite measure of neurofibrillary tangles and amyloid plaques) scores. The clinical diagnoses of AD and MCI have been described in detail and pathologic confirmation of AD approaches 90% (Bennett et al., 2006, 2002; Schneider et al., 2009). Frozen brain tissue specimens used in this study were from the prefrontal cortical grey matter (Brodmann area 9, 10) and were snap-frozen and stored at -140℃. Paraffin-embedded brain samples were also obtained from the Massachusetts General Hospital and Brigham and Womens Hospital. These samples included young adult cases without neurological abnormalities, aged subjects that did not carry a diagnosis of AD or another neurodegenerative disease and showed neuropathological findings within the normal range for age, and cases of AD, FTD and DLB with clinical histories of these disorders and subsequent pathological confirmation.

Immunohistochemical analysis of human and mouse brain and quantification of nuclear levels

Immunohistochemical analysis of human brain. Immunohistochemical analysis using paraffin-embedded brain sections was performed in the prefrontal cortex (Brodmann areas 9, 10 and 47). Paraffin-embedded tissue sections were first deparaffinized in xylene, then rehydrated with decreasing concentrations of ethanol and placed in water. Sections

then underwent antigen retrieval using either citrate buffer (Vectorlabs, USA) or the Diva decloaker (BioCare, USA). For diaminobenzidine (DAB) labeling, sections were additionally treated with 3% hydrogen peroxide for 30 minutes. They were then washed and blocked with 3% BSA, 0.2% Triton X-100 in PBS for 1 hr at room temperature. Primary antibodies were diluted in 2% BSA, 0.1% Triton in PBS. Following overnight incubations, sections were washed three times with PBS. Secondary antibodies, diluted in 2% BSA, 0.1% Triton in PBS were either biotin-coupled (1:200, Vector Labs, USA) or coupled to Alexa fluorophores (1:300, Invitrogen). For DAB labeling, sections were additionally incubated with a pre-formed biotin-avidin-HRP complex (1:100, VectorLabs). For immunofluorescence labeling, sections were also incubated with 1% Sudan Black in 70% ethanol, for 10 minutes, to suppress lipofuscin autofluorescence. Following washes in PBS, sections were mounted and imaged using confocal or bright field microscopy. The following antibodies have been used for immunolabeling studies: (i) a rabbit polyclonal IgG recognizing a region between residues 1050 and the C-terminus (residue 1097) of REST (Bethyl laboratories, IHC-00141); (ii) a goat polyclonal IgG recognizing the C-terminal region of FoxO1a (LSBio B4151).To quantify immunofluorescence or DAB labeling, images that were randomly acquired in selected brain regions. Antigen-expressing areas within each neuron (such as the nucleus) were selected using the Metamorph image analysis system or ImageJ and the average signal intensity measured. Values were corrected by subtracting the average slide background intensity (measured outside of cells). At least 25 neurons were analyzed for each case. The investigator was blinded to sample origin or diagnosis.

Immunohistochemical and histological analysis of mouse brain. Mice were anesthetized with isofulorane and carbon dioxide and then perfused with cold PBS buffer for 20 minutes. Brains were rapidly removed and placed in 4% PFA overnight. They were then processed for paraffin embedding, according to standard procedures. The investigator was blind to the genotype.

To assess the relationship between the levels of nuclear REST protein and FOXO1,

we performed double-label immunofluorescence for REST and each individual protein or marker. Multiple 20–40× pictures were acquired (at various locations) within the prefrontal cortex displaying pyramidal neurons using an Olympus Fluoview Confocal Microscope. For cases displaying a majority of pyramidal neurons with very high (or very low) nuclear REST levels, fields were also included that displayed lower (or higher, respectively) REST levels, to test for potential correlations between REST and each target. Antigen-expressing areas within each neuron (such as the nucleus or the cytoplasm) were selected using the Metamorph image analysis system and the average signal intensity was measured. Values were corrected by subtracting the average slide background intensity (measured outside of cells). At least 25 pyramidal neurons were quantified for each case.

To determine the number of FOXO1-positive neurons in $REST^{lx/lx}$ and $REST^{-/-}$ mice we imaged coronal brain sections at 20× at the level of the lateral striatum. In each image we selected the region corresponding to cortical layers 4–5 and counted large cells that had clear DAB brown staining. Data are expressed as the number of FOXO1-positive neurons per unit area.

Immunocytochemical analysis of cultured cells

Cells plated on polylysine-coated coverslips were fixed by incubation with 4% (v/v) paraformaldehyde in PBS for 30 minutes at room temperature, followed by three washes in PBS, and then permeabilized with 0.1% Triton X-100 in PBS for 15 minutes at room temperature. After 3 additional washes in PBS, cells were blocked with 10% goat serum in PBS for 1 hour at room temperature. Primary antibodies were diluted to the appropriate concentration using 10% goat serum, and incubated overnight at 4℃. Cells were then washed 3 times in 1% goat serum in PBS for 10 minutes before adding fluorophore-conjugated secondary antibodies for 2 hours at room temperature. Fluorophore labeled cells were then washed in 1% goat serum in PBS for 3× 10 minutes, and then mounted using Prolong Gold mounting medium with DAPI and anti-fade reagent (Invitrogen). The

nucleus was delineated by DAPI-positive staining, and REST and FOXO1 nuclear levels were were manually quantified using ImageJ.

Image acquisition.

Images were acquired using an Olympus Fluoview confocal microscope, or using a bright field microscope coupled to a CCD camera (Diagnostic Instruments, Inc.).

Cell culture

SH-SY5Y, a human neuroblastoma cell line, were from ATCC. Cells were maintained at 37℃ in a 5% CO_2 humidified incubator. Cells were cultured in compete medium (10% fetal bovine serum (FBS, heat inactivated 30 minutes at 56℃), 100 units/mL penicillin, 100 μg/mL strepomycin, 1mM glutamax in Dulbecco's Modified Eagle Medium (DMEM, with 4.5 mg/L D-glucose) (all from Invitrogen)). Cells were split every 2–3 days. 4×10^5 cells/mL cells were plated per well unless otherwise stated.

MEFs were derived from $REST^{lx/lx}$ mice (Chapter 2). MEFs were cultured the same as SH-SY5Y cells except they were split every 2 days. MEFs were immortalized with SV40 T antigen and used for up to 10 passages. To generate $REST^{-/-}$ MEFs $REST^{lx/lx}$ MEFs were infected with a Cre virus, and knockout was confirmed by PCR genotyping.

To generate stable FOXO1-DN and control lines, SH-SY5Y cells were transiently transfected with FOXO1-DN plasmid or control plasmid using Lipofectamine 2000. Two days later medium was changed to medium containing 2 μg/mL neomycin with medium changes every 3 days. Cells were maintained under selection for two weeks before use.

Cell culture treatments

Treatments were performed by changing medium to fresh medium with the specified concentrations of the compound. H_2O_2 and paraquat were prepared in water.

Assessment of cell viability

Cell viability was assessed using a chromogenic assay that involves the biological reduction by viable cells of the tetrazolium compound 3-(4,5-dimethylthiazol-2-yl)-5-(3-carboxymethoxyphenyl)-2-(4-sulfophenyl)-2H-tetrazolium (MTS). Treatments and assays were performed in 96-well plates in 100 μl complete medium with the specified compounds. After treatments, cell medium was changed to 120 μl complete medium containing 20 μl MTS reagent following manufacturer's instructions and assayed 1–4 hours later. Absorbance at 490 nm was measured using a plate reader.

RT-qPCR

To extract RNA Trizol (Invitrogen) with DNase I digestion for brain tissue and Trizol or miRNeasy mini kit with on-column DNase I digestion for cells. Primers were designed using NCBI primer-BLAST to span exon boundaries if possible. PCR or real-time PCR were run for 40 cycles. The purity of RT-qPCR products was determined by single peak melting curves. β-actin was used normalization.

Primers

Table 3.1: **Primer sequences for mammalian experiments.**

Gene	Note	Sequence (5' to 3')
β-actin	RT-qPCR	F: CATGTACGTTGCTATCCAGGC
		R: CTCCTTAATGTCACGCACGAT
REST	RT-qPCR	F: GCCGCACCTCAGCTTATTATG
		R: CCGGCATCAGTTCTGCCAT
FOXO1	RT-qPCR	F: TCGTCATAATCTGTCCCTACACA
		R: CGGCTTCGGCTCTTAGCAAA
IGFBP3	RT-qPCR	F: AGAGCACAGATACCCAGAACT
		R: GGTGATTCAGTGTGTCTTCCATT

Western blotting

Tissues were homogenized using RIPA-DOC buffer supplemented with protease and phosphatase inhibitors (Complete and Phosphostop, Roche). A sonication step was performed prior to centrifugation at 10,000 rpm for 10 min at 4C. The supernatant was removed and the protein concentration determined (BioRad protein assay). $2\times$ laemmli buffer containing beta mercaptoethanol was added. Cells were directly lysed in $2\times$ laemmli buffer. Approximately 20 μg protein was loaded per lane and resolved by 4–20% Mini-PROTEAN TGX precast gels (Biorad). Western blots were quantified by densitometry using the ImageJ software. Bands of interest were normalized to beta-actin which served as a loading control.

Microarray analysis

SH-SY5Y cells that express REST-GFP were isolated by FACS into low, middle and high expression populations based on GFP intensity, and the corresponding REST levels were determined by RT-qPCR. Gene expression profiling was performed using Affymetrix U133plus2 microarrays. Expression data were normalized by gcrma and analyzed using the limma Bioconductor package using a moderated t-test in R. Benjamini and Hochberg false discovery rate (FDR) was calculated in R. Only genes that met all of the following criteria were considered: A. significantly different compared to control with FDR < 0.05 in both REST overexpression and REST knockdown; B. REST overexpression and REST knockdown had opposite direction of change relative to control; and C. annotated with GO biological process response to oxidative stress; response to reactive oxygen species; response to hydrogen peroxide; response to oxygen radical; and response to superoxide (Tothova $\mathrm{et\ al.}$, 2007).

Generation of recombinant lentiviruses

Viral particles were generated in HEK293T cells by co-transfection of transfer vectors, packaging plasmid (pRSV-REV and pMDLg) and envelope plasmid (pCMV-VSVG) using Lipofectamine 2000 (Invitrogen). Cells were cultured for 2 days and the medium was collected, centrifuged at 1000$\times$g for 5 min, and passed through a 0.45 μm low protein binding filter (VWR).

Lentiviral transduction

Approximately 8×10^4 SH-SY5Y cells or 1×10^4 MEFs were plated in a 6-well dish. 14–20 hours later medium was changed and lentiviral containing supernatants were added. 2 days later medium was changed and cells were split. Transduced cells were used typically 4–7 days after transduction.

cDNA constructs and shRNAs

Lentiviral constructs for overexpressing REST in FUGW vector and knocking down REST in pGIPZ vector have been described (Chapter 2, Lu $\mathrm{et\ al.}$ (2014)). sh-FOXO1 hairpin was created in PLVTHM vector (Wiznerowicz and Trono, 2003) with FOXO1 targeting sequence `GAGCGTGCCCTACTTCAAG`. sh-con for sh-FOXO1 had targeting sequence `GCGCGATAGCGCTAATAAT`.

RNA-seq data and expression analysis

RNA-seq data was generated and processed by Rush Alzheimer's Disease Center from ROSMAP participants. RUSH processed data as follows. We have extracted RNA from the gray matter of the dorsolateral prefrontal cortex of 724 subjects from the ROS and MAP cohorts. These samples were extracted using Qiagen's miRNeasey mini kit (cat. no.

217004) and the RNase free DNase Set (cat. no. 79254). These samples were quantified by Nanodrop and quality was evaluated by Agilent Bioanalyzer. The Broad Institutes's Genomics Platform performed RNA-Seq library preparation using the strand specific dUTP method (Levin $\mathrm{et\ al.}$, 2010) with poly-A selection (Adiconis $\mathrm{et\ al.}$, 2013). This method begins with poly-A selection followed by first strand specific cDNA synthesis, and then uses dUTP for second strand specific cDNA synthesis followed by fragmentation and Illunmina adapter ligation for library construction. We have completed RNA-Seq with 582 of the samples that met quality (Bioanalyzer RNA integrity (RIN) score $>$5) and quantity thresholds (5 μg). Sequencing was performed on the Illumina HiSeq with 101 bp paired-end reads and achieved coverage of 150M reads of the first 12 samples. These 12 samples will serve as a deep coverage reference and included 2 males and 2 females of non-impaired, mild cognitive impaired, and Alzheimer's cases. The remaining samples were sequenced with coverage of 50M reads. The libraries were constructed and pooled according to the RIN scores such that similar RIN scores would be pooled together. Varying RIN scores results in a larger spread of insert sizes during library construction and leads to uneven coverage distribution throughout the pool. In our sample set, we noticed that samples with lower RIN scores between 5 and 6 had more adapter contamination. An additional 57 samples were submitted at a later date to the platform and run on an updated protocol requiring only 250ng of input RNA. This protocol is a modification of Illumina's TruSeq protocol to include long insert sizes and also be strand specific. Then RNA-Seq data were processed by our parallelized and automacte pipeline. These pipeline include trimming the begining and endding bases from each read, identifying and trimming adapter sequences from reads, detecting and removing rRNA reads, aligning reads to reference genome. We used the non-gapped aligner Bowtie to align reads to transcriptome reference and then applied RSEM to estiamte expression levels for all transcripts. The FPKM values were the outcome of our data RNA-Seq pipeline. We applied quantile normalization method to FPKM first and then used combat package to remove potential batch effect.

From this processed data we selected data from 179 cognitively-intact aged individuals which was log-transformed for analysis. Genes with variance 0 or expressed by less than 25% of the individuals were removed leaving 25786 genes. Each remaining gene's expression was regressed on REST or FOXO1 using a linear model and the significance of the regression coefficient was corrected for $(25786 - 1) \times 2 = 51570$ tests by the Bonferroni correction method.

C. elegans strains

The N2 Bristol strain was used as the wild-type background for these studies. C. elegans strains were cultured at 20℃ under standard conditions (Brenner, 1974). The following mutations and chromosome rearrangements were used: LGI: *spr-4*(by105) (Lakowski $\mathrm{et\ al.}$, 2003), *spr-4*(tm465) (Lu $\mathrm{et\ al.}$, 2014), *daf-16*(mu86) (Kenyon $\mathrm{et\ al.}$, 1993), hT2[bli-4(e937) qIs48] (I;III); LGIII:*daf-2*(e1370) (Kenyon $\mathrm{et\ al.}$, 1993); LGV: spr-1(ok2144) (Jarriault and Greenwald, 2002); and LGX: *spr-3*(ok2525) (Lu $\mathrm{et\ al.}$, 2014); EG7215(oxTi334 [eft-3p::TdTomato::h2b::unc-54 3'UTR + Cbr-unc-119(+)]). All strains, except for *spr-4*(tm465), were provided by the Caenorhabditis Genetics Center (CGC), which is funded by the NIH Office of Research Infrastructure Programs (P40 OD010440). Strains obtained from external sources which had been outcrossed previously were outcrossed to lab strain N2 worms twice. Worms which had not been outcrossed previously were outcrossed six times before use.

spr-5 mutants exhibit transgenerational effects, including increased defects in double strand break repair and germline apoptosis (Katz $\mathrm{et\ al.}$, 2009; Nottke $\mathrm{et\ al.}$, 2011) as well as lifespan effects (Greer 2016, Cell Research). Although we have not fully evaluated the transgenerational phenotypes of *spr-3* and *spr-4* alleles, as a precaution, all assays were performed with animals no more than 5 generations removed from a heterozygote ancestor. To facilitate this, *spr-4* alleles were carried over the ht2 balancer described above, while *spr-3*(ok2525) was carried over the MosTIC (Robert $\mathrm{et\ al.}$, 2009) insertion

oxTi335, which carries a eft-3::tdTomato::h2b fluorescent fusion construct integrated in the X chromosome at 4,348,071bp. Since *spr-3* is located on the X chromosome at 4,514,00 bp, this effectively marked wildtype *spr-3*, allowing us to maintain heterozygous stocks of our double and single mutants.

The *daf-16*::gfp fusion line TJ356, bearing transgene zIs356 [*daf-16*p::*daf-16*a/b::GFP + rol-6], was mildly anesthetized with 0.01% tetramizole and outcrossed to lab wildtype males (10/hermaphrodite) twice, and then mated to *spr-4*(by105);*spr-3*(ok2525) double mutants. Double mutants bearing zIs356 were recovered and propagated.

RNAi in *C. elegans*

Feeding RNAi experiments were performed at 20°C as described (Kamath and Ahringer, 2003). A feeding clone containing a full length *daf-2* cDNA was a received from the Blackwell lab. Control RNAi was performed by feeding HT115 bacteria carrying the empty pL440 vector. Clones were sequence validated and, where indicated, knockdown was confirmed by RT-qPCR.

Microinjection and transgenic strains

For rescue strains transgenic *C. elegans* lines were generated by microinjecting the relevant constructs into the gonads of the indicated strains (Evans TC Wormbook 2006). Prab-3::mCherry (pGH8, Addgene: 19359) or pmyo-2::mCherry (pCFJ90, Addgene 19327): were used as coinjection markers. Three independent lines that demonstrated reliable transmission of the marker were propagated as described above for each experiment. For the dCas9::VP64 experiments, a peft-3::dCas9::VP64::tbb-2 utr construct was cloned using the Wormgate Gateway recombination system into the pCFJ151 MosSCI destination vector (Cloning, genotyping and plasmids). The EG6699 strain, bearing the ttTi5605, MosSCI integration site on chromosome II (at 8.42 MB) was raised on HT115 and microinjected as

Table 3.2: *C. elegans* strains used in this chapter.

Strain	Genotype	Notes
BAY1	*spr-4(by105);spr-3(ok2525)*	
BAY2	*spr-4(tm465);daf-2(e1370)*	
BAY3	*spr-4(by105);daf-2(e1370)*	
BAY4	*spr-4(by105);daf-2(e1370);spr-3(ok2525)*	
BAY6	*spr-4(by105);spr-3(ok2525);* *zIS356 I[daf-16p::daf-16a/b::GFP+ rol-6]*	Made by mating BAY4 to TJ356
BAY7	*unc-119(ed3);* *yanSI1[peft-3::dCAS9::VP64::tbb-2utr; Cbr-unc-119]*	yanSI is a MOSsci integration at ttTI5605 site(II: 8.42 MB) in strain EG6699. Integration plasmid was generated via 3-way gateway reaction with pCFJ150 and plasmids containing eft-3 promoter(ID: 1031@E02 promoterome), tbb-2 utr (pCM1.36), and a full length dcas9::VP64 transgene cloned into pDONR201.
BAY8	*unc-119(ed3); yanEx1;yanSI1*	yanEx 1 is an extrachromosomal array carrying 4 spr-4 targetting sgRNAs, injected at 5ng/ul each, along with 5ng/ul myo-2::mcherry;unc54utr (pCFJ90)
BAY9	*unc-119(ed3); yanEx2;yanSI1*	yanEx 2 is an extrachromosomal array carrying 4 spr-4 targetting sgRNAs, injected at 5ng/ul each, along with 5ng/ul myo-2::mcherry;unc54utr (pCFJ90)
BAY10	*unc-119(ed3); yanEx3;yanSI1*	yanEx 3 is an extrachromosomal array carrying 4 spr-4 targetting sgRNAs, injected at 5ng/ul each, along with 5ng/ul myo-2::mcherry;unc54utr (pCFJ90)
BAY11	*yanEx1*	yanEx 1 is an extrachromosomal array carrying 4 spr-4 targetting sgRNAs, injected at 5ng/ul each, along with 5ng/ul myo-2::mcherry;unc54utr (pCFJ90)
BAY12	*yanEx2*	yanEx 2 is an extrachromosomal array carrying 4 spr-4 targetting sgRNAs, injected at 5ng/ul each, along with 5ng/ul myo-2::mcherry;unc54utr (pCFJ90)
BAY13	*yanEx3*	yanEx 3 is an extrachromosomal array carrying 4 spr-4 targetting sgRNAs, injected at 5ng/ul each, along with 5ng/ul myo-2::mcherry;unc54utr (pCFJ90)
BAY14	*spr-4(tm465);unc-119(ed3);yanSI1;yanEx1*	
BAY15	*spr-4(tm465);unc-119(ed3);yanSI1;yanEx3*	
BAY16	*spr-4(tm465);yanEx1*	
BAY17	*spr-4(tm465);yanEx3*	
BAY19	*yanEx4*	extrachromosomal array consisting of 50ng/ul pkL79 (full length daf-16::gfp fosmid) and 5ng/ul pCFJ90 (myo-2::mCherry)
BAY20	*yanEx5*	extrachromosomal array consisting of 50ng/ul pkL79 (full length daf-16::gfp fosmid) and 5ng/ul pCFJ90 (myo-2::mCherry)
BAY21	*yanEx6*	extrachromosomal array consisting of 5ng/ul myo-2::mCherry and 50ng/ul 1kb DNA ladder (NEB)
BAY22	*yanEx7*	extrachromosomal array consisting of 5ng/ul myo-2::mCherry and 50ng/ul 1kb DNA ladder (NEB)
BAY23	*spr-4(by105);spr-3(ok2525);yanEx4*	generated by crossing BAY11 to BAY1
BAY24	*spr-4(by105);spr-3(ok2525);yanEx5*	generated by crossing BAY12 to BAY1
BAY25	*spr-4(by105);spr-3(ok2525);yanEx6*	generated by crossing BAY13 to BAY1
BAY26	*spr-4(by105);spr-3(ok2525);yanEx7*	generated by crossing BAY14 to BAY1
BAY27	*yanIS1[pspr-4::spr-4::GFP::spr-4utr]*	Created by microparticle bombardment of HT1593(unc-119(ed3)) worms with the transgenome construct: 3167840880351681 C09 containing a GFP-tagged spr-4 allele
TJ356	zIs356 IV[daf-16p::daf-16a/b::GFP + rol-6]	outcrossed to lab N2 strains 2x
EG6699	*ttTi5605 II; unc-119(ed3) III; oxEx1578.*	outcrossed to lab N2 strains 4x
HT1593	unc-119(ed3)	outcrossed to lab N2 strains 7x

described (Frøkjaer-Jensen et al., 2010). Integration was confirmed by genotyping, as well as the absence of unc- progeny. These worms were then microinjected with a cocktail of 4 sgRNAs (5ng/ul each) generated by nested overlap PCR (see Cloning, genotyping and plasmids), along with a pGH8 myo-2::mcherry (10 ng/μl) as a marker. 3 transgenic lines from independent injects were selected. The SPR-4::GFP reporter line was generated by microparticle bombardment using the fusion construct and bombardment protocol as described (Sarov et al., 2012) (see Cloning and Genotyping for additional detail).

Transcript analysis in *C. elegans*

To analyze RNA from the transgenic lines, 100 worms (24 hours post-L4) of each strain (including controls) were placed into 1.5 mL M9 buffer. Worms were washed once in M9, pelleted by centrifugation, resuspended in 200 μl Trizol, vortexed for 2 minutes and flash frozen in liquid nitrogen. Worms were then freeze-cracked by thawing in a 37℃ water bath and re-freezing in liquid nitrogen. This was repeated 2 more times. After the final thaw, 100 μl of Trizol was added and the tubes were maintained at room temperature for 5 minutes. RNA was then extracted with 140 μl of chloroform, precipitated with an equal volume of 70% ethanol and transferred to an RNeasy spin column (Qiagen) and purified. RT-qPCR was performed directly from isolated RNA, using 1 ng of RNA and the Qiagen One Step qPCR mix. All reactions were performed in triplicate.

C. elegans lifespans and stress treatments

For heat shock experiments, 2 replicates per genotype of 30 adult worms (12–24 hours post L4) were transferred to NGM agar plates seeded with OP50 E. coli. For N2 (wt) background animals, the plates were placed in at 34 ℃ incubator for 5 hours. Worms with a *daf-2* mutation were heatshocked for 6.5 hours, in order to induce an equivalent mortality rate (compared to N2). In both cases, worms were transferred back to 20℃, and

scored daily for viability (as assessed by reactive movement to prodding with a platinum wire) up to 72 hours post heat shock. For paraquat experiments, freshly resuspended paraquat (1M stock, methyl viologen, Sigma 856177-1G) was added at 5, or 15 mM (*daf-2* experiments) along with 100 μg/mL FUDR (Sigma, F0503-1G) NGM media before pouring. Within 48 hours, plates were seeded with OP50, and 25–30 adult worms per genotype were transferred from NGM plates, and scored daily for viability (as assessed by reactive movement to prodding with a platinum wire). Lifespan experiments were performed at 20 ℃ unless otherwise noted. For each genotype, 25–30 day 1 worms were transferred to NGM plates containing 100 μg/mL FUDR. Worms were scored for viability every other day, and transferred to fresh plates between day 10 and day 14. For *daf-2* mutant worms, worms were moved again at day 20–24. For all viability-measuring experiments, worms that had burst (interior leaking out through the vulva) or bagged (interior hatching of progeny) were discarded from the plate.

Quantification of DAF-16::GFP fluorescence

For quantification of DAF-16::GFP from the zIs356 transgene, 25–30 worms were transferred to an Eppendorf tube containing M9 buffer, washed once in M9 and pelleted. The supernatant was removed and the pellet was frozen in liquid nitrogen. The day before imaging, worm pellets were thawed in PBS with 4% paraformaldehyde (ThermoFisher) and fixed for 30 minutes at room temperature while rocking. The PFA was removed by washing twice with PBS, with 0.025% Triton (PBST, to prevent sticking), and the worms were stained with DAPI for 10 minutes at room temperature. The DAPI was removed with a final wash in PBST, and the pellet was resuspended in 15 μl of ProLong Gold mounting media (Life Technologies). The worms were transferred, in 12.5 μl of mounting media, to a slide, and gently placed under a coverslip, which was then sealed with clear nailpolish (E.M.S.). Slides were imaged on an Olympus Fluoview confocal microscope, using manufacturer settings for GFP and DAPI (488 and 405 laser, respectively) within 2

weeks of mounting, and all slides compared with each other were imaged on the same day, in the same imaging session. Worms were imaged via a 40$\times$ objective with a 2$\times$ digital zoom. For every worm, Z-stack image series were taken at 2 μm step sizes (roughly 13–15 images per series). To quantify nuclear GFP levels, these Z-stacks were opened in ImageJ (NIH) and flattened using a maximum intensity Z-stack projection. For pharyngeal nuclei, 3 regions of interest (ROI) were selected based on DAPI staining of nuclei, on either side of the pharynx and behind it, encompassing the bulk of the nuclei in that area. Gut nuclei were individually selected using the same ROI tool. These were then used as the ROIs within which to measure GFP fluorescence, using the ImageJ intensity measuring tool.

Cloning and genotyping

Full length *spr-4* was isolated from fosmid DNA (WRM0628bF09, from the Sanger Institute collection) by PCR amplification with primers specific to the promoter regions (1.5 kb upstream of the transcriptional start site) and the UTR. The PCR product was sequence verified and used directly for injection. Human REST was isolated from cDNA and cloned into the vector pD152.79 MCS, downstream of the dpy-30 promoter and upstream of GFP. Sequencing verified the correct reading frame. The SPR-4::GFP fusion fosmid used in bombardment (Clone: 3167840880351681 C09) was provided by the Transgenome consortium (Sarov $\mathrm{et\ al.}$, 2012). This fosmid was also used for PCR-amplification (using the primers described above) of the *spr-4* gene where SPR-4::GFP strains were generated by microinjection.

Primers used for *C. elegans* experiments

Table 3.3: S4-N-B/C are primers for spr-4 overexpression by sgRNAs. For guide RNA internal primers the underlined portion is the sgRNA targeting sequence (5-3') with a GG present in the target sequence, but not the guides themselves.

Name	Sequence (5' to 3')	Use
spr-4(by105) fwd	GTGCCAAATCATATGCGGCT	Primers for genotyping spr-4(by105)
spr-4(by105) REV	ATCCGTACCCTTGTCCACTG	Primers for genotyping spr-4(by105)
spr-4(tm465) fwd	ACAATCTACGGCGCTCGAAA	Primers for genotyping spr-4(tm465)
spr-4(tm465) REV	AGAGGCATCCCAATGCAAGT	Primers for genotyping spr-4(tm465)
daf-2(e1370) fwd	ACCTGGAGTCGCTCAAGTTTTG	Primers for genotyping daf-2(e1370)
daf-2(e1370)REV	TGCTTCGCTTTCATCGGTGTC	Primers for genotyping daf-2(e1370)
Spr-3(ok2525) fwd	tagaactgtgttgtagat	Primers for genotyping spr-3(ok2525)
Spr-3(ok2525) REV	aagagctacttgtcgaaggat	Primers for genotyping spr-3(ok2525)
U6 Forward (A, U6 F)	GATCGATTGAATTCCTCCAAGAACTCGTACAAAAATGCTCTGAAGTAGG	primers to generate guide RNAs by overlap PCR
Tracer reverse (D, U6, R)	GATTACGCCAAGCTTCACAGCCGAC	primers to generate guide RNAs by overlap PCR
S4-1-C Fwd	TGACTCGTACAGTCAGAAAGGTTTTAGAGCTAGAAATAGCAAGTTAAAATAAGGCTAG	interior target specific primers
S4-2-C Fwd	GTACATTGGTGATCTTGATTGTTTTAGAGCTAGAAATAGCAAGTTAAAATAAGGCTAG	interior target specific primers
S4-3-C Fwd	TAACATAAATGTTCGTTTATGTTTTAGAGCTAGAAATAGCAAGTTAAAATAAGGCTAG	interior target specific primers
S4-4-C Fwd	GATACAAAACGCTTAATTTCGTTTTAGAGCTAGAAATAGCAAGTTAAAATAAGGCTAG	interior target specific primers
S4-5-C Fwd	GAATCAAGAATTTTCATAGGGTTTTAGAGCTAGAAATAGCAAGTTAAAATAAGGCTAG	interior target specific primers
S4-6-C Fwd	ATATAAATTCATTCCAAGGTGTTTTAGAGCTAGAAATAGCAAGTTAAAATAAGGCTAG	interior target specific primers
S4-1-B Rev	CTTTCTGACTGTACGAGTCAGAAACATTTAGATTTGCAATTCAATTATATAGGGACCATTT	interior target specific primers
S4-2-B Rev	AATCAAGATCACCAATGTACGAAACATTTAGATTTGCAATTCAATTATATAGGGACCATTT	interior target specific primers
S4-3-B Rev	ATAAACGAACATTTATGTTAGAAACATTTAGATTTGCAATTCAATTATATAGGGACCATTT	interior target specific primers
S4-4-B Rev	GAAATTAAGCGTTTTGTATCGAAACATTTAGATTTGCAATTCAATTATATAGGGACCATTT	interior target specific primers
S4-5-B Rev	CCTATGAAAATTCTTGATTCGAAACATTTAGATTTGCAATTCAATTATATAGGGACCATTT	interior target specific primers
S4-6-B Rev	ACCTTGGAATGAATTTATATGAAACATTTAGATTTGCAATTCAATTATATAGGGACCATTT	interior target specific primers

Chapter 4

REST and age-related cognitive decline

Author Contributions

L.A. performed experiments including immunofluorescence analysis of human brain and quantification of REST nuclear levels. D.D., L.A. and B.A.Y. contributed to the overall study design. D.D. and L.A. performed informatics analysis. D.A.B. contributed tissue samples, cognitive test scores and neuropathological data. B.A.Y. directed the study and B.A.Y., L.A. and D.D. wrote the manuscript, which was edited by all the coauthors. Candidate performed all informatic analysis presented in this chapter.

Introduction

Although several genetic and neuropathological factors contributing to cognitive decline and Alzheimer's disease (AD) have been discovered we still have an incomplete understanding of what causes AD or contributes to the rate of cognitive decline during aging. We showed that nuclear REST levels increase in neurons from cognitively-intact aged individuals but not those with AD (Chapter 2, Lu $\mathrm{et\ al.}$ (2014)). There, REST nuclear levels were shown to positively correlate with cognitive function proximate to death in a cross-sectional analysis

although several questions remained. First, what is the relationship between REST nuclear levels and longitudinal cognitive decline? Are REST nuclear levels are associated with cognitive function independently of neuropathologies? Finally, how much of the variability in cognitive decline do REST nuclear levels account for? To investigate these questions we utilized longitudinal cognitive data and a mixed model analysis to determine how REST nuclear levels influence longitudinal cognitive decline while accounting for neuropathologies. Here we provide evidence that REST nuclear levels are a critical determinant of longitudinal cognitive preservation during aging independent of neuropathologies.

Results

Given that altered REST activity explains a significant fraction of gene expression changes during brain aging (Chapter 2, Lu $\mathrm{et\ al.}$ (2014)) we sought to understand the contribution of REST to cognitive decline and AD neuropathologies during aging. We utilized individuals from the Religious Orders Study and Memory and Aging Project (ROSMAP) at RUSH which are large cohorts with longitudinal cognitive, post-mortem neuropathological, and molecular data from elderly individuals (Bennett $\mathrm{et\ al.}$, 2012$\mathrm{a,b}$). In 122 individuals aged 71–103 from the ROSMAP cohort we quantified REST nuclear levels, as an approximation of active REST, in pyramidal neurons from prefrontal cortex, and we limited our analyses to these individuals as our subset of ROSMAP.

To overview cognitive decline during aging in ROSMAP we created spaghetti plots of global cognitive scores (Figure 4.1). With longitudinal cognitive data one can compute mean cognitive change during aging and an individual's deviation from the mean or "random slope" (Figure 4.2). These plots show there is a large variation in cognitive decline during aging.

To investigate how REST is related to AD neuropathology we first assessed correlations between the neuropathological variables and REST nuclear levels (Table 4.1). Notably,

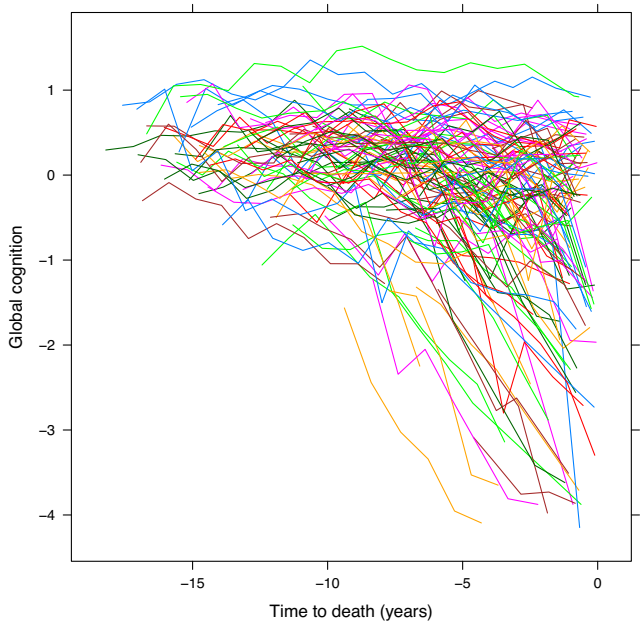

Figure 4.1: **Spaghetti plots of individual global cognitive scores in ROSMAP.**

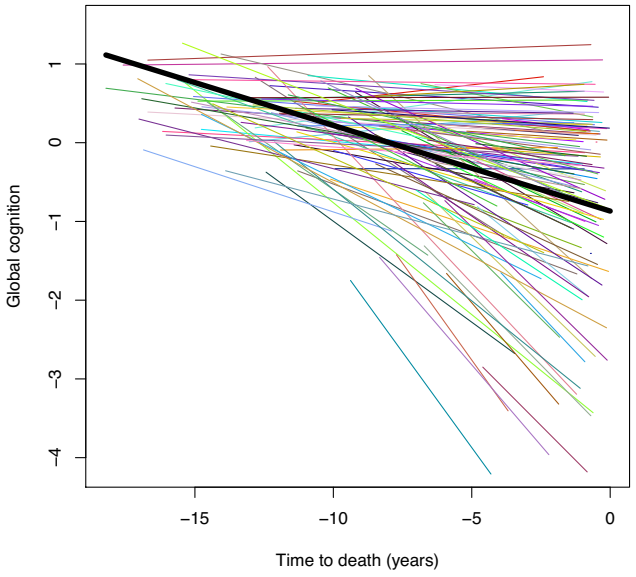

Figure 4.2: **Model-derived individual cognitive random slopes in ROSMAP.** The mean cognitive decline is shown as the bold black line.

REST nuclear levels are significantly inversely correlated with tangles and amyloid and positively correlated with AD age of onset potentially implicating a protective role.

To investigate the relationship between REST nuclear levels and longitudinal cognitive function we initially performed a linear regression of individual-specific random global cognitive slopes on REST nuclear levels (Figure 4.3). This analysis showed that there was a significant correlation between REST nuclear levels and rate of cognitive decline and that individuals with higher REST nuclear levels had a lower degree of cognitive decline during aging. The model was least accurate for individuals with severe AD having MMSE scores ≤ 8 which may suggest that once AD has progressed to late stages of the disease REST nuclear levels are no longer able to influence cognitive function.

To expand on this analysis we used a linear mixed model to investigate the contribution of additional variables in addition to REST nuclear levels to longitudinal cognitive decline. We used measures known to be important for brain aging and AD including quantitative measures of amyloid, tangles, neocortical lewy bodies, gross infarcts, and microinfarcts. First, we determined the association of each neuropathological variable and REST nuclear levels with cognitive decline (Table 4.2). REST nuclear levels are the second most significant contributor to cognitive decline. Then we determined the association all of the neuropathological variables with and without REST nuclear levels simultaneously with cognitive decline (Table 4.3). REST nuclear levels are the second most significant contributor to cognitive decline, and the model with REST nuclear levels and its interaction with time is a significantly better model than the model without REST nuclear levels ($P = 1.141 \times 10^{-6}$, ANOVA). If time was instead modeled forward, as years from birth instead of years to death, the results were nearly identical (data not shown). One interesting observation is how the coefficient of time, which models the cognitive change of the average individual, changes with the inclusion of the REST nuclear levels term (Table 4.3). When the neuropathologies in the full model without REST nuclear levels are accounted for time is not significant although it is significant in the reference model with time as the only term (Table 4.2, time

Table 4.1: **Correlations between neuropathological variables and REST nuclear levels in ROSMAP**. A. Spearman correlations. B. P-value of correlation. Only significant ($P < 0.05$) correlations are shown.

A	amyloid	tangles	gross infarctions	microinfarctions	neocortical lewy bodies	sex	AD age of onset
REST nuclear levels	-0.22	-0.42					0.33
amyloid		0.61					
tangles							
gross infarctions				0.23	-0.19		
microinfarctions							
neocortical lewy bodies							
sex							

B	amyloid	tangles	gross infarctions	microinfarctions	neocortical lewy bodies	sex	AD age of onset
REST nuclear levels	0.014	2.5×10^{-6}					0.024
amyloid		1.4×10^{-13}					
tangles							
gross infarctions				0.0099	0.032		
microinfarctions							
neocortical lewy bodies							
sex							

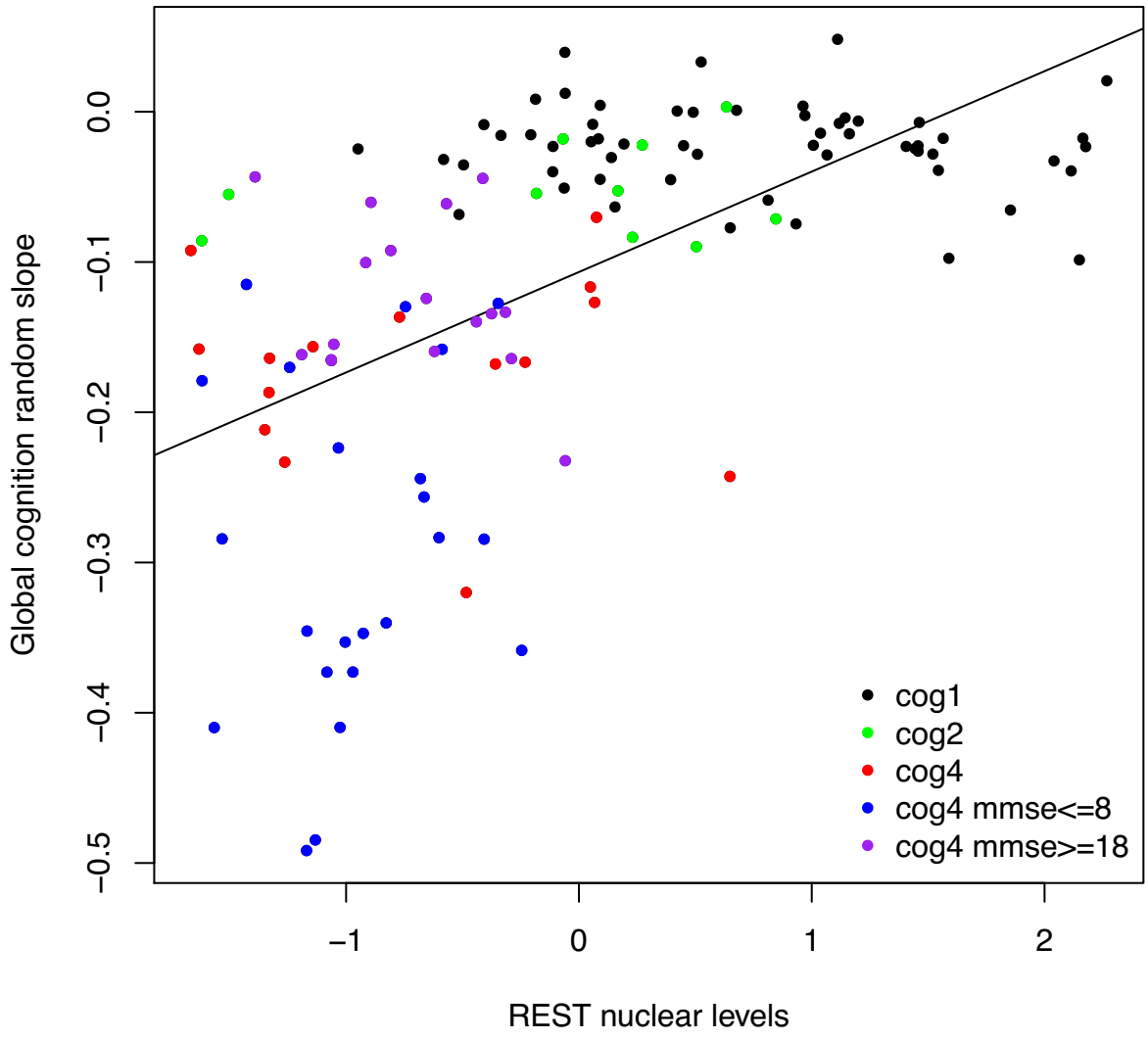

Figure 4.3: **REST nuclear levels positively correlate with reduced longitudinal cognitive decline in ROSMAP.** A linear mixed model with term time to death was used to calculate a random slope per individual for global cognition. Linear regression of global cognitive random slope on REST nuclear levels is shown. Particular AD subsets are identified (mild AD MMSE ≥ 18; severe AD MMSE ≤ 8). REST nuclear levels (estimate $= 0.067$, SE $= 0.0088$, $P = 6.55 \times 10^{-12}$). Model (Residual SE $= 0.098$, DF $= 120$, Adjusted $R^2 = 0.32$; model $P = 6.55 \times 10^{-12}$). cog1, cognitively-intact aged; cog2, MCI; cog4, AD.

row). With the inclusion of REST nuclear levels in the full model, time becomes significant again and the average person declines with time which implies that REST nuclear levels account for a significant amount of the positive component of the time coefficient.

Table 4.2: **Association of each neuropathological variable and REST nuclear levels with rate of cognitive decline in separate models in ROSMAP.** Mixed model analysis of the contribution of each neuropathological variable and REST nuclear levels to rate of global cognitive change during aging. In separate models each independent variable was used singly and its interaction with time to determine if it was significantly correlated with cognitive decline and its effect size. SE, standard error.

	estimate	SE	P
time	-0.11	0.012	4×10^{-15}
amyloid	-0.0075	0.0027	0.0062
tangles	-0.0088	0.0008	$< 2 \times 10^{-16}$
grossinfarctions	-0.016	0.025	0.52
microinfarctions	-0.032	0.024	0.18
neocortical lewy bodies	-0.1	0.037	0.0064
REST nuclear levels	0.071	0.0095	4.5×10^{-11}

As AD is a heterogenous disease with many individuals having high levels of AD neuropathology but no cognitive symptoms we would like to know if REST nuclear levels provide any additional information explaining why an individual might have high degrees of neuropathology yet remain cognitively intact. To investigate this heterogenity of cognitive decline we performed an analysis of the percentage of between-subjects variation in cognitive decline explained by each term and all of the terms in the mixed model (Table 4.4). REST nuclear levels on their own explain 36% of the variation in cognitive decline and additional 9% of the variation in cognitive decline after accounting for traditional AD-related neuropathologies. This confirms that REST nuclear levels are an important contributor to the variability in cognitive decline. Our full model without REST nuclear levels explains 62% of the variance (Table 4.4) while the same full model in the same cohort explained

Table 4.3: **Association of each neuropathological variable and REST nuclear levels with rate of cognitive decline in ROSMAP.** Mixed model analysis of the contribution of each neuropathological variable and REST nuclear levels to rate of global cognitive change during aging. A. Model without REST nuclear levels. B. Model with REST nuclear levels. SE, standard error.

A	estimate	SE	P
time	-0.018	0.014	0.22
amyloid	-0.00052	0.002	0.79
tangles	-0.0087	0.00083	$< 2 \times 10^{-16}$
gross infarctions	-0.013	0.018	0.48
microinfarctions	-0.017	0.017	0.32
neocortical lewy bodies	-0.097	0.026	0.00039

B	estimate	SE	P
time	-0.028	0.013	0.034
amyloid	-0.00036	0.0018	0.84
tangles	-0.0074	0.00084	8.88×10^{-16}
gross infarctions	-0.0078	0.016	0.63
microinfarctions	-0.025	0.016	0.13
neocortical lewy bodies	-0.077	0.024	0.0022
REST nuclear levels	0.038	0.0079	5.49×10^{-6}

only 41% of the variance in the original paper (Boyle $\mathrm{et\ al.}$, 2013a). This is likely due to the original paper using 856 subjects while we used only 122 due to requiring samples also had measured REST nuclear levels.

Table 4.4: **Analysis of the percentage of between-subjects variation in cognitive decline explained by each model term and the full model with and without REST nuclear levels in ROSMAP.** Mixed model analysis of the contribution of each neuropathological variable and REST nuclear levels to the rate of global cognitive change during aging computed as in Table 4.2 and Table 4.3.

	total variance	reduction	% variance explained
Reference model (time only)	0.015		
amyloid	0.014	0.00099	6.5
tangles	0.0068	0.0084	55
grossinfarctions	0.015	5.8×10^{-5}	0.38
microinfarctions	0.015	0.00024	1.6
neocortical lewy bodies	0.014	0.0011	6.9
REST nuclear levels	0.0098	0.0054	36
Full model without REST	0.0058	0.0094	62
Full model with REST	0.0045	0.011	71

Lastly, to investigate how different amounts of REST nuclear levels impact cognitive decline, individuals were stratified into groups by their relative REST nuclear levels which showed that individuals with high REST nuclear levels had significantly lower degrees of cognitive decline during aging (Figure 4.4).

Discussion

Upon death many individuals meet neuropathological criteria for AD yet do not meet criteria for clinical AD diagnosis (Crystal $\mathrm{et\ al.}$, 1988). Understanding what accounts for this discrepancy will help elucidate the mechanisms underlying cognitive decline and clarify the role of neuropathologies in the process. Here we examined the relationship between

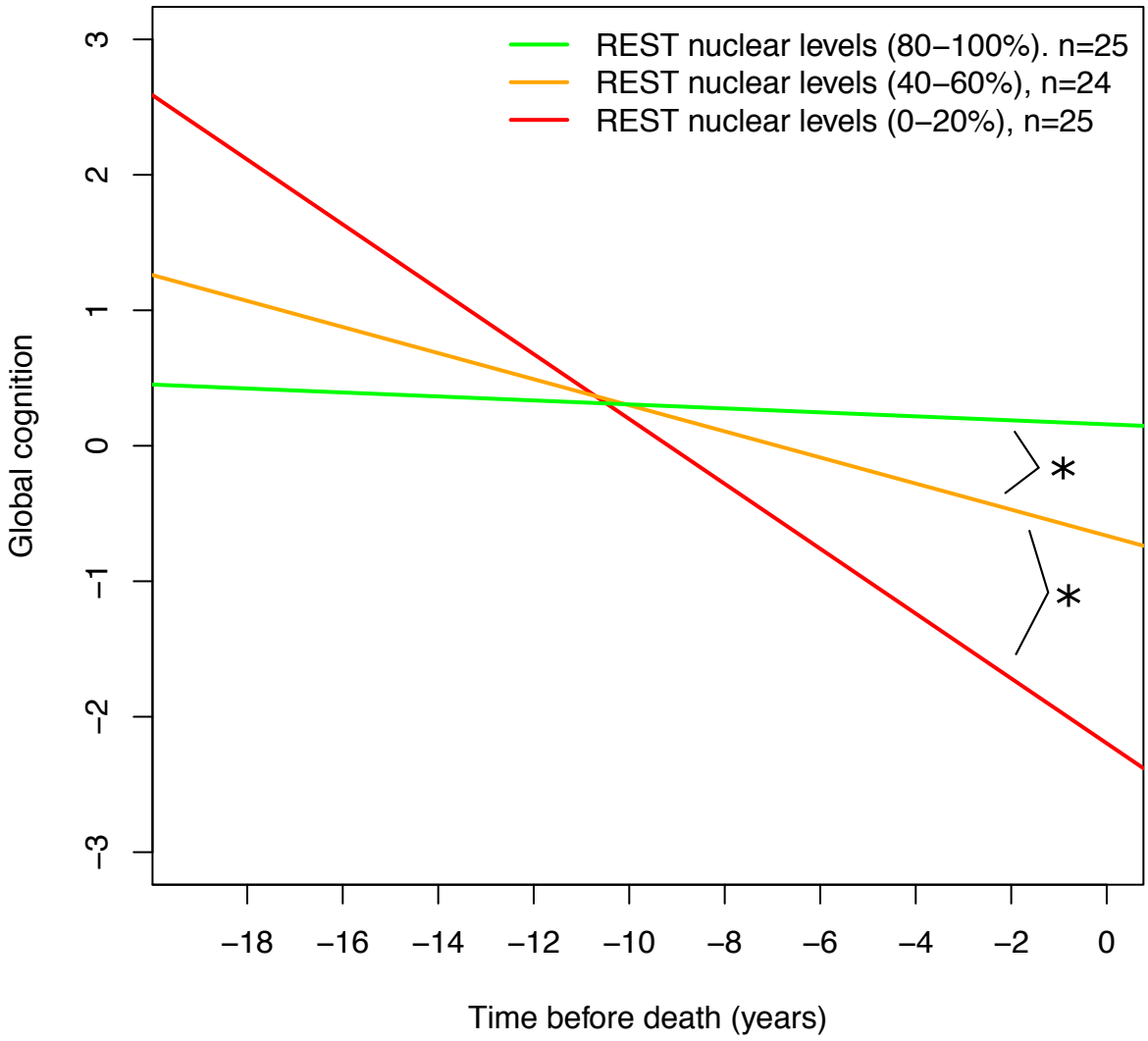

Figure 4.4: **REST nuclear levels positively correlate with reduced cognitive decline in ROSMAP.** Global cognitive decline was calculated for each individual using the linear mixed model-derived coefficients and their neuropathological variable and REST nuclear levels. Then individuals were stratified by REST nuclear levels into highest 20% (80–100%), middle 20% (60–80%), and bottom 20% (0–20%) and their global cognitive decline trajectories averaged to create the graph. * $P < 0.05$ (difference between group slopes) by Wilcoxon rank sum test.

REST nuclear levels and AD neuropathologies in longitudinal cognitive decline. We provide evidence that REST nuclear levels positively correlate with individual cognitive function during aging by a linear mixed model analysis of longitudinal cognitive function (Table 4.2). Further, REST nuclear levels were the second most significant contributor to cognitive function during aging even after accounting for AD neuropathologies (Table 4.3, Figure 4.4), and REST nuclear levels correlated with increased AD age of onset and decreased AD neuropathology (Table 4.1). Finally, REST nuclear levels explain a significant fraction of the variability of cognitive decline (Table 4.4) on their own and after accounting for AD neuropathologies.

However, in our cohort a large fraction of the variability in cognitive decline still remained unexplained (Table 4.4). There are many potential factors that influence cognitive decline that were not included in our analysis including markers of inflammation, measures of "neural reserve" such as higher neuronal density in particular brain regions (Katzman et al., 1988; Wilson et al., 2013) and levels of presynaptic proteins such as complexin-1 and SNAP-25-syntaxin interaction which explain between-subjects variability in cognitive decline after accounting for AD neuropathologies (Boyle et al., 2013a), small vessel disease (Marchant et al., 2013), hippocampal sclerosis (Corey-Bloom et al., 1997), Transactive response DNA binding protein 43 (TDP-43) levels (Tremblay et al., 2011), and other undiscovered pathological processes. Another potential issue is that these neuropathological markers are measured at death so their levels and duration of impact on cognitive decline can only be estimated. Finally, due to our small cohort size we were restricted to a linear model of the contribution of REST nuclear levels to cognitive decline. A nonlinear analysis that models accelerated cognitive decline proximate to death more accurately would likely provide further insight into the contributions of REST nuclear levels to preterminal and terminal rates of cognitive decline.

Our results strongly support the hypothesis that REST is critical determinant of cognitive preservation during aging independent of neuropathologies. They also suggest that

therapies designed to regulate REST nuclear levels may be a viable mechanism for promoting healthy cognitive aging. Notably, lithium treatment, which can activate WNT signaling, which can regulate REST (Lu et al., 2014; Nishihara et al., 2003), reduces AD neuropathology and cognitive impairment in mouse models of AD (Caccamo et al., 2007; Toledo and Inestrosa, 2010).

Methods

Brain sample procurement

Postmortem human brain material was procured in accordance with institutional guidelines governed by approved protocols. Tissue samples were procured from the Rush University Medical Center from participants in the Religious Order Study (ROS) and Rush Memory and Aging Project (MAP) at the Rush Alzheimers Disease Center, which are longitudinal, clinical-pathologic studies of aging, cognitive decline and AD (Bennett et al., 2012a,b). Study participants agreed to comprehensive annual clinical and neuropsychological evaluation and brain donation at death.

Cognitive function tests and neuropathology

Measures of cognitive function were derived from neuropsychiatric assessments performed longitudinally in the Religious Orders Study and the Rush Memory and Aging Project (MAP). This population includes individuals across the cognitive spectrum, ranging from normal to AD. Cognitive testing and neuropathological data have been described previously (Bennett et al., 2012a,b; Boyle et al., 2013a,b). Briefly, we used a summary measure of global cognitive function which consisted of an average of the z-scores of 19 cognitive tests measuring episodic, semantic, and working memory, processing speed, and perceptual orientation. The follow-up rate exceeds 95% and the autopsy rate exceeds 90%.

Autopsy cases in the Religious Orders and MAP studies underwent a uniform structured neuropathologic evaluation of AD, including quantification of amyloid, tangles, neocortical lewy bodies, gross infarctions, and microinfarctions (Boyle et al., 2013a). The clinical diagnoses of AD and MCI have been described in detail and pathologic confirmation of AD approaches 90% (Bennett et al., 2006, 2002; Schneider et al., 2009). Amyloid was measured using 10D5 antibody and quantified (Boyle et al., 2013a). Tangles were measured using AT8 antibody against phosphorylated tau and quantified (Boyle et al., 2013a). Neocortical lewy bodies were measured using an antibody against α-synuclein and scored as present or absent (Boyle et al., 2013a). Gross infarctions and microinfarctions were scored as present or absent (Boyle et al., 2013a). REST nuclear levels were determined by immunohistochemical analysis and quantification as described below. REST nuclear levels were standardized to have mean 0 and standard deviation 1.

Immunofluorescence analysis of human brain and quantification of REST nuclear levels

Immunofluorescence analysis using paraffin-embedded brain sections was performed in the the prefrontal cortex (Broadmann areas 9, 10 and 47). Paraffin-embedded tissue sections were first deparaffinized in xylene, then rehydrated with decreasing concentrations of ethanol and placed in water. Sections then underwent antigen retrieval using either citrate buffer (Vectorlabs, USA) or the Diva decloaker (BioCare, USA). They were then washed and blocked with 3% BSA, 0.2% Triton X-100 in PBS for 1 hr at room temperature. The primary antibody detecting REST, a rabbit polyclonal IgG recognizing a region between residues 1050 and the C-terminus (residue 1097) (Bethyl laboratories, IHC-00141), was diluted in 2% BSA, 0.1% Triton in PBS. Following overnight incubations, sections were washed three times with PBS. Secondary antibodies, diluted in 2% BSA, 0.1% Triton in PBS, were coupled to Alexa fluorophores (1:300, Invitrogen). Sections were then incubated with

1% Sudan Black in 70% ethanol, for 10 minutes, to suppress lipofuscin autofluorescence. Following washes in PBS, sections were mounted and imaged using confocal microscopy. Images were acquired using an Olympus Fluoview confocal microscope. No image processing was performed on the acquired images. To quantify immunofluorescence, images were randomly acquired in selected brain regions. Antigen-expressing areas within each neuron and in cellular compartments (such as the nucleus) were selected using the Metamorph image analysis system and the average signal intensity measured. Values were corrected by subtracting the average slide background intensity (measured outside of cells). Between 50–100 neurons were analyzed for each case. The investigator was blinded to sample origin or diagnosis.

Statistical analyses of longitudinal data

We used a linear mixed model to analyze the contribution of neuropathological variables and REST nuclear levels to the rate of cognitive decline. This model uses repeated measurements on each individual to estimate an individual's slope ("random slope") and intercept deviation from the mean slope and intercept of the group. We modeled time as years to death, and the coefficient of time corresponds to the mean cognitive change proximate to death while an individual's random slope corresponds to his difference from the mean cognitive change. To create the full model to analyze the contribution of neuropathological variables and REST nuclear levels to cognitive decline we added terms for each neuropathological variable and REST nuclear levels and their interaction with time. Thus, our full model consisted of terms for time, each neuropathological variable and REST nuclear levels, and the interaction of each neuropathological variable and REST nuclear levels with time. A significant variable-time interaction coefficient represents a difference from the mean cognitive slope due to that variable. Analysis was performed in R using the lme4 package.

Chapter 5

miR-132/miR-212, a REST-regulated target, in aging, oxidative stress, and FOXO1 regulation

Introduction

Several studies have investigated mRNA and protein changes during brain aging (Lu $\mathrm{et\ al.}$, 2004; Vanguilder and Freeman, 2011), but few have looked at miRNAs. Understanding how miRNAs change during brain aging will be important because of the large number of targets and networks each miRNA can regulate, and because miRNAs can regulate stress responses and maintain homeostasis (Leung and Sharp, 2010). As our lab's original study of mRNA transcriptional changes during human brain aging (Lu $\mathrm{et\ al.}$, 2004) did not investigate miRNAs, we sought to determine how miRNAs change during brain aging. Here we profile miRNA changes during brain aging and find that miR-132/miR-212 levels are decreased in cognitively-intact aged individuals and centenarians, and further decreased in AD. miR-132/miR-212 are predicted to target several genes that protect against oxidative stress, and we show that they are pro-apopototic and sensitize to oxidative stress *in vitro*

and target FOXO1, a critical regulator of oxidative stress responses. miR-132/miR-212 are also known to be regulated by REST (Conaco et al., 2006; Johnson et al., 2008), and we show REST regulates miR-132/miR-212 during aging.

Results

miR-132/miR-212 levels are decreased during brain aging and Alzheimer's disease

To investigate miRNA expression changes during human brain aging, we profiled miRNAs from young and aged prefrontal cortex gray matter (Table 5.1) using miRNA microarrays. Of the 313 miRNAs measured, only 9 were significantly different between young and aged (Table 5.2, Figure 5.1). Based on the fact that miR-132 and miR-212 have a conserved REST RE1 binding site (Wu and Xie, 2006) and the fundamental role of REST in brain aging and AD (Lu et al., 2014) we decided to focus on these two miRNAs which were strongly decreased during aging. That miR-132/miR-212 are decreased during aging would be consistent with a role for REST in their downregulation since aged individuals have increased nuclear REST (Lu et al., 2014). We validated the microarray data expression changes using RT-qPCR for the mature miRNAs for select targets using additional individuals (Table 5.1). RNA sample quality/RNA integrity number, determined using the Agilent Bioanalyzer, was at least 5.5 for all samples to avoid issues with degraded RNA (Ibberson et al., 2009). We observed similar fold changes for miR-132 (Figure 5.2), miR-212 (Figure 5.3), and mir19b (data not shown) by RT-qPCR and microarray. miR-132/miR-212 levels were similarly decreased in centenarians showing that reduced miR-132/miR-212 levels are a common feature of brain aging of cognitively-intact individuals at least 70 years old.

Based on the hypothesis that the decrease in miR-132/miR-212 during aging is neu-

Table 5.1: **Human prefrontal cortex samples used for miRNA analysis.**

sample			
age	sex	application	
24	M	microarray	RT-qPCR
25	F	microarray	RT-qPCR
25	F		RT-qPCR
26	M		RT-qPCR
26	F		RT-qPCR
27	F	microarray	RT-qPCR
29	F	microarray	RT-qPCR
33	F		RT-qPCR
34	F		RT-qPCR
35	M		RT-qPCR
37	M		RT-qPCR
71	M		RT-qPCR
71	M		RT-qPCR
71	F	microarray	RT-qPCR
72	M		RT-qPCR
74	F		RT-qPCR
75	F		RT-qPCR
76	F		RT-qPCR
76	F		RT-qPCR
77	F		RT-qPCR
77	F		RT-qPCR
78	M		RT-qPCR
79	F		RT-qPCR
86	M	microarray	
87	F	microarray	
90	F	microarray	
95	M		RT-qPCR
95	F		RT-qPCR
96	F		RT-qPCR
98	F		RT-qPCR
100	F		RT-qPCR
100	F		RT-qPCR
100	F		RT-qPCR
101	F		RT-qPCR
101	F		RT-qPCR
103	F		RT-qPCR
104	M		RT-qPCR
105	F		RT-qPCR
106	F		RT-qPCR
106	F		RT-qPCR
106	F		RT-qPCR

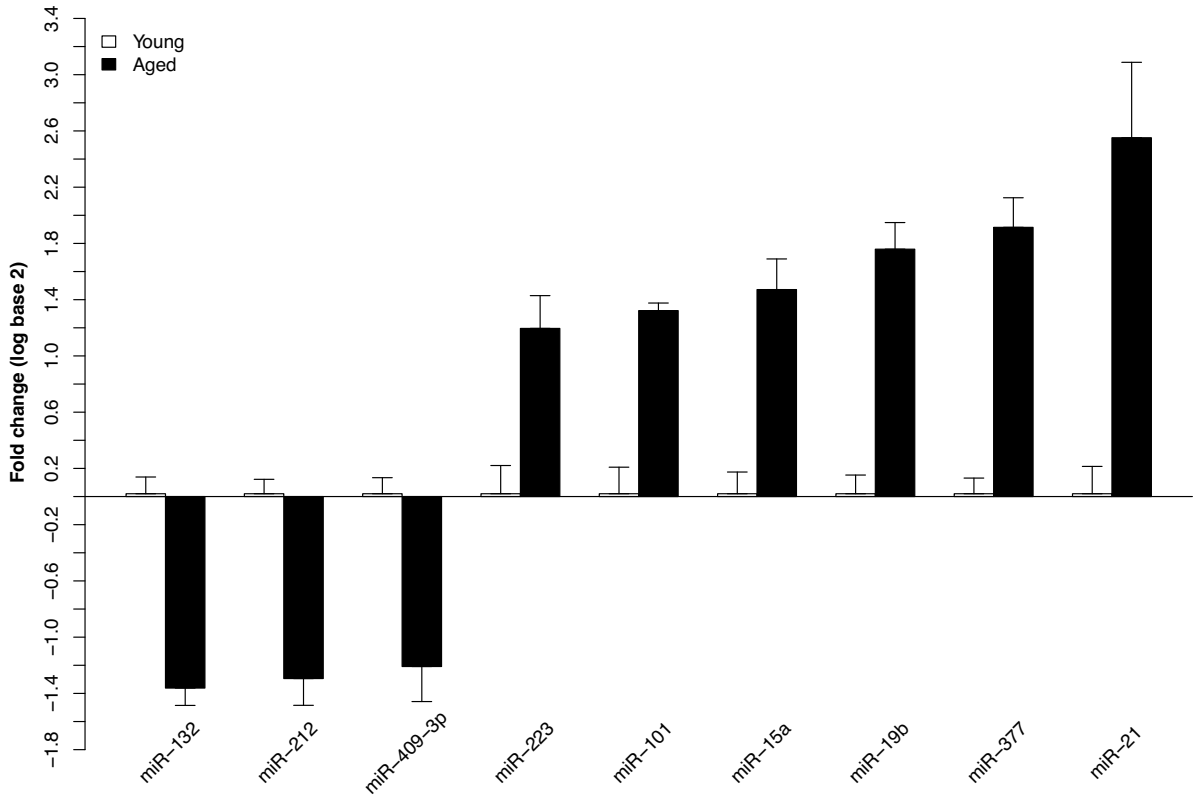

Figure 5.1: **miRNA microarray of young and aged human prefrontal cortex.** miRNAs were considered significantly differentially expressed as in Table 5.2. Data are represented as mean fold change $\pm$ SEM relative to young in a log2 scale.

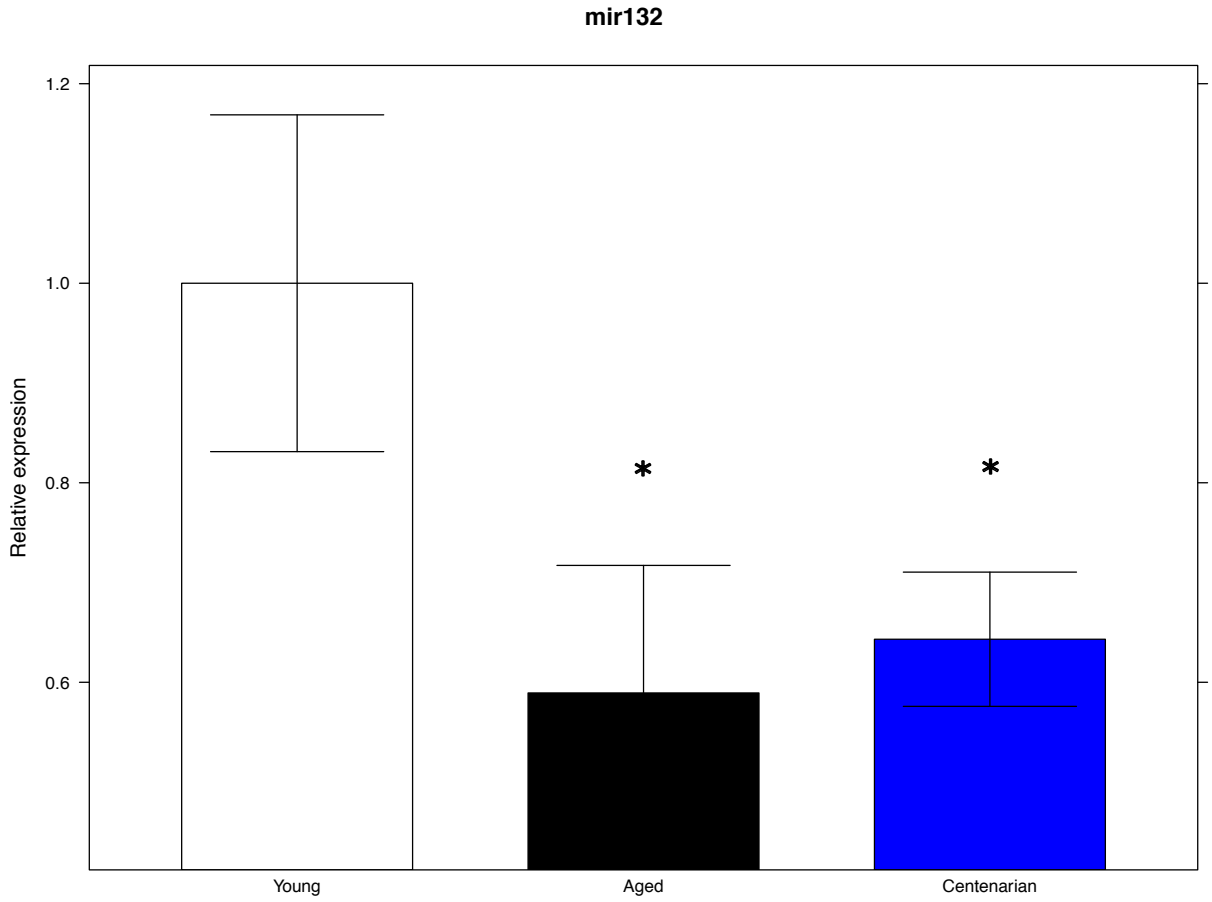

Figure 5.2: **Validation of reduced miR-132 with age by RT-qPCR.** Young (20s–30s); Aged (70s–90s); Centenarian (100–106). mean $\pm$ SEM. Statistical design included planned comparison with Young. *$P < 0.05$ by one-tailed t-test with correction for multiple tests by Holm's method.

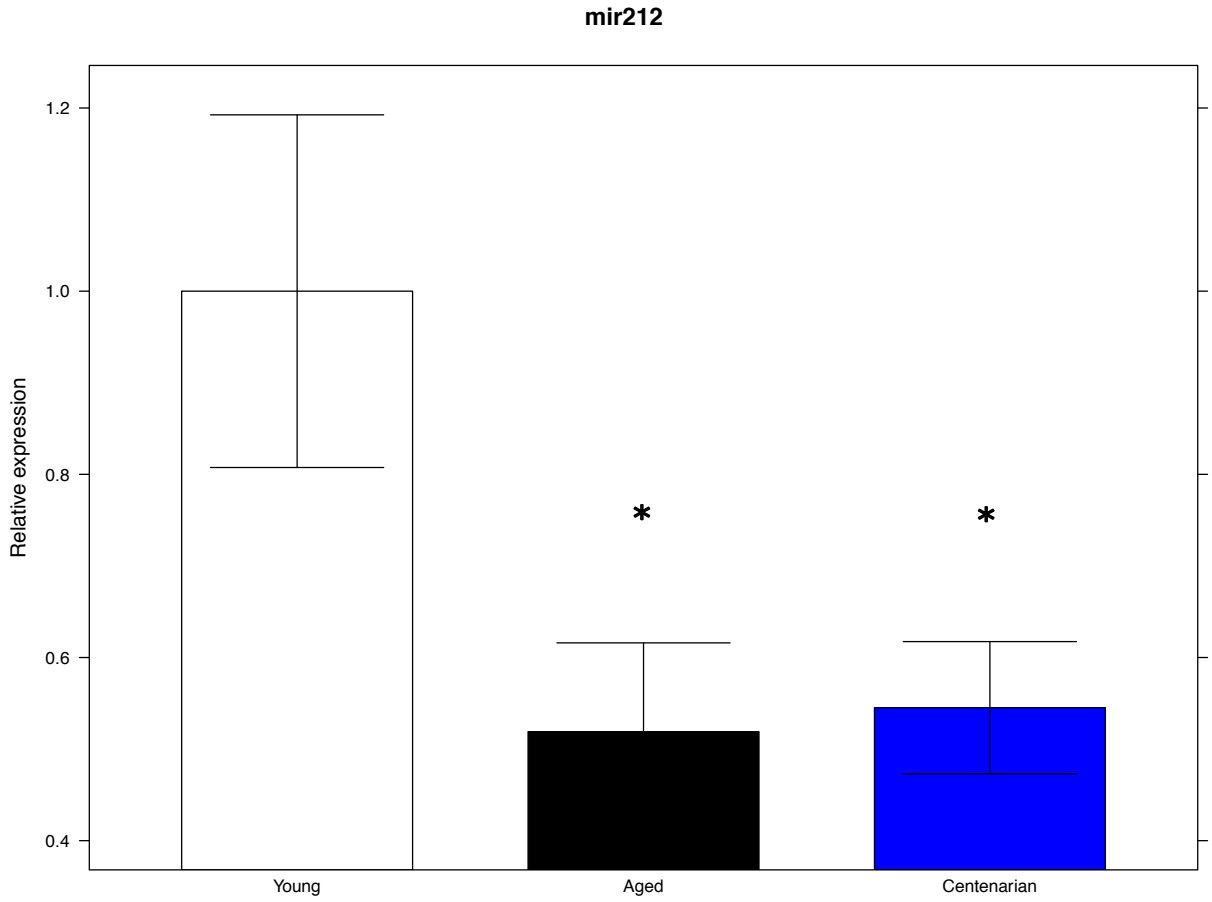

Figure 5.3: **Validation of reduced miR-212 with age by RT-qPCR.** Young (20s–30s); Aged (70s–90s); Centenarian (100–106). mean $\pm$ SEM. Statistical design included planned comparison with Young. *$P < 0.05$ by one-tailed t-test with correction for multiple tests by Holm's method.

Table 5.2: **miRNA microarray of young and aged human prefrontal cortex.** Young ($n = 4$) and Aged ($n = 4$) RNA were hybridized to microarrays. miRNAs with FDR < 0.05 and fold change ≥ 2 were considered significantly differentially expressed. Data are represented as mean fold change relative to Young in a log2 scale.

microRNA	average expression	log2 fold change	P	FDR
miR-223	9.27	1.20	0.00022	0.023
miR-101	10.30	1.32	0.00037	0.029
miR-212	9.10	-1.29	0.00075	0.038
miR-15a	10.39	1.47	0.00106	0.038
miR-409-3p	9.20	-1.21	0.00133	0.038
miR-377	7.55	1.91	0.00131	0.038
miR-19b	9.60	1.76	0.00151	0.038
miR-21	10.45	2.55	0.00157	0.038
miR-132	12.95	-1.36	0.00190	0.040

roprotective, we investigated if they were further reduced in AD. miR-132/miR-212 were significantly decreased approximately 2-fold in AD relative to age-matched cogntively-intact controls (Figure 5.4, Figure 5.5). To further investigate miR-132/miR-212 in AD we measured their levels in prefrontal cortex from AD patients stratified by minimental state examination (MMSE) score which is used to measure cognitive impairment. MMSE $<= 10$ can be considered severe AD with serious cognitive impairment while MMSE $>= 18$ can be considered mild AD with mild cognitive impairment. We performed a similar MMSE stratification and analysis (Lu $\mathrm{et\ al.}$, 2014) showing that upregulation and nuclear localization of REST is important for stress resistance during brain aging, and this process is lost during AD with some results dependent on the degree of cognitive impairment. miR-132 was significantly decreased in severe AD and trended toward a significant decrease in mild AD compared to aged (Figure 5.6). miR-212 trended toward a significant decrease only in severe AD compared to aged (Figure 5.7). In agreement in AD we find that miR-132/miR-212 levels relative to 5S significantly inversely correlate with AD cognitive impairment as measured by MMSE score (miR-132 spearman correlation $\rho = -0.59$, $P = 0.034$; miR-212

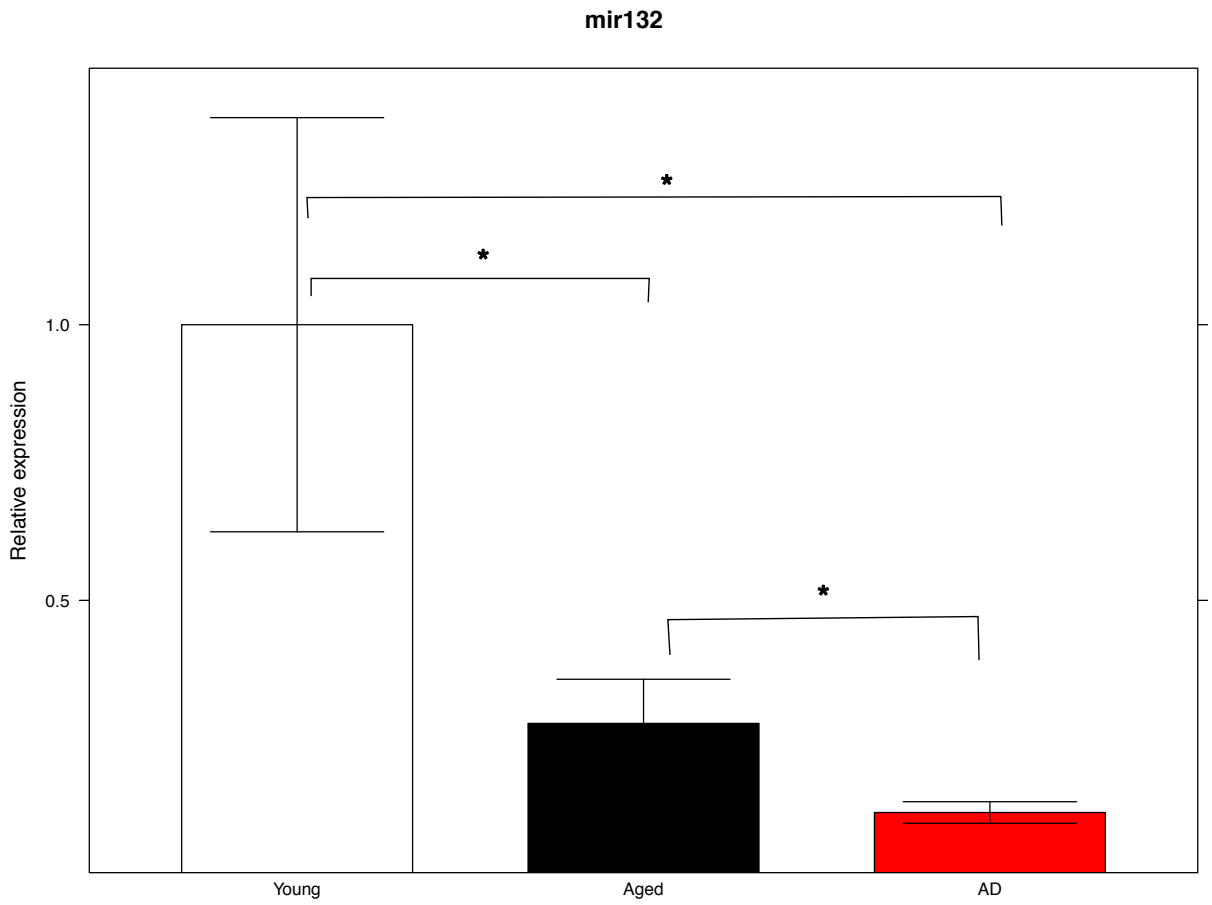

Figure 5.4: **miR-132 levels are decreased in AD cases compared to cognitively-intact aged controls.** Young (20s–30s): $n = 5$; Aged (70s–90s): $n = 15$; AD (80s): $n = 9$. mean $\pm$ SEM, * ANOVA followed by Tukey's HSD test $p < 0.05$.

spearman correlation $\rho = -0.67$, $P = 0.011$).

One caveat to the interpretation that downregulation of miR-132/miR-212 in AD is neuroprotective is that major neuronal death occurs in AD which does not occur during normal aging. Because our RNA was extracted from whole brain tissue miR-132/miR-212 could be decreased simply due to cell death and not downregulated. However, reduced levels of miR-132 cannot be attributed to increased neuronal death at least in mild AD because the neuron-enriched mir-124 is not significantly different between aged and mild AD although it is significantly decreased in severe AD compared to Aged (data not shown).

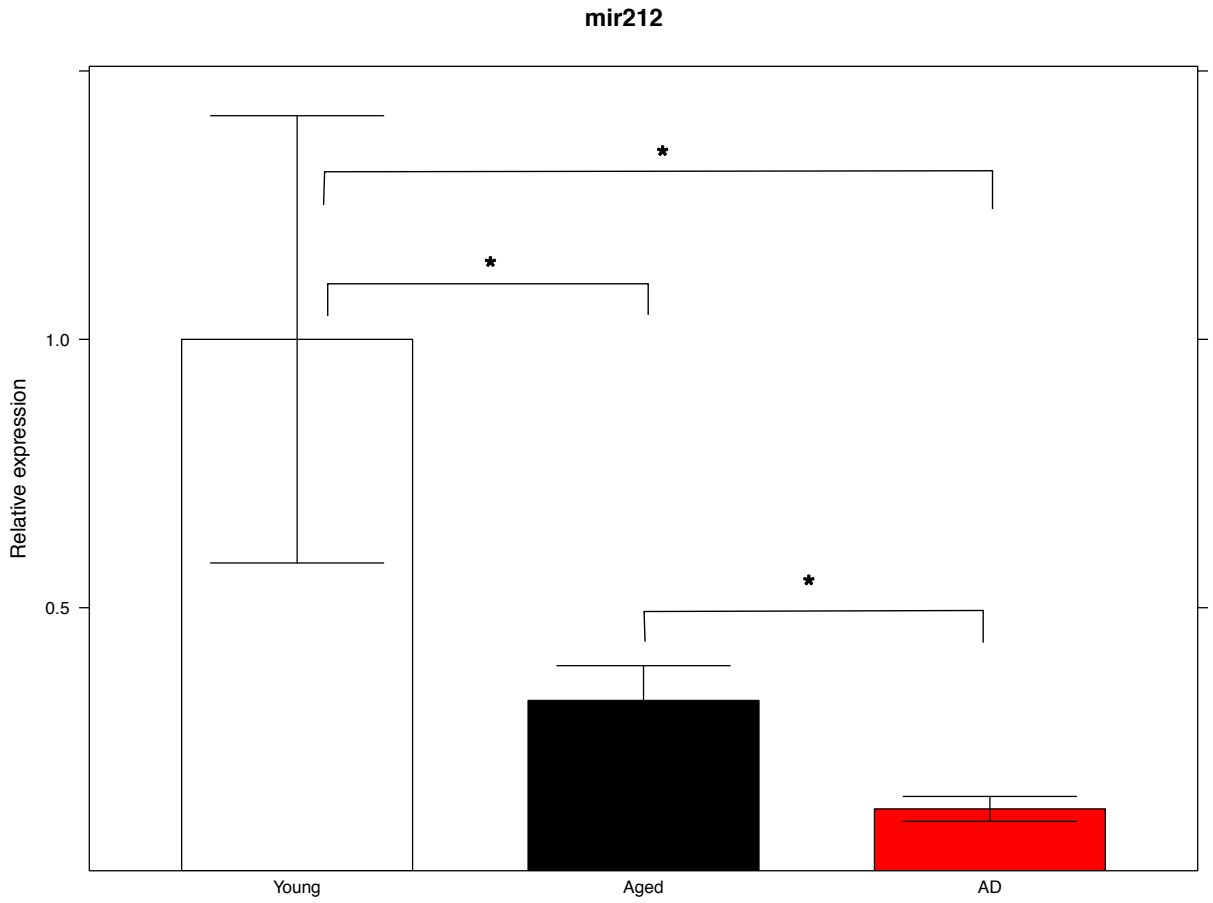

Figure 5.5: **miR-212 levels are decreased in AD cases compared to cognitively-intact aged controls.** Young (20s–30s): $n = 5$; Aged (70s–90s): $n = 15$; AD (80s): $n = 9$. mean $\pm$ SEM, * ANOVA followed by Tukey's HSD test $p < 0.05$.

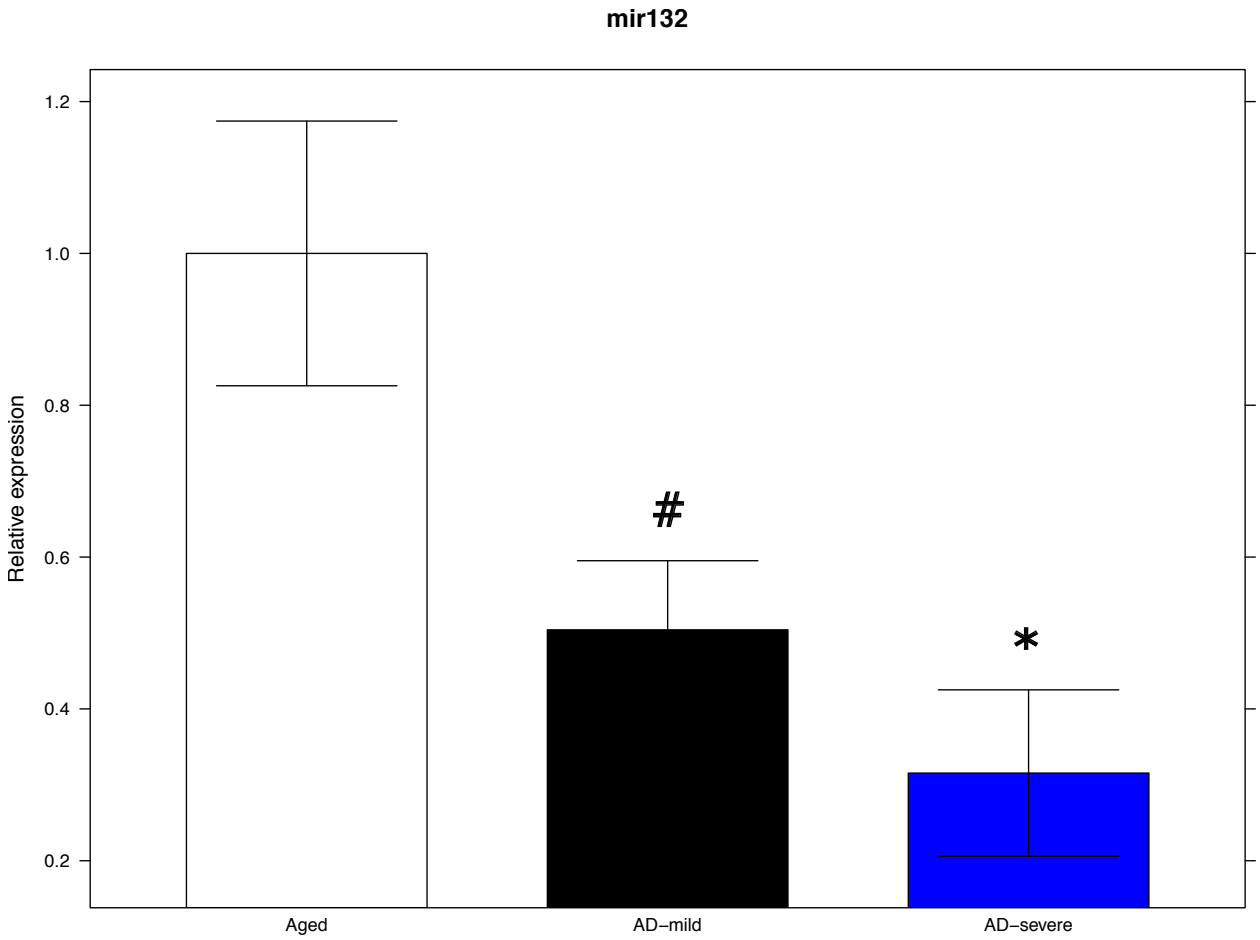

Figure 5.6: **miR-132 levels in AD cases stratified by MMSE compared to cognitively-intact aged controls.** Aged (70s–90s): $n = 15$; AD-mild: $n = 8$; AD-severe: $n = 5$. mean $\pm$ SEM. ANOVA followed by Tukey's HSD test *$p < 0.05$, #$p < 0.10$.

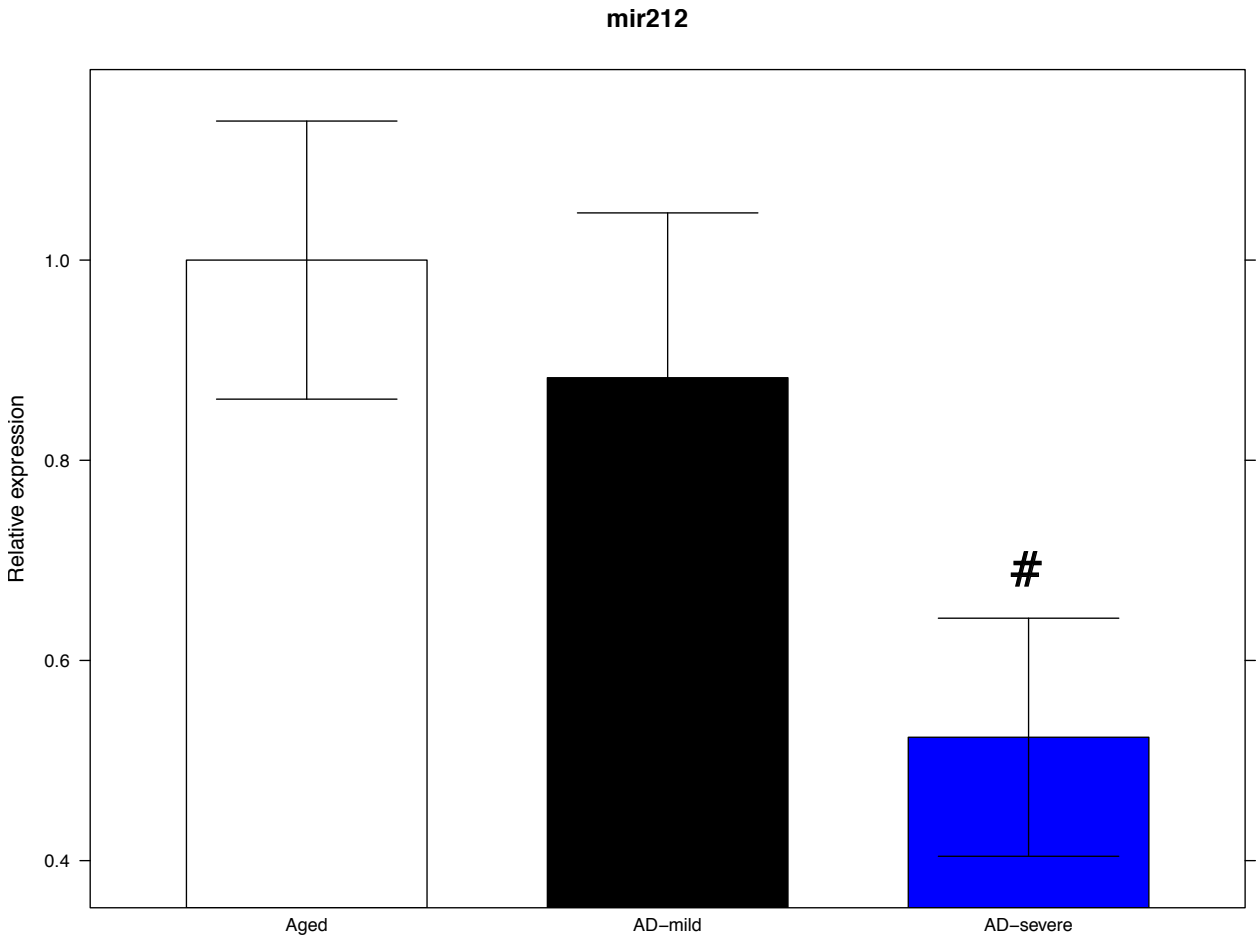

Figure 5.7: **miR-212 levels in AD cases stratified by MMSE compared to cognitively-intact aged controls.** Aged (70s–90s): $n = 15$; AD-mild: $n = 8$; AD-severe: $n = 5$. mean $\pm$ SEM. ANOVA followed by Tukey's HSD test #$p < 0.10$.

miR-132/miR-212 directly regulate FOXO1

The functional consequences of miRNA expression changes are difficult to determine since each miRNA can target many transcripts and each transcript can be targeted by many miRNAs. Additionally, the targets of miRNAs are mostly computationally predicted with each miRNA typically having several thousand predicted targets and very few experimentally validated targets. One way to increase confidence in predicted targets is to utilize several different miRNA target prediction databases. To begin to understand the functional consequences of reduced miR-132/miR-212 levels during brain aging and AD, we used the combined results from 9 miRNA databases to create a high confidence list of predicted targets and focused on those that were protective. We noted that several predicted and validated targets were related to oxidative stress, which increases in the aging brain, including SIRT1 (validated (Strum $\mathrm{et\ al.}$, 2009)), FOXO3 (predicted at analysis, now validated (Ucar $\mathrm{et\ al.}$, 2012)), NFE2L2/NRF2 (predicted at analysis, now validated), SOD2 (predicted at analysis, now validated), NR4A2 (predicted at analysis, now validated (Yang $\mathrm{et\ al.}$, 2012)), and FOXO1 (predicted at analysis, validated here and independently (Lau $\mathrm{et\ al.}$, 2013)). Thus, it appears that miR-132/miR-212 may regulate genes important for oxidative stress, and their downregulation during brain aging would be predicted to derepress and potentially upregulate these genes to reduce oxidative stress.

To test these predictions we decided to focus on FOXO1 and FOXO3 given their involvement in stress resistance, cell death, and aging. We overexpressed miR-132 or miR-212 in SH-SY5Y cells and measured FOXO1 and FOXO3 protein levels by western blot (Figure 5.8). We observed a significant decrease in FOXO1 protein, but we did not observe any change in FOXO3 protein (data not shown). Since the transfection efficiency is only about 50% (data not shown), it is likely miR-132/miR-212 reduce FOXO1 more than these experiments indicate. We also investigated if miR-132/miR-212 can downregulate FOXO1 in retinoic acid-differentiated SH-SY5Y cells which have properties more similar to mature neurons than untreated SH-SY5Y cells. Similarly, overexpression of miR-132 or

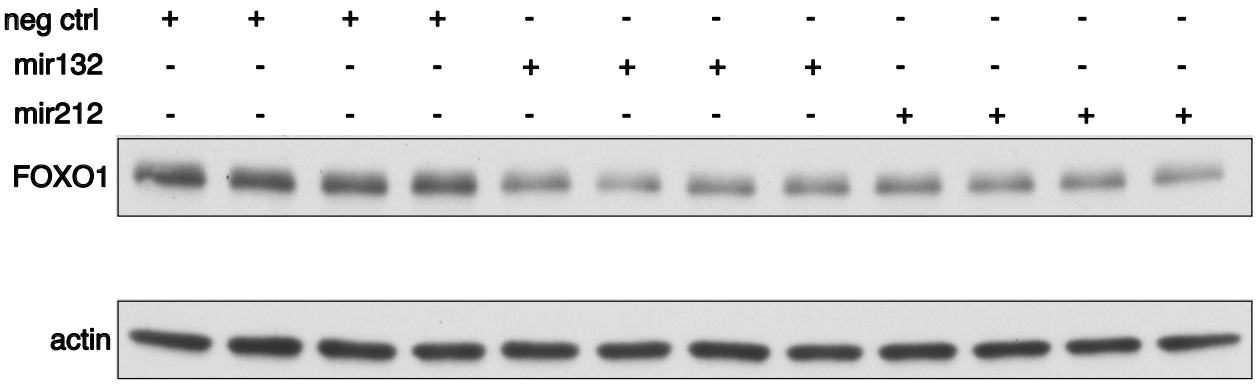

Figure 5.8: **Overexpression of miR-132 or miR-212 decreases FOXO1 protein levels in SH-SY5Y cells.** miR-132 mimic significantly decreased FOXO1 1.7-fold (*) and miR-212 mimic significantly decreased FOXO1 1.6-fold (*) relative to negative control. FOXO1 intensity was normalized to actin intensity. * ANOVA followed by Tukey's HSD test $p < 0.05$.

miR-212 decreased FOXO1 protein levels by western blot (Figure 5.9).

To determine if the regulation of FOXO1 protein level by miR-132/miR-212 has relevance in the aging human brain where miR-132/miR-212 are decreased, we performed a western blot using post-mortem human brain and found that FOXO1 trended toward a 3.6-fold increase in aged compared to young individuals (Figure 3.4B). Again, there was no difference in FOXO3 levels between young and aged individuals similar to the *in vitro* result of overexpressing miR-132/miR-212 (data not shown) so we chose to focus on FOXO1 exclusively.

If miR-132/miR-212 overexpression can downregulate FOXO1 protein levels *in vitro*, do miR-132/miR-212 directly repress FOXO1 via interactions with the 3' UTR or is it indirect? To investigate, we used a luciferase assay where the FOXO1 3' UTR is cloned into the 3' UTR of firefly luciferase with and without mutation of the two miR-132/miR-212 predicted binding sites. Stable SH-SY5Y lines containing these constructs were used because of low luciferase levels in transiently transfected SH-SY5Y cells. This assay gave a small (10–15%), but significant decrease in luciferase levels due to miR-132/miR-212 overexpression compared to control and this decrease was eliminated by the mutation of

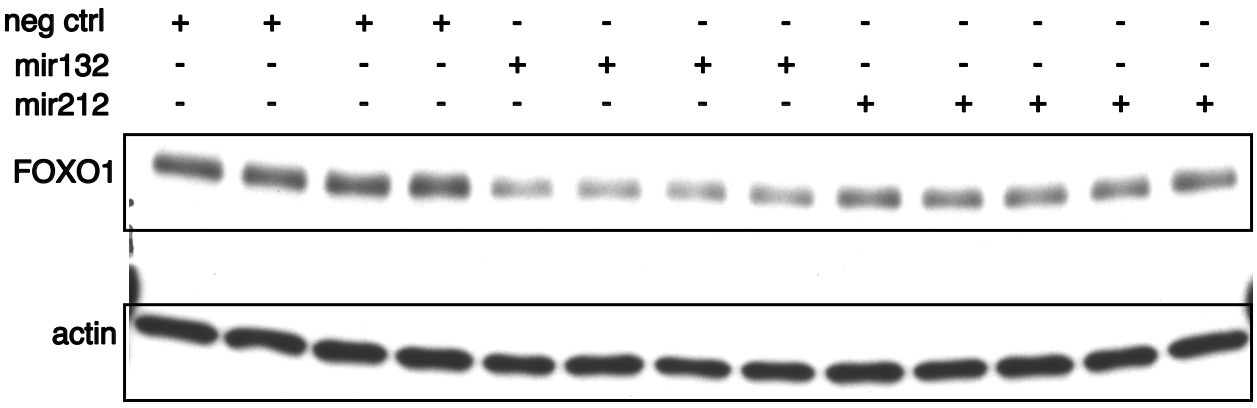

Figure 5.9: **Overexpression of miR-132 or miR-212 decreases FOXO1 protein levels in retinoic acid differentiated SH-SY5Y cells.** miR-132 mimic significantly decreased FOXO1 2-fold (*) and miR-212 mimic significantly decreased FOXO1 1.4-fold (*) relative to negative control. FOXO1 intensity was normalized to actin intensity. * ANOVA followed by Tukey's HSD test $p < 0.05$.

both miR-132/miR-212 seed sequences (Figure 5.10). A 10–20% decrease in luciferase levels is realistic and reproducible for some miRNA-mRNA targeting cases (personal communication, Novina lab). This luciferase assay result showing that miR-132/miR-212 directly represses FOXO1 translation has since been independently published (Lau $\mathrm{et\ al.}$, 2013).

miR-132/miR-212 are pro-apoptotic and sensitize to oxidative stress

To determine if miR-132/miR-212 are associated with stress resistance *in vitro*, we used retinoic acid (RA) differentiated SH-SY5Y cells as a more neuron-like system. To determine cell viability and number we used the MTS assay which provides a composite measure of cell viability and number through reduction of a tetrazolium compound by a NADH-coupled reaction to a colored formazan product which can be easily measured by absorbance in solution. 5–6 days after transient transfection cells had significantly reduced cell viability and number as determined by the MTS assay (Figure 5.11, see 0 mM NAC). Light

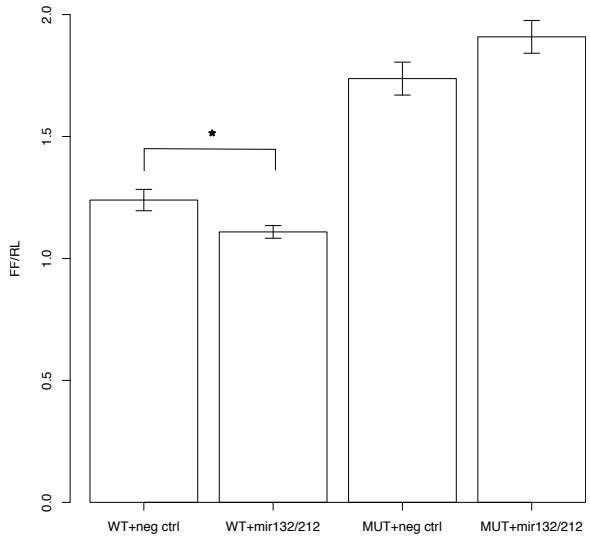

Figure 5.10: **miR-132/miR-212 directly bind to the FOXO1 3'UTR to mediate repression in retinoic acid differentiated SH-SY5Y cells.** Statistical design included planned comparison within WT or mut groups. *$P < 0.05$ by one-tailed t-test with correction for multiple tests by Holm's method.

microscopy indicates this is at least partially due to dying cells (data not shown) which were confirmed to be apoptotic by Hoechst staining showing increased condensed, cleaved chromatin (Figure 5.12).

To determine if this apoptotic phenotype was related to oxidative stress, we treated with the antioxidant N-acetyl-L-cysteine (NAC), a precursor to glutathione, during the 5 day transfection period by adding it to the two medium changes the cells have in this period. NAC was able to rescue the apoptotic phenotype as measured by reduced MTS absorbance in the miR-132/miR-212 overexpression (Figure 5.11). However, the neuronal pro-survival factor BDNF does not rescue the apoptotic phenotype induced by miR-132/miR-212 overexpression (data not shown) which may indicate that the result is dependent on oxidative stress.

As an alternative method of expression of miR-132/miR-212 we created lentiviruses expressing the pre-microRNA form of miR-132 and miR-212 that are expressed by splicing from the 3' UTR of GFP in FUGW vector. We also included approximately 150 bp of

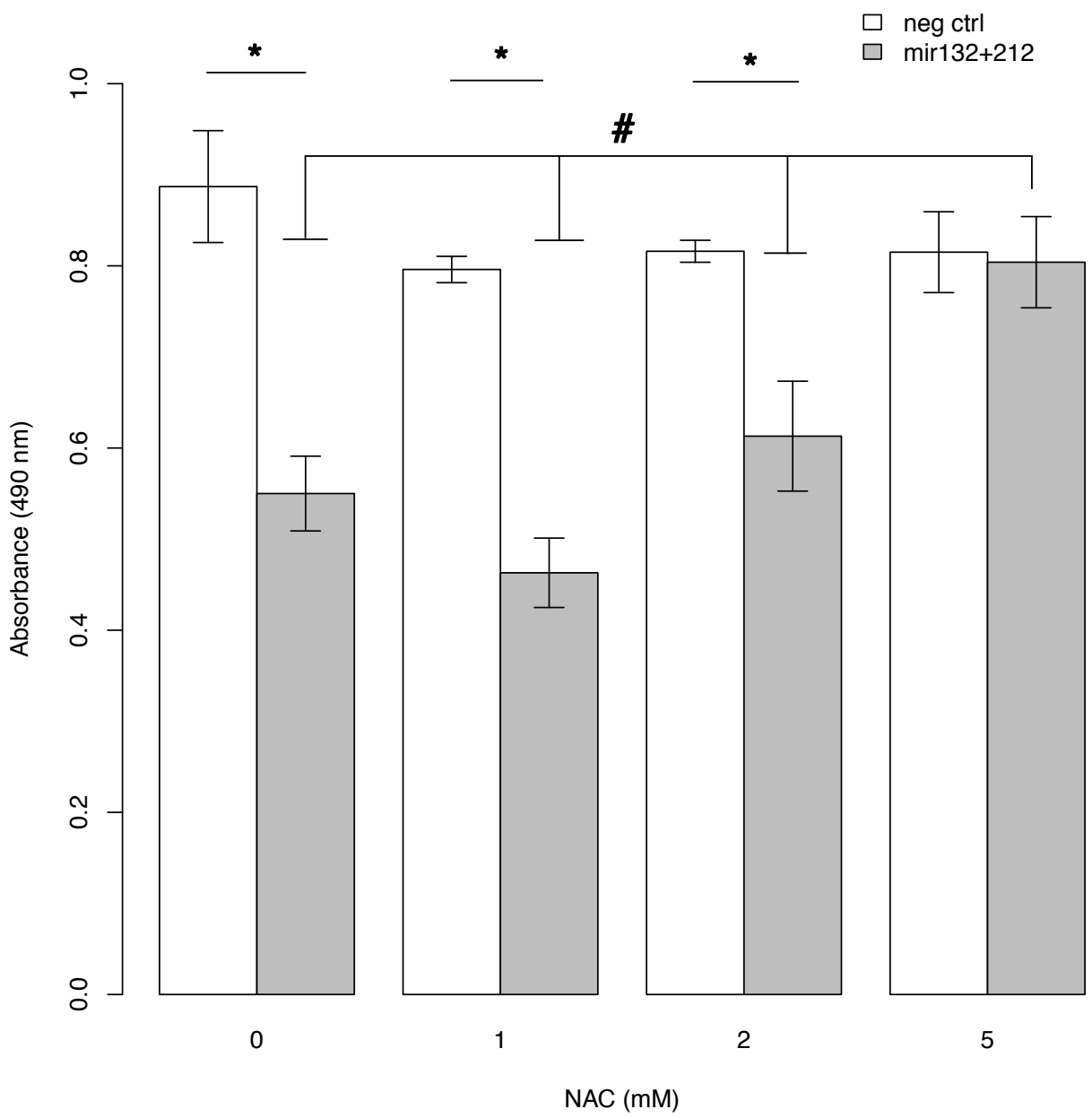

Figure 5.11: **miR-132/miR-212 reduce viability which can be rescued by antioxidant treatment.** MTS assay of RA-differentiated SH-SY5Y transfected with miR-132/miR-212 for 5 days treated with varying amounts of the antioxidant NAC during the transfection period. Note NAC dose-dependent rescue of cell viability. Statistical design included planned comparison within NAC treatment groups and within mir132+212 treatment group to determine rescue. *$P < 0.01$; #$P < 0.01$ compared to mir132+212,5mM NAC, t-test with correction for multiple tests by Holm's method.

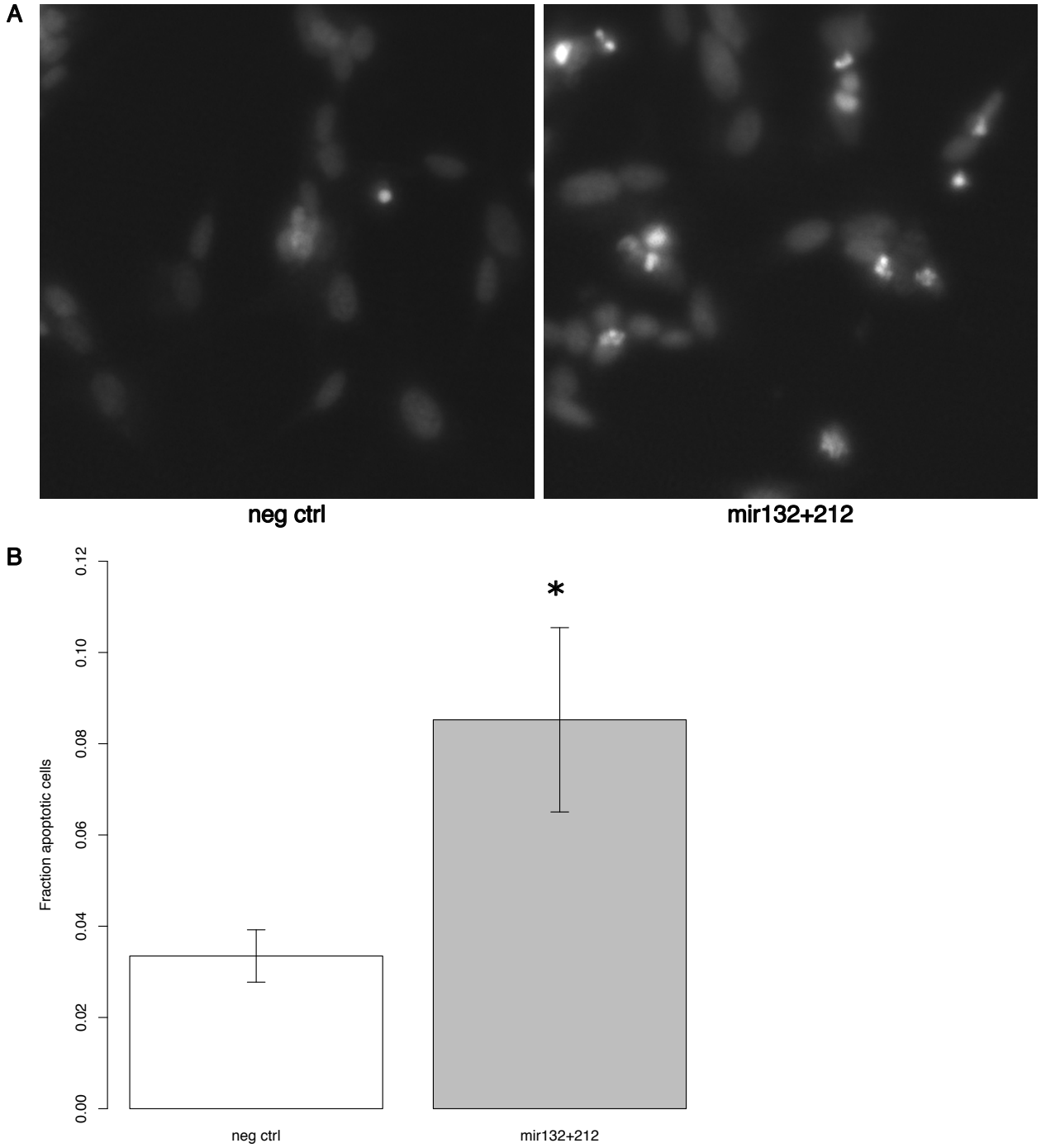

Figure 5.12: **miR-132/miR-212 cause apoptotic cell death.** A. Hoechst staining showing an increase in brightly staining, condensed, cleaved chromatin in apoptotic RA-differentiated SH-SY5Y 5 days after transfection in miR-132/miR-212 overexpressing cells. B. Quantification of fraction of Hoechst-positive per well. *$P < 0.05$, t-test.

genomic context on each side of the pre-microRNA to potentially make expression and splicing more similar to their *in vivo* context. These viruses have essentially 100% transfection efficiency in both differentiated and undifferentiated SH-SY5Y cells (data not shown). We confirmed that the viruses produce mature miR-132/miR-212 (Figure 5.13, Figure 5.14). The miR-132 virus produces 10–15-fold overexpression while the miR-212 virus produces only 1.5–2.5-fold overexpression. Similarly, SH-SY5Y cells normally express miR-132 much more highly than miR-212 even though these miRNAs are expressed from the same transcript.

Using these viruses we created stable SH-SY5Y lines expressing miR-132/miR-212 or a control virus expressing only GFP. The miR-132 overexpressing line in particular and in many cases the miR-132/miR-212 overexpressing line (with less miR-132 expression) are significantly more sensitive to oxidiative stress from H_2O_2 compared to control in undifferentiated (Figure 5.15) and differentiated (Figure 5.16) cells. The differences compared to control are usually in the 10–50% range for 75 and 100 μM H_2O_2. Overall, these results suggest that miR-132/miR-212 sensitize cells to oxidative stress.

Finally, we were interested if the cell death phenotype from transiently transfecting miR-132/miR-212 as double stranded RNAs in RA-differentiated SH-SY5Y was due to FOXO1 downregulation. Because SH-SY5Y cells have low transfectability we created stable FOXO1, constitutively active, predominately nuclear FOXO1 (FOXO1A3), due to mutation of the three AKT phosphorylation sites to alanine, and vector only (pcDNA3) lines using G418 selection. These FOXO1 constructs do not have a 3' UTR and therefore should be resistant to direct miR-132/miR-212 regulation. We sorted the FOXO1 stable lines for GFP expression to obtain a pure population of cells and confirmed FOXO1 expression (data not shown). Transfection of miR-132/miR-212 results in approximately 50% reduction in cell viability/number compared to negative control miRNA in the control (Figure 5.11) while the FOXO1 constructs provide 10–20% rescue (Figure 5.17). The small magnitude of rescue implies that FOXO1 regulation by miR-132/miR-212 only partially contributes

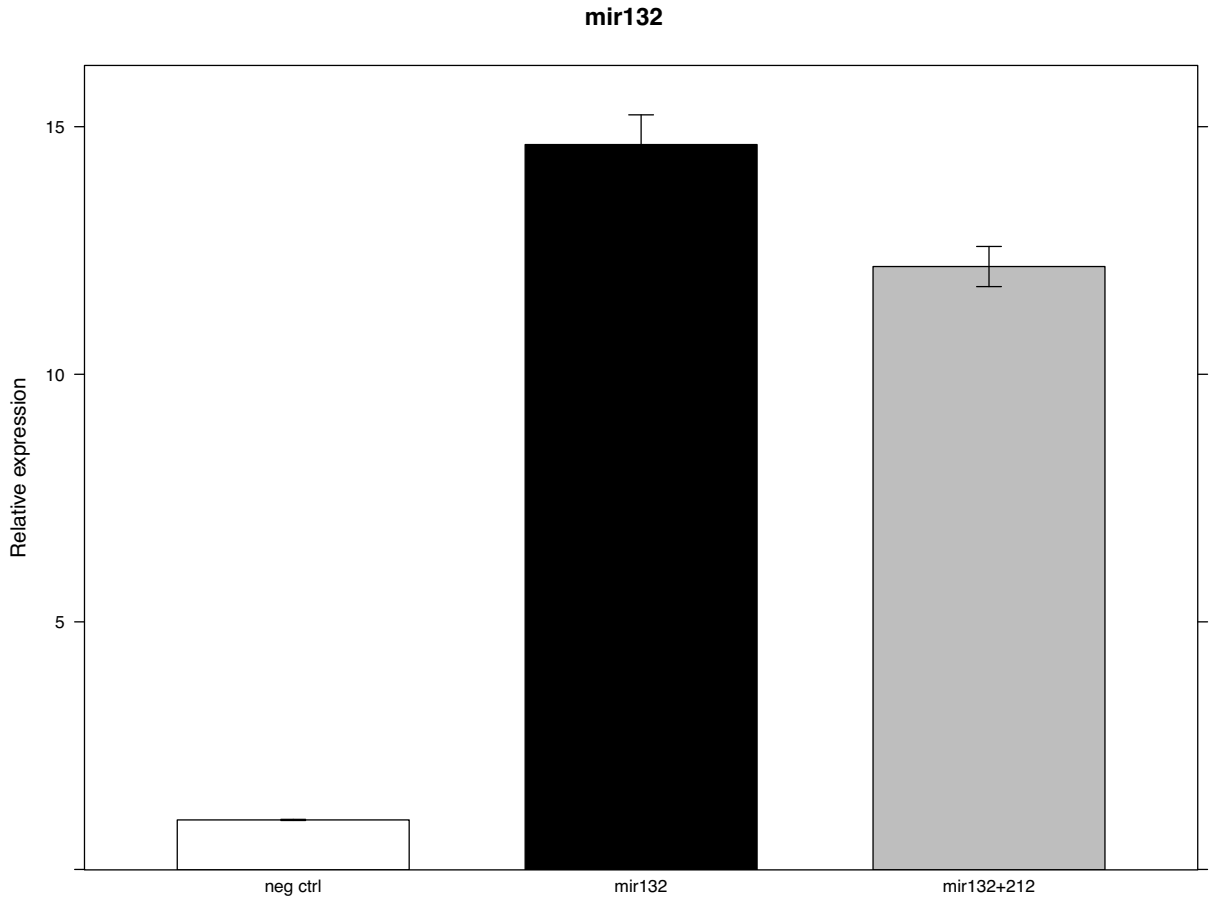

Figure 5.13: **Lentivirus constructs express mature miR-132.** RT-qPCR expression analysis of mature miR-132 SH-SY5Y cells that have been infected with either control virus (neg ctrl), miR-132-expressing virus (miR-132), or both miR-132 and miR-212-expressing virus. Expression values were normalized by 5S, U6, and U91 expression.

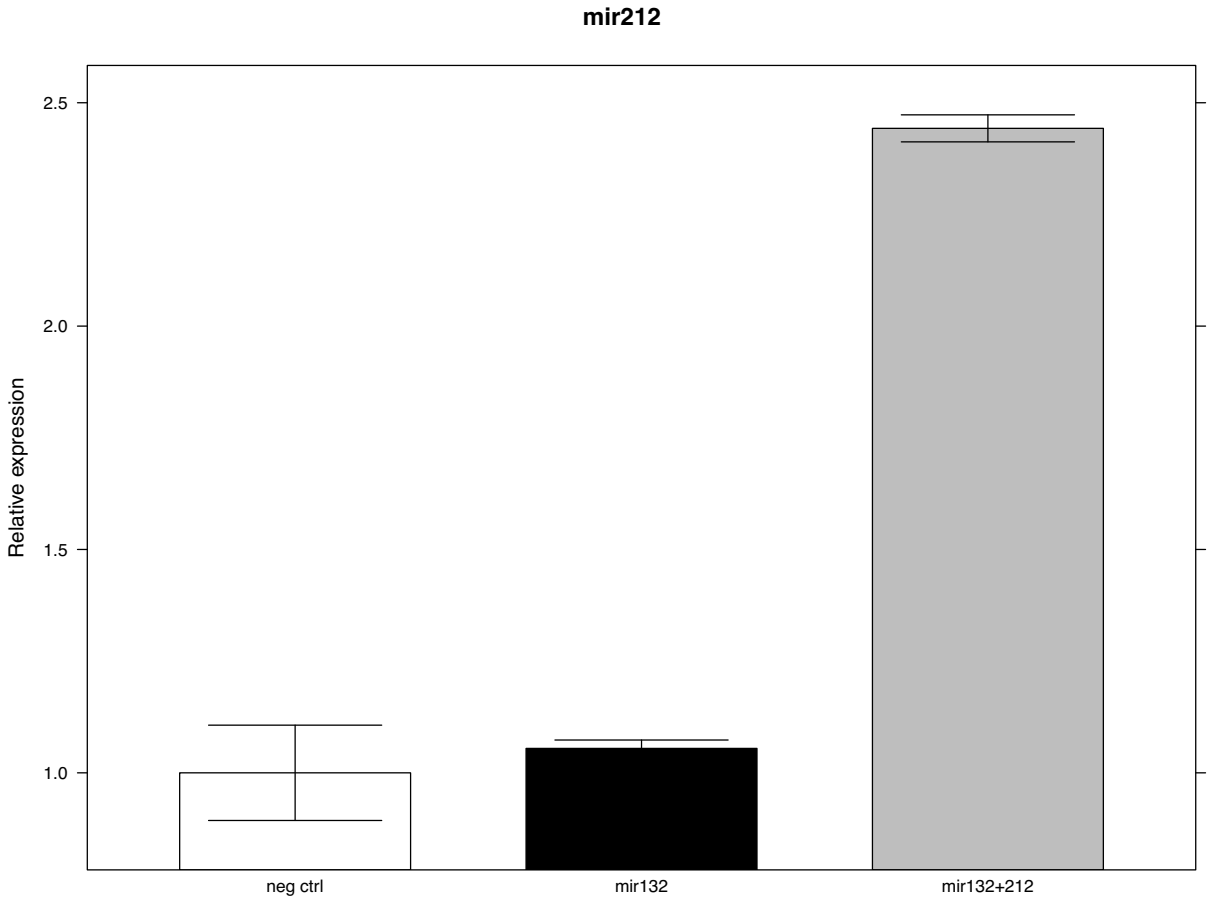

Figure 5.14: **Lentivirus constructs express mature miR-212.** RT-qPCR expression analysis of mature miR-212 SH-SY5Y cells that have been infected with either control virus (neg ctrl), miR-132-expressing virus (miR-132), or both miR-132 and miR-212-expressing virus. Expression values were normalized by 5S, U6, and U91 expression.

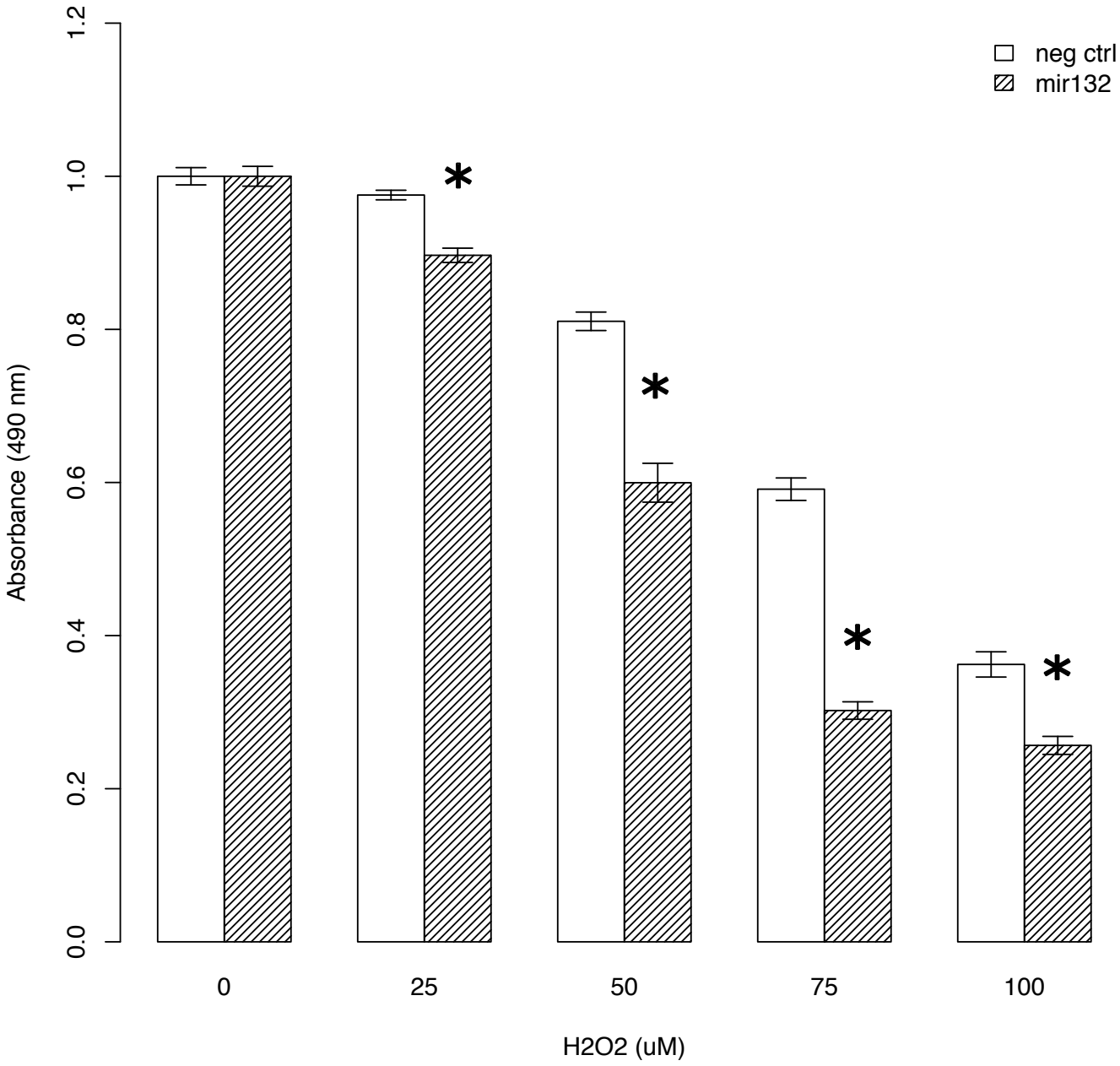

Figure 5.15: **miR-132 sensitizes to oxidative stress.** Virus-infected SH-SY5Y cells were treated for 60 minutes with H_2O_2 and cell viability was determined using MTS assay. Statistical design included planned comparison against control within treatment groups. *$P < 0.05$ by t-test with correction for multiple tests by Holm's method.

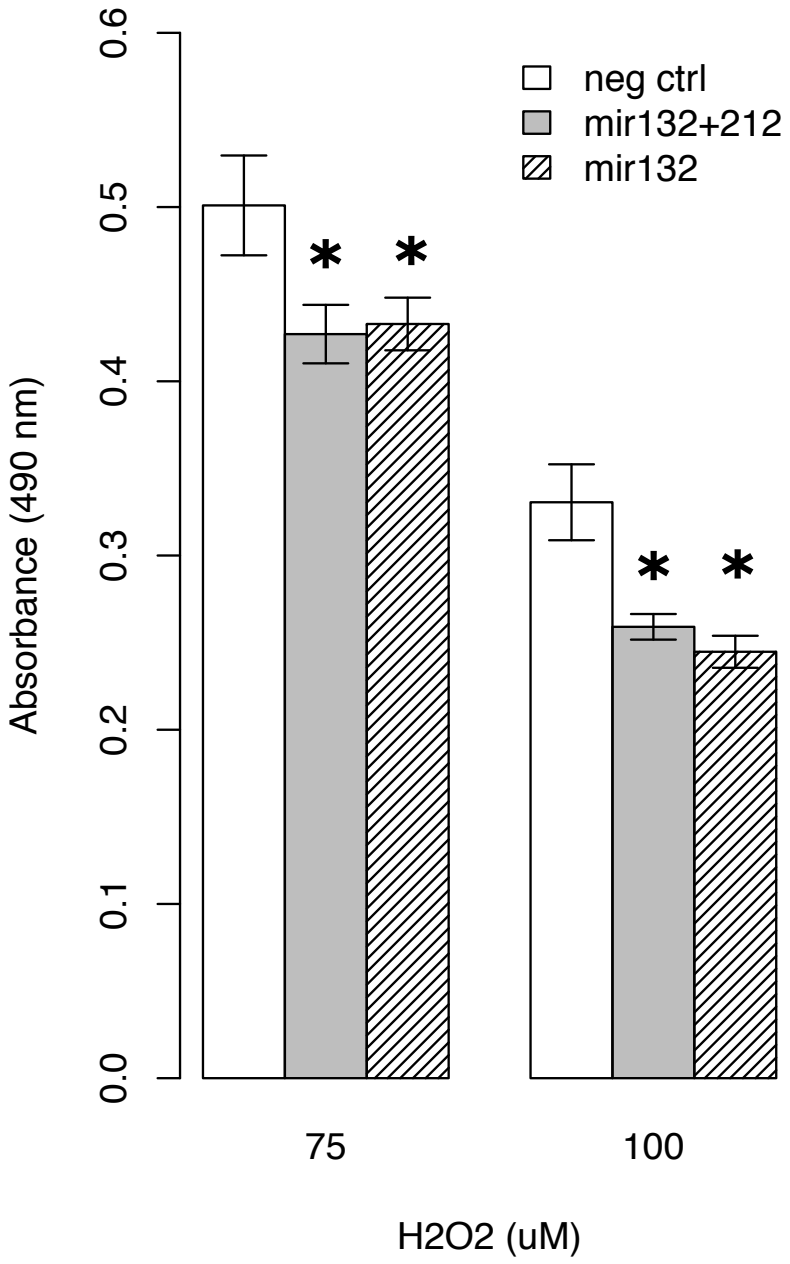

Figure 5.16: **miR-132/miR-212 sensitize to oxidative stress.** Virus-infected SH-SY5Y cells were differentiated with retinoic for 5 days and then were treated for 60 minutes with H_2O_2 and cell viability was determined using MTS assay. Statistical design included planned comparison against control within treatment groups. *$P < 0.05$ by t-test with correction for multiple tests by Holm's method.

to the cell death phenotype. Given that miR-132/miR-212 can directly regulate several other protective genes such as SOD2, NRF2, and SIRT1, that restoration of FOXO1 levels provides only a partial rescue of the phenotype is not unexpected.

REST regulates miR-132/miR-212 during brain aging

Since miR-132/miR-212 are decreased during aging one candidate mechanism is increased repression of expression. There is a well-conserved REST RE1 binding motif between miR-132/miR-212, and nuclear REST levels increase during aging (Lu et al., 2014). REST has also been shown to bind to this RE1 site in mouse (Conaco et al., 2006).

To investigate if REST may regulate miR-132/miR-212 during human brain aging we performed ChIP-qPCR for REST in young and aged prefrontal cortex using primers near the REST RE1 binding site. We designed primers that were as close as possible to the RE1 site but could not design a pair flanking the RE1 due to the highly repetitive nature and high GC content of the region. We found a significant 1.7–2.7-fold increase in REST binding to the region near the miR-132/miR-212 RE1 site using both of these primers in the aged population (Figure 5.18) where miR-132/miR-212 levels are decreased. Thus, increased REST during aging may be responsible for decreased miR-132/miR-212 during aging.

To investigate whether REST is required for miR-132/miR-212 downregulation during brain aging we analyzed whole brain knockout of REST using Nestin-Cre;$REST^{lx/lx}$ and control Nestin-Cre;$REST^{wt/wt}$ mice during aging. Even as early as 8 months miR-132/miR-212 levels are decreased in Nestin-Cre;$REST^{wt/wt}$ mice compared to young mice (Figure 5.19, Figure 5.20). Notably, miR-132/miR-212 levels are not decreased during aging in Nestin-Cre;$REST^{lx/lx}$ mice implicating a role for REST in their downregulation during brain aging.

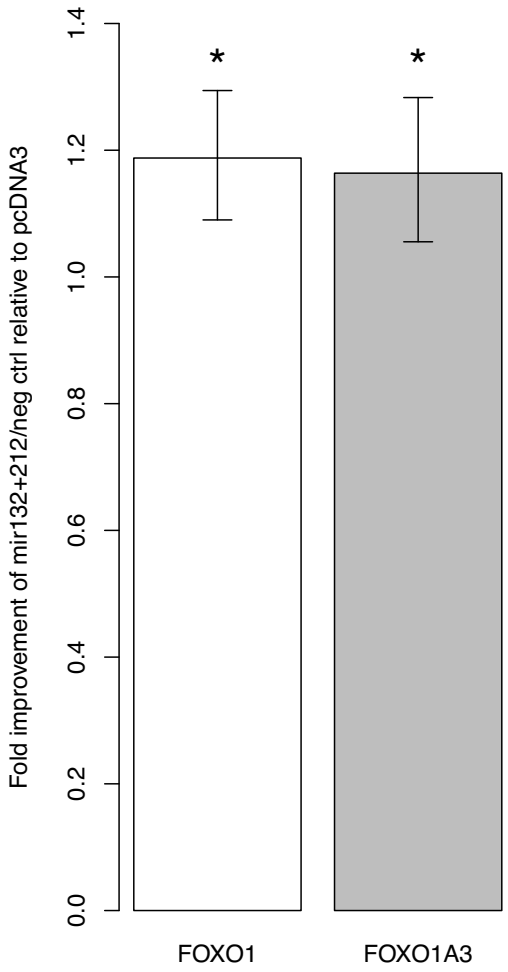

Figure 5.17: **Restoration of FOXO1 partially rescues miR-132/miR-212 apoptotic cell death phenotype.** FOXO1, FOXO1A3, and pcDNA3 stable RA-differentiated SH-SY5Y were transiently transfected with miR-132/miR-212 or negative control. 5 days later MTS assay was performed. Mean fold improvement vs pcDNA3 with 95% confidence interval derived from 3 independent experiments is shown. *$P < 0.05$ fixed effects inverse variance meta-analysis with correction for multiple tests by Holm's method.

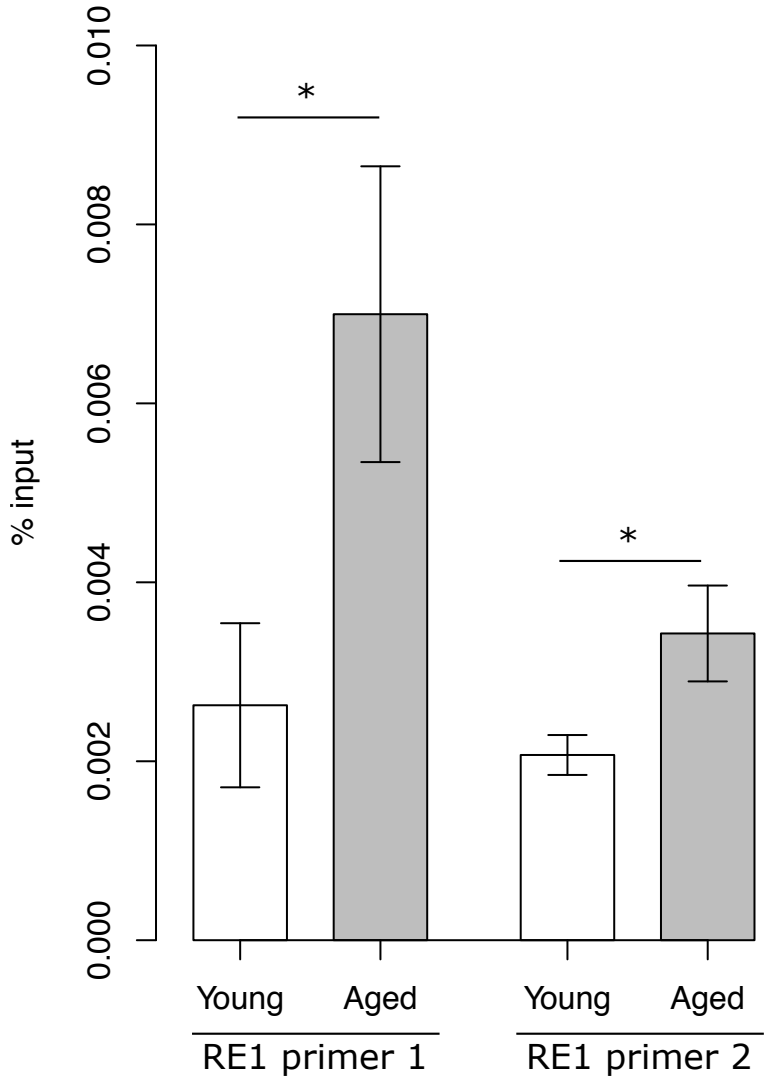

Figure 5.18: **Increased REST binding to miR-132/miR-212 RE1 site during aging.** We analyzed REST binding by ChIP-qPCR for REST using primers near the RE1 site between miR-132/miR-212 in human prefrontal cortex samples. RE1 primer 1 pair (Zhang $\mathrm{et\ al.}$, 2011a) amplifies a product 173 bp upstream of the RE1 while RE1 primer 2 pair amplifies a product 635 bp downstream of the RE1 near the transcription start site. Young, $n = 6$; Aged, $n = 9$. *$P < 0.05$, t-test.

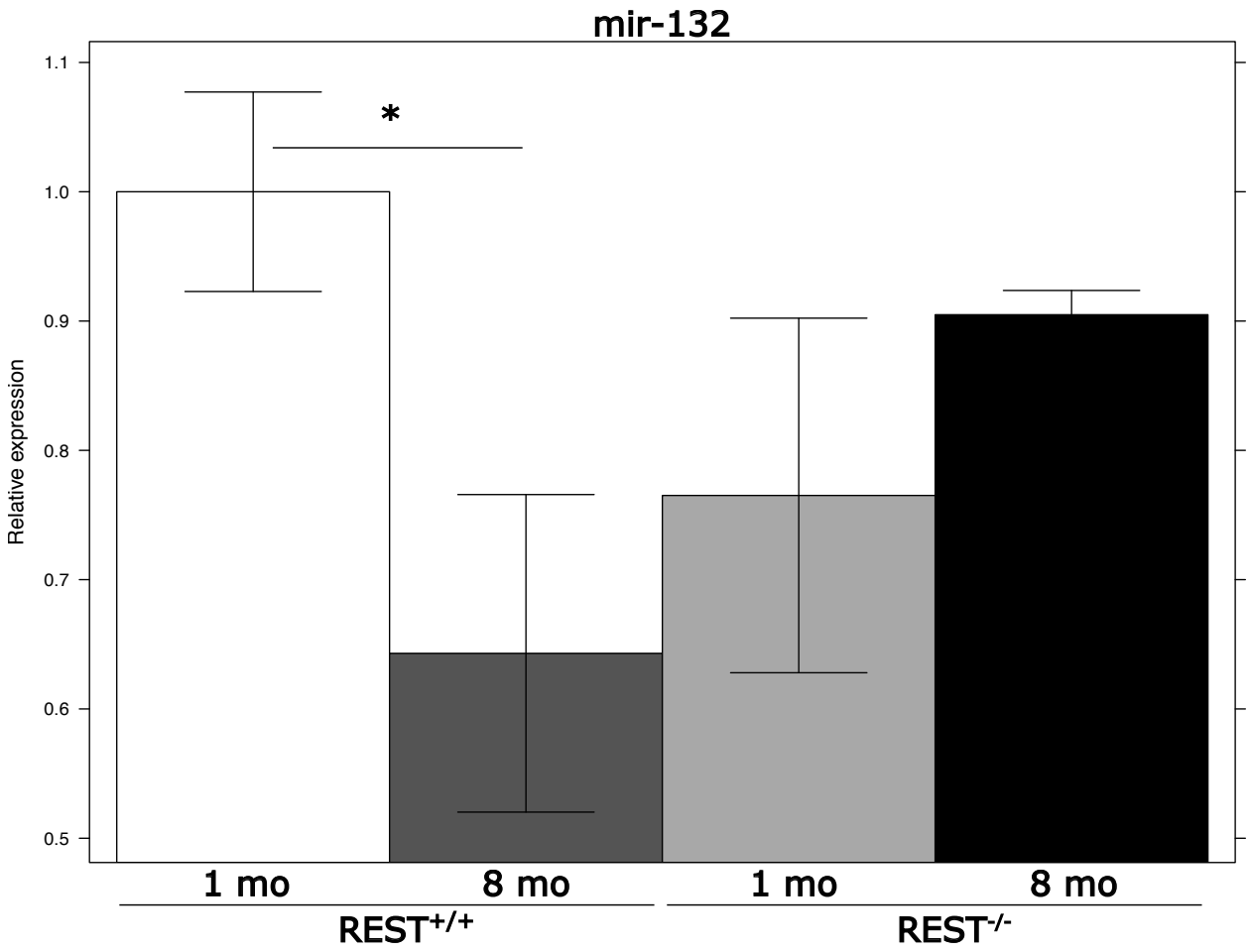

Figure 5.19: **REST is required for downregulation of miR-132 during mouse brain aging.** RNA was extracted from frontal cortex of Nestin-Cre;REST$^{lx/lx}$ (REST$^{-/-}$) or control Nestin-Cre;REST$^{wt/wt}$ (REST$^{+/+}$) mice at age 1 month and 8 months. $n = 4$ mice per group. Statistical design included planned comparison within genotype groups. *$P < 0.05$ by one-tailed t-test with correction for multiple tests by Holm's method.

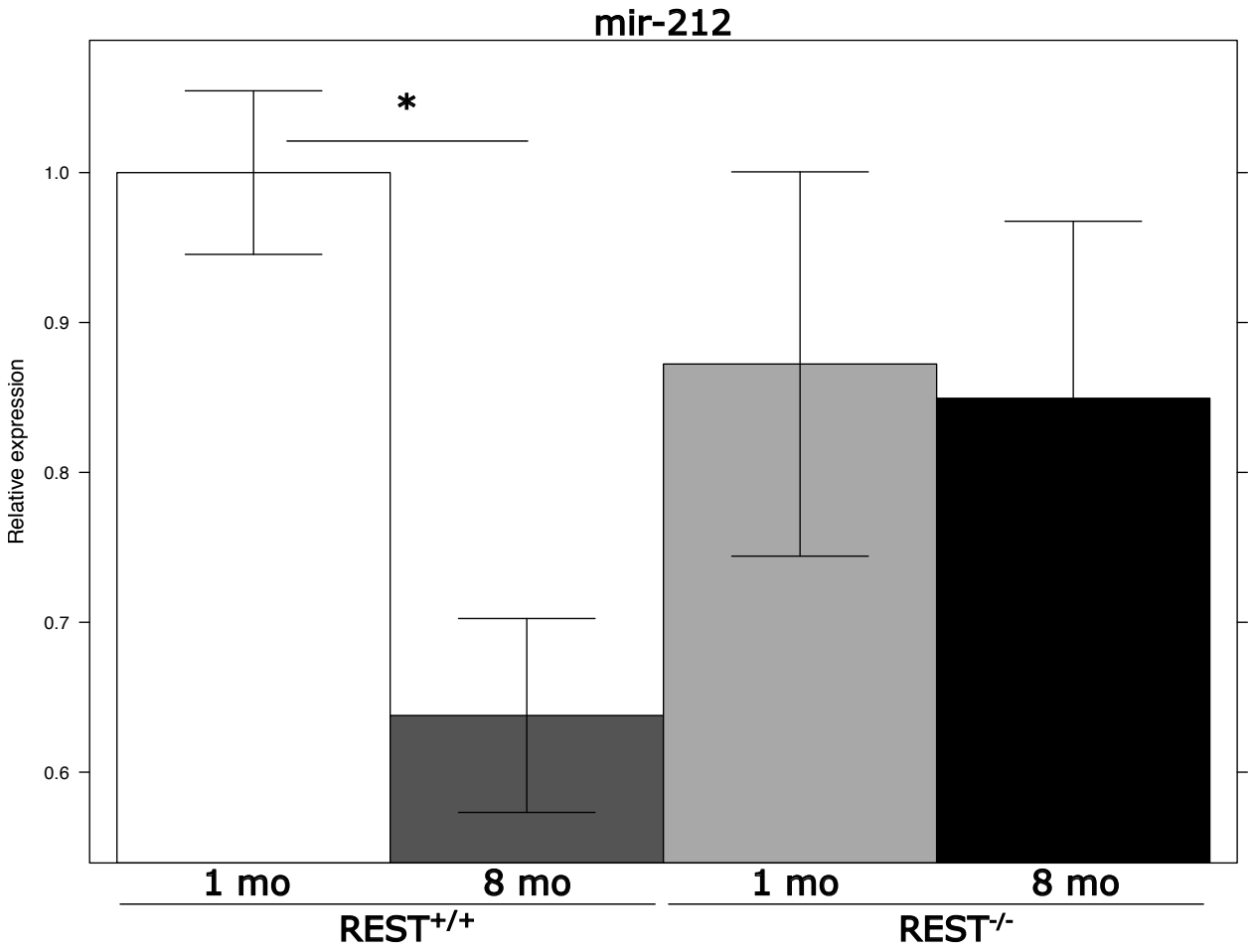

Figure 5.20: **REST is required for downregulation of miR-212 during mouse brain aging.** RNA was extracted from frontal cortex of Nestin-Cre;REST$^{lx/lx}$ (REST$^{-/-}$) or control Nestin-Cre;REST$^{wt/wt}$ (REST$^{+/+}$) mice at age 1 month and 8 months. $n = 4$ mice per group. Statistical design included planned comparison within genotype groups. *$P < 0.05$ by one-tailed t-test with correction for multiple tests by Holm's method.

Discussion

miR-132/miR-212 have been shown to be involved in many fundamental neuronal processes yet high levels of miR-132/miR-212 are detrimental impairing learning (Hansen et al., 2013) and short term memory (Scott et al., 2012) while low levels after status epilepticus are protective (Jimenez-Mateos et al., 2011). Thus, decreased miR-132/miR-212 levels during brain aging could be neuroprotective. Indeed, we find that high levels of miR-132/miR-212 are detrimental by sensitizing to oxidative stress and promoting apoptosis. Since oxidative stress increases in normal brain aging and AD has pronounced cell death the downregulation of these miR-132/miR-212 may be a neuroprotective response. In agreement, miR-132/miR-212 have been shown to directly regulate several critical targets involved in oxidative stress including FOXO3, NFE2L2/NRF2, SOD2, and SIRT1, and FOXO1 as we have shown here. FOXO1 has been shown to promote survival during oxidative stress by regulating SOD2, catalase, and GADD45alpha and activating the thioredoxin pathway. Similarly, FOXO1 deficiency correlates with increased ROS (Sengupta et al., 2011). Our data showing that miR-132/miR-212 directly regulate FOXO1 may have relevance to human brain aging since FOXO1 is increased in aged individuals. This may indicate that one mechanism the aged brain deals with increasing oxidative stress is by increasing the amount of FOXO1 to provide neuroprotection. However, the protection from oxidative stress may come at the cost of decreased neuronal function, and it would be interesting to determine whether the reduced levels of miR-132/miR-212 during aging contribute to decreased neural plasticity and cognition during aging.

Other groups have found that miR-132/miR-212 are decreased in AD relative to aged as well and that FOXO1 levels are correspondingly increased in AD (Lau et al., 2013). The potentially increased FOXO1 during AD may protect against amyloid-β-induced oxidative stress. One report that conflicts with some of our results (Wong et al., 2013) focused on the phenotypic consequences of decreased miR-132 in AD and miR-132 regulation of FOXO3

in mouse primary cultures. They show miR-132 overexpression protects against apoptosis and H_2O_2-induced oxidative stress and show similar magnitude of rescue by knocking down FOXO3 as we see by overexpressing FOXO1. However, FOXO1 is not a predicted target of miR-132 in mouse, and we never saw regulation of FOXO3 by miR-132/miR-212 in our human SH-SY5Y system suggesting differences in the experimental systems or species-specific differences.

Given that increased REST nuclear levels may distinguish cognitively-intact aged from those that develop AD, and REST provides neuroprotection, it is interesting that we see increased binding of REST to miR-132/miR-212 in human brain aging and that REST is required for miR-132/miR-212 downregulation during mouse brain aging. One potential mechanism for the REST regulation of FOXO1 in the aging brain is that REST represses miR-132/miR-212 which derepresses FOXO1. It would be important to know if any of the stress resistance provided by REST during brain aging is through downregulation of miR-132/miR-212 and derepression of FOXO1. miR-132/miR-212 are also CREB-regulated (Vo $\mathrm{et\ al.}$, 2005) and CREB signaling decreases during aging. Another interesting area to investigate would be the impact of reduced CREB signaling during aging and AD on miR-132/miR-212.

Overall these experiments indicate that miR-132/miR-212 are downregulated during human brain aging, inversely correlate with increased FOXO1 levels likely due to their ability to directly repress FOXO1 translation, and that REST may be directly responsible for repressing their expression by binding to the conserved RE1 site between miR-132 and miR-212.

Methods

Brain sample procurement.

Postmortem human brain material was procured in accordance with institutional guidelines governed by approved protocols. Tissue samples were procured from the Rush University Medical Center, the University of Maryland, Duke University, the Brigham and Womens Hospital, and the Massachusetts General Hospital. Tissue samples from Rush University Medical Center were derived from participants in the Religious Order Study (ROS) and Rush Memory and Aging Project (MAP) at the Rush Alzheimers Disease Center, which are longitudinal, clinical-pathologic studies of aging, cognitive decline and AD (Bennett $\mathrm{et\ al.}$, 2012$\mathrm{a,b}$). Study participants agreed to comprehensive annual clinical and neuropsychological evaluation and brain donation at death.

Chemicals and antibodies

DMSO, retinoic acid, NAC, H_2O_2 were from Sigma. Antibodies: FOXO1 (Cell Signaling Technology C29H4), beta-actin (Sigma A2103).

miRNA microarray and analysis

miRNA microarray profiling was performed on young and aged post-mortem human prefrontal cortex gray matter at LC Sciences. Microarray data were processed by background subtraction of the median 10^{th} percentile and scale normalization and analyzed using the limma Bioconductor package using a moderated t-test. Benjamini and Hochberg false discovery rate (FDR) was calculated in R.

miRNA RT-qPCR

To extract RNA Trizol (Invitrogen) with DNase I digestion for brain tissue and Trizol or miRNeasy mini kit with on-column DNase I digestion for cells. First, cDNA was created using Qiagen miScript RT kit. Then, mature miRNA was measured using Qiagen miScript SYBR green PCR kit and Qiagen miScript primer assays for miR-132, miR-212, U25, U91, and 5S. miRNAs were normalized to the geometric mean of the small RNA reference transcripts specified, SNORD25 (U25), SCARNA17 (U91), 5S rRNA, or U6. Quantification was performed using the Comparative ct method.

miRNA target prediction

We combined 7 miRNA target prediction databases and 2 experimentally validated databases using the algorithm: transcript T is a target of miRNA M if at least 4 of 7 databases predict M targets T or if an experimentally validated database indicates M targets T.

Cell culture

SH-SY5Y, a human neuroblastoma cell line, were from ATCC. Cells were maintained at 37℃ in a 5% CO_2 humidified incubator. Cells were cultured in compete medium (10% fetal bovine serum (FBS, heat inactivated 30 minutes at 56℃), 100 units/mL penicillin, 100 μg/mL strepomycin, 1mM glutamax in Dulbecco's Modified Eagle Medium (DMEM, with 4.5 mg/L D-glucose) (all from Invitrogen)). Cells were split every 2–3 days. 4×10^5 cells/mL cells were plated per well unless otherwise stated.

Retinoic acid differentiation of SH-SY5Y cells

SH-SY5Y cells were plated at 4×10^4 cells/mL in plates in complete medium. 24 hours later medium was changed to complete medium with 10 μM retinoic acid. Medium with retinoic acid was changed every 3 days. Cells were used for assays or transfection after 5 days of differentiation.

miRNA overexpression reagents

For miRNA overexpression we used miRNA mimics which are short double stranded RNA oligonucleotides from Qiagen. For negative control overexpression we used AllStars Negative Control siRNA from Qiagen. Lipofectamine 2000 was used as the transfection reagent. Transfection efficiency was approximately 50%. We also created lentiviruses expressing the pre-microRNA form of miR-132 and miR-212 that are expressed by splicing from the 3' UTR of GFP in FUGW vector and included approximately 150 bp of genomic context on each side of the pre-microRNA.

miRNA overexpression

SH-SY5Y cells were plated in 24-well plates at 2×10^5 cells per well in 500 μl growth medium or in 96-well plates at 4×10^4 cells per well in 100 μl growth medium. 24 hours later when cells were approximately 30% confluent medium was changed to fresh growth medium without antibiotics and transfected with mimics using Lipofectamine 2000 according to the manufacturer's protocol. For miR-132, miR-212, and negative control overexpression we used mimics at 100 nM final concentration. For miR-132/miR-212 joint overexpression we used each at 50 nM. Medium was changed 8–24 hours after transfection to remove complexes. Cells were collected or assayed 48 hours after transfection. For retinoic acid differentiated SH-SY5Y experiments, cells were collected or assayed 120 hours after transfection.

Mutation of FOXO1 3' UTR miR-132/miR-212 predicted binding sites

We cloned the entire FOXO1 3' UTR into 3' UTR of firefly luciferase in pmirglo vector. We computationally searched through the 16384 potential mutations of the seed sequence to choose two that maximally eliminated binding to miR-132/miR-212 by RNAhybrid while creating as few new binding sites as possible. We mutated the two predicted miR-132/miR-212 seed sequences to the two computationally predicted ones using Quikchange II XL kit.

Luciferase assays

We performed luciferase assays in retinoic acid differentiated SH-SY5Y cells that had stably integrated either the WT or mutated FOXO1 3'UTR luciferase plasmid. In a 96-well plate we transiently transfected miR-132/miR-212 or negative control and 48 hours later we performed luciferase assay using the Dual luciferase assay from Promega following manufacturer's protocol. We measured firefly luciferase activity and normalized to renilla luciferase activity to control for differences in cell number per well.

Cell culture treatments

Treatments were performed by changing medium to fresh medium with the specified concentrations of the compound. H_2O_2 and NAC were prepared in water. Retinoic acid was prepared in DMSO.

Hoechst staining and quantification of apoptotic cells

Cells were fixed for 20 minutes in 4% paraformaldehyde in $1\times$ PBS at room temperature, washed with $1\times$ PBS, stained with hoechst, and imaged. Cells were classified as apoptotic if they had characteristic bright punctate staining indicative of cleaved chromatin.

Assessment of cell viability

Cell viability was assessed using a chromogenic assay that involves the biological reduction by viable cells of the tetrazolium compound 3-(4,5-dimethylthiazol-2-yl)-5-(3-carboxymethoxyphenyl)-2-(4-sulfophenyl)-2H-tetrazolium (MTS). Treatments and assays were performed in 96-well plates in 100 μl complete medium with the specified compounds. After treatments, cell medium was changed to 120 μl complete medium containing 20 μl MTS reagent following manufacturer's instructions and assayed 1–4 hours later. Absorbance at 490 nm was measured using a plate reader.

Western blotting

Tissues were homogenized using RIPA-DOC buffer supplemented with protease and phosphatase inhibitors (Complete and Phosphostop, Roche). A sonication step was performed prior to centrifugation at 10,000 rpm for 10 min at 4C. The supernatant was removed and the protein concentration determined (BioRad protein assay). 2$\times$ laemmli buffer containing beta mercaptoethanol was added. Cells were directly lysed in 2$\times$ laemmli buffer. Approximately 20 μg protein was loaded per lane and resolved by 4–20% Mini-PROTEAN TGX precast gels (Biorad). Western blots were quantified by densitometry using the ImageJ software. Bands of interest were normalized to beta-actin which served as a loading control.

Generation of recombinant lentiviruses

Viral particles were generated in HEK293T cells by co-transfection of transfer vectors, packaging plasmid (pRSV-REV and pMDLg) and envelope plasmid (pCMV-VSVG) using Lipofectamine 2000 (Invitrogen). Cells were cultured for 2 days and the medium was collected, centrifuged at 1000$\times$g for 5 min, and passed through a 0.45 μm low protein binding filter (VWR).

Lentiviral transduction

Approximately 8×10^4 SH-SY5Y cells were plated in a 6-well dish. 14–20 hours later medium was changed and lentiviral containing supernatants were added. 2 days later medium was changed and cells were split for assays.

Acknowledgements

Tao Lu (Yankner lab) performed RNA extraction and sent samples for miRNA microarray analysis in 2005. Tao Lu performed ChIP for REST in aged human brains and provided DNA for analysis. Liviu Aron (Yankner lab) provided frozen $REST^{lx/lx}$ and $REST^{-/-}$ mouse brain tissue. Candidate performed all other experiments and analyses.

Chapter 6

Conclusion

The mechanisms that protect neurons against stress and prevent neurodegeneration throughout the lifetime of an organism are incompletely understood. Here we provide evidence that REST is critical for neuronal and cognitive preservation in aged humans. REST has been extensively studied as a repressor of neuronal genes during development, but its role in protective functions during aging had been largely unknown. We find that REST is induced in neurons of cognitively-intact aged individuals, but not those with AD. Moreover, REST provides neuroprotection from diverse stresses, including oxidative stress, and protects against neuronal apoptosis and AD pathology. Chromatin immunoprecipitation analysis suggests that REST protects against apoptosis and AD pathology through direct binding and repression of pro-apoptotic genes and genes that contribute to AD pathology. However, the mechanisms by which REST provides oxidative stress resistance were less clear. We unexpectedly found that REST regulates FOXO1, a fundamental regulator of the response to oxidative stress. REST regulates FOXO1 protein levels and nuclear localization *in vitro* through several mechanisms including insulin/IGF-1 signaling and FOXO1 expression. Moreover, REST protects against oxidative stress partially through regulation of FOXO1 suggesting that the oxidative stress sensitivity of REST-deficient cells is due, in part, to reduced FOXO1. REST nuclear levels are also correlated with

FOXO1 nuclear levels in pyramidal neurons of the human prefrontal cortex in young and aged individuals. In cognitively-intact aged individuals REST and FOXO1 expression is highly correlated, and their expression is also correlated with several genes involved in directly protecting against oxidative stress but not correlated with canonical FOXO1 pro-apoptotic genes supporting the idea that REST may provide neuroprotection by inducing FOXO1 specifically tuned for stress resistance. How FOXO1 only activates protective and not pro-apoptotic genes is unknown, but may be due to REST-mediated repression of FOXO1 pro-apoptotic targets or altered post-translational modifications of FOXO1 such as deacetylation.

To investigate if the neuroprotective functions of REST were associated with cognitive preservation during aging we measured REST nuclear levels by immunoflourescence in humans. REST nuclear levels in pyramidal cortical neurons were shown to positively correlate with cognitive function proximate to death in a cross-sectional analysis. However, whether this association was an artifact of a cross-sectional analysis and would also be found in a longitudinal analysis was unknown. We found that REST nuclear levels were associated with reduced longitudinal cognitive decline during late life aging by a linear mixed model analysis, and were the second most significant contributor to cognitive decline during aging while accounting for AD neuropathologies. REST nuclear levels also explain a significant fraction of the variability of cognitive decline suggesting that regulation of REST is a critical determinant of cognitive function during aging and account for the heterogeneity in interindividual cognitive decline. Finally, we found that REST nuclear levels were correlated with increased AD age of onset and decreased AD neuropathology further implying a protective role in AD.

To understand other candidate regulators of brain aging, we also profiled miRNAs in the human prefrontal cortex and found that miR-132/miR-212, canonical REST-regulated miRNAs regulating diverse neuronal and cognitive processes, are decreased during aging in cognitively-intact individuals and centenarians, and further decreased in AD. miR-132/miR-

212 directly regulate FOXO1 suggesting an additional mechanism by which REST may regulate FOXO1 *in vivo*. miR-132/miR-212 overexpression is pro-apoptotic and sensitizes to oxidative stress. We found increased REST binding to a conserved REST RE1 binding site between miR-132/miR-212 in the prefrontal cortex of aged individuals, and that REST is required for downregulation of miR-132/miR-212 during mouse brain aging. This suggests that decreased miR-132/miR-212 levels during brain aging could be neuroprotective and may be an additional mechanism by which REST provides neuroprotection.

It remains unclear, however, if there are any detrimental effects of increased REST nuclear levels during aging. REST represses neuronal gene expression, and REST expression is negatively correlated with neuronal gene expression during aging which could be considered detrimental. Neuronal function has a high energy demand, and, consequently, a high metabolic rate and mitochondrially produced oxidative stress. Perhaps preservation of neurons during a human lifespan requires submaximal neuronal function provided by an age-dependent induction of REST? In agreement, we find that centenarians typically have the highest REST nuclear levels.

We have provided several independent lines of evidence that REST is a fundamental regulator of brain aging, and delineate potential mechanisms by which REST may provide stress resistance such as through FOXO1. Therefore, clarifying the molecular mechanisms that regulate REST during aging may be key to understanding the transition between healthy brain aging and neurodegeneration. With this knowledge, designing therapies to regulate REST nuclear levels may be viable as a near-term mechanism to promote healthy cognitive aging.

Appendix

Appendix Tables 2.1, 2.2, 2.3, 2.4a, and 2.4b are provided as separate spreadsheets.

References

Abrajano, J. J., Qureshi, I. A., Gokhan, S., Zheng, D., Bergman, A. and Mehler, M. F. (2009). REST and CoREST modulate neuronal subtype specification, maturation and maintenance. PLoS One *4*, e7936.

Adiconis, X., Borges-Rivera, D., Satija, R., DeLuca, D. S., Busby, M. A., Berlin, A. M., Sivachenko, A., Thompson, D. A., Wysoker, A., Fennell, T., Gnirke, A., Pochet, N., Regev, A. and Levin, J. Z. (2013). Comparative analysis of RNA sequencing methods for degraded or low-input samples. Nat Methods *10*, 623–9.

Alcendor, R. R., Gao, S., Zhai, P., Zablocki, D., Holle, E., Yu, X., Tian, B., Wagner, T., Vatner, S. F. and Sadoshima, J. (2007). Sirt1 regulates aging and resistance to oxidative stress in the heart. Circ Res *100*, 1512–1521.

Andrews-Hanna, J. R., Snyder, A. Z., Vincent, J. L., Lustig, C., Head, D., Raichle, M. E. and Buckner, R. L. (2007). Disruption of large-scale brain systems in advanced aging. Neuron *56*, 924–35.

Ballas, N., Grunseich, C., Lu, D. D., Speh, J. C. and Mandel, G. (2005). REST and its corepressors mediate plasticity of neuronal gene chromatin throughout neurogenesis. Cell *121*, 645–57.

Ballas, N. and Mandel, G. (2005). The many faces of REST oversee epigenetic programming of neuronal genes. Curr Opin Neurobiol *15*, 500–6.

Bassuk, A. G., Wallace, R. H., Buhr, A., Buller, A. R., Afawi, Z., Shimojo, M., Miyata, S., Chen, S., Gonzalez-Alegre, P., Griesbach, H. L., Wu, S., Nashelsky, M., Vladar, E. K., Antic, D., Ferguson, P. J., Cirak, S., Voit, T., Scott, M. P., Axelrod, J. D., Gurnett, C., Daoud, A. S., Kivity, S., Neufeld, M. Y., Mazarib, A., Straussberg, R., Walid, S., Korczyn, A. D., Slusarski, D. C., Berkovic, S. F. and El-Shanti, H. I. (2008). A homozygous mutation in human PRICKLE1 causes an autosomal-recessive progressive myoclonus epilepsy-ataxia syndrome. Am J Hum Genet *83*, 572–81.

Bennett, D. A., Schneider, J. A., Aggarwal, N. T., Arvanitakis, Z., Shah, R. C., Kelly, J. F., Fox, J. H., Cochran, E. J., Arends, D., Treinkman, A. D. and Wilson, R. S. (2006). Decision rules guiding the clinical diagnosis of Alzheimer's disease in two community-based cohort studies compared to standard practice in a clinic-based cohort study. Neuroepidemiology *27*, 169–76.

Bennett, D. A., Schneider, J. A., Arvanitakis, Z. and Wilson, R. S. (2012a). Overview and findings from the religious orders study. Curr Alzheimer Res *9*, 628–45.

Bennett, D. A., Schneider, J. A., Buchman, A. S., Barnes, L. L., Boyle, P. A. and Wilson, R. S. (2012b). Overview and findings from the rush Memory and Aging Project. Curr Alzheimer Res *9*, 646–63.

Bennett, D. A., Wilson, R. S., Schneider, J. A., Evans, D. A., Beckett, L. A., Aggarwal, N. T., Barnes, L. L., Fox, J. H. and Bach, J. (2002). Natural history of mild cognitive impairment in older persons. Neurology *59*, 198–205.

Bolstad, B. M., Irizarry, R. A., Astrand, M. and Speed, T. P. (2003). A comparison of normalization methods for high density oligonucleotide array data based on variance and bias. Bioinformatics *19*, 185–193.

Boulias, K. and Horvitz, H. R. (2012). The C. elegans microRNA mir-71 acts in neurons to promote germline-mediated longevity through regulation of DAF-16/FOXO. Cell Metab *15*, 439–50.

Boyle, P. A., Wilson, R. S., Yu, L., Barr, A. M., Honer, W. G., Schneider, J. A. and Bennett, D. A. (2013a). Much of late life cognitive decline is not due to common neurodegenerative pathologies. Ann Neurol *74*, 478–89.

Boyle, P. A., Yu, L., Wilson, R. S., Schneider, J. A. and Bennett, D. A. (2013b). Relation of neuropathology with cognitive decline among older persons without dementia. Front Aging Neurosci *5*, 50.

Braak, H. and Braak, E. (1991). Neuropathological stageing of Alzheimer-related changes. Acta Neuropathol *82*, 239–59.

Brenner, S. (1974). The genetics of Caenorhabditis elegans. Genetics *77*, 71–94.

Bruce, A. W., Donaldson, I. J., Wood, I. C., Yerbury, S. A., Sadowski, M. I., Chapman, M., Göttgens, B. and Buckley, N. J. (2004). Genome-wide analysis of repressor element 1 silencing transcription factor/neuron-restrictive silencing factor (REST/NRSF) target genes. Proc Natl Acad Sci U S A *101*, 10458–10463.

Brunet, A., Bonni, A., Zigmond, M. J., Lin, M. Z., Juo, P., Hu, L. S., Anderson, M. J., Arden, K. C., Blenis, J. and Greenberg, M. E. (1999). Akt promotes cell survival by phosphorylating and inhibiting a Forkhead transcription factor. Cell *96*, 857–868.

Brunet, A., Sweeney, L. B., Sturgill, J. F., Chua, K. F., Greer, P. L., Lin, Y., Tran, H., Ross, S. E., Mostoslavsky, R., Cohen, H. Y., Hu, L. S., Cheng, H.-L., Jedrychowski, M. P., Gygi, S. P., Sinclair, D. A., Alt, F. W. and Greenberg, M. E. (2004). Stress-dependent regulation of FOXO transcription factors by the SIRT1 deacetylase. Science *303*, 2011–5.

Burke, S. N. and Barnes, C. A. (2006). Neural plasticity in the ageing brain. Nat Rev Neurosci *7*, 30–40.

Bus, J. S. and Gibson, J. E. (1984). Paraquat: model for oxidant-initiated toxicity. Environ Health Perspect *55*, 37–46.

Busciglio, J. and Yankner, B. A. (1995). Apoptosis and increased generation of reactive oxygen species in Down's syndrome neurons in vitro. Nature *378*, 776–9.

Caccamo, A., Oddo, S., Tran, L. X. and LaFerla, F. M. (2007). Lithium reduces tau phosphorylation but not A beta or working memory deficits in a transgenic model with both plaques and tangles. Am J Pathol *170*, 1669–75.

Calderone, A., Jover, T., Noh, K. M., Tanaka, H., Yokota, H., Lin, Y., Grooms, S. Y., Regis, R., Bennett, M. V. and Zukin, R. S. (2003). Ischemic insults derepress the gene silencer REST in neurons destined to die. J Neurosci *23*, 2112–2121.

Calixto, A., Chelur, D., Topalidou, I., Chen, X. and Chalfie, M. (2010). Enhanced neuronal RNAi in C. elegans using SID-1. Nat Methods *7*, 554–9.

Castello, P. R., Drechsel, D. A. and Patel, M. (2007). Mitochondria are a major source of paraquat-induced reactive oxygen species production in the brain. J Biol Chem *282*, 14186–93.

Chen, Z. F., Paquette, A. J. and Anderson, D. J. (1998). NRSF/REST is required in vivo for repression of multiple neuronal target genes during embryogenesis. Nat Genet *20*, 136–142.

Cheng, H.-Y. M., Papp, J. W., Varlamova, O., Dziema, H., Russell, B., Curfman, J. P., Nakazawa, T., Shimizu, K., Okamura, H., Impey, S. and Obrietan, K. (2007). microRNA modulation of circadian-clock period and entrainment. Neuron *54*, 813–29.

Choi, J., Oh, S., Lee, D., Oh, H. J., Park, J. Y., Lee, S. B. and Lim, D. S. (2009). Mst1-FoxO signaling protects Naïve T lymphocytes from cellular oxidative stress in mice. PLoS One *4*.

Chong, J. A., Tapia-Ramírez, J., Kim, S., Toledo-Aral, J. J., Zheng, Y., Boutros, M. C., Altshuller, Y. M., Frohman, M. A., Kraner, S. D. and Mandel, G. (1995). REST: a mammalian silencer protein that restricts sodium channel gene expression to neurons. Cell *80*, 949–57.

Cochemé, H. M. and Murphy, M. P. (2008). Complex I is the major site of mitochondrial superoxide production by paraquat. J Biol Chem *283*, 1786–98.

Conaco, C., Otto, S., Han, J. J. and Mandel, G. (2006). Reciprocal actions of REST and a microRNA promote neuronal identity. Proc Natl Acad Sci U S A *103*, 2422–2427.

Corey-Bloom, J., Sabbagh, M. N., Bondi, M. W., Hansen, L., Alford, M. F., Masliah, E. and Thal, L. J. (1997). Hippocampal sclerosis contributes to dementia in the elderly. Neurology *48*, 154–60.

Cruchaga, C., Karch, C. M., Jin, S. C., Benitez, B. A., Cai, Y., Guerreiro, R., Harari, O., Norton, J., Budde, J., Bertelsen, S., Jeng, A. T., Cooper, B., Skorupa, T., Carrell, D., Levitch, D., Hsu, S., Choi, J., Ryten, M., UK Brain Expression Consortium, Hardy, J., Ryten, M., Trabzuni, D., Weale, M. E., Ramasamy, A., Smith, C., Sassi, C., Bras, J., Gibbs, J. R., Hernandez, D. G., Lupton, M. K., Powell, J., Forabosco, P., Ridge, P. G., Corcoran, C. D., Tschanz, J. T., Norton, M. C., Munger, R. G., Schmutz, C., Leary, M., Demirci, F. Y., Bamne, M. N., Wang, X., Lopez, O. L., Ganguli, M., Medway, C., Turton, J., Lord, J., Braae, A., Barber, I., Brown, K., Alzheimer's Research UK Consortium, Passmore, P., Craig, D., Johnston, J., McGuinness, B., Todd, S., Heun, R., Kölsch, H., Kehoe, P. G., Hooper, N. M., Vardy, E. R. L. C., Mann, D. M., Pickering-Brown, S., Brown, K., Kalsheker, N., Lowe, J., Morgan, K., David Smith, A., Wilcock, G., Warden, D., Holmes, C., Pastor, P., Lorenzo-Betancor, O., Brkanac, Z., Scott, E., Topol, E., Morgan, K., Rogaeva, E., Singleton, A. B., Hardy, J., Kamboh, M. I., St George-Hyslop, P., Cairns, N., Morris, J. C., Kauwe, J. S. K. and Goate, A. M. (2014). Rare coding variants in the phospholipase D3 gene confer risk for Alzheimer's disease. Nature *505*, 550–4.

Crystal, H., Dickson, D., Fuld, P., Masur, D., Scott, R., Mehler, M., Masdeu, J., Kawas, C., Aronson, M. and Wolfson, L. (1988). Clinico-pathologic studies in dementia: non-demented subjects with pathologically confirmed Alzheimer's disease. Neurology *38*, 1682–7.

Datta, M. and Bhattacharyya, N. P. (2011). Regulation of RE1 protein silencing transcription factor (REST) expression by HIP1 protein interactor (HIPPI). J Biol Chem *286*, 33759–69.

Datta, M., Choudhury, A., Lahiri, A. and Bhattacharyya, N. P. (2011). Genome wide gene expression regulation by HIP1 Protein Interactor, HIPPI: prediction and validation. BMC Genomics *12*, 463.

De Jager, P. L., Shulman, J. M., Chibnik, L. B., Keenan, B. T., Raj, T., Wilson, R. S., Yu, L., Leurgans, S. E., Tran, D., Aubin, C., Anderson, C. D., Biffi, A., Corneveaux, J. J., Huentelman, M. J., Alzheimer's Disease Neuroimaging Initiative, Rosand, J., Daly, M. J., Myers, A. J., Reiman, E. M., Bennett, D. A. and Evans, D. A. (2012). A genome-wide scan for common variants affecting the rate of age-related cognitive decline. Neurobiol Aging *33*, 1017.e1–15.

Dyrks, T., Dyrks, E., Masters, C. L. and Beyreuther, K. (1993). Amyloidogenicity of rodent and human beta A4 sequences. FEBS Lett *324*, 231–6.

Fabian, M. R., Sonenberg, N. and Filipowicz, W. (2010). Regulation of mRNA translation and stability by microRNAs. Annu Rev Biochem *79*, 351–79.

Fischer, A., Sananbenesi, F., Wang, X., Dobbin, M. and Tsai, L.-H. (2007). Recovery of learning and memory is associated with chromatin remodelling. Nature *447*, 178–82.

Formosa, A., Lena, A. M., Markert, E. K., Cortelli, S., Miano, R., Mauriello, A., Croce, N., Vandesompele, J., Mestdagh, P., Finazzi-Agrò, E., Levine, A. J., Melino, G., Bernardini, S.

and Candi, E. (2013). DNA methylation silences miR-132 in prostate cancer. Oncogene *32*, 127–34.

Frøkjaer-Jensen, C., Davis, M. W., Hollopeter, G., Taylor, J., Harris, T. W., Nix, P., Lofgren, R., Prestgard-Duke, M., Bastiani, M., Moerman, D. G. and Jorgensen, E. M. (2010). Targeted gene deletions in C. elegans using transposon excision. Nat Methods *7*, 451–3.

Gems, D., Sutton, A. J., Sundermeyer, M. L., Albert, P. S., King, K. V., Edgley, M. L., Larsen, P. L. and Riddle, D. L. (1998). Two pleiotropic classes of daf-2 mutation affect larval arrest, adult behavior, reproduction and longevity in Caenorhabditis elegans. Genetics *150*, 129–55.

Giannakopoulos, P., Herrmann, F. R., Bussière, T., Bouras, C., Kövari, E., Perl, D. P., Morrison, J. H., Gold, G. and Hof, P. R. (2003). Tangle and neuron numbers, but not amyloid load, predict cognitive status in Alzheimer's disease. Neurology *60*, 1495–500.

Gilbert, L. A., Larson, M. H., Morsut, L., Liu, Z., Brar, G. A., Torres, S. E., Stern-Ginossar, N., Brandman, O., Whitehead, E. H., Doudna, J. A., Lim, W. A., Weissman, J. S. and Qi, L. S. (2013). CRISPR-mediated modular RNA-guided regulation of transcription in eukaryotes. Cell *154*, 442–51.

Gómez-Isla, T., Price, J. L., McKeel, Jr, D. W., Morris, J. C., Growdon, J. H. and Hyman, B. T. (1996). Profound loss of layer II entorhinal cortex neurons occurs in very mild Alzheimer's disease. J Neurosci *16*, 4491–500.

Gräff, J. and Tsai, L.-H. (2013). Histone acetylation: molecular mnemonics on the chromatin. Nat Rev Neurosci *14*, 97–111.

Greer, E. L. and Brunet, A. (2005). FOXO transcription factors at the interface between longevity and tumor suppression. Oncogene *24*, 7410–25.

Grune, T., Jung, T., Merker, K. and Davies, K. J. A. (2004). Decreased proteolysis caused by protein aggregates, inclusion bodies, plaques, lipofuscin, ceroid, and 'aggresomes' during oxidative stress, aging, and disease. Int J Biochem Cell Biol *36*, 2519–30.

Haigis, M. C. and Yankner, B. A. (2010). The aging stress response. Mol Cell *40*, 333–44.

Halliwell, B. (2006). Oxidative stress and neurodegeneration: where are we now? J Neurochem *97*, 1634–58.

Halliwell, B. and Gutteridge, J. M. (1984). Oxygen toxicity, oxygen radicals, transition metals and disease. Biochem J *219*, 1–14.

Hamilton, B., Dong, Y., Shindo, M., Liu, W., Odell, I., Ruvkun, G. and Lee, S. S. (2005). A systematic RNAi screen for longevity genes in C. elegans. Genes Dev *19*, 1544–55.

Hansen, K. F., Karelina, K., Sakamoto, K., Wayman, G. A., Impey, S. and Obrietan, K. (2013). miRNA-132: a dynamic regulator of cognitive capacity. Brain Struct Funct *218*, 817–31.

Hansen, M., Hsu, A.-L., Dillin, A. and Kenyon, C. (2005). New genes tied to endocrine, metabolic, and dietary regulation of lifespan from a Caenorhabditis elegans genomic RNAi screen. PLoS Genet *1*, 119–28.

Harman, D. (1956). Aging: a theory based on free radical and radiation chemistry. J Gerontol *11*, 298–300.

Hebert, L. E., Scherr, P. A., Bienias, J. L., Bennett, D. A. and Evans, D. A. (2003). Alzheimer disease in the US population: prevalence estimates using the 2000 census. Arch Neurol *60*, 1119–22.

Hedden, T. and Gabrieli, J. D. E. (2004). Insights into the ageing mind: a view from cognitive neuroscience. Nat Rev Neurosci *5*, 87–96.

Holtzman, D. M., Herz, J. and Bu, G. (2012). Apolipoprotein E and apolipoprotein E receptors: normal biology and roles in Alzheimer disease. Cold Spring Harb Perspect Med *2*, a006312.

Holtzman, D. M., Morris, J. C. and Goate, A. M. (2011). Alzheimer's disease: the challenge of the second century. Sci Transl Med *3*, 77sr1.

Hu, X.-L., Cheng, X., Cai, L., Tan, G.-H., Xu, L., Feng, X.-Y., Lu, T.-J., Xiong, H., Fei, J. and Xiong, Z.-Q. (2011). Conditional deletion of NRSF in forebrain neurons accelerates epileptogenesis in the kindling model. Cereb Cortex *21*, 2158–65.

Ibberson, D., Benes, V., Muckenthaler, M. U. and Castoldi, M. (2009). RNA degradation compromises the reliability of microRNA expression profiling. BMC Biotechnol *9*, 102–102.

Jarriault, S. and Greenwald, I. (2002). Suppressors of the egg-laying defective phenotype of sel-12 presenilin mutants implicate the CoREST corepressor complex in LIN-12/Notch signaling in C. elegans. Genes Dev *16*, 2713–28.

Jimenez-Mateos, E. M., Bray, I., Sanz-Rodriguez, A., Engel, T., McKiernan, R. C., Mouri, G., Tanaka, K., Sano, T., Saugstad, J. A., Simon, R. P., Stallings, R. L. and Henshall, D. C. (2011). miRNA Expression profile after status epilepticus and hippocampal neuroprotection by targeting miR-132. Am J Pathol *179*, 2519–32.

Johnson, D. S., Mortazavi, A., Myers, R. M. and Wold, B. (2007). Genome-wide mapping of in vivo protein-DNA interactions. Science *316*, 1497–502.

Johnson, R., Zuccato, C., Belyaev, N. D., Guest, D. J., Cattaneo, E. and Buckley, N. J. (2008). A microRNA-based gene dysregulation pathway in Huntington's disease. Neurobiol Dis *29*, 438–45.

Johnson, T. E., Henderson, S., Murakami, S., de Castro, E., de Castro, S. H., Cypser, J., Rikke, B., Tedesco, P. and Link, C. (2002). Longevity genes in the nematode Caenorhabditis elegans also mediate increased resistance to stress and prevent disease. J Inherit Metab Dis *25*, 197–206.

Jonsson, T., Stefansson, H., Steinberg, S., Jonsdottir, I., Jonsson, P. V., Snaedal, J., Bjornsson, S., Huttenlocher, J., Levey, A. I., Lah, J. J., Rujescu, D., Hampel, H., Giegling, I., Andreassen, O. A., Engedal, K., Ulstein, I., Djurovic, S., Ibrahim-Verbaas, C., Hofman, A., Ikram, M. A., van Duijn, C. M., Thorsteinsdottir, U., Kong, A. and Stefansson, K. (2013). Variant of TREM2 associated with the risk of Alzheimer's disease. N Engl J Med *368*, 107–16.

Kamath, R. S. and Ahringer, J. (2003). Genome-wide RNAi screening in Caenorhabditis elegans. Methods *30*, 313–21.

Kaneko, N., Hwang, J.-Y., Gertner, M., Pontarelli, F. and Zukin, R. S. (2014). Casein kinase 1 suppresses activation of REST in insulted hippocampal neurons and halts ischemia-induced neuronal death. J Neurosci *34*, 6030–9.

Karch, C. M., Cruchaga, C. and Goate, A. M. (2014). Alzheimer's disease genetics: from the bench to the clinic. Neuron *83*, 11–26.

Katz, D. J., Edwards, T. M., Reinke, V. and Kelly, W. G. (2009). A C. elegans LSD1 demethylase contributes to germline immortality by reprogramming epigenetic memory. Cell *137*, 308–20.

Katzman, R., Terry, R., DeTeresa, R., Brown, T., Davies, P., Fuld, P., Renbing, X. and Peck, A. (1988). Clinical, pathological, and neurochemical changes in dementia: a subgroup with preserved mental status and numerous neocortical plaques. Ann Neurol *23*, 138–44.

Kenyon, C., Chang, J., Gensch, E., Rudner, A. and Tabtiang, R. (1993). A C. elegans mutant that lives twice as long as wild type. Nature *366*, 461–464.

Kenyon, C. J. (2010). The genetics of ageing. Nature *464*, 504–12.

Kimble, J. and Hirsh, D. (1979). The postembryonic cell lineages of the hermaphrodite and male gonads in Caenorhabditis elegans. Dev Biol *70*, 396–417.

Klotz, L.-O., Sánchez-Ramos, C., Prieto-Arroyo, I., Urbánek, P., Steinbrenner, H. and Monsalve, M. (2015). Redox regulation of FoxO transcription factors. Redox Biol *6*, 51–72.

Lakowski, B., Eimer, S., Göbel, C., Böttcher, A., Wagler, B. and Baumeister, R. (2003). Two suppressors of sel-12 encode C2H2 zinc-finger proteins that regulate presenilin transcription in Caenorhabditis elegans. Development *130*, 2117–2128.

Lambert, J. C., Ibrahim-Verbaas, C. A., Harold, D., Naj, A. C., Sims, R., Bellenguez, C., DeStafano, A. L., Bis, J. C., Beecham, G. W., Grenier-Boley, B., Russo, G., Thorton-Wells, T. A., Jones, N., Smith, A. V., Chouraki, V., Thomas, C., Ikram, M. A., Zelenika, D., Vardarajan, B. N., Kamatani, Y., Lin, C. F., Gerrish, A., Schmidt, H., Kunkle, B., Dunstan, M. L., Ruiz, A., Bihoreau, M. T., Choi, S. H., Reitz, C., Pasquier, F., Cruchaga, C., Craig, D., Amin, N., Berr, C., Lopez, O. L., De Jager, P. L., Deramecourt, V., Johnston, J. A.,

Evans, D., Lovestone, S., Letenneur, L., Morón, F. J., Rubinsztein, D. C., Eiriksdottir, G., Sleegers, K., Goate, A. M., Fiévet, N., Huentelman, M. W., Gill, M., Brown, K., Kamboh, M. I., Keller, L., Barberger-Gateau, P., McGuiness, B., Larson, E. B., Green, R., Myers, A. J., Dufouil, C., Todd, S., Wallon, D., Love, S., Rogaeva, E., Gallacher, J., St George-Hyslop, P., Clarimon, J., Lleo, A., Bayer, A., Tsuang, D. W., Yu, L., Tsolaki, M., Bossù, P., Spalletta, G., Proitsi, P., Collinge, J., Sorbi, S., Sanchez-Garcia, F., Fox, N. C., Hardy, J., Deniz Naranjo, M. C., Bosco, P., Clarke, R., Brayne, C., Galimberti, D., Mancuso, M., Matthews, F., European Alzheimer's Disease Initiative (EADI), Genetic and Environmental Risk in Alzheimer's Disease, Alzheimer's Disease Genetic Consortium, Cohorts for Heart and Aging Research in Genomic Epidemiology, Moebus, S., Mecocci, P., Del Zompo, M., Maier, W., Hampel, H., Pilotto, A., Bullido, M., Panza, F., Caffarra, P., Nacmias, B., Gilbert, J. R., Mayhaus, M., Lannefelt, L., Hakonarson, H., Pichler, S., Carrasquillo, M. M., Ingelsson, M., Beekly, D., Alvarez, V., Zou, F., Valladares, O., Younkin, S. G., Coto, E., Hamilton-Nelson, K. L., Gu, W., Razquin, C., Pastor, P., Mateo, I., Owen, M. J., Faber, K. M., Jonsson, P. V., Combarros, O., O'Donovan, M. C., Cantwell, L. B., Soininen, H., Blacker, D., Mead, S., Mosley, Jr, T. H., Bennett, D. A., Harris, T. B., Fratiglioni, L., Holmes, C., de Bruijn, R. F., Passmore, P., Montine, T. J., Bettens, K., Rotter, J. I., Brice, A., Morgan, K., Foroud, T. M., Kukull, W. A., Hannequin, D., Powell, J. F., Nalls, M. A., Ritchie, K., Lunetta, K. L., Kauwe, J. S., Boerwinkle, E., Riemenschneider, M., Boada, M., Hiltuenen, M., Martin, E. R., Schmidt, R., Rujescu, D., Wang, L. S., Dartigues, J. F., Mayeux, R., Tzourio, C., Hofman, A., Nöthen, M. M., Graff, C., Psaty, B. M., Jones, L., Haines, J. L., Holmans, P. A., Lathrop, M., Pericak-Vance, M. A., Launer, L. J., Farrer, L. A., van Duijn, C. M., Van Broeckhoven, C., Moskvina, V., Seshadri, S., Williams, J., Schellenberg, G. D. and Amouyel, P. (2013). Meta-analysis of 74,046 individuals identifies 11 new susceptibility loci for Alzheimer's disease. Nat Genet *45*, 1452–8.

Landis, J. N. and Murphy, C. T. (2010). Integration of diverse inputs in the regulation of Caenorhabditis elegans DAF-16/FOXO. Dev Dyn *239*, 1405–12.

Lau, P., Bossers, K., Janky, R., Salta, E., Frigerio, C. S., Barbash, S., Rothman, R., Sierksma, A. S. R., Thathiah, A., Greenberg, D., Papadopoulou, A. S., Achsel, T., Ayoubi, T., Soreq, H., Verhaagen, J., Swaab, D. F., Aerts, S. and De Strooper, B. (2013). Alteration of the microRNA network during the progression of Alzheimer's disease. EMBO Mol Med *5*, 1613–34.

Lee, C. K., Weindruch, R. and Prolla, T. A. (2000). Gene-expression profile of the ageing brain in mice. Nat Genet *25*, 294–297.

Leung, A. K. L. and Sharp, P. A. (2010). MicroRNA functions in stress responses. Mol Cell *40*, 205–15.

Levin, J. Z., Yassour, M., Adiconis, X., Nusbaum, C., Thompson, D. A., Friedman, N., Gnirke, A. and Regev, A. (2010). Comprehensive comparative analysis of strand-specific RNA sequencing methods. Nat Methods *7*, 709–15.

Li, C. and Wong, W. H. (2001). Model-based analysis of oligonucleotide arrays: expression index computation and outlier detection. Proc Natl Acad Sci U S A *98*, 31–6.

Li, X.-J. and Li, S.-H. (2005). HAP1 and intracellular trafficking. Trends Pharmacol Sci *26*, 1–3.

Li, Y., Wang, W.-J., Cao, H., Lu, J., Wu, C., Hu, F.-Y., Guo, J., Zhao, L., Yang, F., Zhang, Y.-X., Li, W., Zheng, G.-Y., Cui, H., Chen, X., Zhu, Z., He, H., Dong, B., Mo, X., Zeng, Y. and Tian, X.-L. (2009). Genetic association of FOXO1A and FOXO3A with longevity trait in Han Chinese populations. Hum Mol Genet *18*, 4897–904.

Lin, K., Dorman, J. B., Rodan, A. and Kenyon, C. (1997). daf-16: An HNF-3/forkhead family member that can function to double the life-span of Caenorhabditis elegans. Science *278*, 1319–1322.

Lipinski, M. M., Zheng, B., Lu, T., Yan, Z., Py, B. F., Ng, A., Xavier, R. J., Li, C., Yankner, B. A., Scherzer, C. R. and Yuan, J. (2010). Genome-wide analysis reveals mechanisms modulating autophagy in normal brain aging and in Alzheimer's disease. Proc Natl Acad Sci U S A *107*, 14164–9.

Lithgow, G. J., White, T. M., Melov, S. and Johnson, T. E. (1995). Thermotolerance and extended life-span conferred by single-gene mutations and induced by thermal stress. Proc Natl Acad Sci U S A *92*, 7540–4.

Liu, J., Head, E., Gharib, A. M., Yuan, W., Ingersoll, R. T., Hagen, T. M., Cotman, C. W. and Ames, B. N. (2002). Memory loss in old rats is associated with brain mitochondrial decay and RNA/DNA oxidation: partial reversal by feeding acetyl-L-carnitine and/or R-alpha -lipoic acid. Proc Natl Acad Sci U S A *99*, 2356–61.

Loerch, P. M., Lu, T., Dakin, K. A., Vann, J. M., Isaacs, A., Geula, C., Wang, J., Pan, Y., Gabuzda, D. H., Li, C., Prolla, T. A. and Yankner, B. A. (2008). Evolution of the aging brain transcriptome and synaptic regulation. PLoS One *3*, e3329.

Lois, C., Hong, E. J., Pease, S., Brown, E. J. and Baltimore, D. (2002). Germline transmission and tissue-specific expression of transgenes delivered by lentiviral vectors. Science *295*, 868–72.

Lorenzo, A., Yuan, M., Zhang, Z., Paganetti, P. A., Sturchler-Pierrat, C., Staufenbiel, M., Mautino, J., Vigo, F. S., Sommer, B. and Yankner, B. A. (2000). Amyloid beta interacts with the amyloid precursor protein: a potential toxic mechanism in Alzheimer's disease. Nat Neurosci *3*, 460–4.

Lu, T., Aron, L., Zullo, J., Pan, Y., Kim, H., Chen, Y., Yang, T.-H., Kim, H.-M., Drake, D., Liu, X. S., Bennett, D. A., Colaiácovo, M. P. and Yankner, B. A. (2014). REST and stress resistance in ageing and Alzheimer's disease. Nature *507*, 448–54.

Lu, T., Pan, Y., Kao, S. Y., Li, C., Kohane, I., Chan, J. and Yankner, B. A. (2004). Gene regulation and DNA damage in the ageing human brain. Nature *429*, 883–891.

Lusardi, T. A., Farr, C. D., Faulkner, C. L., Pignataro, G., Yang, T., Lan, J., Simon, R. P. and Saugstad, J. A. (2010). Ischemic preconditioning regulates expression of microRNAs and a predicted target, MeCP2, in mouse cortex. J Cereb Blood Flow Metab *30*, 744–56.

Maeder, M. L., Linder, S. J., Cascio, V. M., Fu, Y., Ho, Q. H. and Joung, J. K. (2013). CRISPR RNA-guided activation of endogenous human genes. Nat Methods *10*, 977–9.

Magill, S. T., Cambronne, X. A., Luikart, B. W., Lioy, D. T., Leighton, B. H., Westbrook, G. L., Mandel, G. and Goodman, R. H. (2010). microRNA-132 regulates dendritic growth and arborization of newborn neurons in the adult hippocampus. Proc Natl Acad Sci U S A *107*, 20382–7.

Mahadev, K., Wu, X., Zilbering, A., Zhu, L., Lawrence, J. T. and Goldstein, B. J. (2001). Hydrogen peroxide generated during cellular insulin stimulation is integral to activation of the distal insulin signaling cascade in 3T3-L1 adipocytes. J Biol Chem *276*, 48662–9.

Mao, C.-A., Tsai, W.-W., Cho, J.-H., Pan, P., Barton, M. C. and Klein, W. H. (2011). Neuronal transcriptional repressor REST suppresses an Atoh7-independent program for initiating retinal ganglion cell development. Dev Biol *349*, 90–9.

Marchant, N. L., Reed, B. R., Sanossian, N., Madison, C. M., Kriger, S., Dhada, R., Mack, W. J., DeCarli, C., Weiner, M. W., Mungas, D. M., Chui, H. C. and Jagust, W. J. (2013). The aging brain and cognition: contribution of vascular injury and a to mild cognitive dysfunction. JAMA Neurol *70*, 488–95.

Mariani, E., Polidori, M. C., Cherubini, A. and Mecocci, P. (2005). Oxidative stress in brain aging, neurodegenerative and vascular diseases: an overview. J Chromatogr B Analyt Technol Biomed Life Sci *827*, 65–75.

Merritt, C., Rasoloson, D., Ko, D. and Seydoux, G. (2008). 3' UTRs are the primary regulators of gene expression in the C. elegans germline. Curr Biol *18*, 1476–82.

Mulligan, P., Westbrook, T. F., Ottinger, M., Pavlova, N., Chang, B., Macia, E., Shi, Y.-J., Barretina, J., Liu, J., Howley, P. M., Elledge, S. J. and Shi, Y. (2008). CDYL bridges REST and histone methyltransferases for gene repression and suppression of cellular transformation. Mol Cell *32*, 718–26.

Murphy, M. P. (2009). How mitochondria produce reactive oxygen species. Biochem J *417*, 1–13.

Nesti, E., Corson, G. M., McCleskey, M., Oyer, J. A. and Mandel, G. (2014). C-terminal domain small phosphatase 1 and MAP kinase reciprocally control REST stability and neuronal differentiation. Proc Natl Acad Sci U S A *111*, E3929–36.

Nguyen, T., Nioi, P. and Pickett, C. B. (2009). The Nrf2-antioxidant response element signaling pathway and its activation by oxidative stress. J Biol Chem *284*, 13291–5.

Nishihara, S., Tsuda, L. and Ogura, T. (2003). The canonical Wnt pathway directly regulates NRSF/REST expression in chick spinal cord. Biochem Biophys Res Commun *311*, 55–63.

Nottke, A. C., Beese-Sims, S. E., Pantalena, L. F., Reinke, V., Shi, Y. and Colaiácovo, M. P. (2011). SPR-5 is a histone H3K4 demethylase with a role in meiotic double-strand break repair. Proc Natl Acad Sci U S A *108*, 12805–10.

Olsen, L., Klausen, M., Helboe, L., Nielsen, F. C. and Werge, T. (2009). MicroRNAs show mutually exclusive expression patterns in the brain of adult male rats. PLoS One *4*, e7225.

Ooi, L. and Wood, I. C. (2007). Chromatin crosstalk in development and disease: lessons from REST. Nat Rev Genet *8*, 544–54.

Otto, S. J., McCorkle, S. R., Hover, J., Conaco, C., Han, J.-J., Impey, S., Yochum, G. S., Dunn, J. J., Goodman, R. H. and Mandel, G. (2007). A new binding motif for the transcriptional repressor REST uncovers large gene networks devoted to neuronal functions. J Neurosci *27*, 6729–39.

Paik, J.-h., Ding, Z., Narurkar, R., Ramkissoon, S., Muller, F., Kamoun, W. S., Chae, S.-S., Zheng, H., Ying, H., Mahoney, J., Hiller, D., Jiang, S., Protopopov, A., Wong, W. H., Chin, L., Ligon, K. L. and DePinho, R. A. (2009). FoxOs cooperatively regulate diverse pathways governing neural stem cell homeostasis. Cell Stem Cell *5*, 540–53.

Palm, K., Belluardo, N., Metsis, M. and Timmusk, T. (1998). Neuronal expression of zinc finger transcription factor REST/NRSF/XBR gene. J Neurosci *18*, 1280–1296.

Park, S.-K., Kim, K., Page, G. P., Allison, D. B., Weindruch, R. and Prolla, T. A. (2009). Gene expression profiling of aging in multiple mouse strains: identification of aging biomarkers and impact of dietary antioxidants. Aging Cell *8*, 484–95.

Peters, A., Sethares, C. and Moss, M. B. (1998). The effects of aging on layer 1 in area 46 of prefrontal cortex in the rhesus monkey. Cereb Cortex *8*, 671–84.

Pozzi, D., Lignani, G., Ferrea, E., Contestabile, A., Paonessa, F., D'Alessandro, R., Lippiello, P., Boido, D., Fassio, A., Meldolesi, J., Valtorta, F., Benfenati, F. and Baldelli, P. (2013). REST/NRSF-mediated intrinsic homeostasis protects neuronal networks from hyperexcitability. EMBO J *32*, 2994–3007.

Qiang, L., Banks, A. S. and Accili, D. (2010). Uncoupling of acetylation from phosphorylation regulates FoxO1 function independent of its subcellular localization. J Biol Chem *285*, 27396–401.

Ravache, M., Weber, C., Mérienne, K. and Trottier, Y. (2010). Transcriptional activation of REST by Sp1 in Huntington's disease models. PLoS One *5*, e14311.

Remenyi, J., Hunter, C. J., Cole, C., Ando, H., Impey, S., Monk, C. E., Martin, K. J., Barton, G. J., Hutvagner, G. and Arthur, J. S. C. (2010). Regulation of the miR-212/132 locus by MSK1 and CREB in response to neurotrophins. Biochem J *428*, 281–91.

Robert, V. J. P., Katic, I. and Bessereau, J.-L. (2009). Mos1 transposition as a tool to engineer the Caenorhabditis elegans genome by homologous recombination. Methods *49*, 263–9.

Ronan, J. L., Wu, W. and Crabtree, G. R. (2013). From neural development to cognition: unexpected roles for chromatin. Nat Rev Genet *14*, 347–59.

Rong, J., Li, S.-H. and Li, X.-J. (2007). Regulation of intracellular HAP1 trafficking. J Neurosci Res *85*, 3025–9.

Rowe, W. B., Blalock, E. M., Chen, K.-C., Kadish, I., Wang, D., Barrett, J. E., Thibault, O., Porter, N. M., Rose, G. M. and Landfield, P. W. (2007). Hippocampal expression analyses reveal selective association of immediate-early, neuroenergetic, and myelinogenic pathways with cognitive impairment in aged rats. J Neurosci *27*, 3098–110.

Sarov, M., Murray, J. I., Schanze, K., Pozniakovski, A., Niu, W., Angermann, K., Hasse, S., Rupprecht, M., Vinis, E., Tinney, M., Preston, E., Zinke, A., Enst, S., Teichgraber, T., Janette, J., Reis, K., Janosch, S., Schloissnig, S., Ejsmont, R. K., Slightam, C., Xu, X., Kim, S. K., Reinke, V., Stewart, A. F., Snyder, M., Waterston, R. H. and Hyman, A. A. (2012). A genome-scale resource for in vivo tag-based protein function exploration in C. elegans. Cell *150*, 855–66.

Schneider, J. A., Arvanitakis, Z., Leurgans, S. E. and Bennett, D. A. (2009). The neuropathology of probable Alzheimer disease and mild cognitive impairment. Ann Neurol *66*, 200–8.

Schoenherr, C. J. and Anderson, D. J. (1995). The neuron-restrictive silencer factor (NRSF): a coordinate repressor of multiple neuron-specific genes. Science *267*, 1360–1363.

Schriner, S. E., Linford, N. J., Martin, G. M., Treuting, P., Ogburn, C. E., Emond, M., Coskun, P. E., Ladiges, W., Wolf, N., Van Remmen, H., Wallace, D. C. and Rabinovitch, P. S. (2005). Extension of murine life span by overexpression of catalase targeted to mitochondria. Science *308*, 1909–11.

Scott, H. L., Tamagnini, F., Narduzzo, K. E., Howarth, J. L., Lee, Y.-B., Wong, L.-F., Brown, M. W., Warburton, E. C., Bashir, Z. I. and Uney, J. B. (2012). MicroRNA-132 regulates recognition memory and synaptic plasticity in the perirhinal cortex. Eur J Neurosci *36*, 2941–8.

Sempere, L. F., Freemantle, S., Pitha-Rowe, I., Moss, E., Dmitrovsky, E. and Ambros, V. (2004). Expression profiling of mammalian microRNAs uncovers a subset of brain-expressed microRNAs with possible roles in murine and human neuronal differentiation. Genome Biol *5*.

Sengupta, A., Molkentin, J. D., Paik, J. H., DePinho, R. A. and Yutzey, K. E. (2011). FoxO transcription factors promote cardiomyocyte survival upon induction of oxidative stress. J Biol Chem *286*, 7468–7478.

Shaltiel, G., Hanan, M., Wolf, Y., Barbash, S., Kovalev, E., Shoham, S. and Soreq, H. (2013). Hippocampal microRNA-132 mediates stress-inducible cognitive deficits through its acetylcholinesterase target. Brain Struct Funct *218*, 59–72.

Shao, D., Zhai, P., Del Re, D. P., Sciarretta, S., Yabuta, N., Nojima, H., Lim, D.-S., Pan, D. and Sadoshima, J. (2014). A functional interaction between Hippo-YAP signalling and FoxO1 mediates the oxidative stress response. Nat Commun *5*, 3315.

Shimojo, M. (2006). Characterization of the nuclear targeting signal of REST/NRSF. Neurosci Lett *398*, 161–6.

Shimojo, M. (2008). Huntingtin regulates RE1-silencing transcription factor/neuron-restrictive silencer factor (REST/NRSF) nuclear trafficking indirectly through a complex with REST/NRSF-interacting LIM domain protein (RILP) and dynactin p150 Glued. J Biol Chem *283*, 34880–6.

Shimojo, M. and Hersh, L. B. (2003). REST/NRSF-interacting LIM domain protein, a putative nuclear translocation receptor. Mol Cell Biol *23*, 9025–31.

Shimojo, M. and Hersh, L. B. (2006). Characterization of the REST/NRSF-interacting LIM domain protein (RILP): localization and interaction with REST/NRSF. J Neurochem *96*, 1130–8.

Siegmund, K. D., Connor, C. M., Campan, M., Long, T. I., Weisenberger, D. J., Biniszkiewicz, D., Jaenisch, R., Laird, P. W. and Akbarian, S. (2007). DNA methylation in the human cerebral cortex is dynamically regulated throughout the life span and involves differentiated neurons. PLoS One *2*, e895.

Singh, S., Ramamoorthy, M., Vaughan, C., Yeudall, W. A., Deb, S. and Palit Deb, S. (2013). Human oncoprotein MDM2 activates the Akt signaling pathway through an interaction with the repressor element-1 silencing transcription factor conferring a survival advantage to cancer cells. Cell Death Differ *20*, 558–66.

Spalding, K. L., Bhardwaj, R. D., Buchholz, B. A., Druid, H. and Frisén, J. (2005). Retrospective birth dating of cells in humans. Cell *122*, 133–43.

Strum, J. C., Johnson, J. H., Ward, J., Xie, H., Feild, J., Hester, A., Alford, A. and Waters, K. M. (2009). MicroRNA 132 regulates nutritional stress-induced chemokine production through repression of SirT1. Mol Endocrinol *23*, 1876–84.

Sulston, J. E. and Horvitz, H. R. (1977). Post-embryonic cell lineages of the nematode, Caenorhabditis elegans. Dev Biol *56*, 110–156.

Sultana, R., Perluigi, M. and Butterfield, D. A. (2006). Protein oxidation and lipid peroxidation in brain of subjects with Alzheimer's disease: insights into mechanism of neurodegeneration from redox proteomics. Antioxid Redox Signal *8*, 2021–37.

Toledo, E. M. and Inestrosa, N. C. (2010). Activation of Wnt signaling by lithium and rosiglitazone reduced spatial memory impairment and neurodegeneration in brains of an APPswe/PSEN1DeltaE9 mouse model of Alzheimer's disease. Mol Psychiatry *15*, 272–85, 228.

Tothova, Z., Kollipara, R., Huntly, B. J., Lee, B. H., Castrillon, D. H., Cullen, D. E., McDowell, E. P., Lazo-Kallanian, S., Williams, I. R., Sears, C., Armstrong, S. A., Passegué, E., DePinho, R. A. and Gilliland, D. G. (2007). FoxOs are critical mediators of hematopoietic stem cell resistance to physiologic oxidative stress. Cell *128*, 325–39.

Tremblay, C., St-Amour, I., Schneider, J., Bennett, D. A. and Calon, F. (2011). Accumulation of transactive response DNA binding protein 43 in mild cognitive impairment and Alzheimer disease. J Neuropathol Exp Neurol *70*, 788–98.

Treusch, S., Hamamichi, S., Goodman, J. L., Matlack, K. E. S., Chung, C. Y., Baru, V., Shulman, J. M., Parrado, A., Bevis, B. J., Valastyan, J. S., Han, H., Lindhagen-Persson, M., Reiman, E. M., Evans, D. A., Bennett, D. A., Olofsson, A., DeJager, P. L., Tanzi, R. E., Caldwell, K. A., Caldwell, G. A. and Lindquist, S. (2011). Functional links between A toxicity, endocytic trafficking, and Alzheimer's disease risk factors in yeast. Science *334*, 1241–5.

Troncoso, J. C., Costello, A., Watson, Jr, A. L. and Johnson, G. V. (1993). In vitro polymerization of oxidized tau into filaments. Brain Res *613*, 313–6.

Tusher, V. G., Tibshirani, R. and Chu, G. (2001). Significance analysis of microarrays applied to the ionizing radiation response. Proc Natl Acad Sci U S A *98*, 5116–5121.

Ucar, A., Gupta, S. K., Fiedler, J., Erikci, E., Kardasinski, M., Batkai, S., Dangwal, S., Kumarswamy, R., Bang, C., Holzmann, A., Remke, J., Caprio, M., Jentzsch, C., Engelhardt, S., Geisendorf, S., Glas, C., Hofmann, T. G., Nessling, M., Richter, K., Schiffer, M., Carrier, L., Napp, L. C., Bauersachs, J., Chowdhury, K. and Thum, T. (2012). The miRNA-212/132 family regulates both cardiac hypertrophy and cardiomyocyte autophagy. Nat Commun *3*, 1078.

van der Horst, A. and Burgering, B. M. T. (2007). Stressing the role of FoxO proteins in lifespan and disease. Nat Rev Mol Cell Biol *8*, 440–50.

Van Raamsdonk, J. M. and Hekimi, S. (2009). Deletion of the mitochondrial superoxide dismutase sod-2 extends lifespan in Caenorhabditis elegans. PLoS Genet *5*, e1000361.

Vanguilder, H. D. and Freeman, W. M. (2011). The hippocampal neuroproteome with aging and cognitive decline: past progress and future directions. Front Aging Neurosci *3*, 8.

Vo, N., Klein, M. E., Varlamova, O., Keller, D. M., Yamamoto, T., Goodman, R. H. and Impey, S. (2005). A cAMP-response element binding protein-induced microRNA regulates neuronal morphogenesis. Proc Natl Acad Sci U S A *102*, 16426–16431.

Wang, L., Brugge, J. S. and Janes, K. A. (2011). Intersection of FOXO- and RUNX1-mediated gene expression programs in single breast epithelial cells during morphogenesis and tumor progression. Proc Natl Acad Sci U S A *108*, E803–12.

Wayman, G. A., Davare, M., Ando, H., Fortin, D., Varlamova, O., Cheng, H. Y., Marks, D., Obrietan, K., Soderling, T. R., Goodman, R. H. and Impey, S. (2008). An activity-regulated microRNA controls dendritic plasticity by down-regulating p250GAP. Proc Natl Acad Sci U S A *105*, 9093–9098.

Wen, C., Levitan, D., Li, X. and Greenwald, I. (2000). spr-2, a suppressor of the egg-laying defect caused by loss of sel-12 presenilin in Caenorhabditis elegans, is a member of the SET protein subfamily. Proc Natl Acad Sci U S A *97*, 14524–9.

Westbrook, T. F., Hu, G., Ang, X. L., Mulligan, P., Pavlova, N. N., Liang, A., Leng, Y., Maehr, R., Shi, Y., Harper, J. W. and Elledge, S. J. (2008). SCFbeta-TRCP controls oncogenic transformation and neural differentiation through REST degradation. Nature *452*, 370–4.

Westbrook, T. F., Martin, E. S., Schlabach, M. R., Leng, Y., Liang, A. C., Feng, B., Zhao, J. J., Roberts, T. M., Mandel, G., Hannon, G. J., Depinho, R. A., Chin, L. and Elledge, S. J. (2005). A genetic screen for candidate tumor suppressors identifies REST. Cell *121*, 837–48.

Willert, J., Epping, M., Pollack, J. R., Brown, P. O. and Nusse, R. (2002). A transcriptional response to Wnt protein in human embryonic carcinoma cells. BMC Dev Biol *2*, 8.

Wilson, R. S., Nag, S., Boyle, P. A., Hizel, L. P., Yu, L., Buchman, A. S., Schneider, J. A. and Bennett, D. A. (2013). Neural reserve, neuronal density in the locus ceruleus, and cognitive decline. Neurology *80*, 1202–8.

Wiznerowicz, M. and Trono, D. (2003). Conditional suppression of cellular genes: lentivirus vector-mediated drug-inducible RNA interference. J Virol *77*, 8957–61.

Wong, H.-K. A., Veremeyko, T., Patel, N., Lemere, C. A., Walsh, D. M., Esau, C., Vanderburg, C. and Krichevsky, A. M. (2013). De-repression of FOXO3a death axis by microRNA-132 and -212 causes neuronal apoptosis in Alzheimer's disease. Hum Mol Genet *22*, 3077–92.

Wu, J. and Xie, X. (2006). Comparative sequence analysis reveals an intricate network among REST, CREB and miRNA in mediating neuronal gene expression. Genome Biol *7*, R85.

Xie, Q., Chen, J. and Yuan, Z. (2012). Post-translational regulation of FOXO. Acta Biochim Biophys Sin (Shanghai) *44*, 897–901.

Yang, D., Li, T., Wang, Y., Tang, Y., Cui, H., Tang, Y., Zhang, X., Chen, D., Shen, N. and Le, W. (2012). miR-132 regulates the differentiation of dopamine neurons by directly targeting Nurr1 expression. J Cell Sci *125*, 1673–82.

Yang, Y., Hou, H., Haller, E. M., Nicosia, S. V. and Bai, W. (2005). Suppression of FOXO1 activity by FHL2 through SIRT1-mediated deacetylation. EMBO J *24*, 1021–32.

Yankner, B. A., Lu, T. and Loerch, P. (2008). The aging brain. Annu Rev Pathol *3*, 41–66.

Yu, M., Cai, L., Liang, M., Huang, Y., Gao, H., Lu, S., Fei, J. and Huang, F. (2009). Alteration of NRSF expression exacerbating 1-methyl-4-phenyl-pyridinium ion-induced cell death of SH-SY5Y cells. Neurosci Res *65*, 236–44.

Yu, M., Suo, H., Liu, M., Cai, L., Liu, J., Huang, Y., Xu, J., Wang, Y., Zhu, C., Fei, J. and Huang, F. (2013). NRSF/REST neuronal deficient mice are more vulnerable to the neurotoxin MPTP. Neurobiol Aging *34*, 916–27.

Zecca, L., Youdim, M. B. H., Riederer, P., Connor, J. R. and Crichton, R. R. (2004). Iron, brain ageing and neurodegenerative disorders. Nat Rev Neurosci *5*, 863–73.

Zeiser, E., Frøkjær-Jensen, C., Jorgensen, E. and Ahringer, J. (2011). MosSCI and Gateway Compatible Plasmid Toolkit for Constitutive and Inducible Expression of Transgenes in the C. elegans Germline. PLoS One *6*, e20082.

Zhang, S., Hao, J., Xie, F., Hu, X., Liu, C., Tong, J., Zhou, J., Wu, J. and Shao, C. (2011a). Downregulation of miR-132 by promoter methylation contributes to pancreatic cancer development. Carcinogenesis *32*, 1183–9.

Zhang, X., Tang, N., Hadden, T. J. and Rishi, A. K. (2011b). Akt, FoxO and regulation of apoptosis. Biochim Biophys Acta *1813*, 1978–86.

Zhang, Y., Liu, T., Meyer, C. A., Eeckhoute, J., Johnson, D. S., Bernstein, B. E., Nusbaum, C., Myers, R. M., Brown, M., Li, W. and Liu, X. S. (2008). Model-based analysis of ChIP-Seq (MACS). Genome Biol *9*, R137.

Zhao, Y., Yang, J., Liao, W., Liu, X., Zhang, H., Wang, S., Wang, D., Feng, J., Yu, L. and Zhu, W.-G. (2010). Cytosolic FoxO1 is essential for the induction of autophagy and tumour suppressor activity. Nat Cell Biol *12*, 665–75.